FINAL REPORT

COMPUTER MODELING ANALYSIS IN BRIDGE EVALUATION

PHASE II
DYNAMIC RESPONSE OF CONTINUOUS BEAM BRIDGES
AND SLANT-LEGGED RIGID FRAME BRIDGES

Research Report No. FL/DOT/RMC/0542(2)-4108

Highway Planning and Research Program

HPR Project No. 0510542
State Project No. 99700-8311-119
FIU Project No. 49-80-57-18-144-00

Ton-Lo Wang
Dongzhou Huang

October 1992

Department of Civil and Environmental Engineering
College of Engineering and Design
Florida International University
Miami, Florida

Technical Report Documentation Page

1. Report No.	2. Government Accession No.	3. Recipient's Catalog No.
FL/DOT/RMC/0542(2)-4108		

4. Title and Subtitle	5. Report Date
Computer Modeling Analysis in Bridge Evaluation: Dynamic Analysis of Continuous Beam Bridges and Slant-legged rigid Frame Bridge	October 1992
	6. Performing Organization Code

7. Author(s)	8. Performing Organization Report No.
Ton-Lo Wang and Dongzhou Huang	

9. Performing Organization Name and Address	10. Work Unit No.
Florida International University Department of Civil and Environmental Engineering University Park Miami, Florida 33199	11. Contract or Grant No. WPI 0510542, C-4108
	13. Type of Report and Period Covered Final Report November 1991 - November 1992
12. Sponsoring Agency Name and Address Florida Department of Transportation Research Center, MS30 605 Suwannee Street Tallahassee, Florida 32399-0450	14. Sponsoring Agency Code 99700-8311-119

15. Supplementary Notes

Prepared in cooperation with the Federal Highway Administration

16. Abstract

This is an interim report of the second year's work on computer modeling analysis in highway bridge evaluation. The objective of this investigation is to study the dynamic and impact characteristics of continuous beam bridges and slant-legged rigid frame bridges due to vehicles passing over rough bridge decks.

According to the Type 3, Type 3S2, and Type 3-3 trucks, three nonlinear vehicle models with nine, sixteen, and eighteen degrees of freedom are developed. Six continuous multigirder bridges with different span lengths are designed based on the Standard Plans of Highway Bridge Structures of U. S. Bureau of Public Roads. The continuous multigirder bridges are modeled as grillage beam systems. The effect of transverse stiffness, road surface roughness, vehicle speed, span length, spacing of girders, and damping ratio are analyzed. The slant-legged rigid frame bridge is modeled as a space bar system. The free and force vibration characteristics including parametric study are analyzed.

17. Key Words	18. Distribution Statement
Road Surface Roughness, Highway Trucks, Continuous Multigirder Bridges, Slant-legged rigid bridges, Dynamic Response, Impact.	This document is available to the public through the National Technical Information Service, Springfield, Virginia, 22161

19. Security Classify. (of this report)	20. Security Classify. (of this page)	21. No. of Pages	22. Price
Unclassified	Unclassified	215	

Form DOT F 1700.7 (8-72)

METRIC CONVERSIONS

inch x 25.40 = mm

foot x 0.3048 = m

lb (force) x 4.448 = N

kip (force) x 4.448 = kN

lb (mass) x 454 = g (mass)

kip (mass) x 454 = kg (mass)

kip/in x 0.175 = kN/mm

psi x 6.895 = kPa

ksi x 6.895 = MPa

mph x 1.609 = km/hr

DISCLAIMER

"The opinions, findings and conclusions expresses in this publication are those of the authors and not necessarily those of the Department of Transportation or the U.S. Department of Transportation.

Prepared in cooperation with the State of Florida Department of Transportation and the U.S. Department of Transportation."

ACKNOWLEDGMENTS

The authors wish to express their sincere appreciation to the Florida Department of Transportation (FDOT) for funding this research. Special thanks are also extended to Dr. Mohsen Shahawy, Chief Structural Analyst, Structures Research and Testing Center, FDOT for his valuable advice, suggestions, and comments during the course of this study.

Also, the authors would like to express their thanks to Dr. J. Huang and student assistant Mr. Juan C. Vallarino for their assistance in generating the Figures and Tables.

TABLE OF CONTENTS

LIST OF TABLES

LIST OF FIGURES

CHAPTER I

INTRODUCTION

Nowadays, many existing highway bridges in the United States, including those in Florida, are older than 20 years. In order to insure their safety for the traveling public and to protect their initial investment, the evaluation of existing bridges has become very important. One of the most significant aspects in the bridge evaluation process is how to determine the response of bridge to moving vehicles. Unfortunately, all the existing theories and computer software packages can accurately analyze only the static response to vehicles. Therefore, this research project mainly deals with dynamic response of highway bridges to moving vehicles.

It is well known to most bridge engineers and investigators that the impact or dynamic load of bridges is a complicated subject. It depends on the roughness of roadway, different kinds of vehicles, different types of bridges, the number of vehicles on the bridge, vehicle speeds, and so on. Therefore, this project "Computer Modeling Analysis in Bridge Evaluation" is divided into three phases. In Phase I, the following research items have been accomplished: (1). the generation of different classes of road surface roughness, (2). the development of vehicle computer models to simulate the dynamic responses of highway H20-44 and HS20-44 trucks, (3). the development of computer models for the highway reinforcement concrete, prestressed concrete, and steel simple bridges, (4). the formulation of bridge/vehicle interaction motions, (5). the study of static and dynamic responses in various members of bridges, and (6). the

comparison of results of this computer modeling study with the experimental data and AASHTO standard specifications.

In Phase I, the trucks were modeled as nonlinear space models, while the bridge was modeled as a space beam. The computer program developed in this phase can mainly analyze the response of simply supported beam bridges which can be reasonably treated as one space beam, individually.

In Phase II, the specific objectives of this research are: (1). the development of vehicle models to simulate the actions of Type 3, Type 3S2, and Type 3-3 trucks, (2). the development of bridge models for the continuous bridges and the slant-legged rigid frame bridges, (3). the formulation of the bridge/vehicle interaction motions, (4). the study of the static and dynamic responses in various members of bridges based on different vehicle speeds, vehicle weights, road surface roughness, bridge types, and the lengths of bridge spans, and (5). the comparison of results of this computer modeling study with the AASHTO standard specifications.

The mathematical models for Type 3, Type 3S2, and Type 3-3 trucks with nine, sixteen, and eighteen degrees of freedom, respectively, are described in Chapter 2. Also, the dynamic analysis of these vehicles is studied.

Chapter 3 is primarily devoted to the dynamic analysis of continuous multigirder bridges. The bridge model for six continuous steel bridges is introduced first. Then, a new numerical

procedure for analyzing dynamic response of bridges to moving vehicles is presented. Finally, the free and impact characteristics of continuous multigirder bridges are discussed.

The dynamic behavior of a slant-legged rigid frame highway bridge is examined in Chapter 4. A bridge model of space bar system which involves the effect of axial force caused by dead load is described first. Then, the effect of loading positions, vehicle speed, road roughness, damping ratio, etc. are studied. Also included in Chapter 4 are the maximum impact factors of the bridge and their comparison with ASSHTO specifications.

The significant conclusions and recommendation are given in Chapter 5.

CHAPTER II

HIGHWAY VEHICLE MODELS

2.1 Introduction

.

The study of the characteristics of vehicles, which are the primary loadings of highways and bridges, is very important in determining the response of roads and bridges. In phase I, two vehicle models of H2O-44 and HS20-44 ', trucks have been developed. However, the investigations show that Type 3, Type 3S2, and Type 3-3 trucks correspond better to existing traffic. Also, these three types of trucks are adopted for rating vehicles in the AASHTO Guide Specifications for Strength Evaluation of Existing Steel and Concrete Bridges [8]. For these reasons, this chapter will be devoted to developing these three new vehicle models. First, the derivation of the motion equations of vehicles will be described. Then, the dynamic behaviors of the vehicles passing over different kinds of road surface roughness will be analyzed.

2.2 Vehicle Models

Fig. 2-1 to Fig. 2-4 show the three vehicle models corresponding to Type 3, Type 3S2, and Type 3-3 trucks, respectively. Their dimensions are given in Table 2-1 to Table 2-4, _ including FDOT truck (Type 3S2).

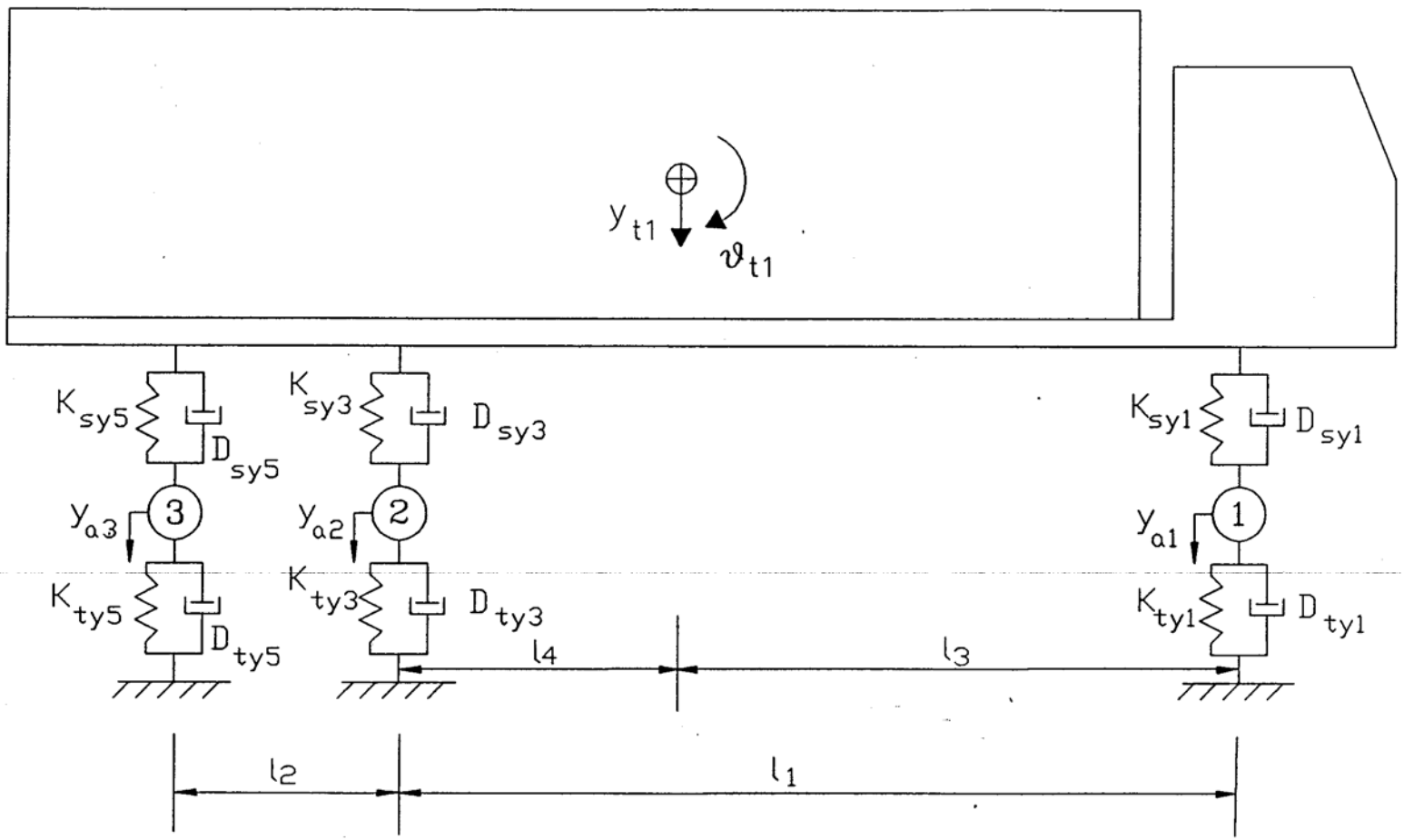

Fig. 2-1. Side View of Type 3 Vehicle Model

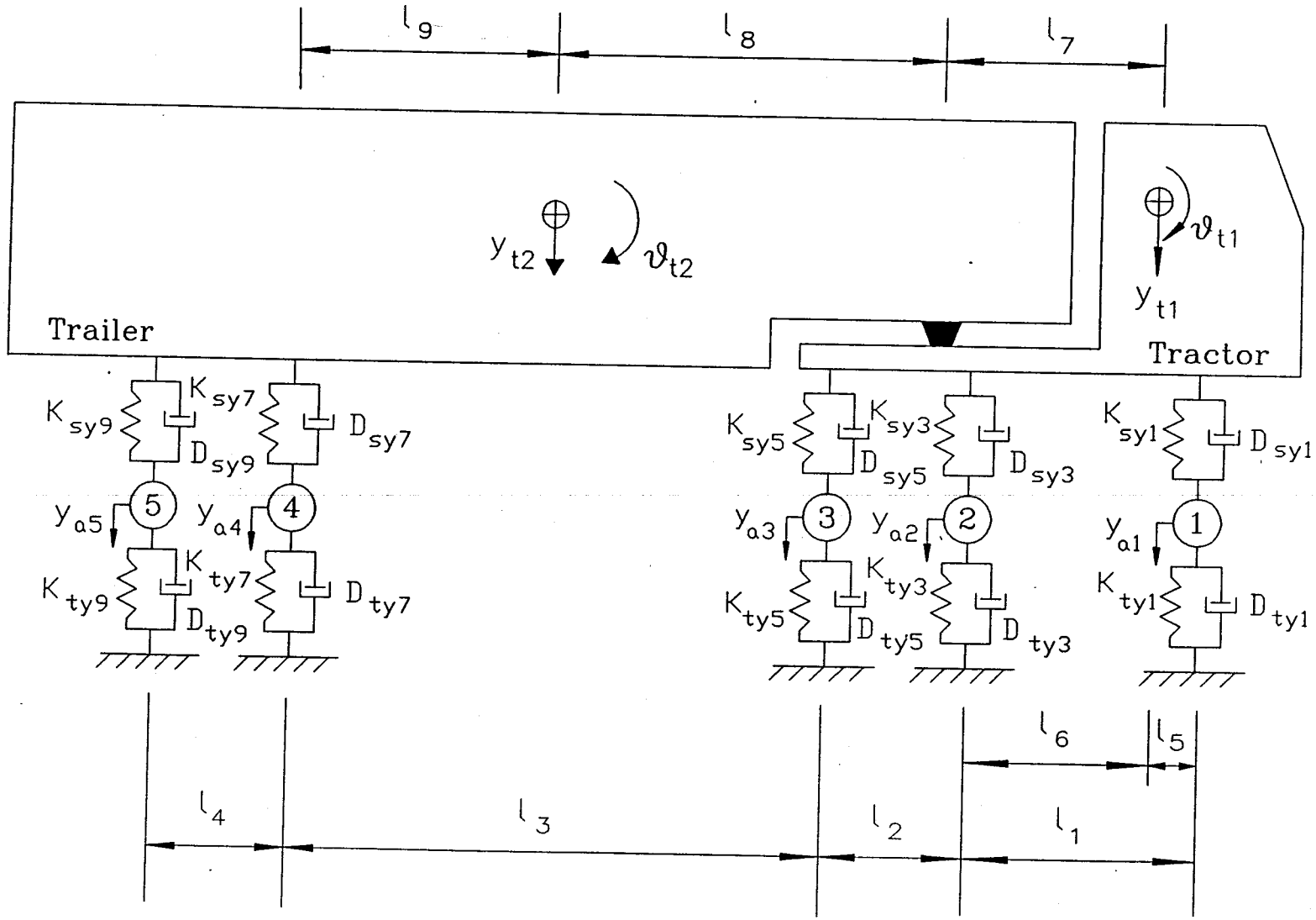

Fig. 2-2. Side View of Type 3S2 Vehicle Model

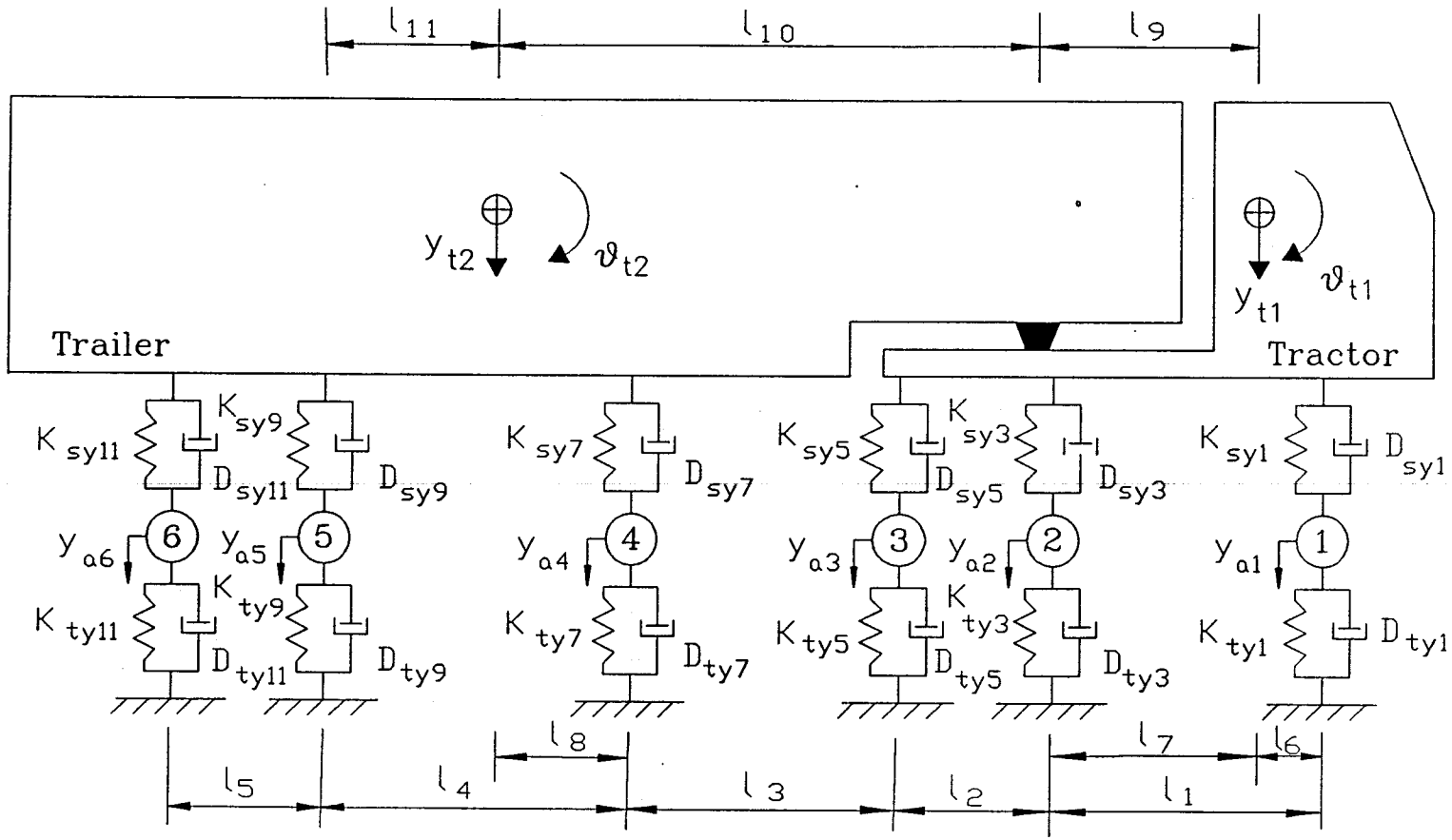

Fig. 2-3. Side View of Type 3-3 Vehicle Model

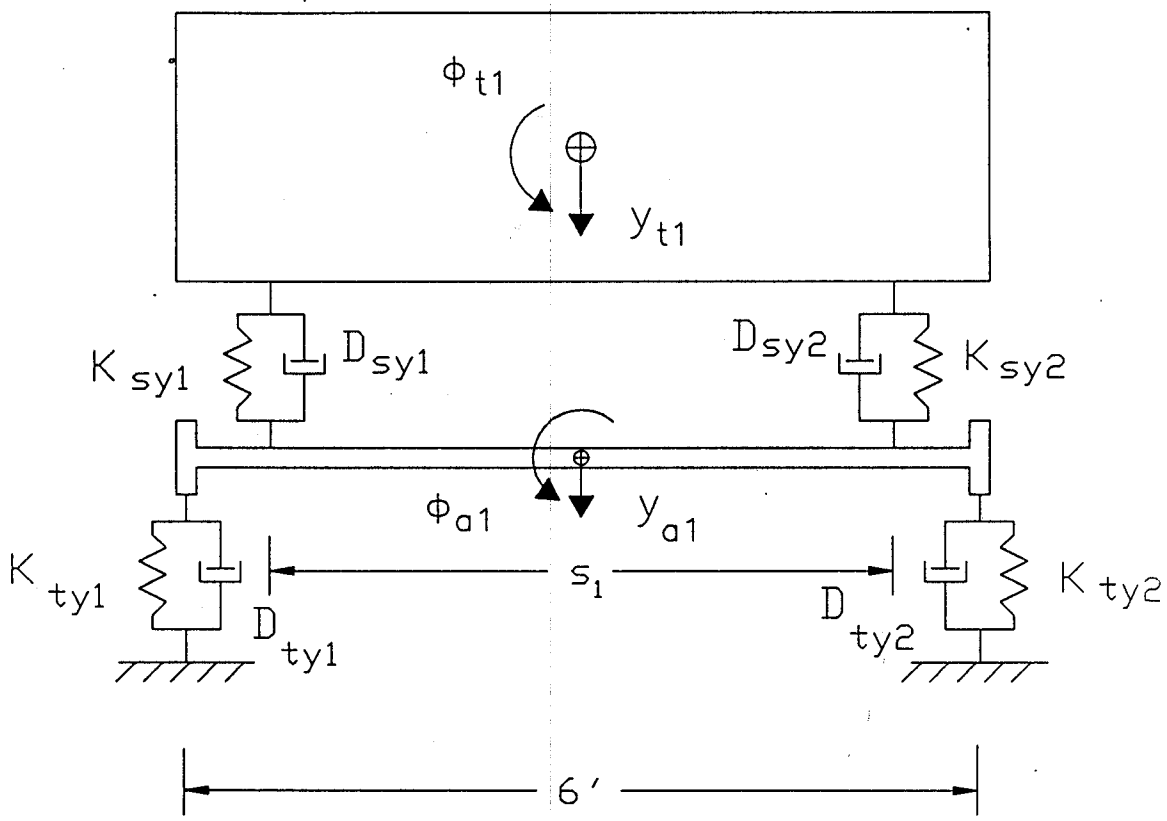

Fig. 2-4. Front View of Type 3, Type 3S2, and Type 3-3 Vehicle Models

Table 2-1. Dimensions of Type 3 Truck

Distance Between Axles (in)		Spacing Between Suspensions and Wheels (in)	
l_1	180	s_1	44
l_2	48	s_2, s_3	36
l_3	136.78	d_1	68
l_4	43.22	d_2, d_3	72

Table 2-2. Dimensions of Type 3S2 Truck

Distance Between Axles (in)		Spacing Between Suspensions and Wheels (in)	
l_1	132	s_1	44
l_2	48	s_2	36
l_3	264	s_3	36
l_4	48	s_4	36
l_5	47.06	s_5	36
l_6	84.94	d_1	68
l_7	96.94	d_2	72
l_8	163.08	d_3	72
l_9	136.92	d_4 d_5	72

Table 2-3. Dimensions of Type 3S2 (FDOT) Truck

Distance Between Axles (in)		Spacing Between Suspensions and Wheels (in)	
l_1	186	s_1	44
l_2	54	s_2	36
l_3	252	s_3	36
l_4	54	s_4	36
l_5	37.79	s_5	36
l_6	151.21	d_1	68
l_7	166.21	d_2	72
l_8	168.14	d_3	72
l_9	122.86	d_4 d_5	72

Table 2-4. Dimensions of Type 3-3 Truck

Distance Between Axles (in)		Spacing Between Suspensions and Wheels (in)	
l_1	180	s_1	44
l_2	48		
l_3	180		
l_4	192	s_2 to s_6	36
l_5	48		
l_6	40.27		
l_7	139.73	d_1	68
l_8	12.65		
l_9	145.73	d_2 to d_6	72
l_{10}	234.65		
l_{11}	179.35		

Figs. 2-1 and 2-4 illustrate the side and front views of Type 3 vehicle model. Four rigid masses represent the truck, steer wheel/axle set, the forward wheel/axle set of the tandem, and the aft wheel/axle set of the tandem, individually. In the model, the truck is assigned three degrees of freedom, corresponding to the vertical displacement (y), rotation about the transverse axis (pitch or θ), and rotation about the longitudinal axis (roll or ϕ). Each wheel axle set is provided with two degrees of freedom in the vertical and roll directions. The total degrees of freedom in the model are nine.

The vehicle model of Type 3S2 truck is shown in Figs. 2-2 and 2-4. The model consists of seven rigid masses as tractor, semi-trailer, steer wheel/axle set, the forward and aft wheel/axle sets of drive tandem, and the forward and aft wheel/axle sets of trailer tandem. Tractor and semi-trailer are assigned three degrees of freedom (y, θ, and ϕ), individually. Two degrees of freedom (y and ϕ) are assigned for each wheel-axle set. The tractor and semi-trailer are interconnected at the pivot point (so-called fifth wheel point, see Fig. 2-2). The total degrees of freedom are sixteen. FDOT testing truck is one of the Type 3S2 truck. Its dimensions are given in Table 2-3.

Similarly, the third vehicle model (refer to Figs. 2-3 and 2-4) with nineteen degrees of freedom is developed to represent Type 3-3 truck, composed of eight rigid masses as tractor, semi-trailer, steer wheel/axle set, the forward and aft wheel/axle sets of drive tandem, the first wheel/axle set of trailer, and the forward and aft wheel/axle sets of trailer tandem. Tractor and semi-trailer are assigned three degrees of freedom (y, θ, and ϕ), individually. Two degrees of

freedom (y and θ) are assigned for each wheel-axle set. The tractor and semi-trailer are interconnected at the pivot point.

Suspension force consists of the linear elastic spring force and the constant interleaf friction force [29]. The load-displacement relationship for friction force, suspension spring force, and the combination of these two forces are given in Phase I interim report [29]. The tire springs are assumed to be linear.

Since the truck is a complex physical system, certain assumptions are made to simplify the model. These assumptions are as follows:

(1) The vehicle runs at a constant speed.

(2) All components move with the same velocity in the longitudinal direction.

(3) Provision is made in the model for wheel lift. Under this condition, the vertical tire stiffnesses are taken as zero.

(4) Each tire contacts the road at a single point.

(5) Force inputs are limited to the vertical direction.

(6) In suspension system, damping elements were assumed to be linear and to be of the viscous type. Damper force is proportional to the velocity. 10% of the critical damping value was used for damping coefficient. In the tires, the damping forces were neglected.

The total potential energy, $V = \sum V_i$, of the system is then computed from the spring stiffnesses and relative displacements, whereas the dissipation energy, $D = \sum D_i$, of the system is obtained from the damping forces. The total kinetic energy, $T = \sum T_i$, of the system is calculated using the mass, mass moment of inertia, and translational as well as rotational

velocities, of the system components. The moment of inertia of all components is assumed to be constant and the weight of each component is considered as the external force on that component.

The equations of motion of the system are derived, using Lagrange's formulation, as follows:

$$\frac{d}{dt}\left(\frac{\partial T}{\partial \dot{q}_i}\right) - \frac{\partial T}{\partial q_i} + \frac{\partial V}{\partial q_i} + \frac{\partial D}{\partial \dot{q}_i} = 0 \qquad (2\text{-}1)$$

where q_i and $\dot{q}_i$ are the generalized displacements and velocities. Details of derivation and the motion equations are presented in Appendix A.

2.3 Vehicle Dynamic Analysis

In order to know the vehicle dynamic characteristics of each model, the maximum dynamic forces of suspensions and tires are calculated in 800-ft simulation length when vehicle models with damped suspension system are running on the different classes of roads.

The equations of motion were solved by using a fourth-order Runge-Kutta Scheme, with an integration time step of 0.005 second. Such a small time step was necessary to avoid numerical instability.

The real percentage of impact acquired from the study is defined as:

$$Imp(\%) = \left[\frac{R_{dm}}{R_{sm}} - 1 \right] x\,100\% \qquad (2\text{-}2)$$

in which R_{dm} and R_{sm} are the absolute maximum responses for dynamic and static studies, respectively.

A summary of the impact factors of suspension and tire forces for different road surface conditions and vehicle speeds is given in Table 2-5 to Table 2-16 and illustrated in Figure 2-5 to Figure 2-28. In these Tables and Figures, we can observe that: (1) the impact factors of both suspension and tire forces increase with vehicle speed in most cases, (2) the impact factors are affected slightly by the vehicle speeds in very good and good roads for both suspension and tire forces, (3) the vehicle speeds influence the impact factors significantly in average and poor roads, (4) the impact factors of both suspension and tire forces obtained from the poor road are the highest among these four different road surface conditions for speed varied from 15 to 75 mph, (5) the lowest impact factors are always found in the very good road, (6) the impact factors of tire forces of tractor axle are much higher than those of trailer axle in Type 3S2 and Type 3-3 vehicles, and (7) generally, the impact of suspensions is much smaller than that of tires.

Table 2-5. Maximum Suspension Forces, Tire Forces, and Impact Factors of Steer Axle of Type 3 Truck with Damped Suspension for Different Road Surface Conditions and Vehicle Speeds.

Steer Axle	Maximum Static Force (kips)	Vehicle Speed (mph)	Road Surface Conditions							
			Very Good		Good		Average		Poor	
			Maximum Dynamic Force (kips)	Impact Factor (%)	Maximum Dynamic Force (kips)	Impact Factor (%)	Maximum Dynamic Force (kips)	Impact Factor (%)	Maximum Dynamic Force (kips)	Impact Factor (%)
Suspension Force	7.345	15	8.216	11.85	8.473	15.36	9.250	25.94	10.319	40.49
		25	8.231	12.06	8.464	15.23	9.166	24.79	10.542	43.52
		35	8.270	12.59	8.629	17.48	9.615	30.91	11.398	55.18
		45	8.300	13.01	8.763	19.31	9.906	34.87	13.088	78.18
		55	8.399	14.35	8.886	20.98	10.519	43.21	13.170	79.31
		65	8.367	13.92	9.268	26.17	10.295	40.16	13.178	79.42
		75	8.410	14.50	9.201	25.27	10.357	41.00	13.390	82.30
Tire Force	8.000	15	8.492	6.15	8.724	9.05	9.761	22.01	11.304	41.31
		25	8.626	7.82	8.977	12.21	10.198	27.47	12.724	59.05
		35	8.674	8.43	9.347	16.84	10.945	36.81	15.535	94.19
		45	8.713	8.91	9.492	18.65	12.210	52.63	16.083	101.04
		55	8.826	10.32	9.716	21.44	12.346	54.33	16.913	111.41
		65	8.950	11.88	10.164	27.05	12.468	55.85	17.651	120.64
		75	8.934	11.68	10.194	27.43	14.063	75.79	17.917	123.96

Table 2-6. Maximum Suspension Forces, Tire Forces, and Impact Factors of Tandem Axle of Type 3 Truck with Damped Suspension for Different Road Surface Conditions and Vehicle Speeds.

Tandem Axle	Maximum Static Force (kips)	Vehicle Speed (mph)	Road Surface Conditions							
			Very Good		Good		Average		Poor	
			Maximum Dynamic Force (kips)	Impact Factor (%)	Maximum Dynamic Force (kips)	Impact Factor (%)	Maximum Dynamic Force (kips)	Impact Factor (%)	Maximum Dynamic Force (kips)	Impact Factor (%)
Suspension Force	7.472	15	9.738	30.32	9.885	32.29	10.289	37.70	11.333	51.66
		25	9.740	30.34	10.029	34.21	10.774	44.19	11.897	59.22
		35	9.764	30.68	10.075	34.83	10.967	46.77	12.423	66.26
		45	9.793	31.05	10.132	35.60	11.272	50.85	13.024	74.29
		55	9.760	30.61	10.159	35.96	11.073	48.19	13.043	74.55
		65	9.810	31.28	10.218	36.75	11.154	49.27	13.409	79.46
		75	9.768	30.73	10.466	40.06	11.138	49.06	13.015	74.18
Tire Force	8.500	15	9.424	10.87	9.915	16.65	10.640	25.18	12.782	50.37
		25	9.699	14.10	10.217	20.19	11.523	35.56	14.171	66.72
		35	9.524	12.05	10.288	21.04	12.133	42.74	16.265	91.35
		45	9.685	13.94	10.508	23.62	12.519	47.28	17.640	107.53
		55	9.844	15.81	10.761	26.60	13.243	55.80	17.671	107.90
		65	9.813	15.45	10.907	28.32	12.870	51.41	18.851	121.77
		75	9.814	15.45	11.308	33.03	13.138	54.56	19.949	134.69

Table 2-7. Maximum Suspension Forces, Tire Forces, and Impact Factors of Steer Axle of Type 3S2 Truck with Damped Suspension for Different Road Surface Conditions and Vehicle Speeds.

Steer Axle	Maximum Static Force (kips)	Vehicle Speed (mph)	Road Surface Conditions							
			Very Good		Good		Average		Poor	
			Maximum Dynamic Force (kips)	Impact Factor (%)	Maximum Dynamic Force (kips)	Impact Factor (%)	Maximum Dynamic Force (kips)	Impact Factor (%)	Maximum Dynamic Force (kips)	Impact Factor (%)
Suspension Force	4.345	15	4.904	12.88	5.036	15.91	5.527	27.23	6.155	41.67
		25	4.893	12.61	5.117	17.77	5.593	28.75	6.547	50.70
		35	4.931	13.49	5.132	18.13	5.589	28.65	6.734	55.00
		45	4.946	13.84	5.194	19.56	5.752	32.40	7.178	65.21
		55	4.946	13.84	5.264	21.17	5.868	35.07	6.630	52.59
		65	4.997	15.01	5.572	28.26	6.011	38.35	6.991	60.91
		75	5.045	16.13	5.452	25.50	6.244	43.71	8.165	87.94
Tire Force	5.000	15	5.282	5.64	5.516	10.33	6.146	22.93	7.881	57.63
		25	5.368	7.37	5.597	11.96	6.593	31.88	7.673	53.48
		35	5.416	8.33	5.694	13.90	6.701	34.03	8.895	77.92
		45	5.426	8.53	6.110	22.21	6.929	38.59	8.834	76.69
		55	5.446	8.94	6.062	21.24	6.840	36.81	9.663	93.29
		65	5.584	11.69	6.296	25.94	6.914	38.29	10.084	101.70
		75	5.555	11.11	6.361	27.23	7.616	52.34	11.500	130.02

Table 2-8. Maximum Suspension Forces, Tire Forces, and Impact Factors of Tandem Tractor Axles of Type 3S2 Truck with Damped Suspension for Different Road Surface Conditions and Vehicle Speeds.

Tandem Tractor Axle	Maximum Static Force (kips)	Vehicle Speed (mph)	Road Surface Conditions							
			Very Good		Good		Average		Poor	
			Maximum Dynamic Force (kips)	Impact Factor (%)	Maximum Dynamic Force (kips)	Impact Factor (%)	Maximum Dynamic Force (kips)	Impact Factor (%)	Maximum Dynamic Force (kips)	Impact Factor (%)
Suspension Force	6.723	15	8.799	30.89	8.916	32.62	9.510	41.46	10.316	53.46
		25	8.942	33.02	9.079	35.06	9.840	46.37	11.052	64.40
		35	8.920	32.69	9.267	37.86	9.845	46.45	10.903	62.19
		45	8.818	31.17	9.089	35.20	9.688	44.12	11.303	68.13
		55	8.824	31.25	9.150	36.11	9.769	45.32	11.685	73.82
		65	8.802	30.94	9.159	36.24	9.807	45.88	11.317	68.35
		75	8.811	31.06	9.300	38.34	9.973	48.36	11.768	75.06
Tire Force	7.750	15	8.832	13.96	9.628	24.23	10.644	37.33	13.302	71.64
		25	9.265	19.54	10.603	36.81	11.896	53.49	15.862	104.66
		35	9.206	18.79	10.292	32.79	12.983	67.51	15.123	95.13
		45	8.860	14.31	10.212	31.76	11.562	49.18	15.796	103.81
		55	8.866	14.39	9.978	28.75	12.196	57.36	15.702	102.60
		65	8.912	14.98	10.212	31.76	12.211	57.55	17.494	125.72
		75	9.025	16.45	10.745	38.64	13.123	69.33	17.277	122.92

Table 2-9. Maximum Suspension Forces, Tire Forces, and Impact Factors of Tandem Trailer Axles of Type 3S2 Truck with Damped Suspension for Different Road Surface Conditions and Vehicle Speeds.

Tandem Trailer Axle	Maximum Static Force (kips)	Vehicle Speed (mph)	Road Surface Conditions							
			Very Good		Good		Average		Poor	
			Maximum Dynamic Force (kips)	Impact Factor (%)	Maximum Dynamic Force (kips)	Impact Factor (%)	Maximum Dynamic Force (kips)	Impact Factor (%)	Maximum Dynamic Force (kips)	Impact Factor (%)
Suspension Force	6.587	15	8.507	29.14	8.638	31.13	9.188	39.49	10.071	52.88
		25	8.568	30.06	8.864	34.56	9.658	46.61	10.706	62.52
		35	8.545	29.71	8.982	36.35	9.733	47.75	12.427	88.66
		45	8.538	29.61	8.924	35.47	9.885	50.06	13.128	99.29
		55	8.554	29.85	9.028	37.05	9.832	49.25	11.648	76.83
		65	8.577	30.21	9.113	38.34	9.984	51.56	13.603	106.50
		75	8.660	31.47	9.028	37.04	10.544	60.06	14.033	113.03
Tire Force	7.750	15	8.378	8.09	8.773	13.19	9.459	22.04	11.720	51.21
		25	8.569	10.57	9.029	16.50	10.701	38.07	12.810	65.28
		35	8.569	10.56	9.559	23.33	10.749	38.69	14.094	81.85
		45	8.653	11.64	9.407	21.37	10.922	40.92	15.909	105.27
		55	8.709	12.37	9.713	25.32	11.593	49.58	16.415	111.80
		65	8.834	13.98	10.073	29.97	11.514	48.56	18.527	139.05
		75	8.824	13.86	10.287	32.73	12.074	55.79	19.081	146.20

Table 2-10. Maximum Suspension Forces, Tire Forces, and Impact Factors of Steer Axle of FDOT (Type 3S2) Truck with Damped Suspension for Different Road Surface Conditions and Vehicle Speeds.

Steer Axle	Maximum Static Force (kips)	Vehicle Speed (mph)	Road Surface Conditions							
			Very Good		Good		Average		Poor	
			Maximum Dynamic Force (kips)	Impact Factor (%)	Maximum Dynamic Force (kips)	Impact Factor (%)	Maximum Dynamic Force (kips)	Impact Factor (%)	Maximum Dynamic Force (kips)	Impact Factor (%)
Suspension Force	5.895	15	6.516	10.53	6.695	13.57	7.118	20.74	7.816	32.59
		25	6.518	10.56	6.789	15.17	7.413	25.74	8.174	38.66
		35	6.497	10.21	6.743	14.37	7.121	20.80	8.874	50.53
		45	6.529	10.75	6.784	15.08	7.408	25.66	8.778	48.90
		55	6.544	11.00	6.879	16.69	7.485	26.97	9.037	53.30
		65	6.559	11.25	7.172	21.66	7.661	29.95	9.975	69.20
		75	6.605	12.04	7.252	23.01	8.354	41.70	10.097	71.27
Tire Force	6.550	15	6.809	3.95	7.030	7.33	7.523	14.85	9.000	37.40
		25	6.849	4.56	7.073	7.98	7.918	20.88	8.975	37.02
		35	6.893	5.23	7.234	10.44	8.005	22.21	9.844	50.29
		45	6.961	6.27	7.340	12.05	8.064	23.11	10.236	56.27
		55	6.945	6.02	7.563	15.47	8.379	27.92	11.064	68.91
		65	6.961	6.28	8.015	22.36	8.627	31.71	12.026	83.59
		75	7.020	7.18	8.168	24.70	9.461	44.43	14.098	115.23

Table 2-11. Maximum Suspension Forces, Tire Forces, and Impact Factors of Tandem Tractor Axles of FODT (Type 3S2) Truck with Damped Suspension for Different Road Surface Conditions and Vehicle Speeds.

Tandem Tractor Axle	Maximum Static Force (kips)	Vehicle Speed (mph)	Road Surface Conditions							
			Very Good		Good		Average		Poor	
			Maximum Dynamic Force (kips)	Impact Factor (%)	Maximum Dynamic Force (kips)	Impact Factor (%)	Maximum Dynamic Force (kips)	Impact Factor (%)	Maximum Dynamic Force (kips)	Impact Factor (%)
Suspension Force	9.272	15	12.792	37.96	12.859	38.68	13.307	43.52	14.182	52.95
		25	12.672	36.66	13.020	40.42	13.382	44.32	14.872	60.40
		35	12.662	36.55	13.205	42.42	14.265	53.85	16.324	76.05
		45	12.776	37.79	13.088	41.15	14.137	52.47	15.830	70.73
		55	12.787	37.91	12.983	40.02	14.096	52.03	15.931	71.81
		65	12.608	35.97	13.284	43.26	14.376	55.04	15.499	67.15
		75	12.691	36.87	13.082	41.09	14.119	52.27	15.928	71.78
Tire Force	10.300	15	11.992	16.43	12.621	22.53	13.896	34.91	16.918	64.25
		25	12.002	16.52	12.900	25.24	14.469	40.48	18.326	77.92
		35	12.804	24.31	14.101	36.90	17.782	72.63	25.819	150.67
		45	12.561	21.95	14.582	41.57	18.576	80.35	21.021	104.09
		55	12.633	22.64	13.600	32.03	16.352	58.75	21.781	111.46
		65	12.322	19.63	13.684	32.85	16.943	64.49	20.567	99.67
		75	12.251	18.95	13.335	29.46	15.846	53.84	23.296	126.17

Table 2-12. Maximum Suspension Forces, Tire Forces, and Impact Factors of Tandem Trailer Axles of FDOT (Type 3S2) Truck with Damped Suspension for Different Road Surface Conditions and Vehicle Speeds.

Tandem Trailer Axle	Maximum Static Force (kips)	Vehicle Speed (mph)	Road Surface Conditions							
			Very Good		Good		Average		Poor	
			Maximum Dynamic Force (kips)	Impact Factor (%)	Maximum Dynamic Force (kips)	Impact Factor (%)	Maximum Dynamic Force (kips)	Impact Factor (%)	Maximum Dynamic Force (kips)	Impact Factor (%)
Suspension Force	10.463	15	13.428	28.35	13.663	30.59	14.681	40.32	15.921	52.16
		25	13.571	29.71	14.051	34.29	15.301	46.24	17.172	64.13
		35	13.773	31.64	14.316	36.83	15.359	46.80	19.968	90.85
		45	13.614	30.12	14.067	34.45	15.860	51.58	19.358	85.01
		55	13.596	29.95	14.170	35.43	15.717	50.22	18.727	78.98
		65	13.737	31.29	14.356	37.21	16.239	55.20	20.850	99.28
		75	13.689	30.83	14.327	36.93	17.073	63.18	22.216	112.33
Tire Force	11.626	15	12.714	9.36	13.152	13.12	14.179	21.96	16.446	41.46
		25	12.907	11.02	13.361	14.93	14.998	29.01	17.768	52.84
		35	12.813	10.21	13.772	18.46	16.081	38.32	19.451	67.31
		45	12.925	11.18	14.051	20.86	16.983	46.08	20.358	75.11
		55	13.176	13.34	14.475	24.51	16.677	43.45	21.231	82.62
		65	13.250	13.97	14.479	24.54	17.185	47.82	23.924	105.78
		75	13.119	12.84	14.867	27.88	17.101	47.09	24.223	108.35

Table 2-13. Maximum Suspension Forces, Tire Forces, and Impact Factors of Steer Axle of Type 3-3 Truck with Damped Suspension for Different Road Surface Conditions and Vehicle Speeds.

Steer Axle	Maximum Static Force (kips)	Vehicle Speed (mph)	Road Surface Conditions							
			Very Good		Good		Average		Poor	
			Maximum Dynamic Force (kips)	Impact Factor (%)	Maximum Dynamic Force (kips)	Impact Factor (%)	Maximum Dynamic Force (kips)	Impact Factor (%)	Maximum Dynamic Force (kips)	Impact Factor (%)
Suspension Force	5.306	15	5.894	11.08	6.057	14.16	6.555	23.54	7.008	32.07
		25	5.917	11.52	6.171	16.31	6.865	29.39	7.299	37.57
		35	5.909	11.37	6.168	16.25	6.633	25.02	7.965	50.12
		45	5.936	11.88	6.178	16.43	6.935	30.70	8.082	52.33
		55	5.930	11.76	6.218	17.18	7.164	35.02	8.429	58.87
		65	5.937	11.90	6.347	19.61	7.028	32.46	7.935	49.54
		75	6.007	13.21	6.460	21.75	7.532	41.96	8.367	57.70
Tire Force	5.961	15	6.168	3.48	6.412	7.57	6.983	17.15	8.087	35.67
		25	6.263	5.06	6.562	10.08	7.487	25.60	8.555	43.53
		35	6.276	5.29	6.698	12.36	7.401	24.17	9.101	52.68
		45	6.313	5.90	6.722	12.77	8.139	36.54	11.227	88.35
		55	6.366	6.80	7.016	17.71	7.970	33.71	10.434	75.04
		65	6.374	6.94	7.174	20.36	8.036	34.81	11.189	87.72
		75	6.422	7.73	7.334	23.03	8.457	41.88	11.763	97.35

Table 2-14. Maximum Suspension Forces, Tire Forces, and Impact Factors of Tandem Tractor Axles of Type 3-3 Truck with Damped Suspension for Different Road Surface Conditions and Vehicle Speeds.

Tandem Tractor Axle	Maximum Static Force (kips)	Vehicle Speed (mph)	Road Surface Conditions							
			Very Good		Good		Average		Poor	
			Maximum Dynamic Force (kips)	Impact Factor (%)	Maximum Dynamic Force (kips)	Impact Factor (%)	Maximum Dynamic Force (kips)	Impact Factor (%)	Maximum Dynamic Force (kips)	Impact Factor (%)
Suspension Force	4.992	15	6.796	36.15	6.893	38.10	7.169	43.61	7.898	58.22
		25	6.705	34.33	6.881	37.85	7.557	51.40	8.302	66.32
		35	6.707	34.37	6.968	39.60	7.293	46.10	8.342	67.12
		45	6.760	35.44	7.023	40.70	7.395	48.15	8.602	72.33
		55	6.680	33.83	6.997	40.18	7.358	47.42	8.786	76.02
		65	6.714	34.50	7.082	41.88	7.576	51.77	8.840	77.10
		75	6.728	34.78	7.156	43.36	7.780	55.87	9.096	82.23
Tire Force	6.019	15	6.724	11.71	7.348	22.07	8.433	40.09	10.127	68.25
		25	7.524	24.99	8.191	36.08	9.286	54.27	11.720	94.71
		35	6.951	15.48	8.004	32.97	9.426	56.60	12.768	112.12
		45	6.904	14.70	7.720	28.26	9.562	58.85	12.032	99.89
		55	6.984	16.02	7.835	30.16	9.144	51.91	12.420	106.34
		65	7.019	16.60	8.116	34.83	10.269	70.60	13.734	128.16
		75	7.334	21.85	8.412	39.75	10.817	79.70	16.082	167.18

Table 2-15. Maximum Suspension Forces, Tire Forces, and Impact Factors of the First Axle of Trailer of Type 3-3 Truck with Damped Suspension for Different Road Surface Conditions and Vehicle Speeds.

The First Axle of Trailer	Maximum Static Force (kips)	Vehicle Speed (mph)	Road Surface Conditions							
			Very Good		Good		Average		Poor	
			Maximum Dynamic Force (kips)	Impact Factor (%)	Maximum Dynamic Force (kips)	Impact Factor (%)	Maximum Dynamic Force (kips)	Impact Factor (%)	Maximum Dynamic Force (kips)	Impact Factor (%)
Suspension Force	6.838	15	9.279	35.70	9.756	42.68	10.288	50.46	11.863	73.50
		25	9.398	37.45	9.654	41.18	10.254	49.96	12.086	76.75
		35	9.374	37.08	9.657	41.22	10.507	53.66	12.434	81.84
		45	9.310	36.15	9.691	41.73	10.561	54.45	13.563	98.35
		55	9.328	36.42	9.746	42.53	10.616	55.26	13.591	98.77
		65	9.333	36.49	9.797	43.28	10.748	57.19	13.542	98.04
		75	9.300	36.01	9.860	44.20	10.939	59.97	14.165	107.16
Tire Force	8.001	15	9.230	15.37	9.651	20.63	10.516	31.43	12.365	54.54
		25	9.207	15.08	9.617	20.20	10.922	36.52	13.590	69.86
		35	9.222	15.26	9.945	24.30	11.550	44.35	14.500	81.23
		45	9.315	16.42	10.170	27.11	11.382	42.26	15.331	91.62
		55	9.276	15.93	10.443	30.52	11.524	44.04	16.150	101.85
		65	9.417	17.70	10.604	32.54	12.091	51.12	18.439	130.47
		75	9.547	19.32	10.613	32.65	12.191	52.38	18.830	135.35

Table 2-16. Maximum Suspension Forces, Tire Forces, and Impact Factors of Tandem Trailer Axles of Type 3-3 Truck with Damped Suspension for Different Road Surface Conditions and Vehicle Speeds.

Tandem Trailer Axle	Maximum Static Force (kips)	Vehicle Speed (mph)	Road Surface Conditions							
			Very Good		Good		Average		Poor	
			Maximum Dynamic Force (kips)	Impact Factor (%)	Maximum Dynamic Force (kips)	Impact Factor (%)	Maximum Dynamic Force (kips)	Impact Factor (%)	Maximum Dynamic Force (kips)	Impact Factor (%)
Suspension Force	5.838	15	7.436	27.37	7.670	31.38	8.069	38.22	9.068	55.33
		25	7.464	27.86	7.635	30.78	8.198	40.43	8.973	53.71
		35	7.492	28.33	7.733	32.46	8.574	46.86	9.922	69.95
		45	7.525	28.90	7.819	33.93	8.435	44.48	10.362	77.50
		55	7.509	28.62	7.888	35.12	8.345	42.95	9.947	70.39
		65	7.508	28.60	7.910	35.49	8.366	43.31	10.667	82.72
		75	7.577	29.80	7.940	36.02	8.412	44.09	11.473	96.53
Tire Force	7.001	15	7.497	7.08	7.901	12.85	8.615	23.06	10.576	51.06
		25	7.549	7.83	8.141	16.28	9.355	33.62	11.192	59.87
		35	7.606	8.64	8.254	17.90	9.467	35.22	12.628	80.38
		45	7.647	9.23	8.395	19.92	10.046	43.50	14.734	110.45
		55	7.731	10.43	8.587	22.65	9.683	38.31	13.725	96.05
		65	7.800	11.42	8.814	25.90	10.134	44.75	15.856	126.48
		75	7.848	12.11	8.939	27.69	10.836	54.78	15.368	119.51

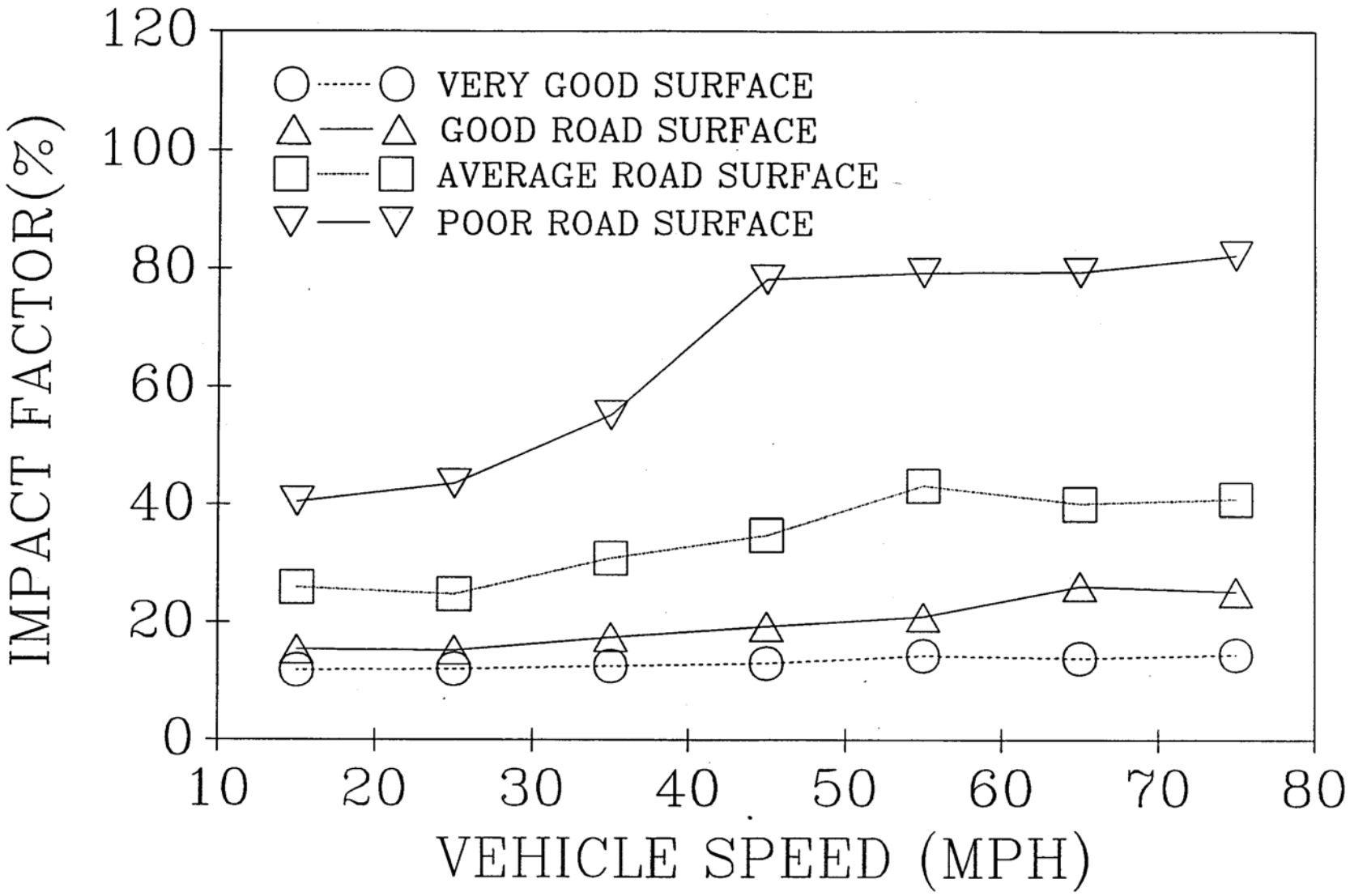

Fig. 2-5. Impact Results of Suspension Forces for the Steer Axle of Type 3 Truck with Damped Suspension

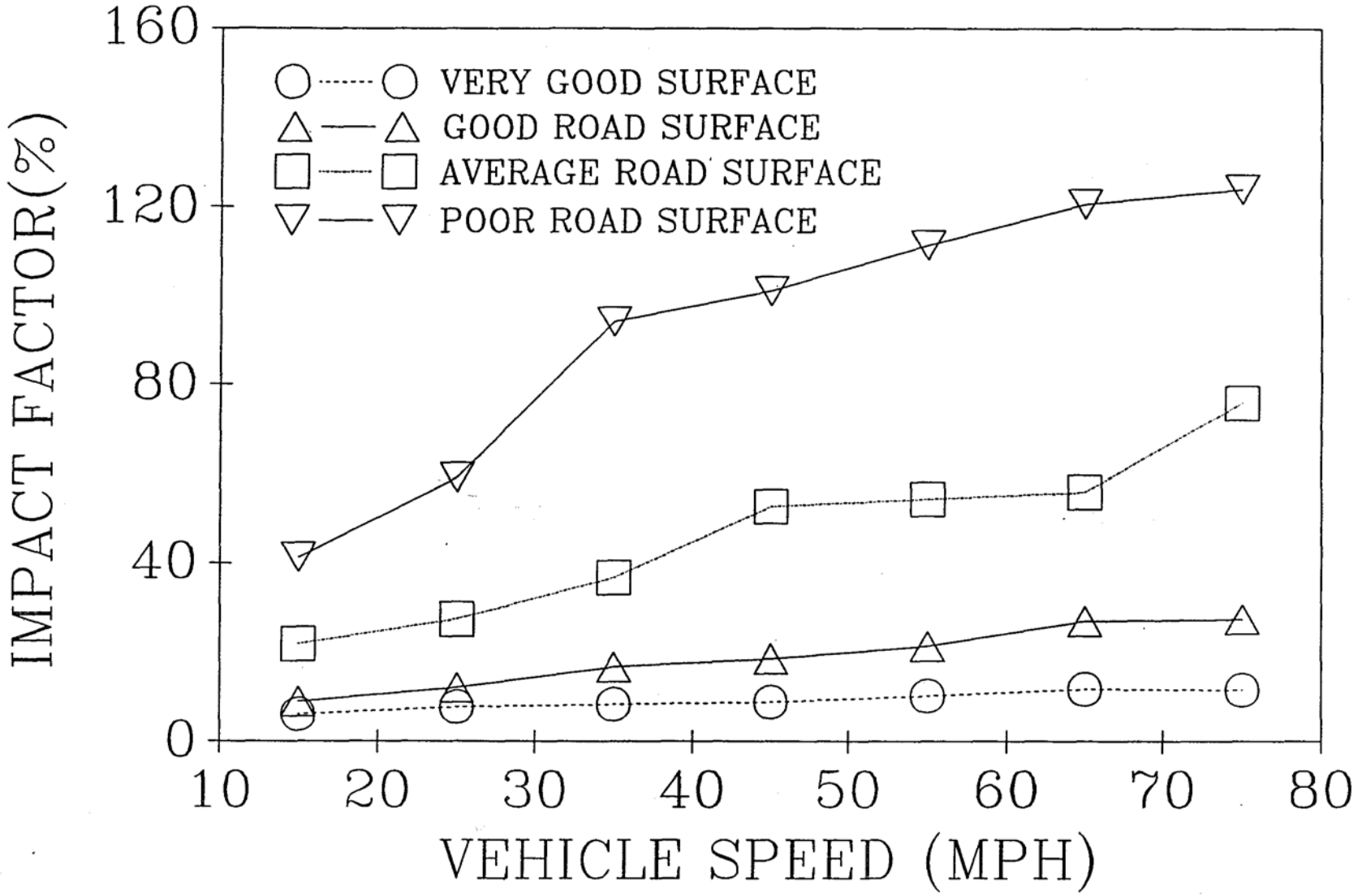

Fig. 2-6. Impact Results of Tire Forces for the Steer Axle of Type 3 Truck with Damped Suspension

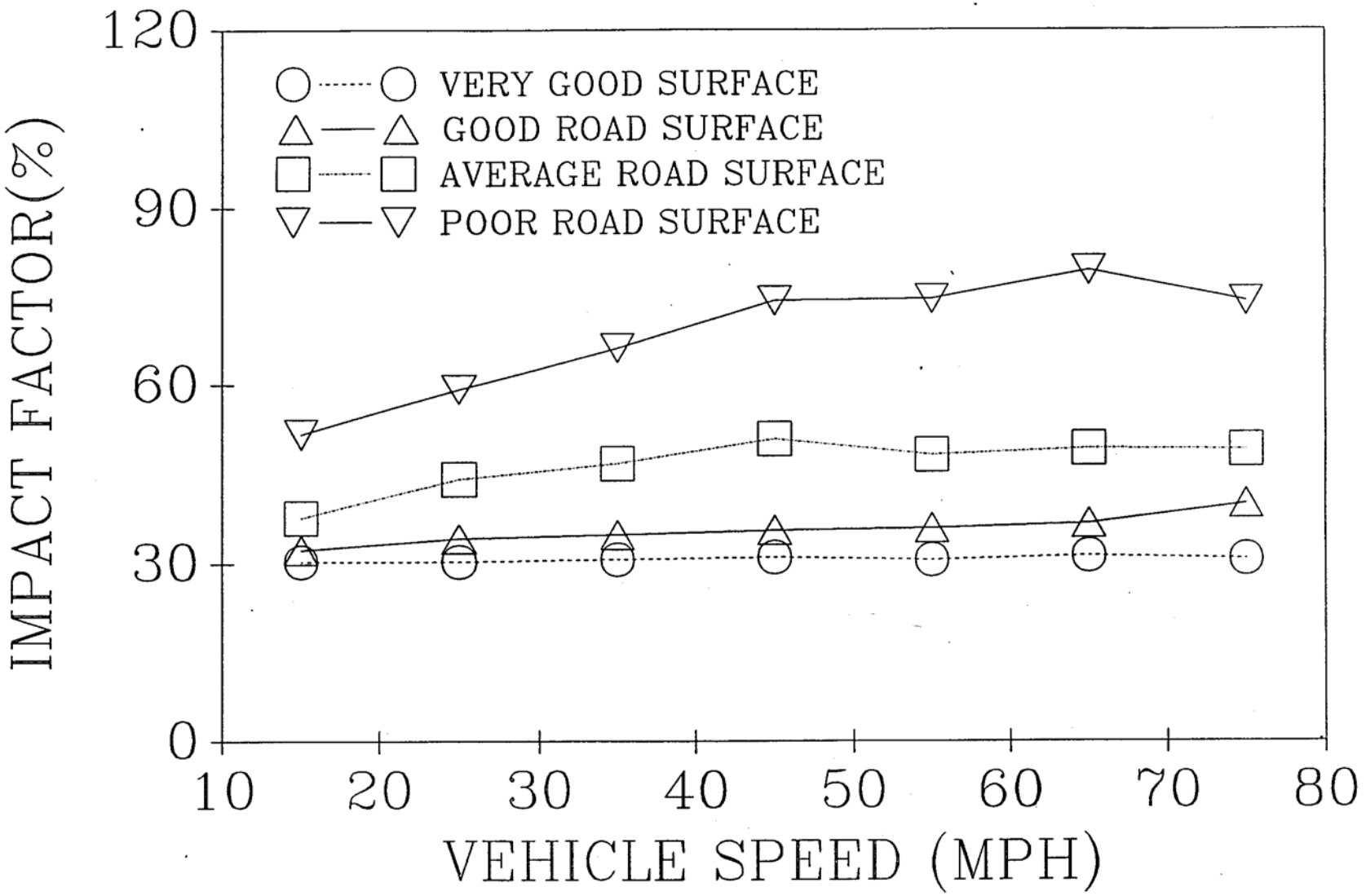

Fig. 2-7. Impact Results of Suspension Forces for the Tandem Axle of Type 3 Truck with Damped Suspension

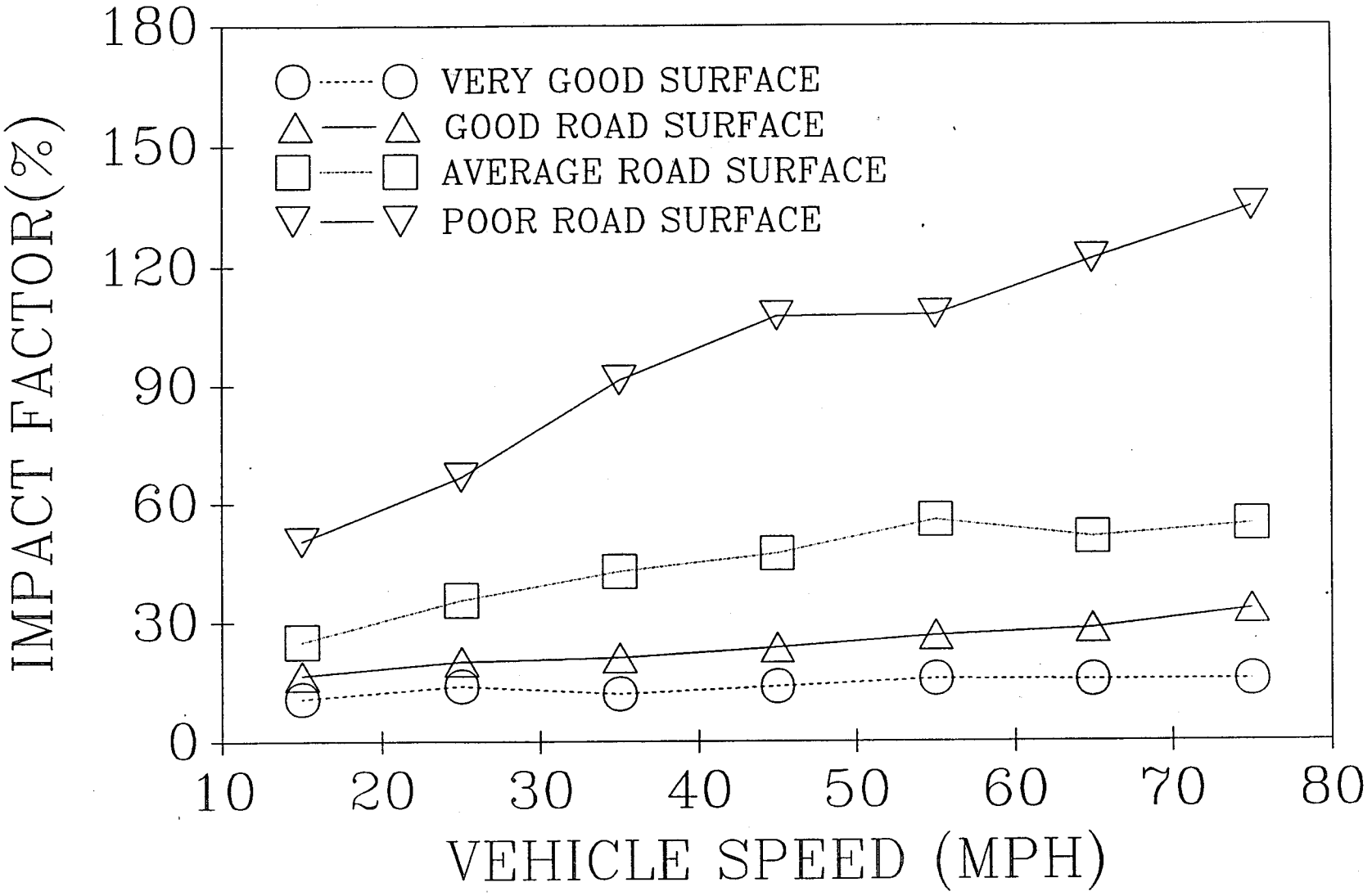

Fig. 2-8. Impact Results of Tire Forces for the Tandem Axle of Type 3 Truck with Damped Suspension

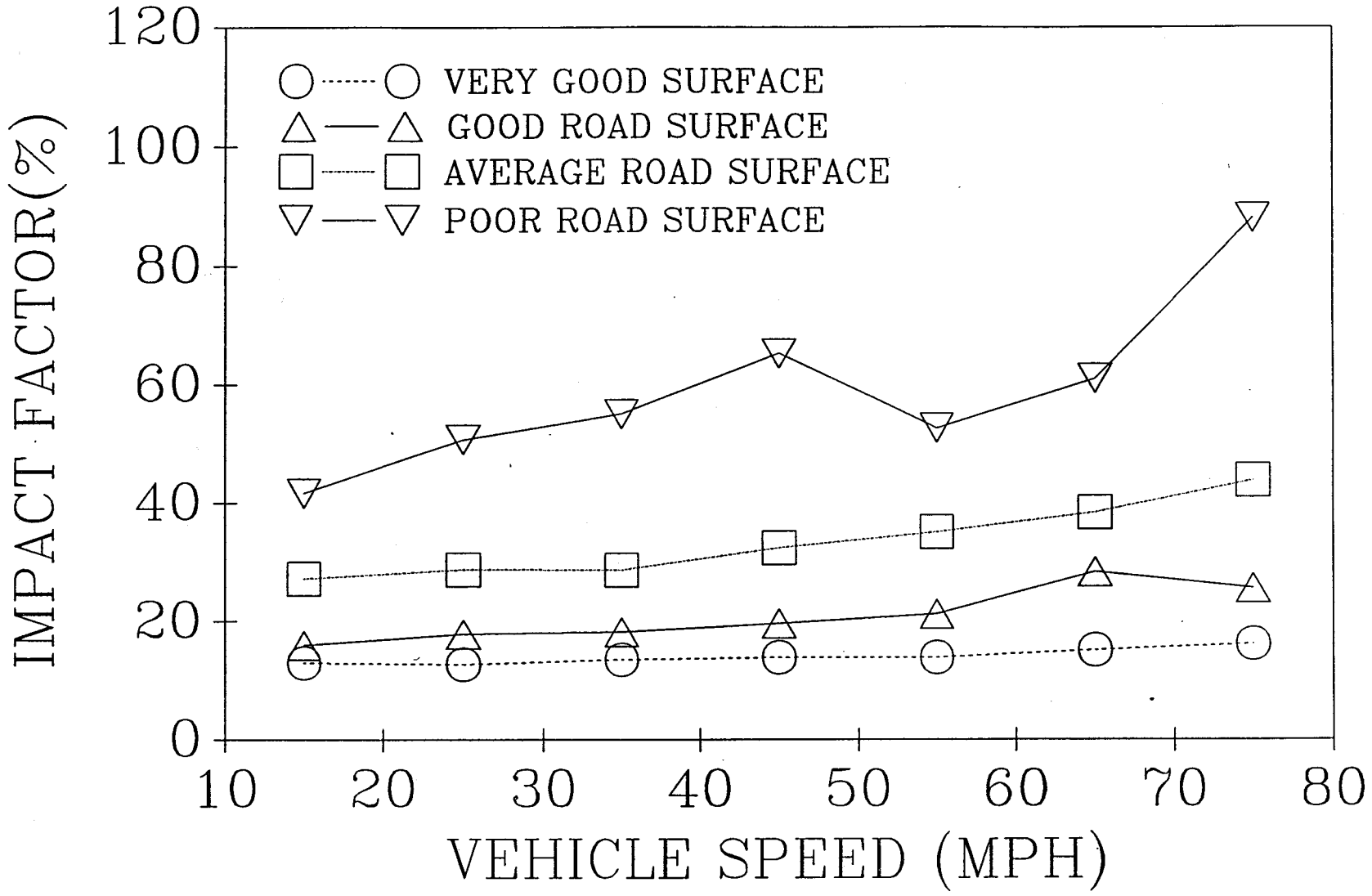

Fig. 2-9. Impact Results of Suspension Forces for the Steer Axle of Type 3S2 Truck with Damped Suspension

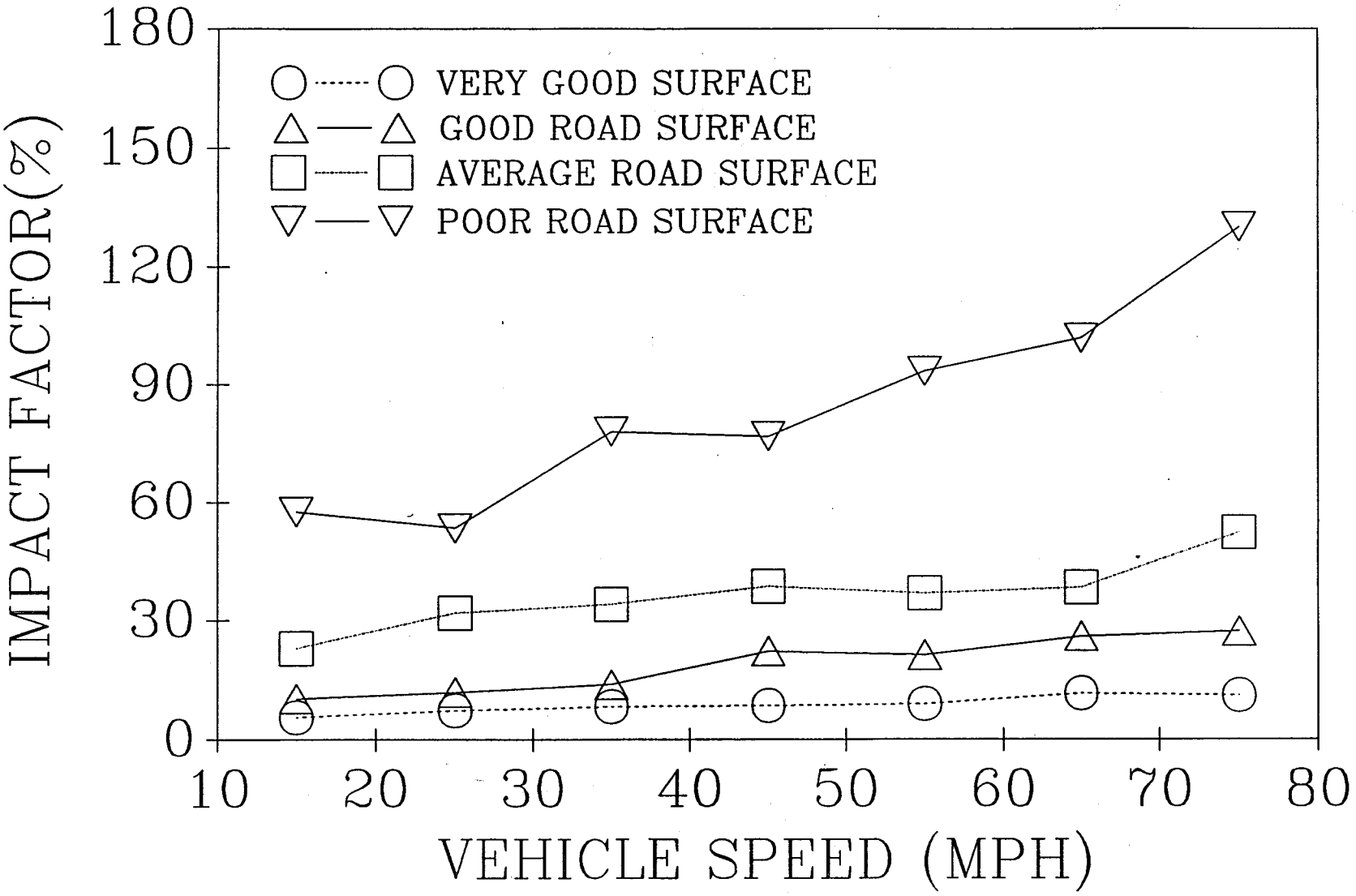

Fig. 2-10. Impact Results of Tire Forces for the Steer Axle of Type 3S2 Truck with Damped Suspension

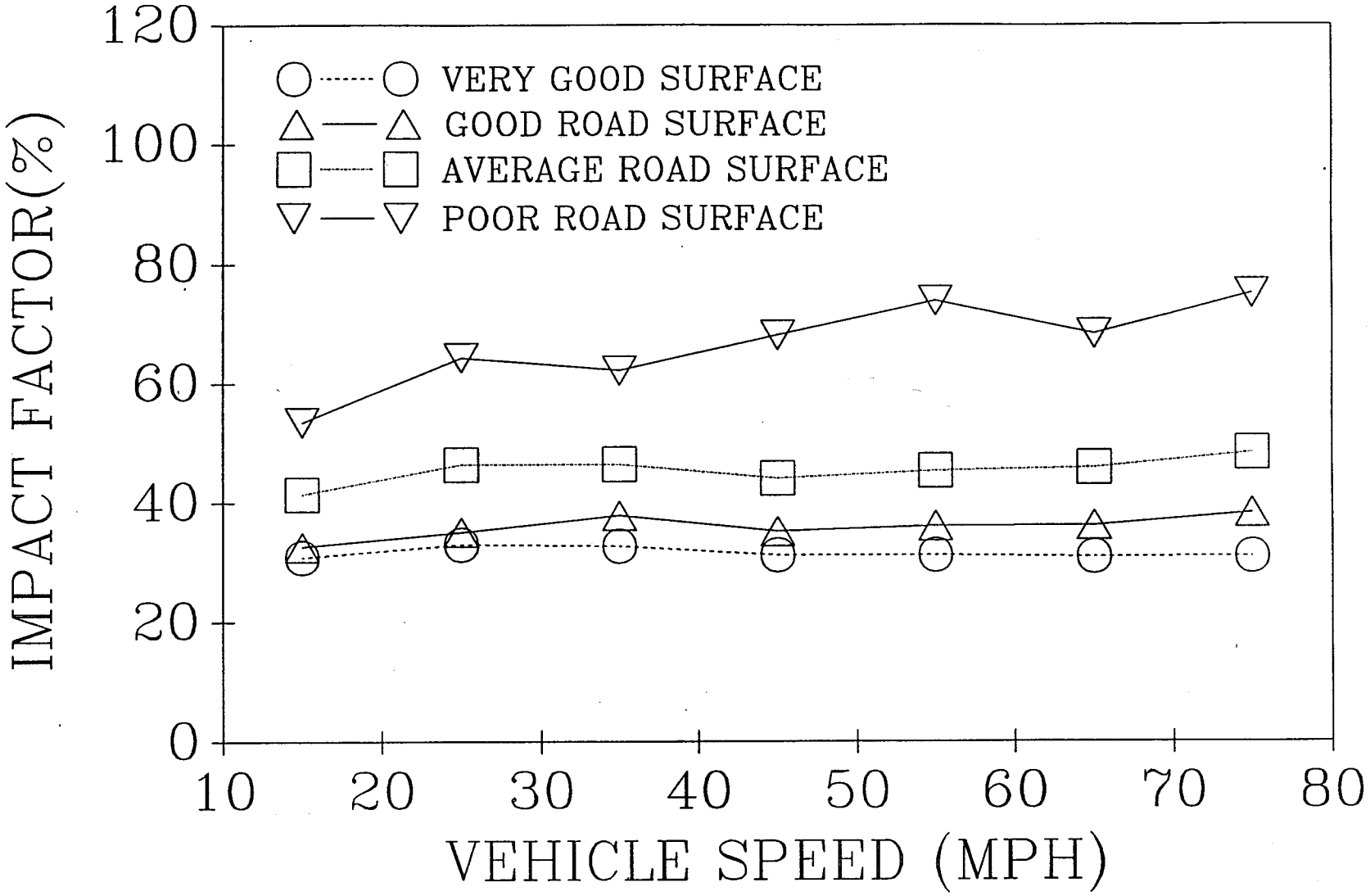

Fig. 2-11. Impact Results of Suspension Forces for the Tandem Tractor Axles of Type 3S2 Truck with Damped Suspension

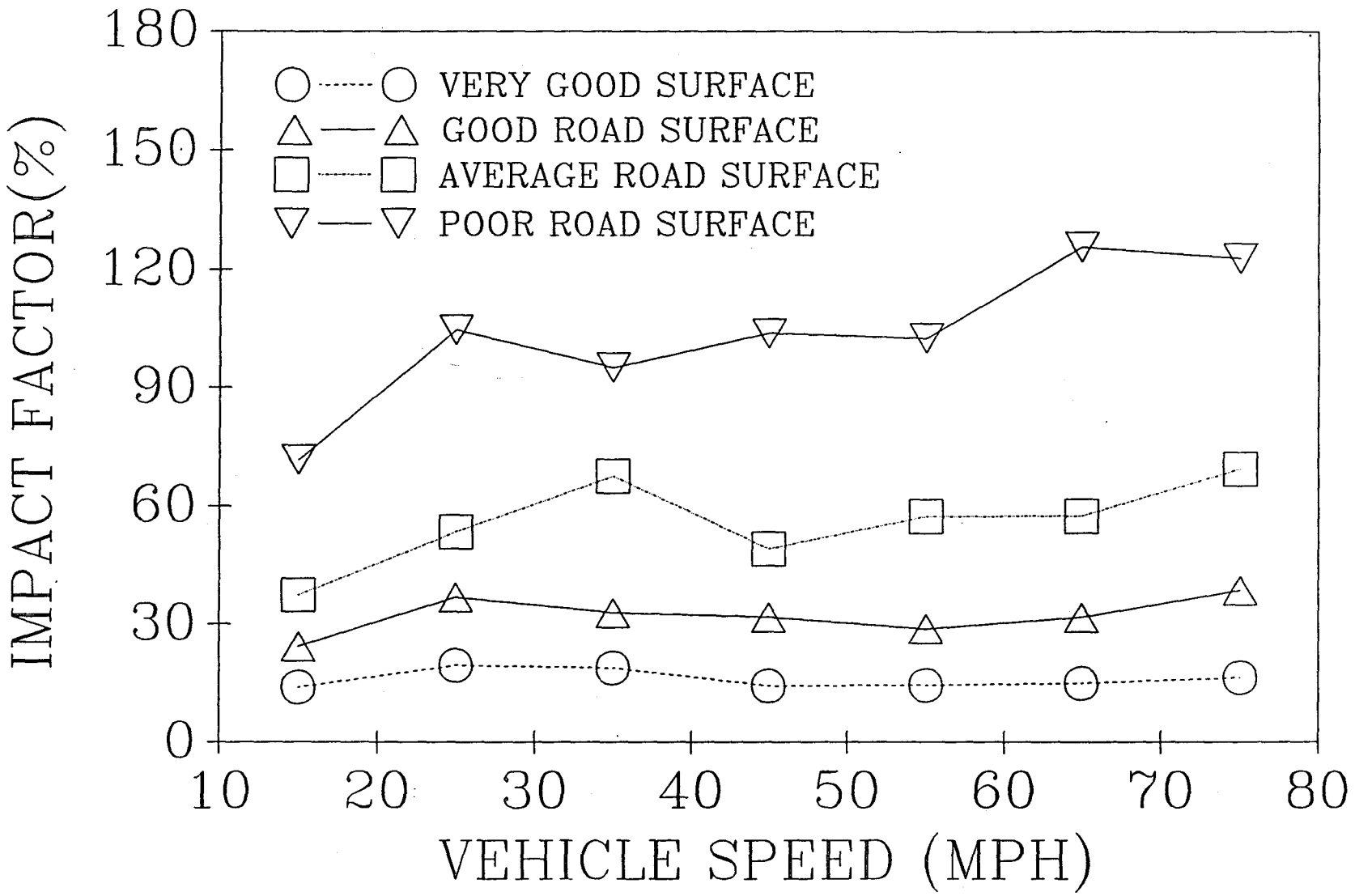

Fig. 2-12. Impact Results of Tire Forces for the Tandem Tractor Axles of Type 3S2 Truck with Damped Suspension

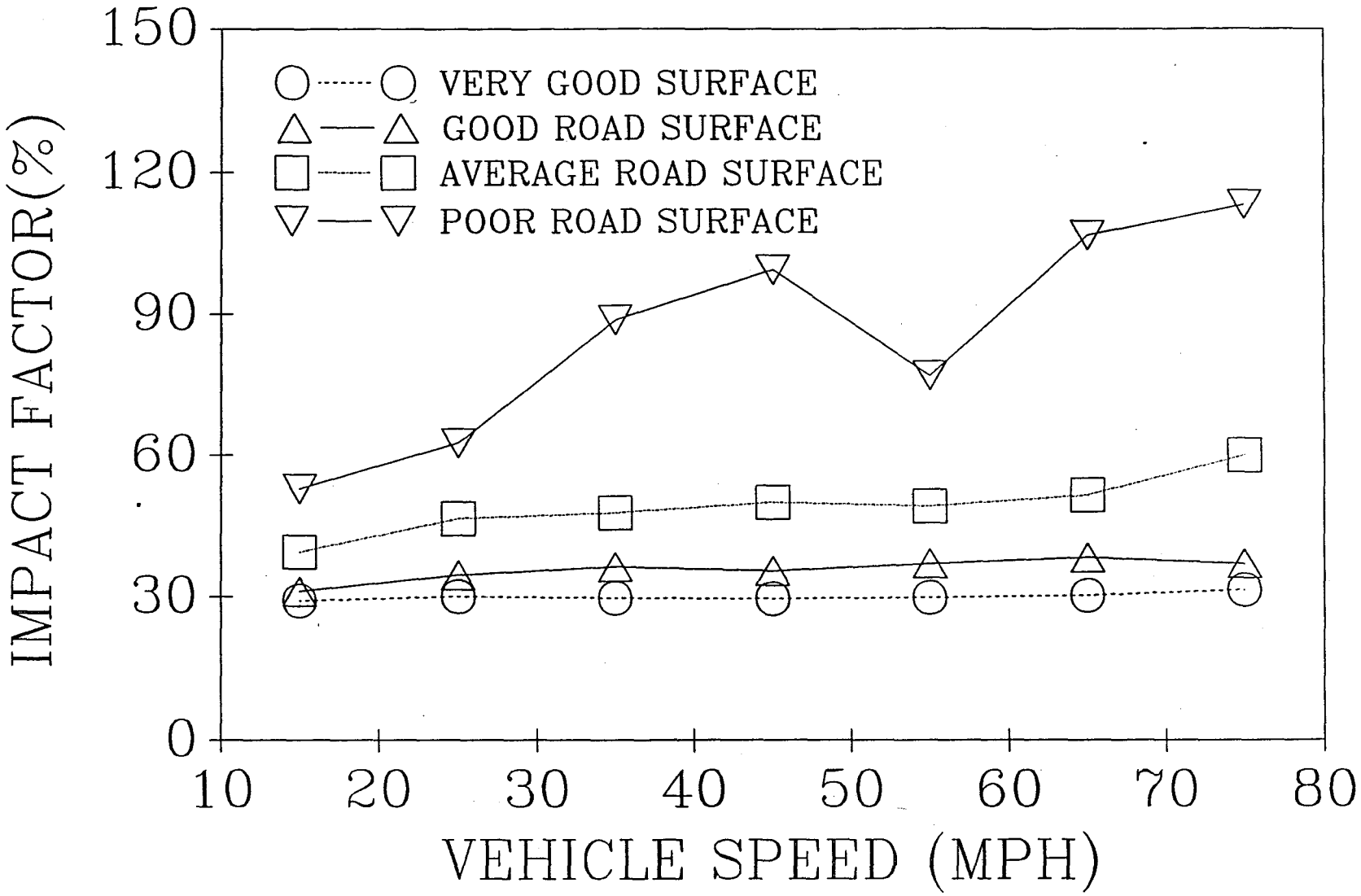

Fig. 2-13. Impact Results of Suspension Forces for the Tandem Trailer Axles of Type 3S2 Truck with Damped Suspension

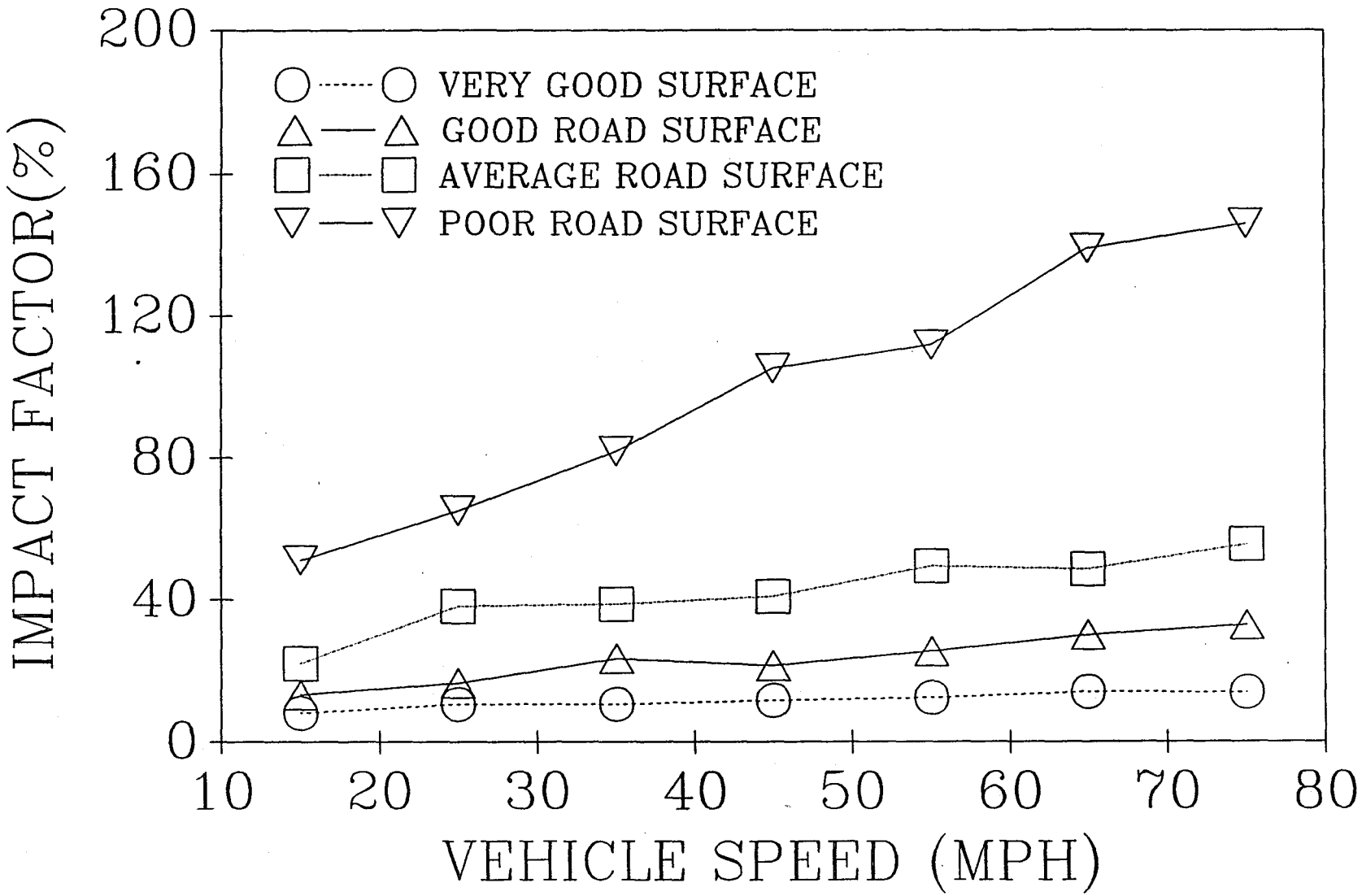

Fig. 2-14. Impact Results of Tire Forces for the Tandem Trailer Axles of Type 3S2 Truck with Damped Suspension

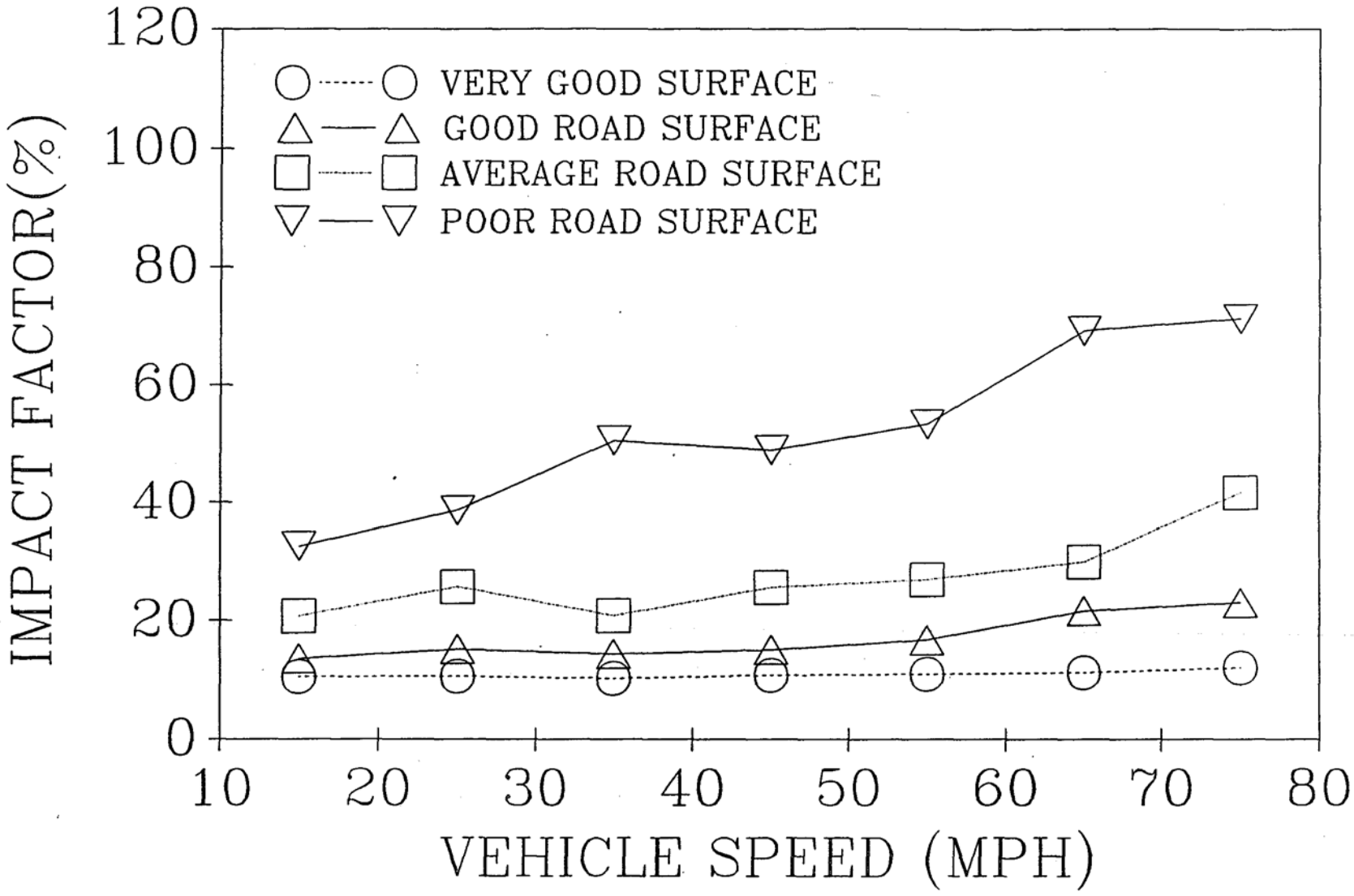

Fig. 2-15. Impact Results of Suspension Forces for the Steer Axle of FDOT (Type 3S2) Truck with Damped Suspension

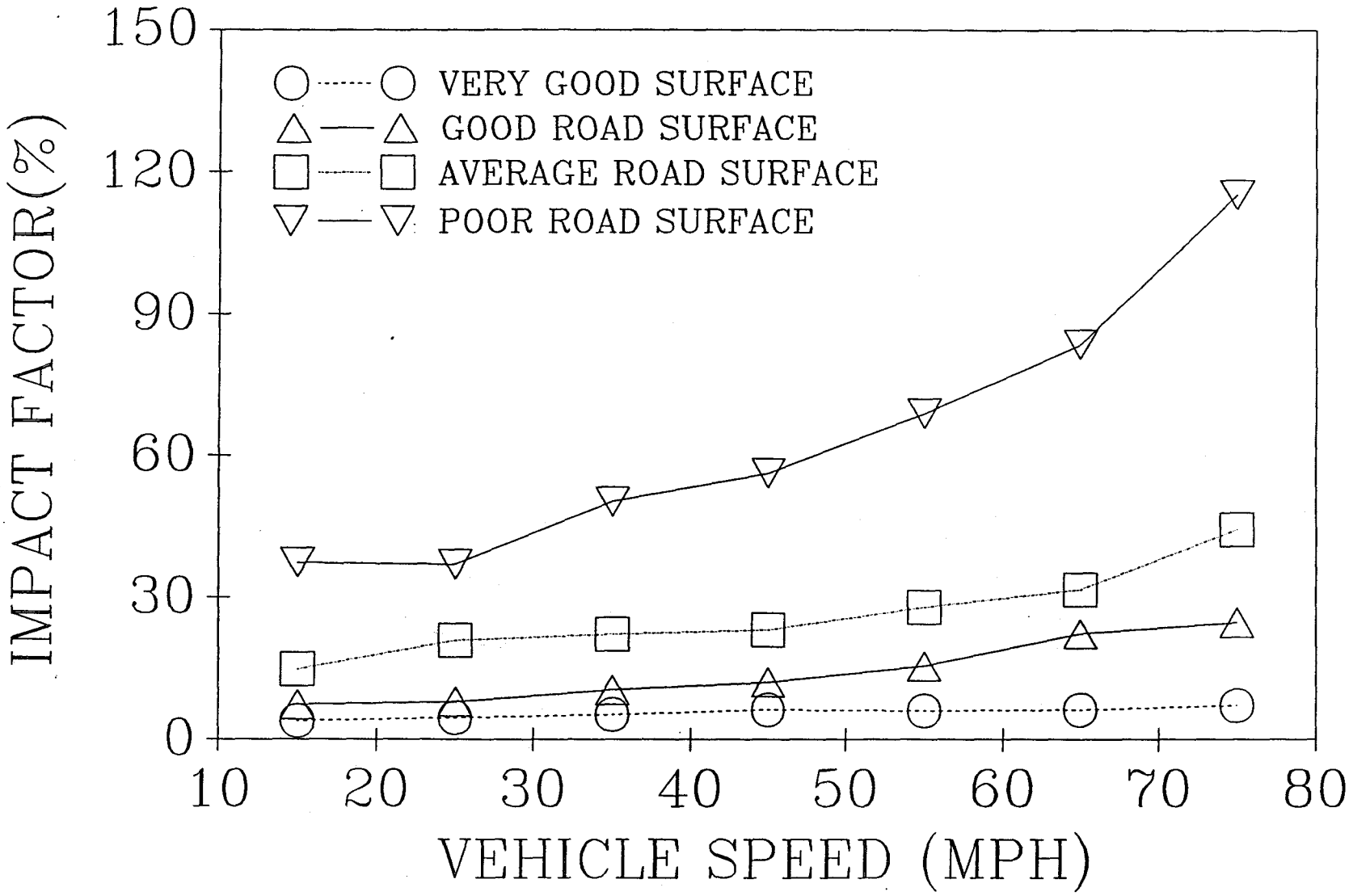

Fig. 2-16. Impact Results of Tire Forces for the Steer Axle of FDOT (Type 3S2) Truck with Damped Suspension

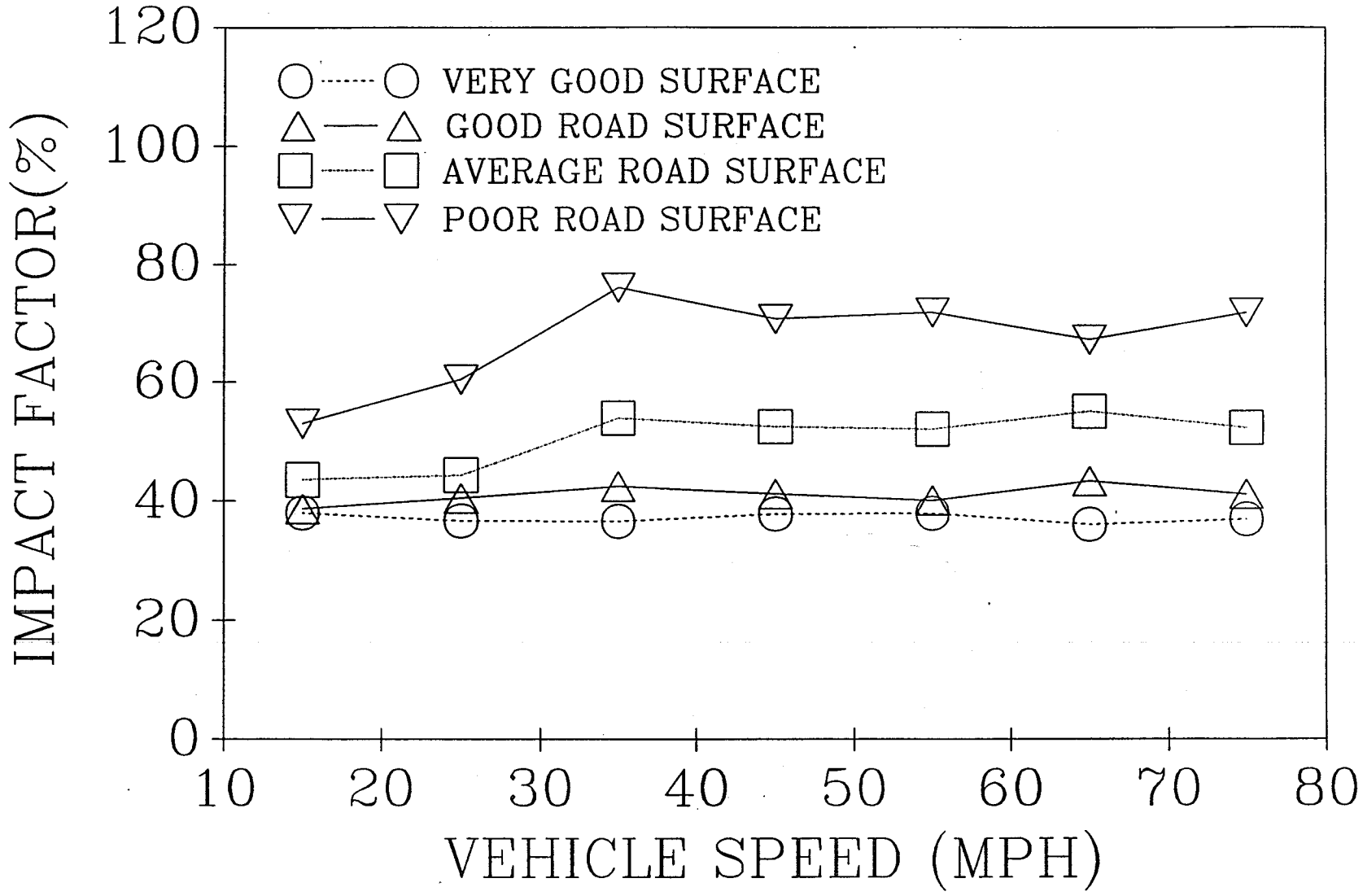

Fig. 2-17. Impact Results of Suspension Forces for Tandem Tractor Axles of FDOT (Type 3S2) Truck with Damped Suspension

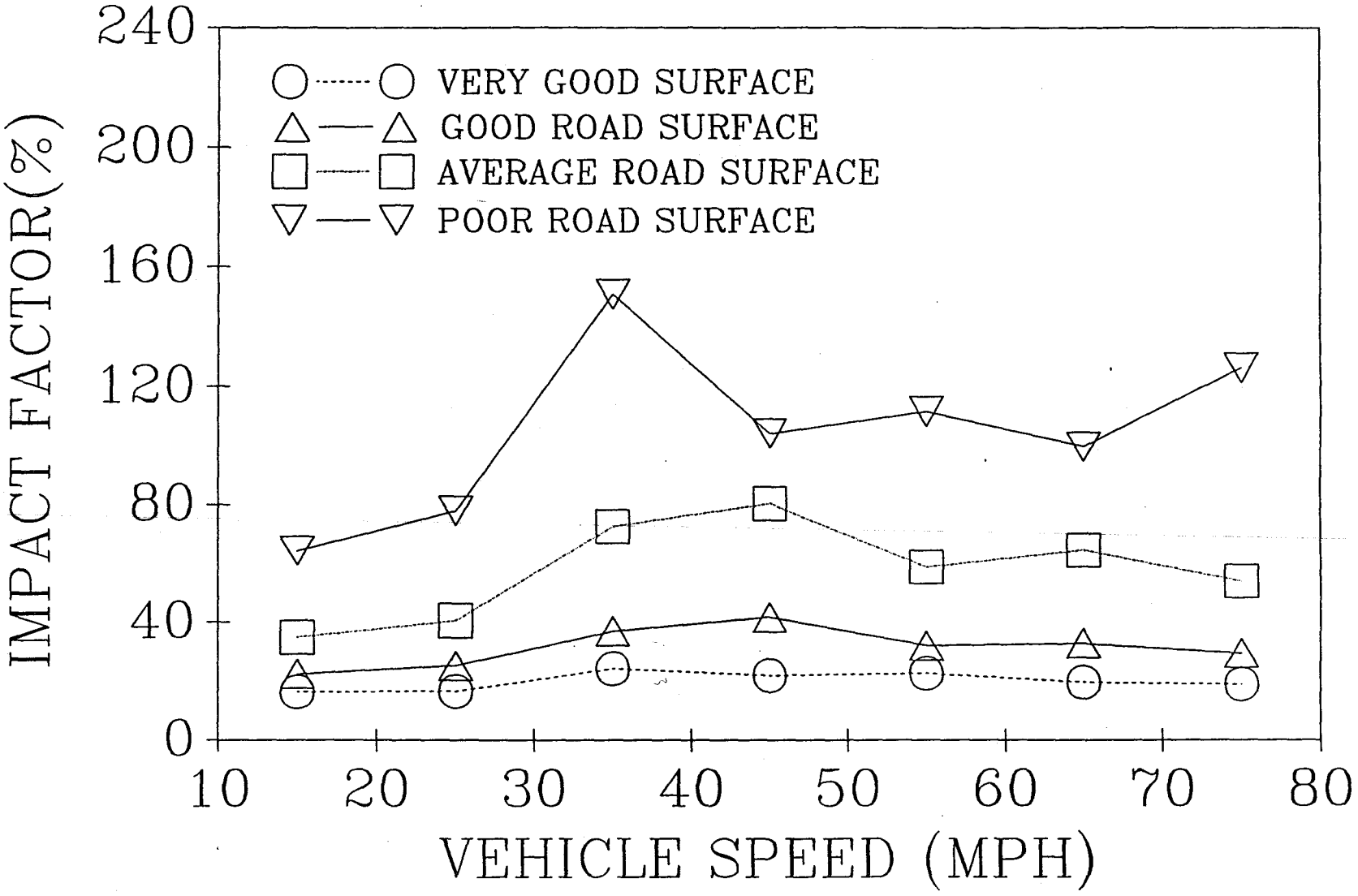

Fig. 2-18. Impact Results of Tire Forces for Tandem Tractor Axles of FDOT (Type 3S2) Truck with Damped Suspension

Fig. 2-19. Impact Results of Suspension Forces for Tandem Trailer Axles of FDOT (Type 3S2) Truck with Damped Suspension

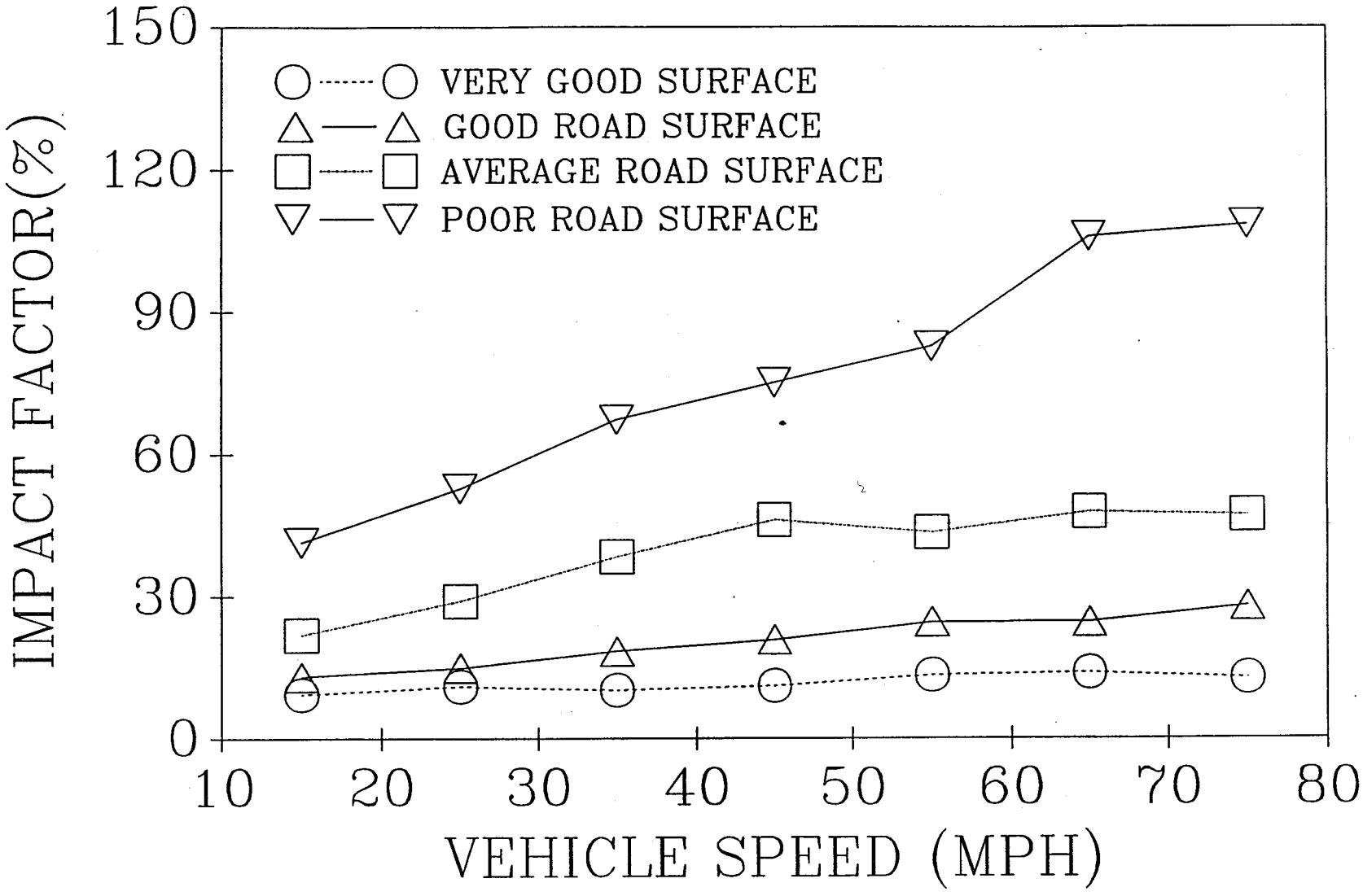

Fig. 2-20. Impact Results of Tire Forces for Tandem Trailer Axles of FDOT (Type 3S2) Truck with Damped Suspension

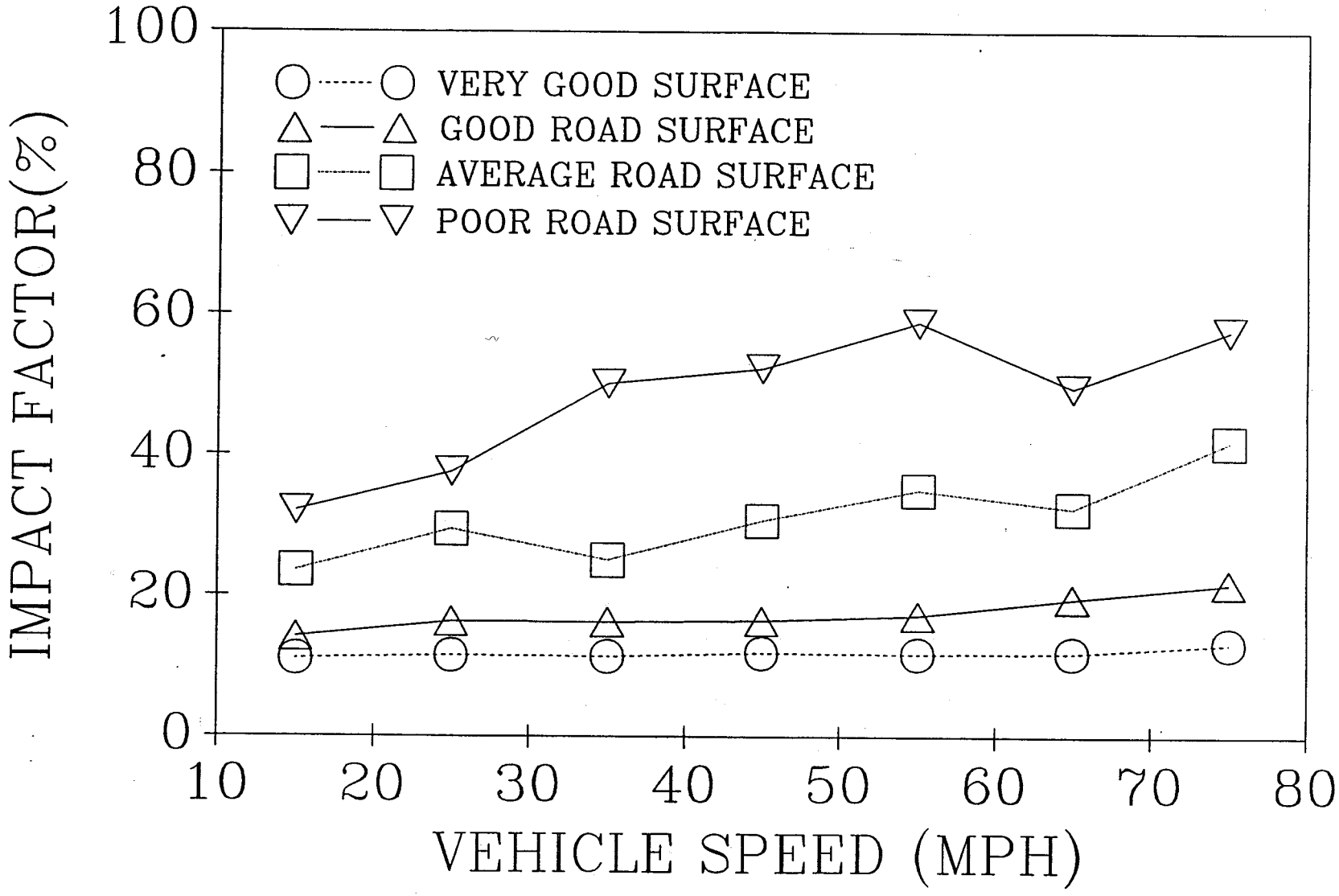

Fig. 2-21. Impact Results of Suspension Forces for the Steer Axle of Type 3-3 Truck with Damped Suspension

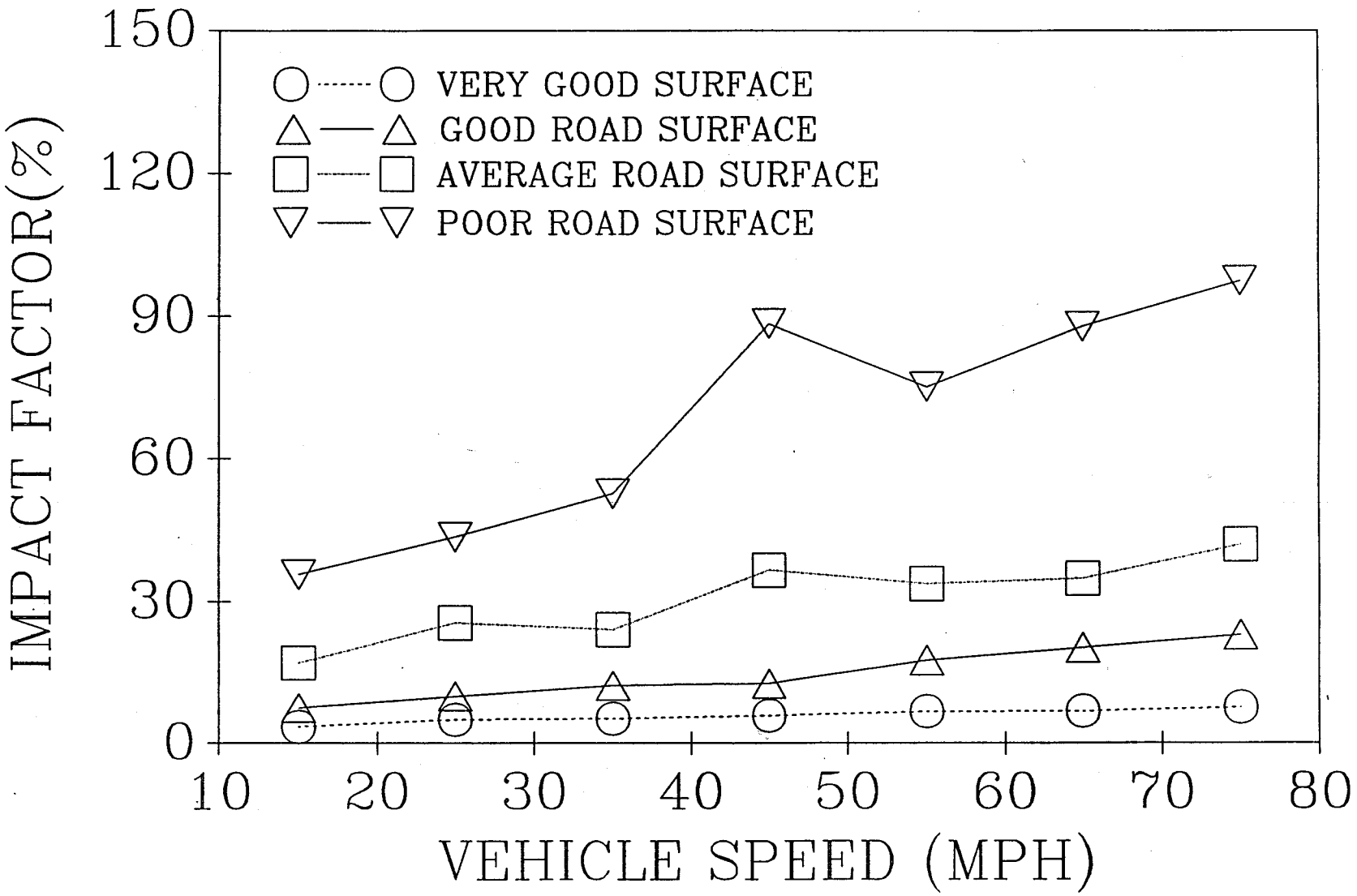

Fig. 2-22. Impact Results of Tire Forces for the Steer Axle of Type 3-3 Truck with Damped Suspension

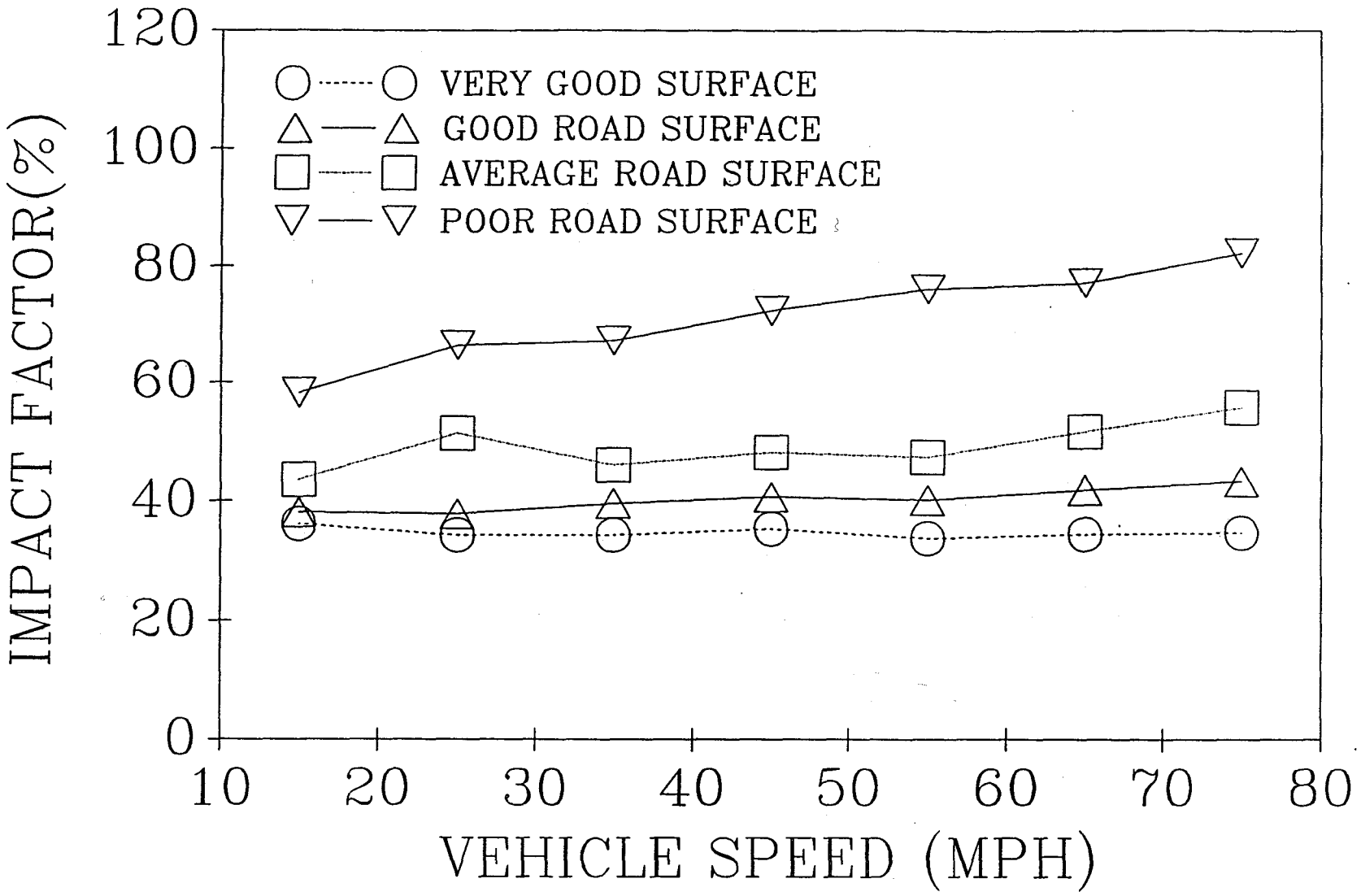

Fig. 2-23. Impact Results of Suspension Forces for Tandem Tractor Axles of Type 3-3 Truck with Damped Suspension

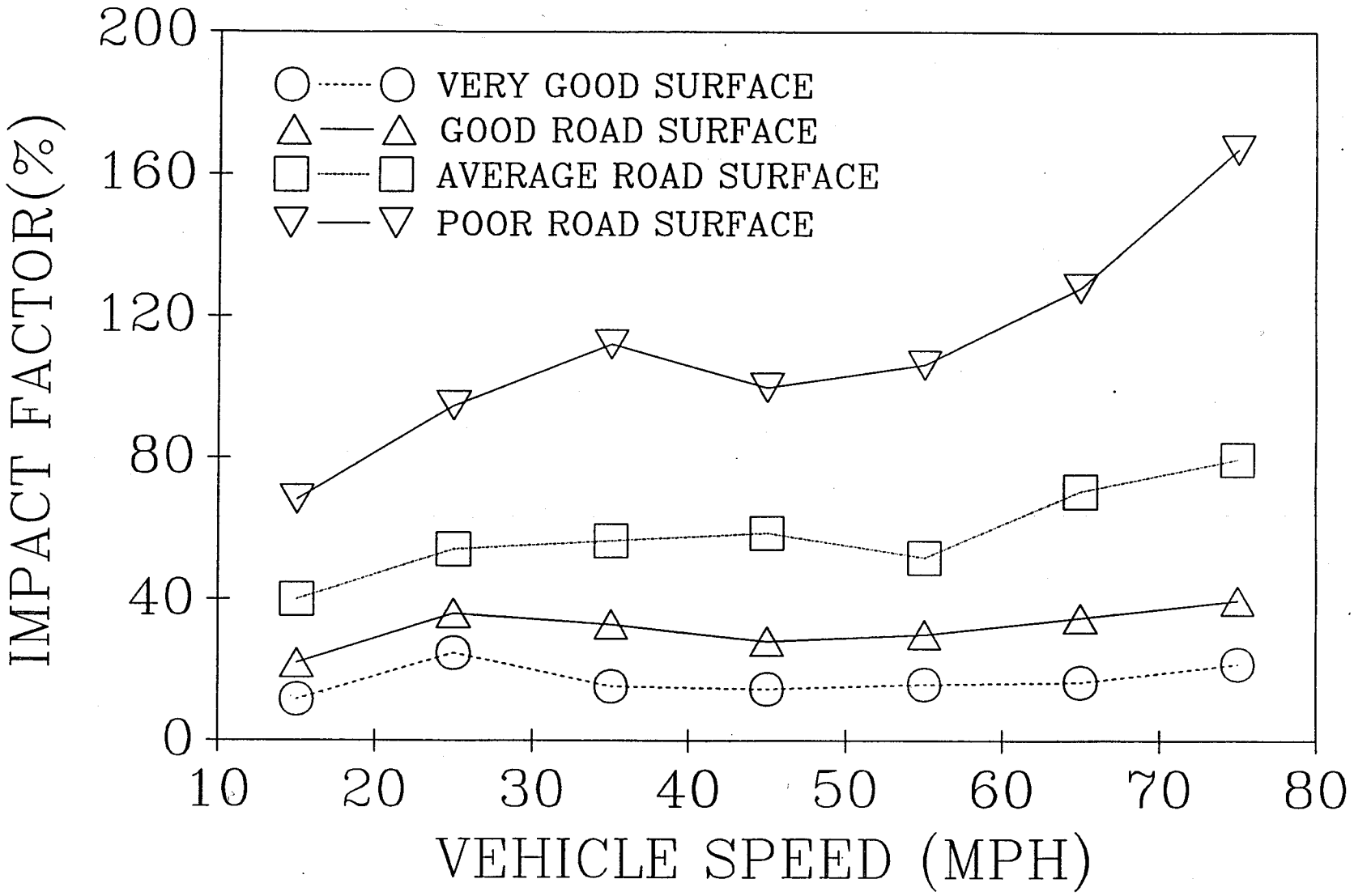

Fig. 2-24. Impact Results of Tire Forces for Tandem Tractor Axles of Type 3-3 Truck with Damped Suspension

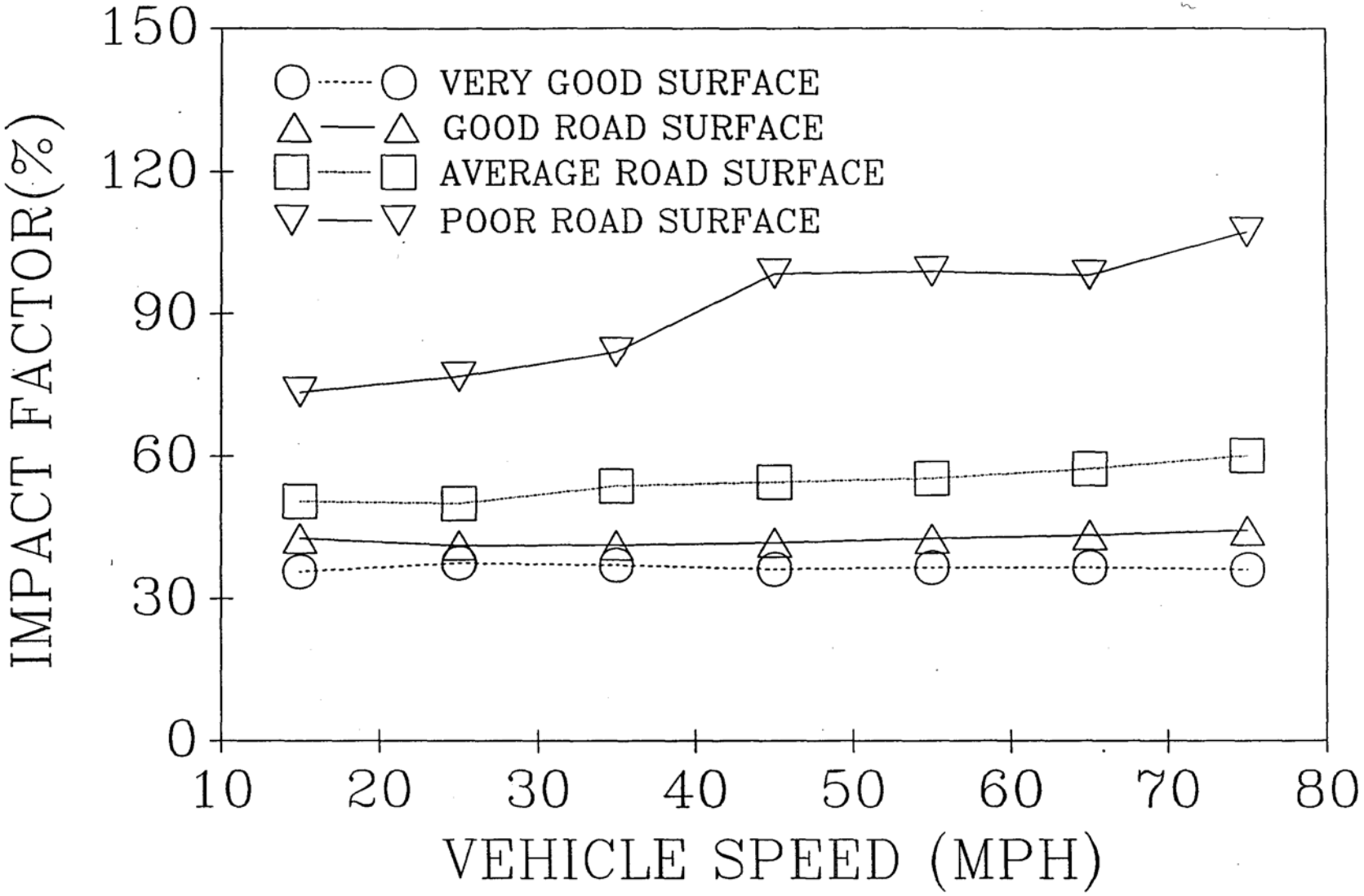

Fig. 2-25. Impact Results of Suspension Forces for the First Axle of Trailer of Type 3-3 Truck with Damped Suspension

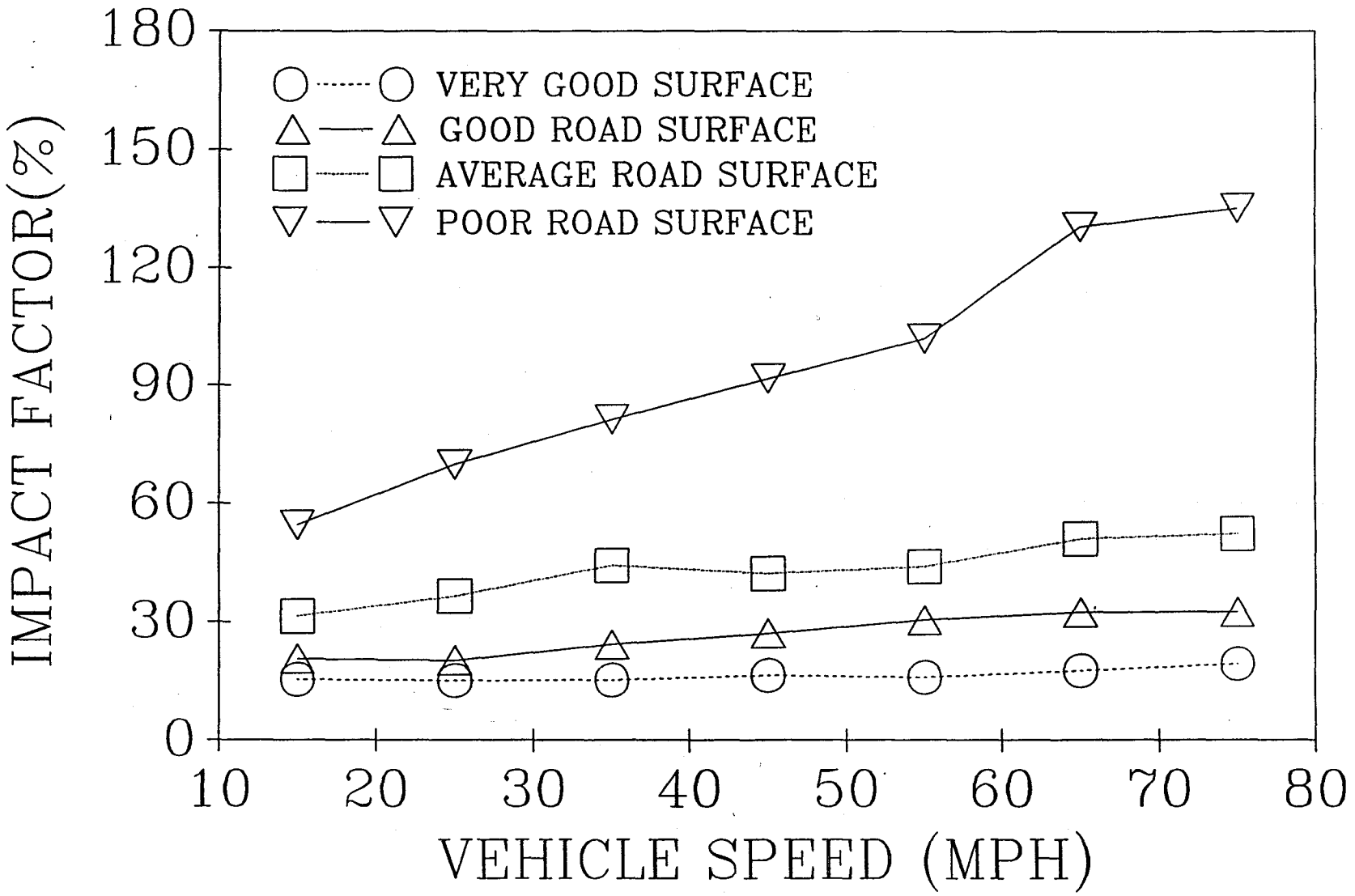

Fig. 2-26. Impact Results of Tire Forces for the First Axle of Trailer of Type 3-3 Truck with Damped Suspension

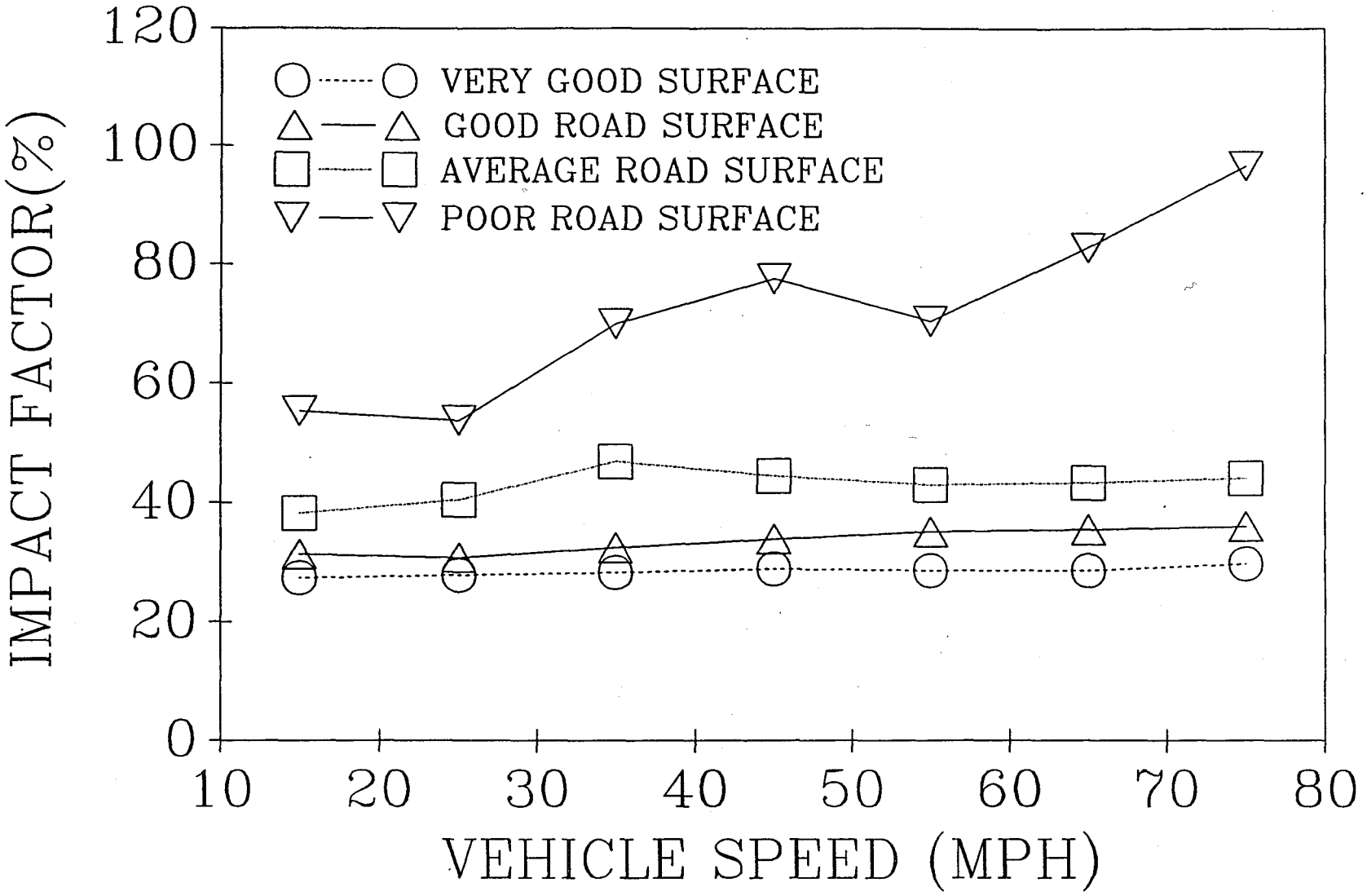

Fig. 2-27. Impact Results of Suspension Forces for Tandem Trailer Axles of Type 3-3 Truck with Damped Suspension

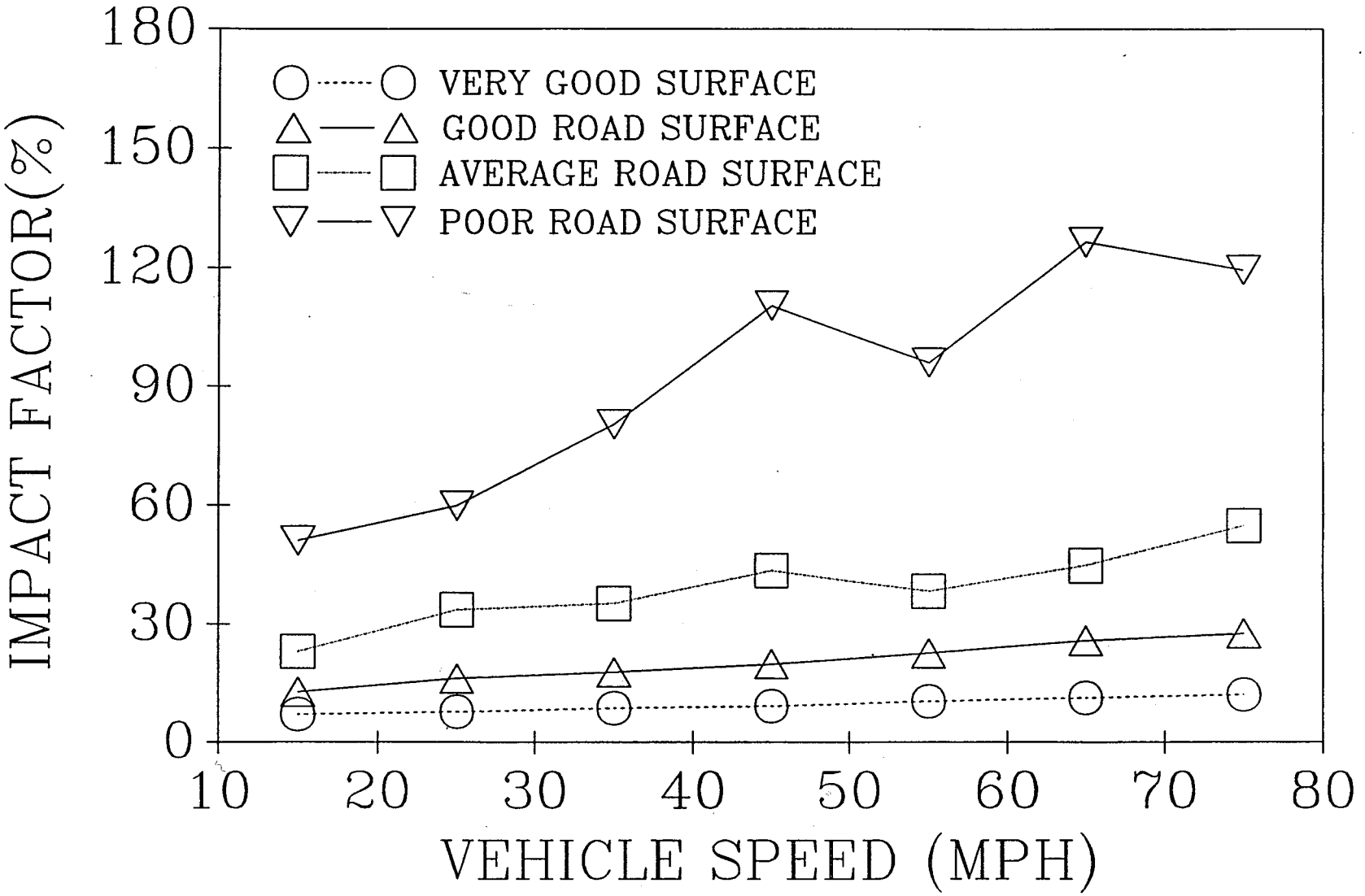

Fig. 2-28. Impact Results of Tire Forces for Tandem Trailer Axles of Type 3-3 Truck with Damped Suspension

CHAPTER III

IMPACT ANALYSIS OF CONTINUOUS MULTIGIRDER

BRIDGES 3.1. General

The continuous multigirder steel bridge is one of the most popular bridge types throughout the world. Its dynamic behavior has been an interesting subject of numerous investigations since the 50's of the twentieth. Under the direction of J. M. Biggs, Louw [18] investigated the response of two-span highway bridges to the single-axle vehicle loading and Chen [1] conducted the model investigation of the vibration of continuous three-span steel, bridges. Early field tests on actual continuous bridges have been reported by Vandegrift [25], Edgarton [6] and Hayes [11]. The most systematic and comprehensive investigations on this subject have been conducted at the University of Illinois [7]. Veletsos and Huang [13, 26] presented a successful numerical approach for determining the response of multi-span bridges, in which both planar bridge model and vehicle model were adopted. Eberhardt and Walker [5] developed a finite element method for the analysis of dynamic response of highway bridges. Ruhl [20] conducted an extensive study of field tests on three-span and two-span bridges.

Most previous investigations treated both continuous beam bridges and vehicles as the planar models [10, 19, 24, 26]. Although three-dimensional models of the continuous bridge and vehicle were used in Eberhardt's study [5], there was little information available concerning the effect of i transverse stiffness, road surface roughness, vehicle speed, span length, etc., on 53

the impact of longitudinal girders at different sections. Therefore, due to the weakness of previous studies, further research on continuous bridge dynamic analysis based on the different aforementioned parameters should be carried out.

The objective of this investigation is to analyze the impact of three-span continuous steel beam bridges with six different span lengths due to vehicles (side by side) moving over different classes of roads with various speeds.

3.2. Equations of Motion

3.2.1. Equations of Motion for Vehicle

HS20-44 truck, which is a major design vehicle in AASHTO specifications [23] is used for later dynamic analysis of continuous beam bridges. The mathematical model for the HS20-44 truck has been developed in Phase I [29]. The model has twelve degrees of freedom (DOF'S). The equations of motion of the system were derived by using Lagrange's formulation. Details of derivation and data are presented in Phase I interim report [29].

3.2.2. Equations of Motion for Bridgg

The continuous multigirder bridge is treated as a grillage beam system (refer to Fig.3-1). The dynamic response of the bridge was analyzed with finite element method. The bridge .was divided into grillage elements (see Fig. 3-2). The node parameters are

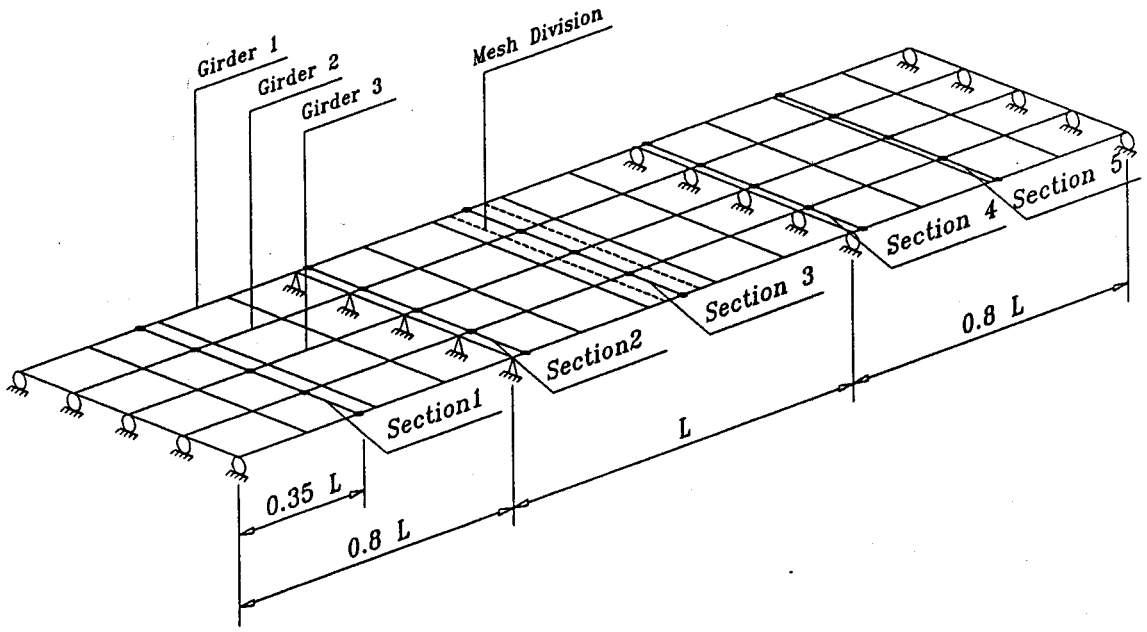

Fig. 3-1. Idealization of Bridge

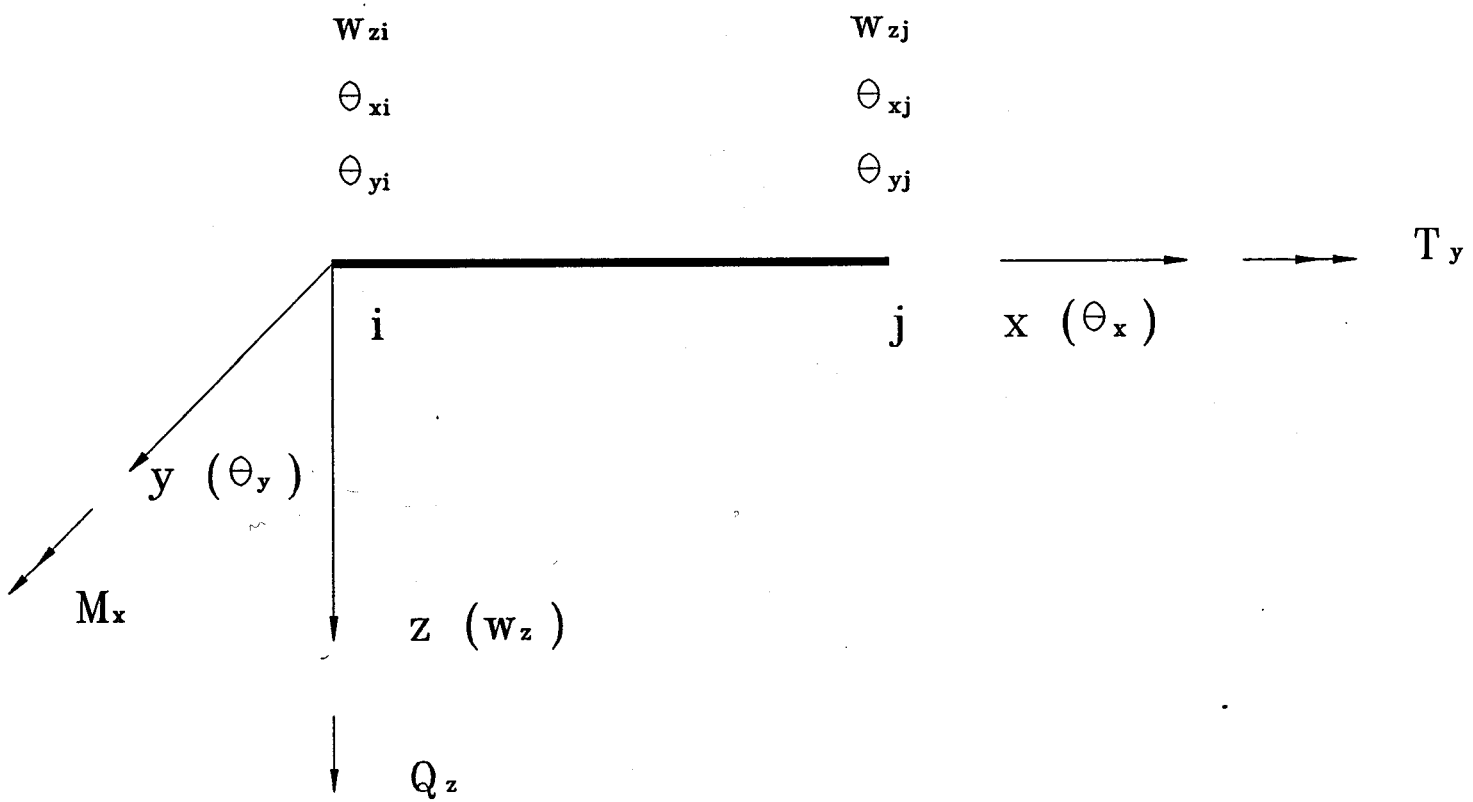

Fig. 3-2. Grillage Element

$$\{\delta\}^e = \begin{Bmatrix} \delta_i \\ \delta_j \end{Bmatrix} \qquad (3-1)$$

in which $\{\delta_i\} = [w_{zi}\ \theta_{xi}\ \theta_{yi}]^T$ = the displacement vector of left joint,

$\{\delta_j\} = [w_{zj}\ \theta_{xj}\ \theta_{yj}]^T$ = the displacement vector of right joint,

w = vertical displacement in z-direction, and

θ_x, θ_y = rotational displacements about x and y axes, respectively.

The equations of motion of the bridge are

$$[M_B]\{\ddot{\delta}\} + [D_B]\{\dot{\delta}\} + [K_B]\{\delta\} = \{F_{BT}\} \qquad (3\text{-}2)$$

in which $[M_B]$ = global mass matrix,

$[K_B]$ = global stiffness matrix,

$[D_B]$ = global damping matrix,

$\{\delta\}$, $\{\dot{\delta}\}$, $\{\ddot{\delta}\}$ = global nodal displacement, velocity, and acceleration vectors, and

$\{F_{BT}\}$ = global nodal loading vector, due to the interaction between the bridge and vehicle.

3.2.3. Interaction Equations Between Vehicle and Bridge

The interaction force of the ith axle between the bridge and vehicle is given as:

$$F^i_{BT} = K_{tyi}U_{tyi} + D_{tyi}\dot{U}_{tyi} \qquad (3\text{-}3)$$

in which K_{tyi} = the tire stiffness of the ith axle,

D_{tyi} = the tire damping coefficient of the ith axle,

U_{tyi} = the relative displacement between the ith axle and bridge = y_{ai} - ($-u_{sri}$) - ($-y_{bi}$),

y_{ai} = the vertical displacement of the ith axle,

u_{sri} = the road surface roughness under the ith axle (positive upwards), and

y_{bi} = the bridge vertical displacement under the ith axle (positive upwards).

A dot-superscript denotes differential with respect to time. The y_{bi} can be evaluated by the nodal displacements $\{\delta\}^e$ of the element and expressed as follows:

$$y_{bi} = [N_3\ 0\ N_1\ N_4\ 0\ N_2]\{\delta\}^e \qquad (3\text{-}4)$$

where

$$N_1 = 1 - \frac{3}{l^2}x_i^2 + \frac{2}{l^3}x_i^3 ,$$

$$N_2 = x_i - \frac{2}{l}x_i^2 + \frac{1}{l^2}x_i^3 ,$$

$$N_3 = \frac{3}{l^2}x_i^2 - \frac{2}{l^3}x_i^3 ,$$

$$N_4 = -\frac{x_i^2}{l} + \frac{x_i^3}{l^2} ,$$

N_i is the displacement interpolation function of the element, x_i is the distance measured from the applied point of F_{BT}^i to the beginning node of the element.

3.3. Road Surface Roughness

The Power Spectral Density (PSD) functions for highway surface roughness have been developed by Dodds and Robson [4] and modified by Wang and Huang [29].

The random numbers which have approximate white noise properties were generated first. Then, these random numbers were passed through the first recursive filter. Finally, the output function will be the road surface roughness. The detail of the procedure and the vertical highway surface profiles for very good, good, average, and poor roads, respectively, have been given in Phase I interim report [29].

3.4. Numerical Methods

The equations of motion of the vehicle are non-linear, while those of the bridge are considered as linear. Considering the different characteristics of those equations of motion, we employ fourth-order Runge-Kutta integration scheme [2, 28] to solve the equations of motion of the vehicle, while the solutions of the bridge were determined by the mode-superposition procedure based on the subspace iteration method. The overall scheme of the procedure is described as follows:

1

The global nodal displacement vector {b} in Eq. (3-2) can be expanded in the form

$$\{S\} \_ [\cdot 1]\{Y\} \qquad (3\text{-}5)$$

in which, the mode shape matrix, [f], corresponding to the free vibration equations of the bridge is given as:

$$[\Phi] = [\ \{\phi_1\}\{\phi_2\} \ldots\ldots \{\phi_n\}\ ] \qquad (3\text{-}6)$$

and $\{Y\}$ is the generalized coordinate vector of n dimensions.

Based on Rayleigh damping matrix [3] and the orthogonality property shown as:

$$[\Phi]^T[M_B][\Phi] = [I], \qquad (3\text{-}7)$$

$$[\Phi]^T[K_B][\Phi] = [\Omega]^2, \qquad (3\text{-}8)$$

where the natural frequency vector, $[\Omega]$, corresponding to Eq. (3-6) is given as:

$$[\Omega] = \begin{bmatrix} \omega_1 & & & 0 \\ & \omega_2 & & \\ & & . & \\ & & . & \\ 0 & & & \omega_n \end{bmatrix} \qquad (3\text{-}9)$$

and [I] is an n x n identity matrix, Eq. (3-2) can be transformed to a set of n independent normal-coordinate equations, i.e.,

$$\{\ddot{Y}\} + 2[\varsigma][\Omega]\{\dot{Y}\} + [\Omega]^2\{Y\} = [\Phi]^T\{F\} \qquad (3\text{-}10)$$

in which $[\varsigma]$ = modal damping ratio matrix. The single DOF equations can be easily solved by any appropriate method. After obtaining $\{Y\}$, the displacements can be determined by Eq.

(3-5). The nodal forces of each element are calculated by

$$\{S\} = \{S_1\} + \{S_2\} \qquad (3\text{-}11)$$

in which $\{S_1\} = [k]^e[\Phi]^e\{Y\}$ and $\{S_2\} = [m]^e[\Phi]^e[\Omega]^2\{Y\}$. The superscript e represents the element and $[m]^e$ is the element mass matrix.

In the mode superposition process, the accurate results can be obtained from the first several modes. The first several modes will be determined by the following subspace iteration method [21]:

The eigenvalue equation for undamping free vibration is shown as:

$$[K_B]\{\delta\} = \omega^2[M_B]\{\delta\} \qquad (3\text{-}12)$$

It can be rewritten in the form of Rayleigh quotient as:

$$\omega^2 = \frac{\{\delta\}^T[K_B]\{\delta\}}{\{\delta\}^T[M_B]\{\delta\}} \qquad (3\text{-}13)$$

First, we assume the first q sets of modes and write the $\{\delta\}$ as

$$\{\delta\} = [X]\{A\} \qquad (3\text{-}14)$$

where [X] = initial assumed modes (q $\ll$ the dimensions of Eq. (3-12)) and

{A} = vector needed to be calculated.

Substituting Eq. (3-14) into Eq. (3-12) and using $\partial\omega^2/\partial\{A\} = 0$, lead to:

$$[K_B]^*\{A\} = \omega^2[M_B]^*\{A\} \tag{3-15}$$

in which $[K_B]^* = [X]^T[K_B][X]$ and $[M_B]^* = [X]^T[M_B][X]$.

Eq. (3-15) can be solved very quickly because its size is much smaller than that of Eq. (3-12). After obtaining q sets of {A} from Eq. (3-15), the second assumed modes [X] can be modified. Repeat the procedure until the desired accuracy of the modes is reached.

The main procedures for dynamic analysis of the bridge are as follows:

1. Evaluate the natural frequencies and the corresponding vibration modes of the bridge.
2. Determine the longitudinal position of each axle of the vehicle on the bridge at time $t+\Delta t$.
3. Assume that the vertical bridge deflection y_{bi} under the ith axle at time $t+\Delta t$, in the first time step of iteration, equals the value of y_{bi} at time t and the initial values of y_{bi} could be zero.
4. Use the fourth-order Runge-Kutta method to solve the equations of motion of the vehicle and calculate the bridge/vehicle interaction forces from Eq. (3-3).
5. Solve Eq. (3-10) to obtain the generalized coordinates {Y} and calculate the vertical bridge deflection y_{bi} at the time $t+\Delta t$, in the second time step of iteration, according to Eqs. (3-5) and (3-4).

6. Repeat step 3 through step 5 by using the latest available values of yb; and other related values until all differences between the previous and derived deflections are less than the prescribed tolerance.

7. Proceed to the next time step and repeat the aforementioned

process. 3.5. Description of Analytical Bridges

In the study of general dynamic characteristics of continuous multigirder bridges, six three-span continuous bridges with steel girders and concrete deck (refer to Figs. 3-3 and 3-4) were designed based on-the Standard Plans for Highway Bridge Superstructures of U. S. Bureau of Public Roads [22].

The lengths of the individual spans are in the ratio of 4:5:4 and the overall length ranges from 130 ft. to 260 ft. The shortest bridge has spans of 40 ft.-50 ft.-40 ft. and the longest bridge has spans of 80 ft.-100 ft.-80 ft. These bridges are of the I-beam type and are designed for the HS20-44 loading. The bridges have a roadway width of 28 ft. and a 7.5 in. thick concrete slab. The entire deck is supported by five steel beams. The typical cross-section of the bridges is shown in Fig. 3-3. Fig. 3-4 shows the plan of the bridge with span of 72 ft.-90 ft.-72 ft. and the others have similar arrangements.

The mass per unit length of each girder of the bridges and the cross-sectional area were considered to be uniform. The flexural rigidities of cross-sections were determined as composite sections which consist of the girders and slab. The primary data of bridges were presented in 63

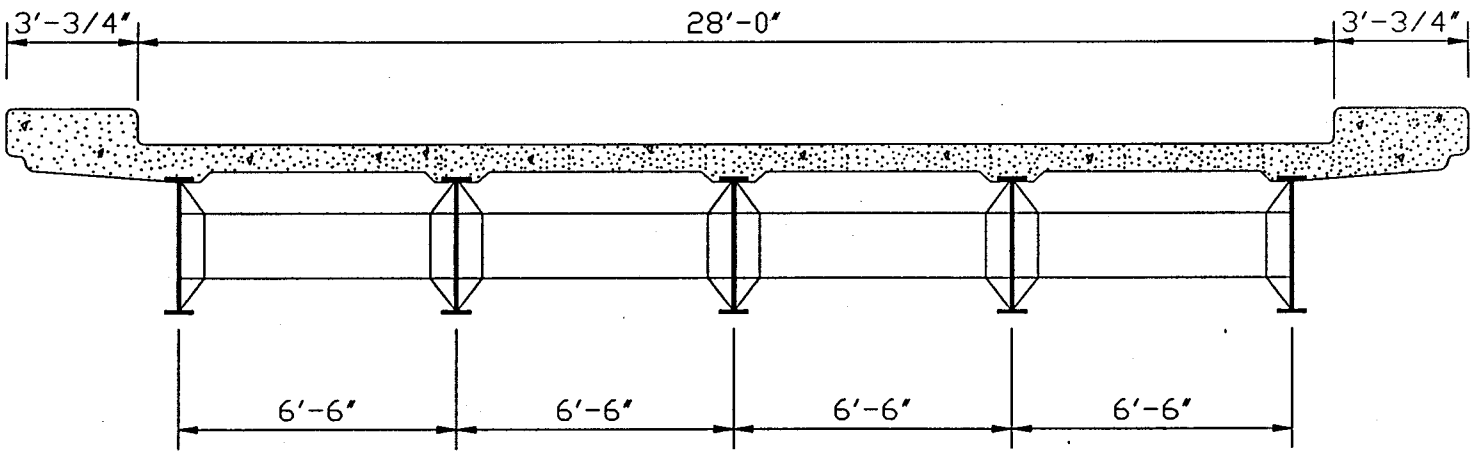

Fig. 3-3. Typical Cross-section

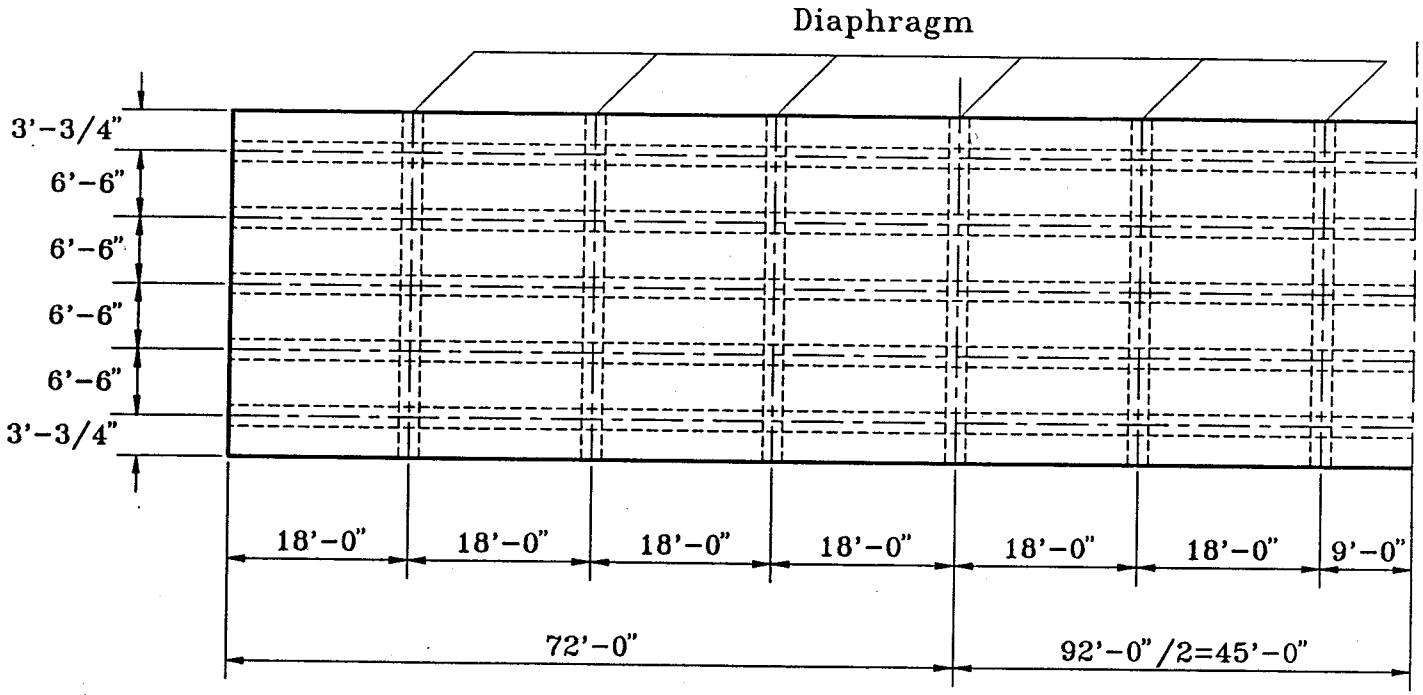

Fig. 3-4. Plan of Bridge

Table 3-1.

3.6. Lnpact Analysis

3.6.1. General

Fig. 3-1 shows the grillage beam model of the continuous multigirder bridges. Along the longitudinal axes of bridges, each girder was divided into 52 elements.

The mode damping coefficients were determined by using an approach described by Clough and Penzien [3]. The bridges were assumed to have damping characteristics that can be modeled as viscous. One percent of critical damping is adopted for the first and second modes according to the experiment results [20].,

The first six frequencies of each bridge are given in Table 3-2. Fig. 3-5 to 3-14 show the first ten vibration modes of the bridge with span'length of 80 ft.-100 ft.-80 ft. The vibration modes of the other bridges have nearly same shapes. From those figures, we can see that modes 1, 3, 6, 8 and 9 are corresponding to bending modes, while modes 2, 4, 5, 7 and 10 corresponding to torsional modes.

In order to obtain the initial displacements and velocities of vehicle DOF'S when the vehicle entered the bridge, the vehicle was started the motion at a distance of 140 ft (42.67 m, i.e., a five-car length) away from the left end of the bridge and continued moving until the entire 66

Table 3-1. Primary Data of Bridges.

Span (ft.)	Longitudinal Girder				Transverse Beam		
	Inertia $(in^4)x10^3$	Torsional Constant (in^4) $x10^3$	Mass per Unit (kps/in)		Inertia $(in^4)x10^3$	Torsional Constant (in^4)	Number of Transverse Beam
			Exter. Girder	Inter. Girder			
40-50-40	9.4276	1.102	0.09542	0.06417	2.255	422	8
48-60-48	16.152	1.105	0.09728	0.06603	2.948	506	10
56-70-56	19.052	1.107	0.09925	0.06800	3.627	591	10
64-80-64	23.368	1.109	0.10140	0.07015	5.293	675	11
72-90-72	27. 954	1.119	0.10479	0.07354	6.447	759	14
80-100-80	31.713	1.125	0.10904	0.07779	7.336	845	14

Table 3-2. Natural Frequencies of Bridges.

No. of Frequency	Span Length (ft.)					
	40-50-40	48-60-48	56-70-56	64-80-64	72-90-72	80-100-80
1	6.466	5.637	4.591	3.843	3.234	2.745
2	6.625	5.651	4.678	3.934	3.339	2.861
3	9.770	8.431	6.907	5.801	4.912	4.191
4	9.807	8.579	6.997	5.864	4.935	4.199
5	11.750	10.162	8.314	6.977	5.897	5.033
6	12.002	10.520	8.592	7.209	6.070	5.154

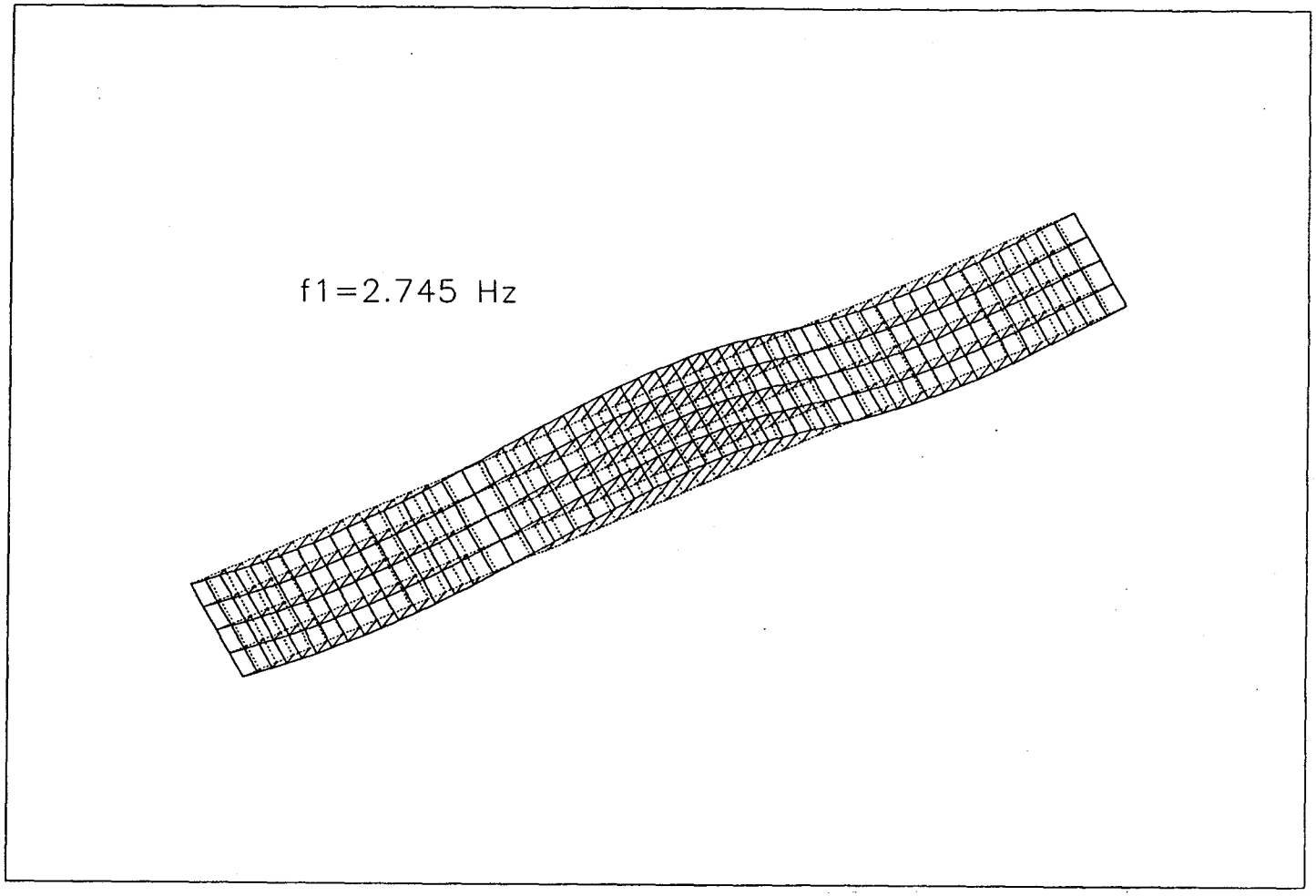

Fig. 3-5. The First Vibration Mode

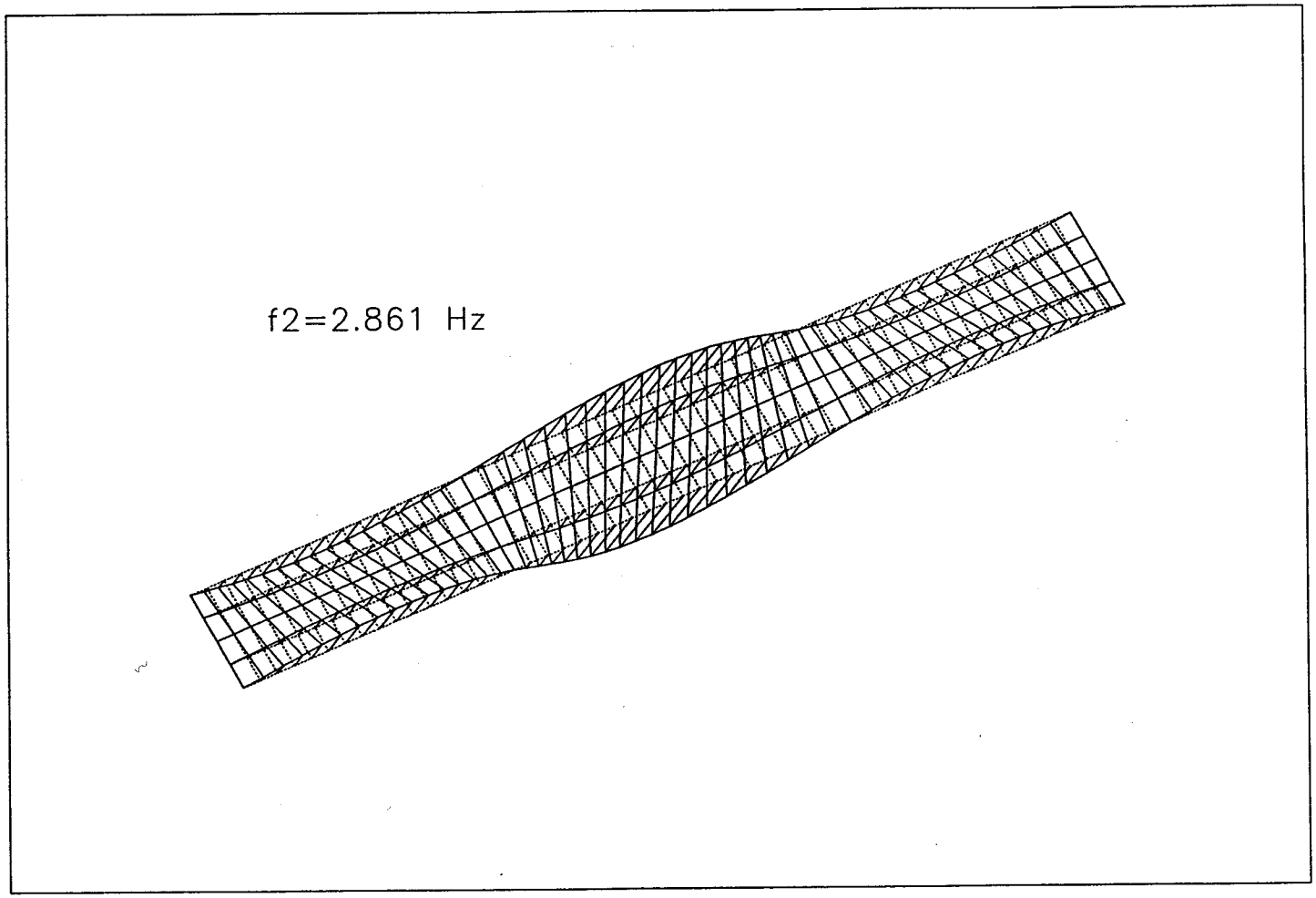

Fig. 3-6. The Second Vibration Mode

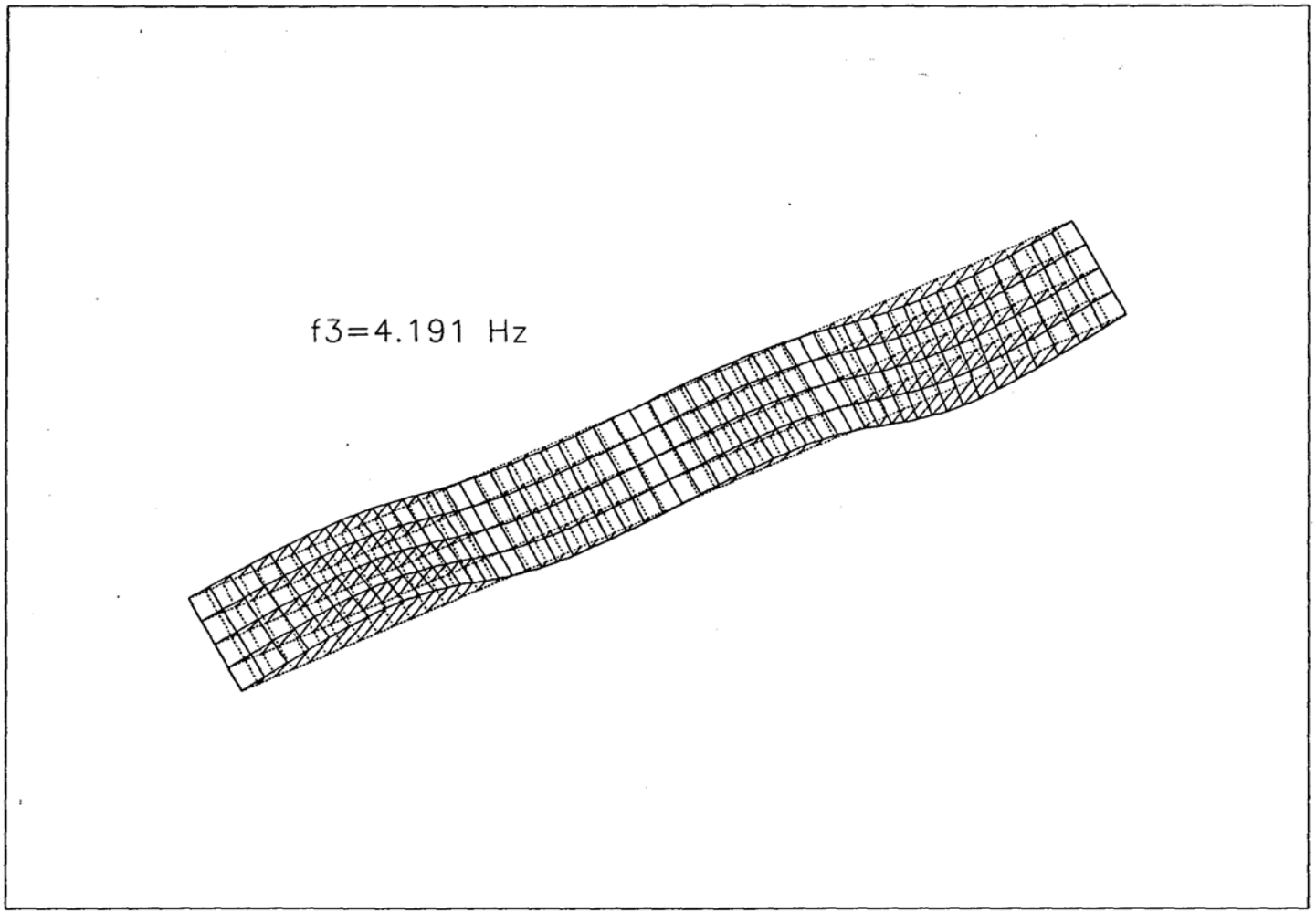

Fig. 3-7. The Third Vibration Mode

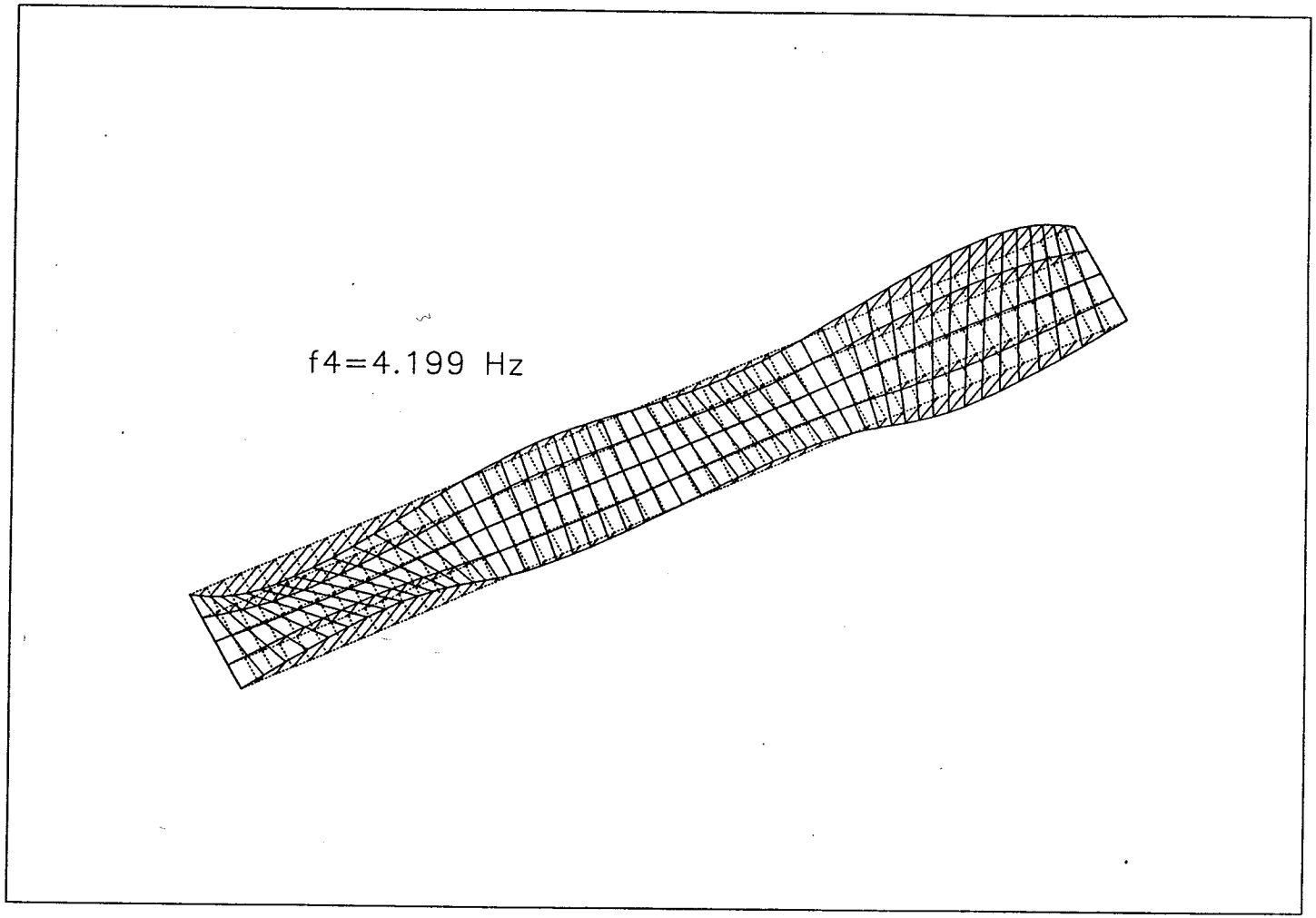

Fig. 3-8. The Fourth Vibration Mode

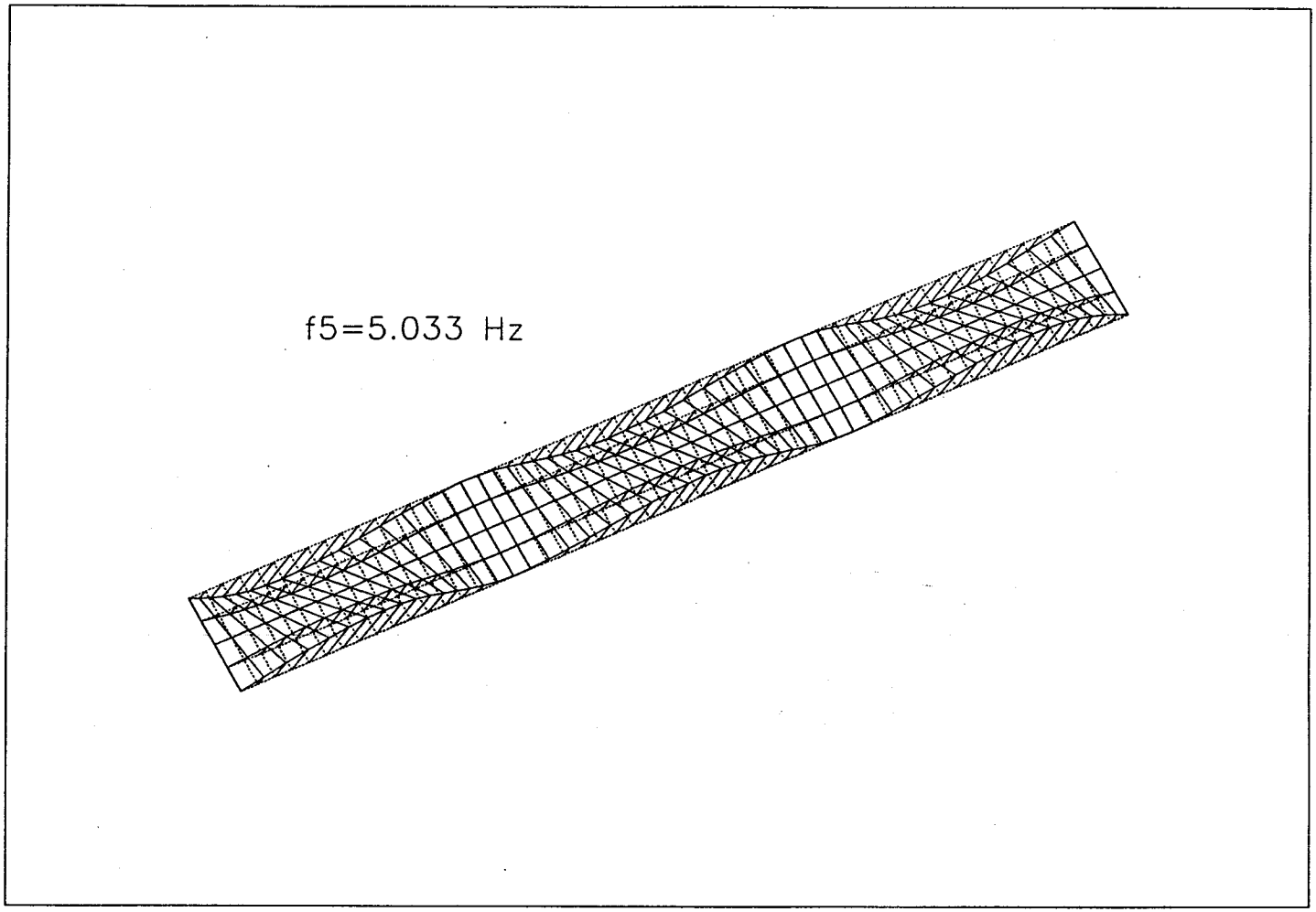

Fig. 3-9. The Fifth Vibration Mode

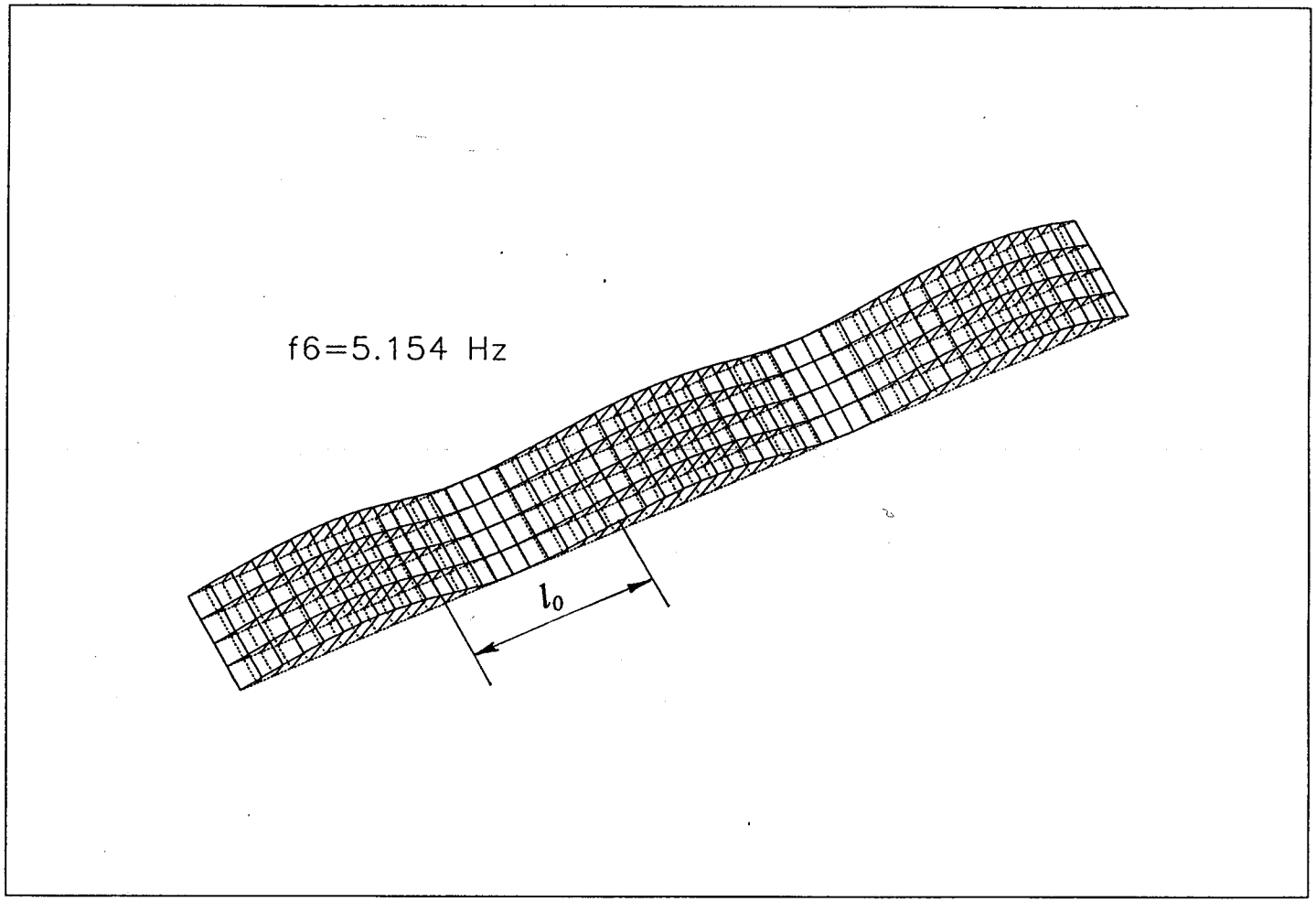

Fig. 3-10. The Sixth Vibration Mode

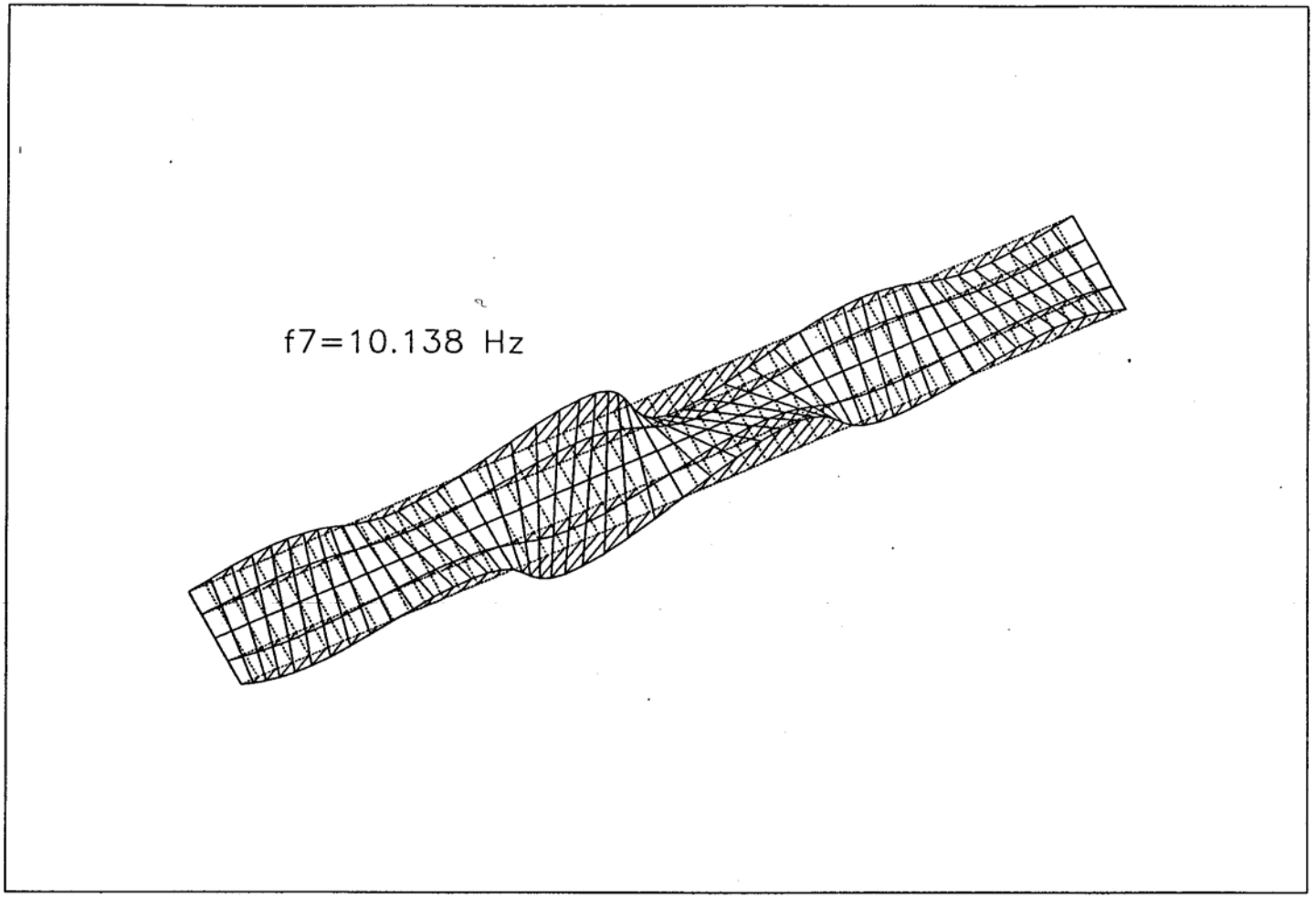

Fig. 3-11. The Seventh Vibration Mode

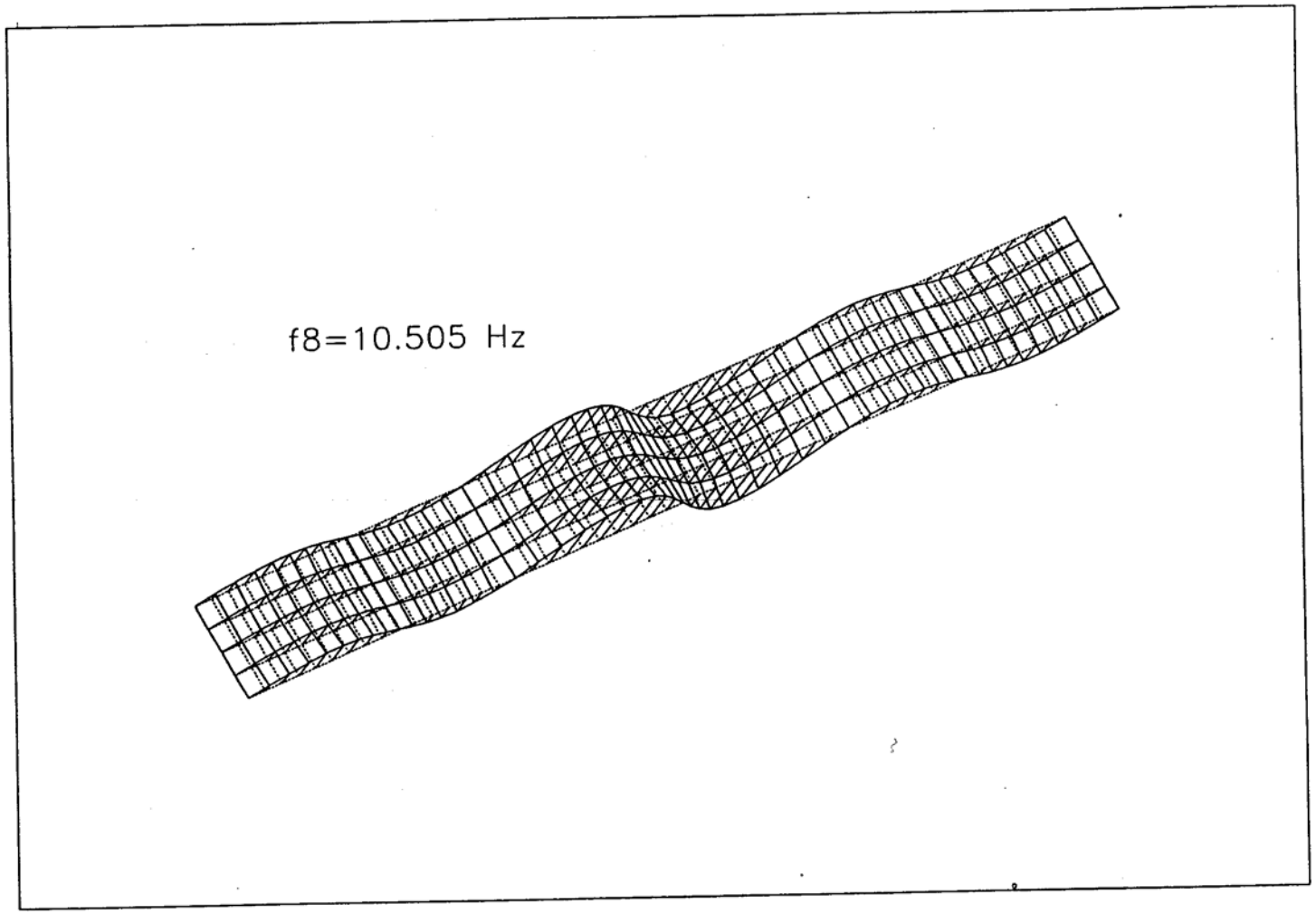

Fig. 3-12. The Eighth Vibration Mode

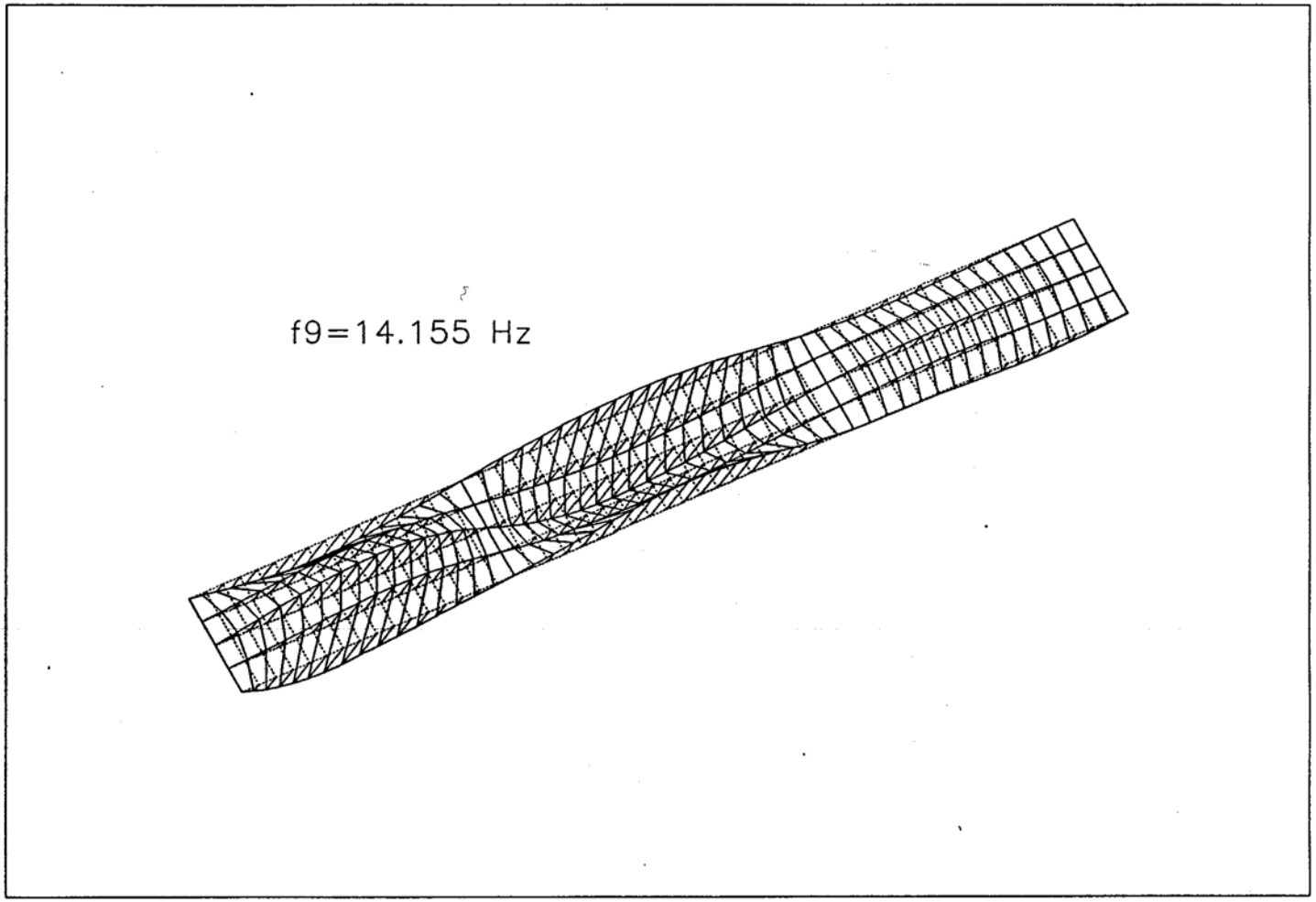

Fig. 3-13. The Ninth Vibration Mode

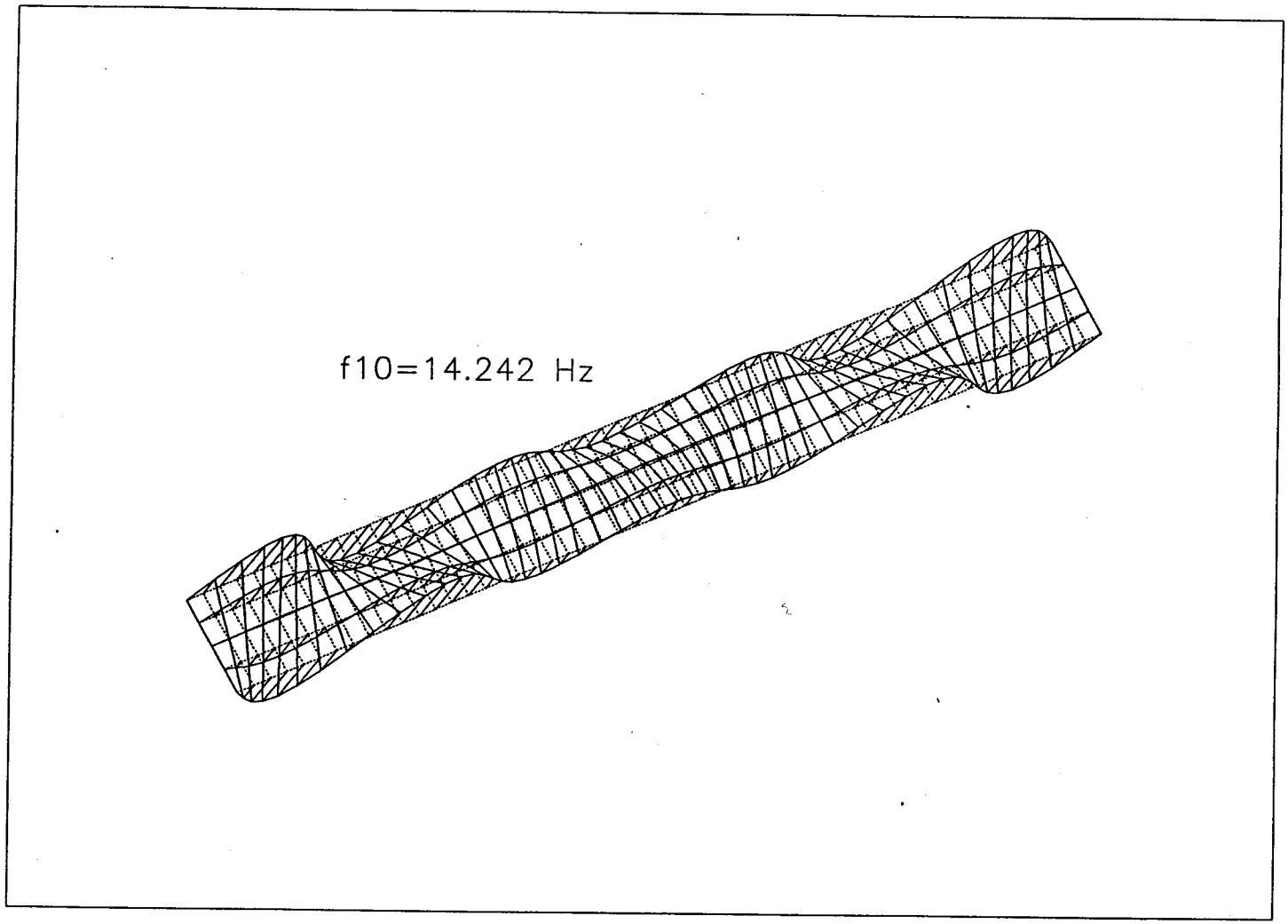

Fig. 3-14. The Tenth Vibration Mode

vehicle cleared the right end of the bridge. The same class of road surface was assumed for both the approach roadways and bridge decks.

In order to get the general dynamic characteristics of each girder, a single vehicle loading (Fig. 3-15), both symmetrically and asymmetrically, was first investigated.

Under the conditions of good road surface and 55 MPH (88.495 km/hr) vehicle speed, the lateral static and dynamic wheel-load distribution factors as well as impact factors for bending moment at Sections 1, 2 and 3 (see Fig. 3-1) are given in Table 3-3. The wheel-load distribution factors acquired for the study is defined as

$$\eta = M_i/M_t \qquad (3\text{-}16)$$

in which $M_t = M/n$,

M = the sum of the bending moment of all girders at one section,

n = number of wheel-load in transverse direction, and

M_i = maximum bending moment of one girder at the section.

The impact factor is defined as

$$I_{mp}(\%) = [R_d/R_s - 1] \times 100\% \qquad (3\text{-}17)$$

in which R_d and R_s = the absolute maximum response for dynamic and static studies,

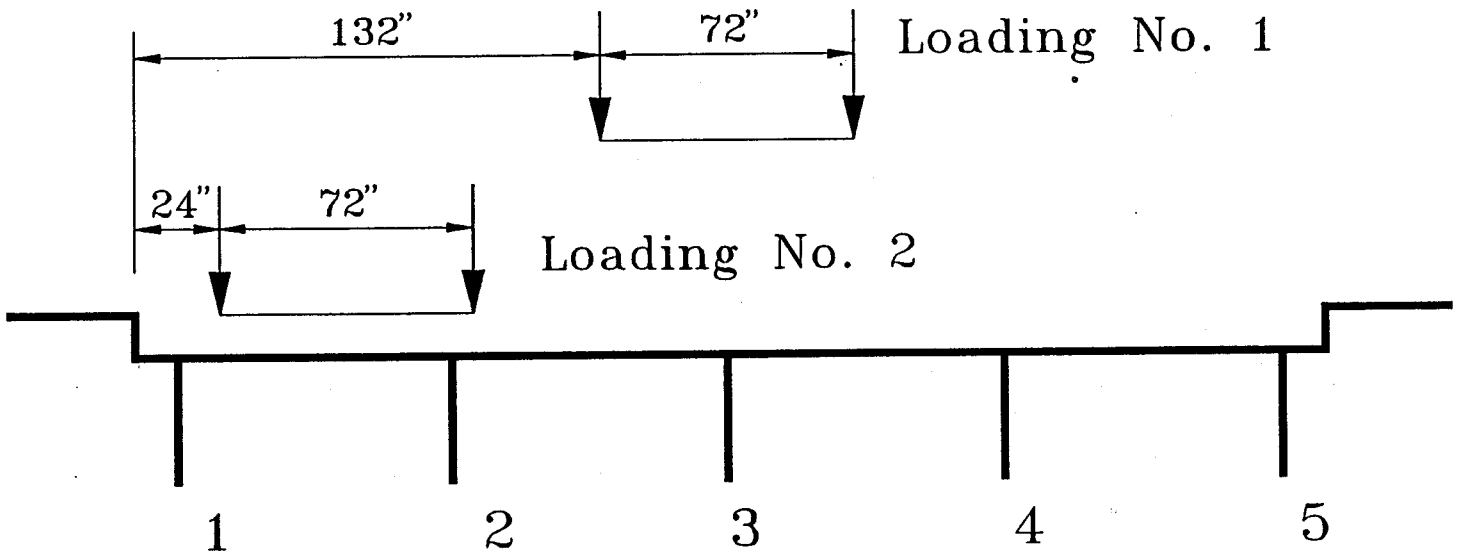

Fig. 3-15. One-truck Loading

Table 3-3. Load Distribution Factor and Impact Factor (one truck loading).

Section			1			2			3		
Girder			1	2	3	1	2	3	1	2	3
Static	Distribution Factor	Load 1	0.321	0.423	0.512	0.318	0.430	0.505	0.320	0.423	0.514
		Load 2	0.873	0.671	0.378	0.926	0.651	0.387	0.870	0.680	0.367
Dynamic	Distribution Factor	Load 1	0.363	0.444	0.477	0.441	0.529	0.565	0.365	0.458	0.512
		Load 2	0.951	0.683	0.411	1.202	0.849	0.508	0.955	0.689	0.419
	Impact Factor	Load 1	13.20	5.06	-7.04	38.65	23.13	11.62	13.88	8.41	-0.58
		Load 2	9.02	2.03	8.73	30.07	30.51	31.45	9.75	1.35	13.88

respectively.

Table 3-3 gives wheel-load factors and impact factors of one bridge with spans of 56 ft.80 ft.-56 ft. for two loading cases. From Rows 3, 5 and 7 in Table 3-3, which shows the results of symmetric loading, it can be observed that the smaller the wheel-load distribution factors are, the larger the impact factors will be. From Rows 4, 6 and 8 in Table 3-3, which lists the results of asymmetric loading, it can be seen that owing to the effect of torsion, the smallest impact factor occurred at Girder 2 instead of exterior girder which has the maximum wheel-load distribution factors at all sections.

3.6.2. Representative History Curves

With good road surface, vehicle speed of 45 MPH (72.41 km/hr) and two-truck loading asymmetrically (see Fig. 3-16, Loading No. 4), the time histories of bending moment at Sections 1 to 4 of Girders 1 to 3 are presented in Figs. 3-17 to 3-28 and the histories of deflection at Section 3 of Girders 1 to 3 are illustrated in Figs. 3-29 to 3-31. The histories of shear of Girders 1 to 3 at Section 2 are shown in Figs. 3-32 to 3-34. In Figs. 3-17 to 3-34, the dotted lines actually represented the influence lines of bending moment, deflection and shear corresponding to the related cross-sections respectively, provided that the two-truck loading was treated as a unit load. Concerning the curves presented in Figs. 3-17 to 3-34, we can see that the dynamic response arises mainly from the participation of the first six natural modes. If we observe Figs. 3-5 to 3-14 and Figs. 3-17 to 3-28, it will be found that the shapes of Modes 1,

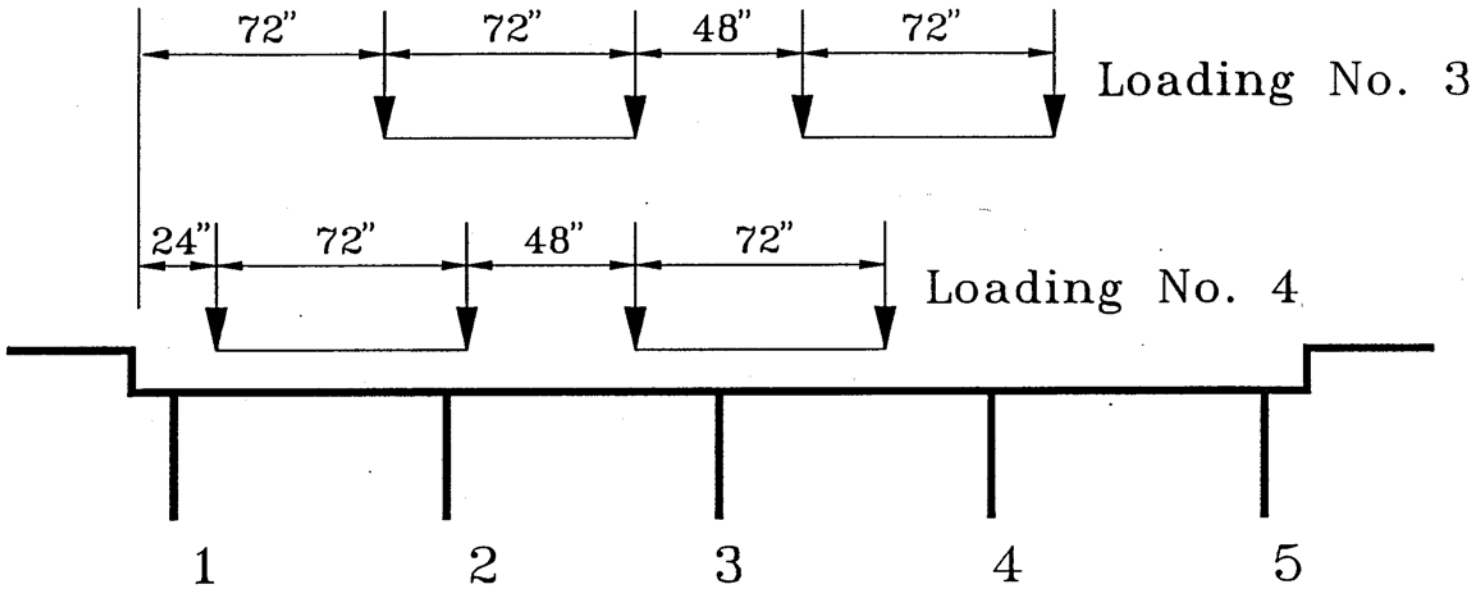

Fig. 3-16. Two-truck Loading

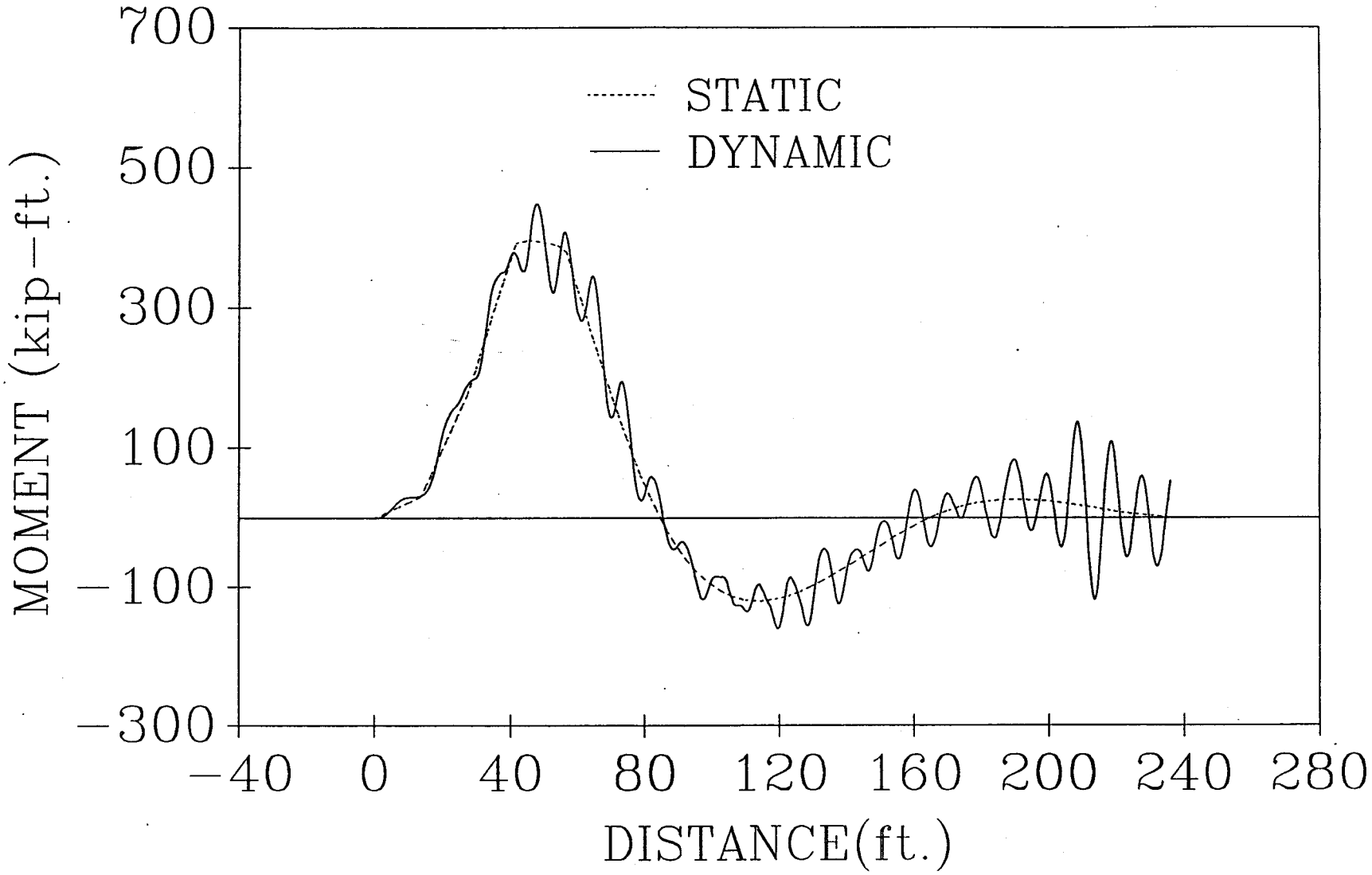

Fig. 3-17. Histories of Bending Moment at Section 1 of Girder 1

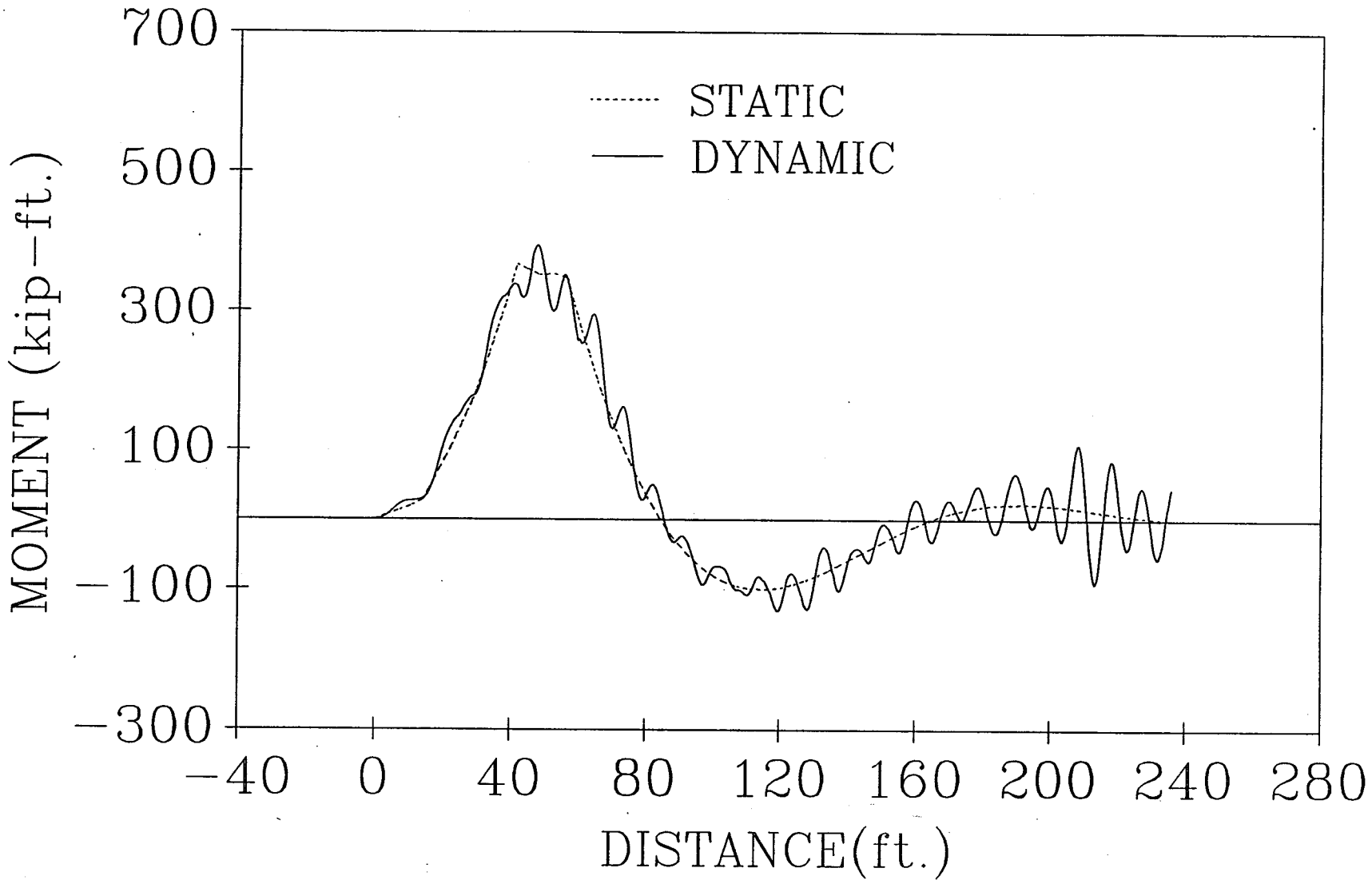

Fig. 3-18. Histories of Bending Moment at Section 1 of Girder 2

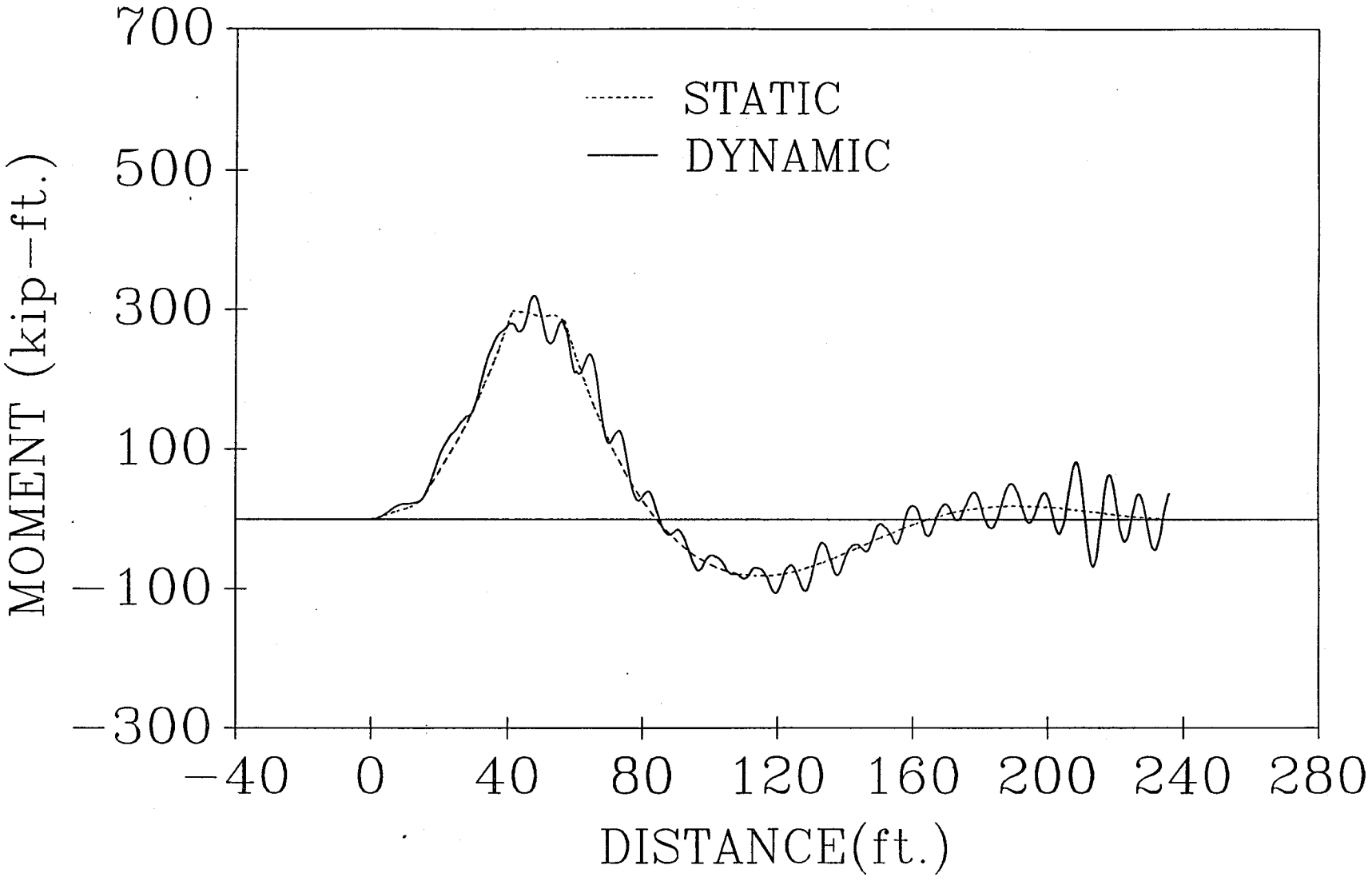

Fig. 3-19. Histories of Bending Moment at Section 1 of Girder 3

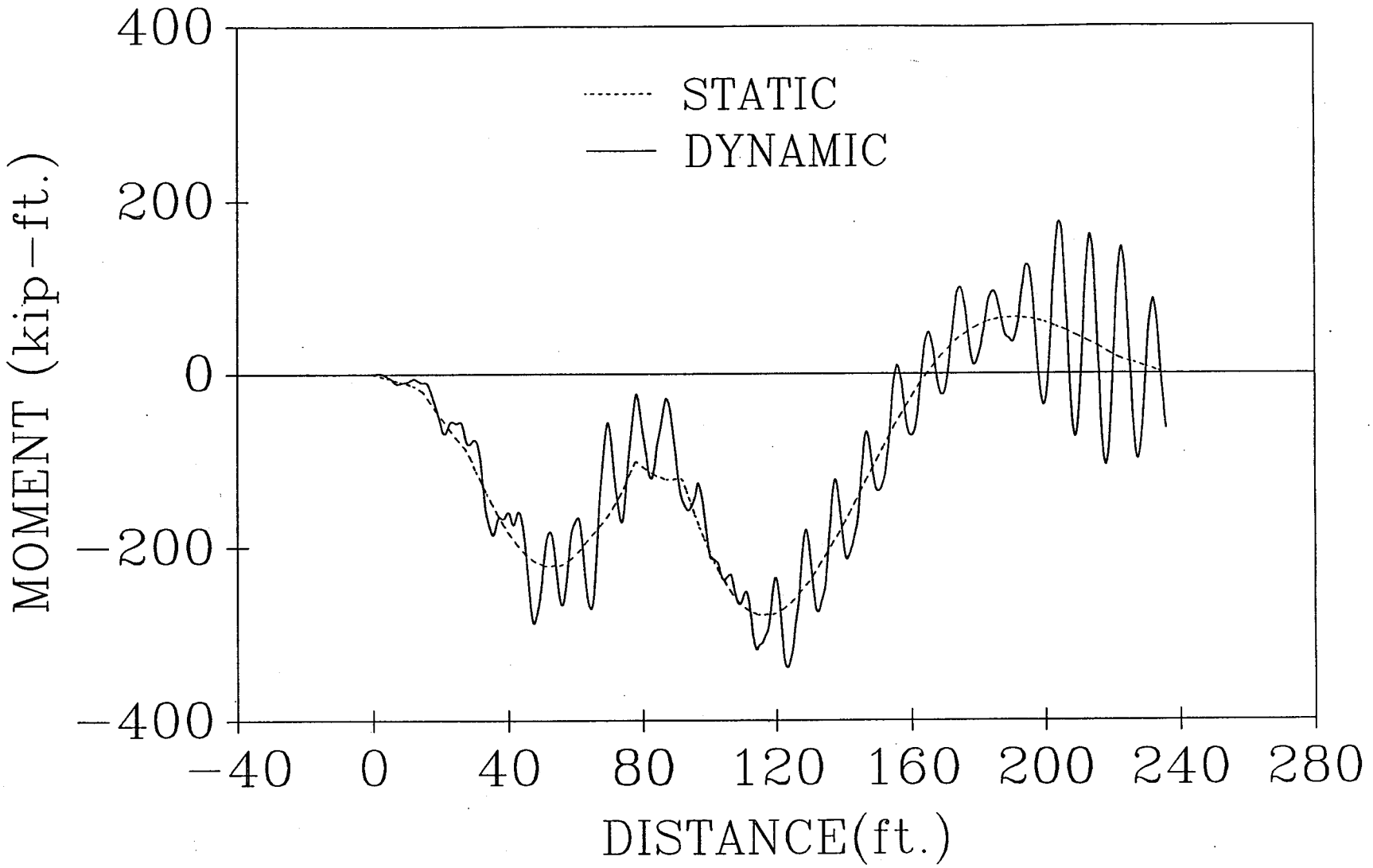

Fig. 3-20. Histories of Bending Moment at Section 2 of Girder 1

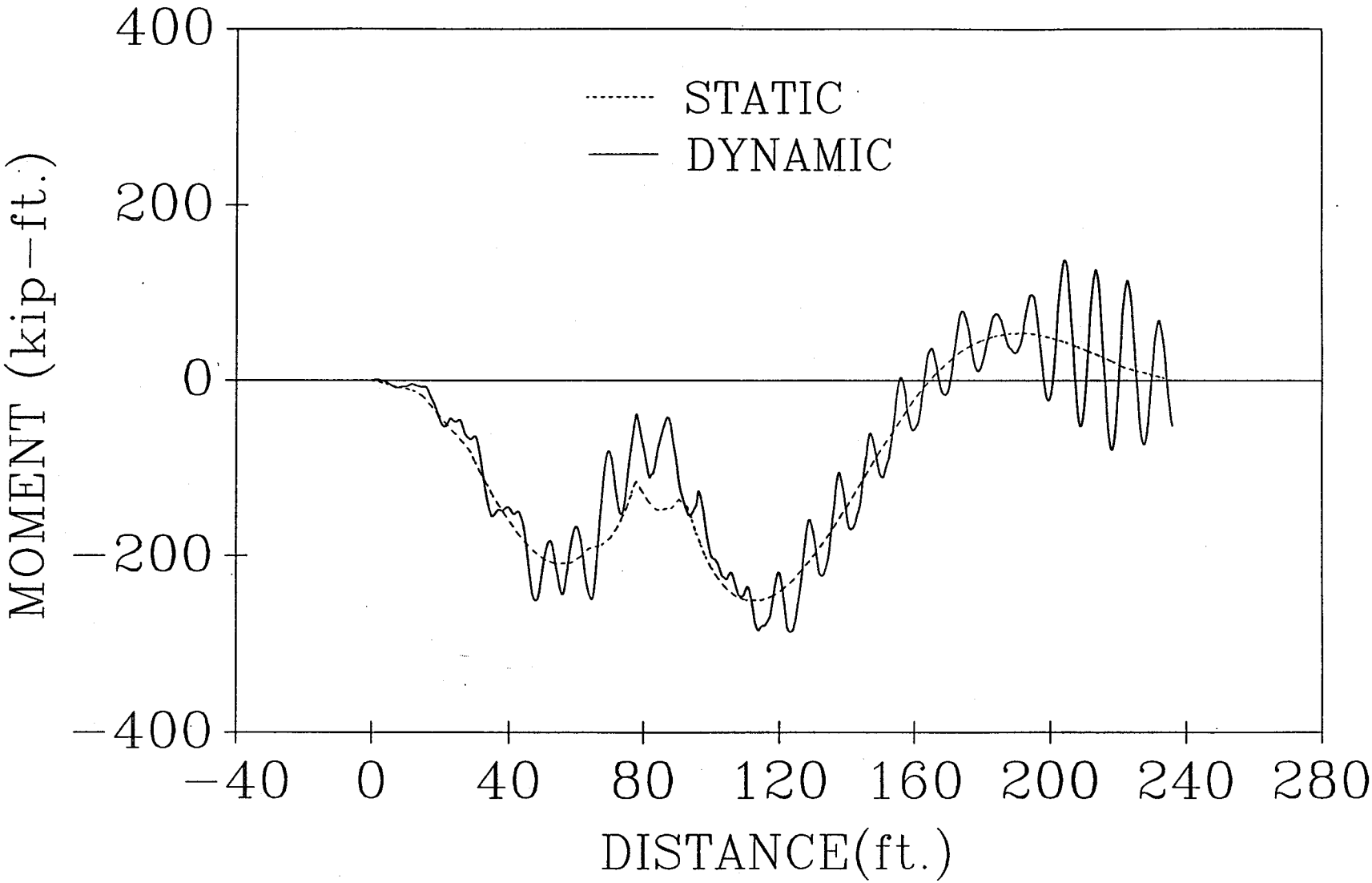

Fig. 3-21. Histories of Bending Moment at Section 2 of Girder 2

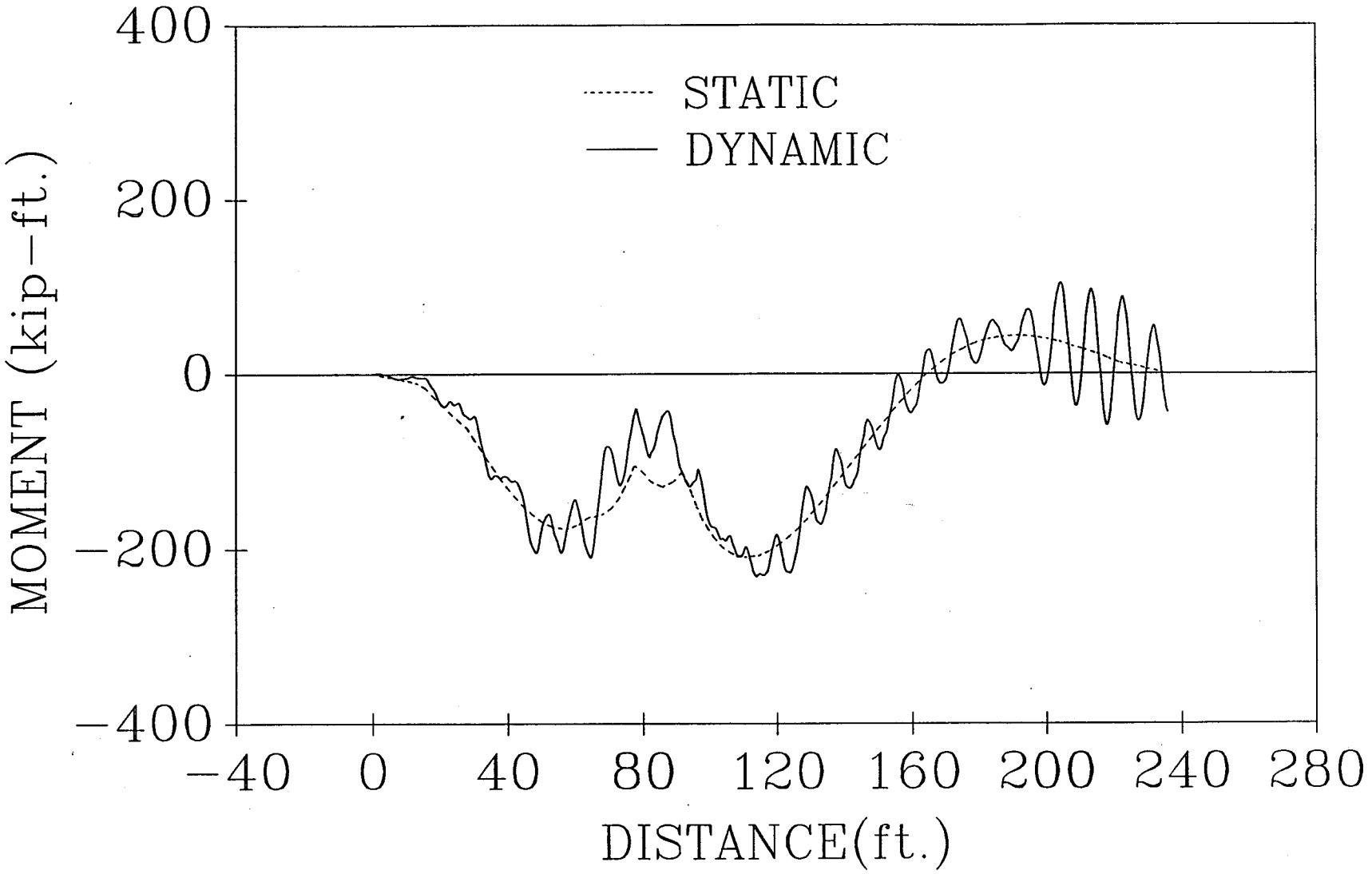

Fig. 3-22. Histories of Bending Moment at Section 2 of Girder 3

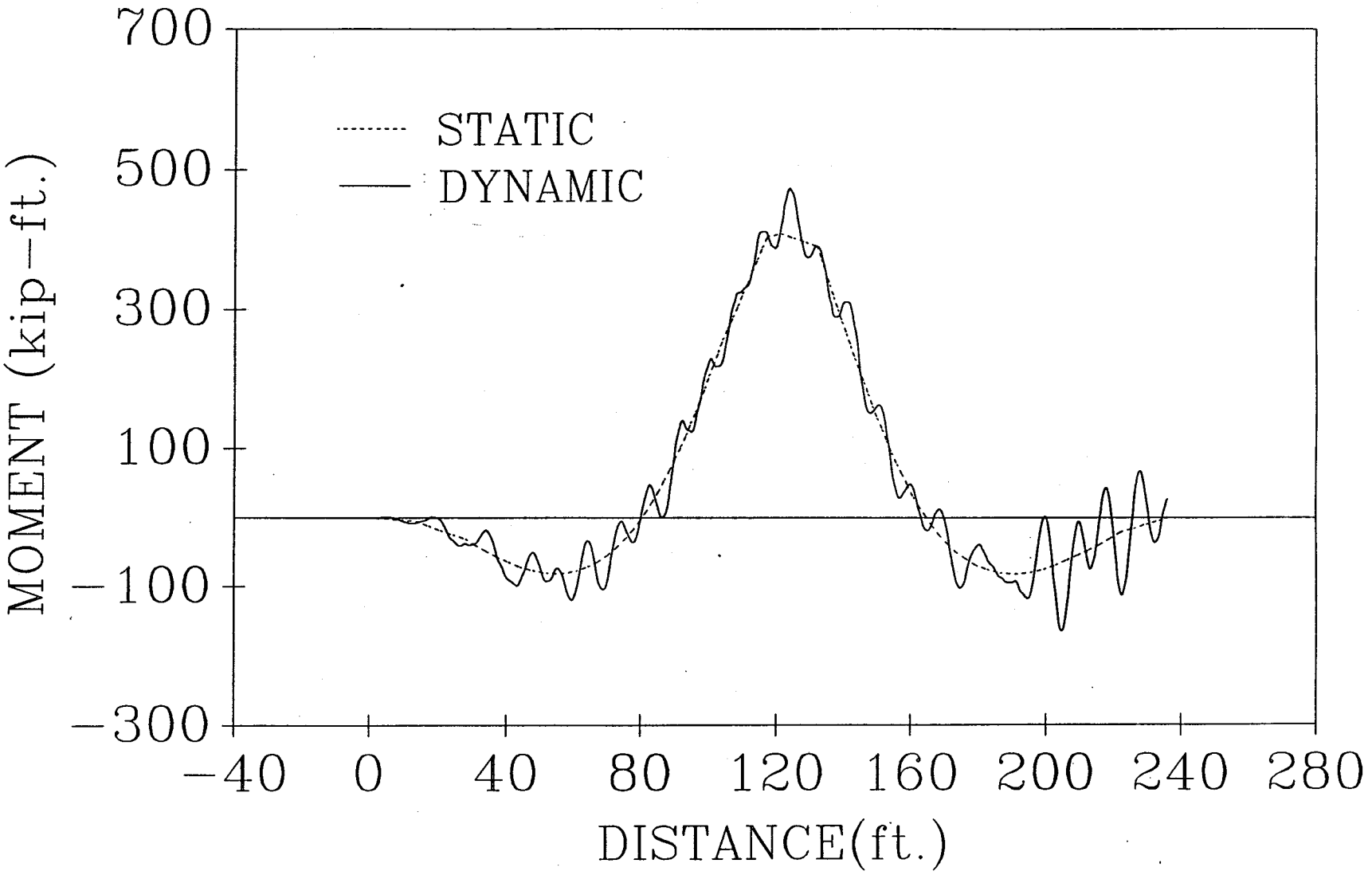

Fig. 3-23. Histories of Bending Moment at Section 3 of Girder 1

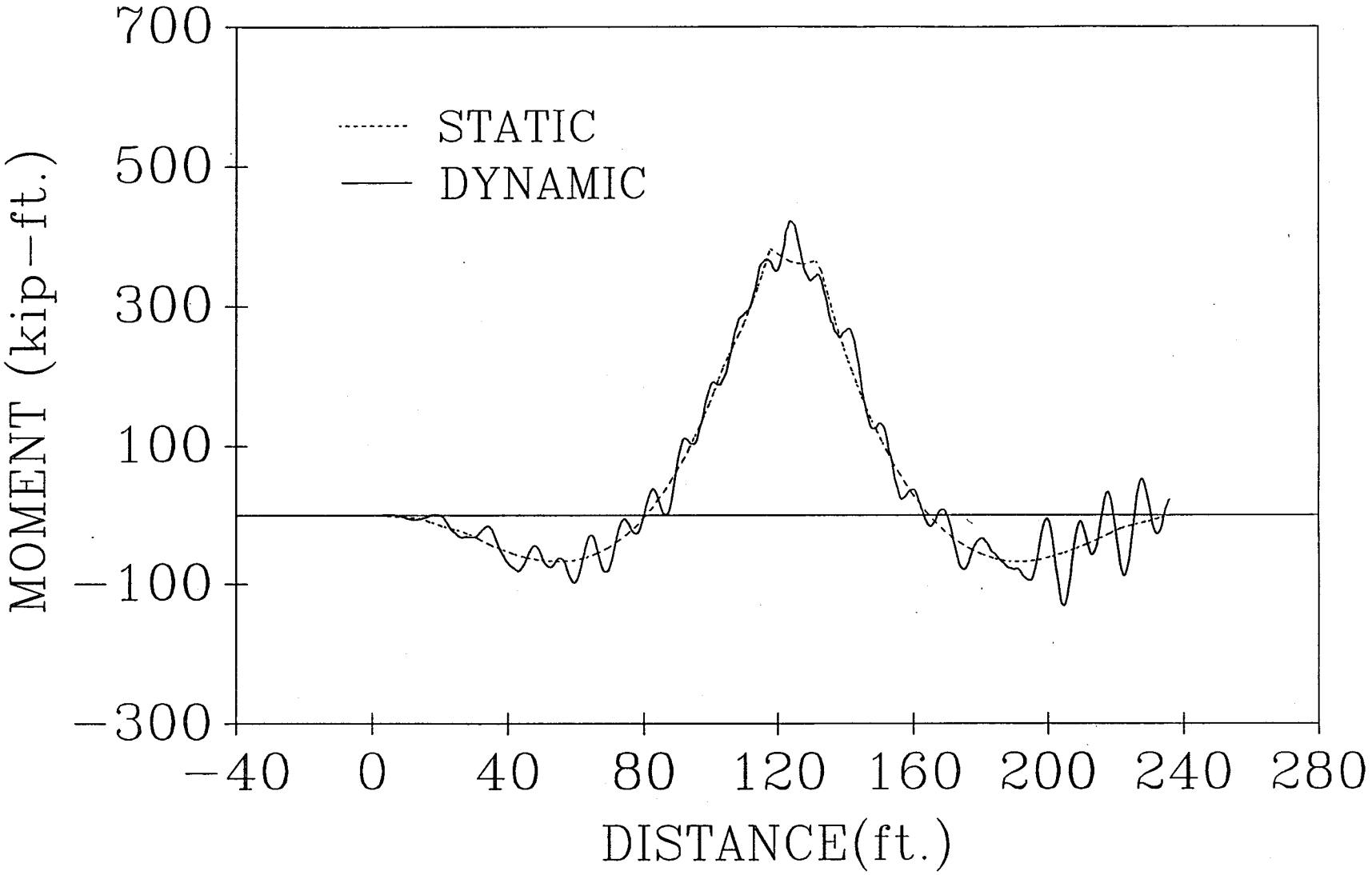

Fig. 3-24. Histories of Bending Moment at Section 3 of Girder 2

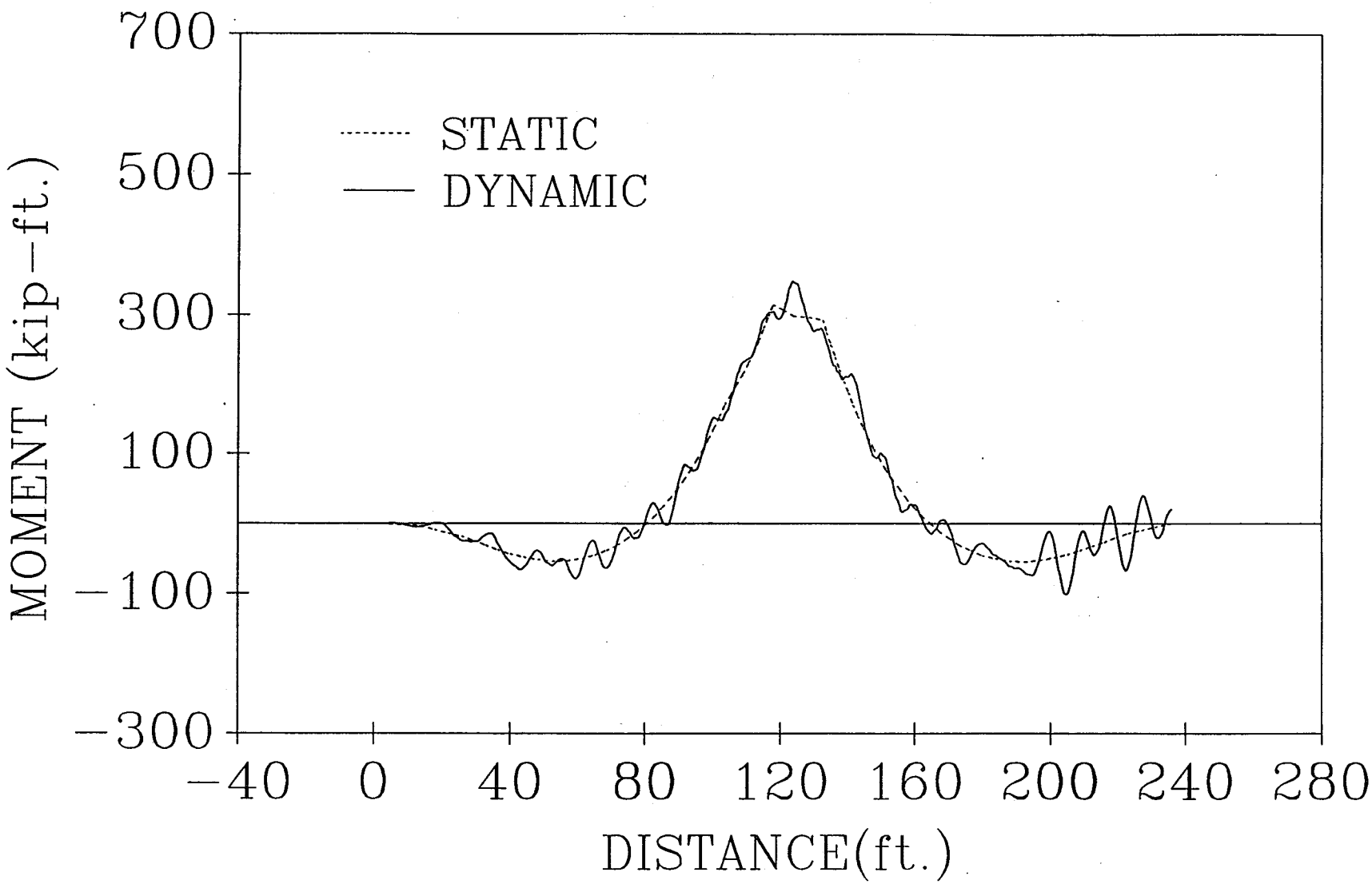

Fig. 3-25. Histories of Bending Moment at Section 3 of Girder 3

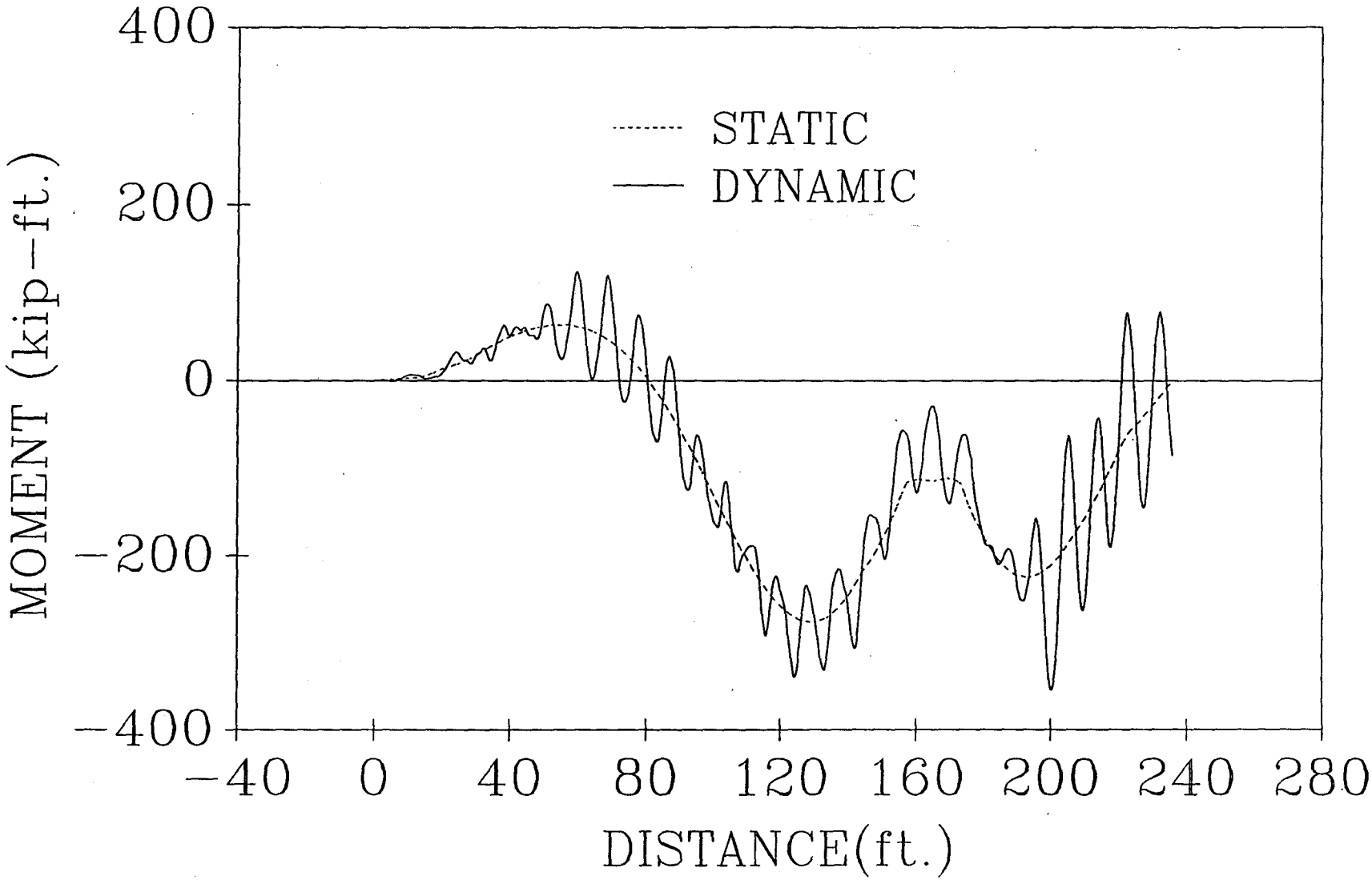

Fig. 3-26. Histories of Bending Moment at Section 4 of Girder 1

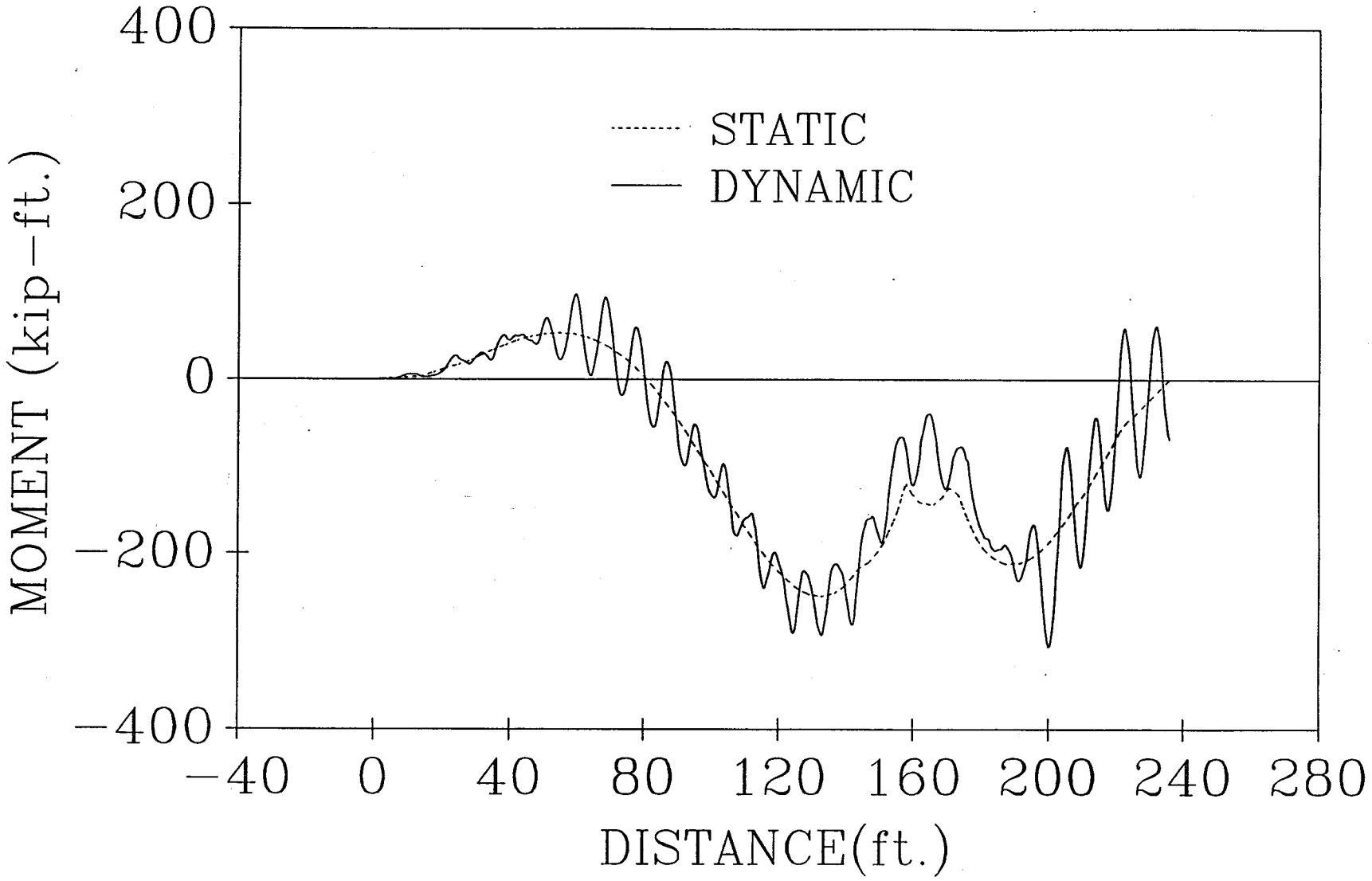

Fig. 3-27. Histories of Bending Moment at Section 4 of Girder 2

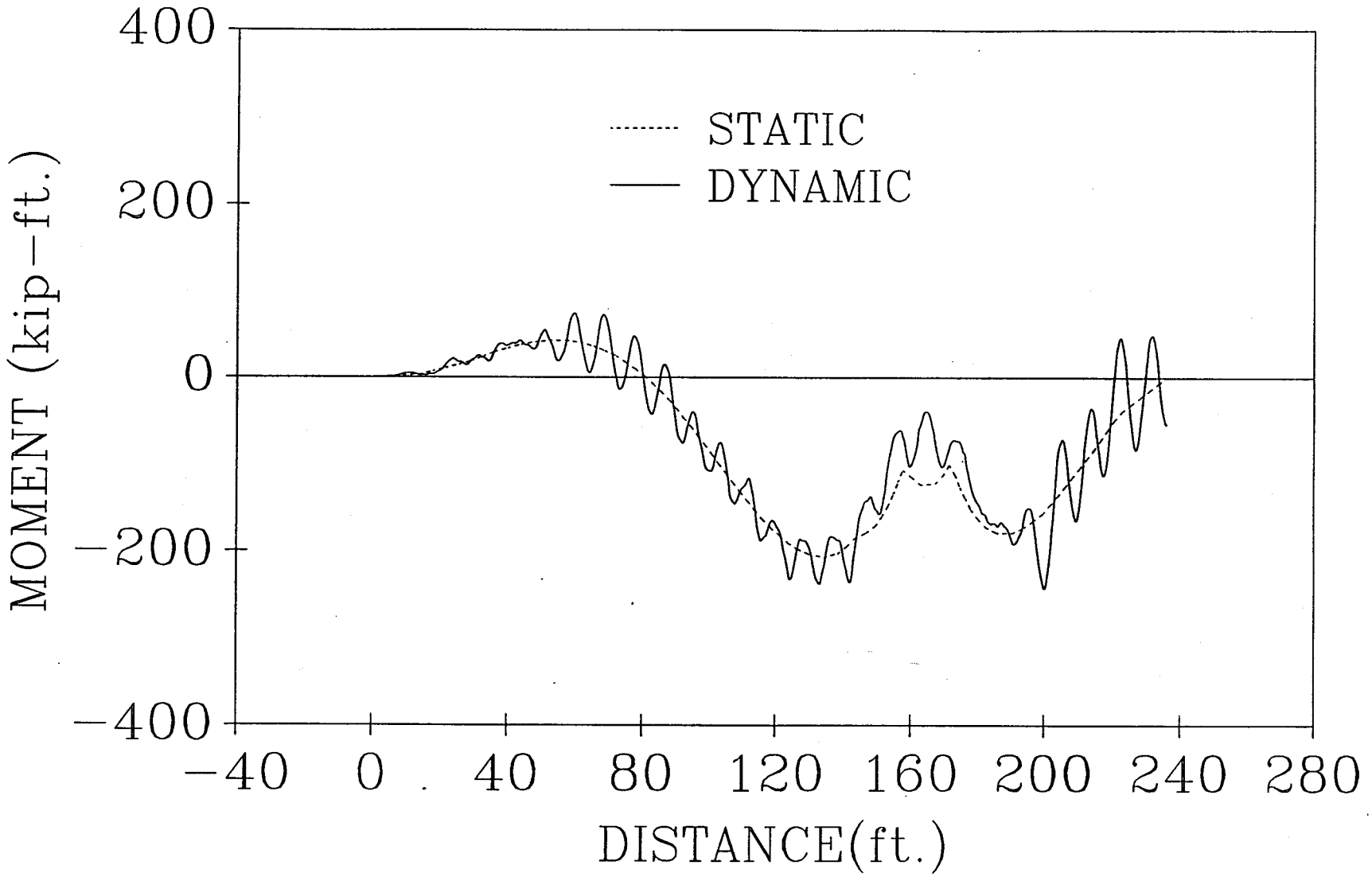

Fig. 3-28. Histories of Bending Moment at Section 4 of Girder 3

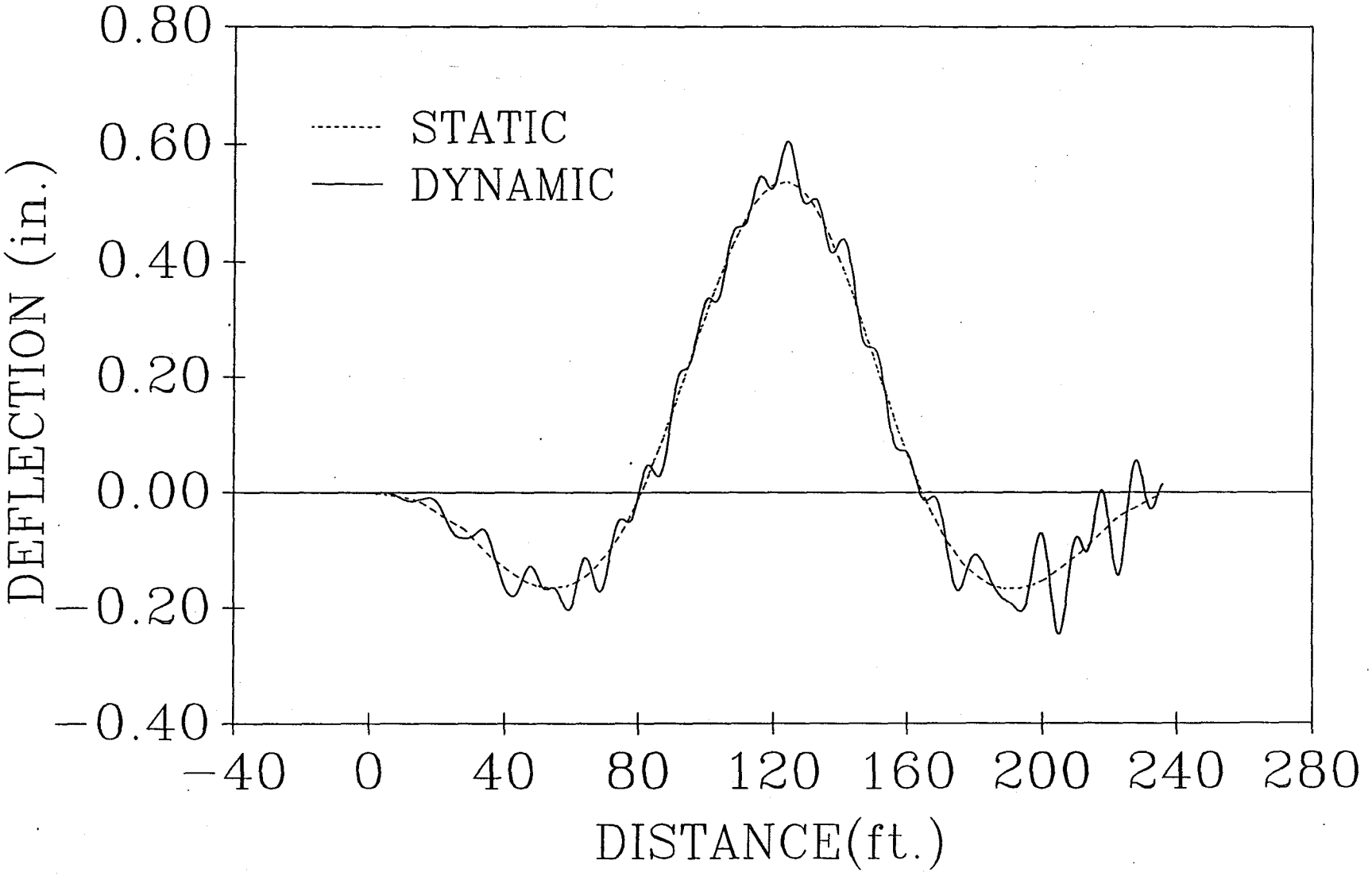

Fig. 3-29. Histories of Deflection at Section 3 of Girder 1

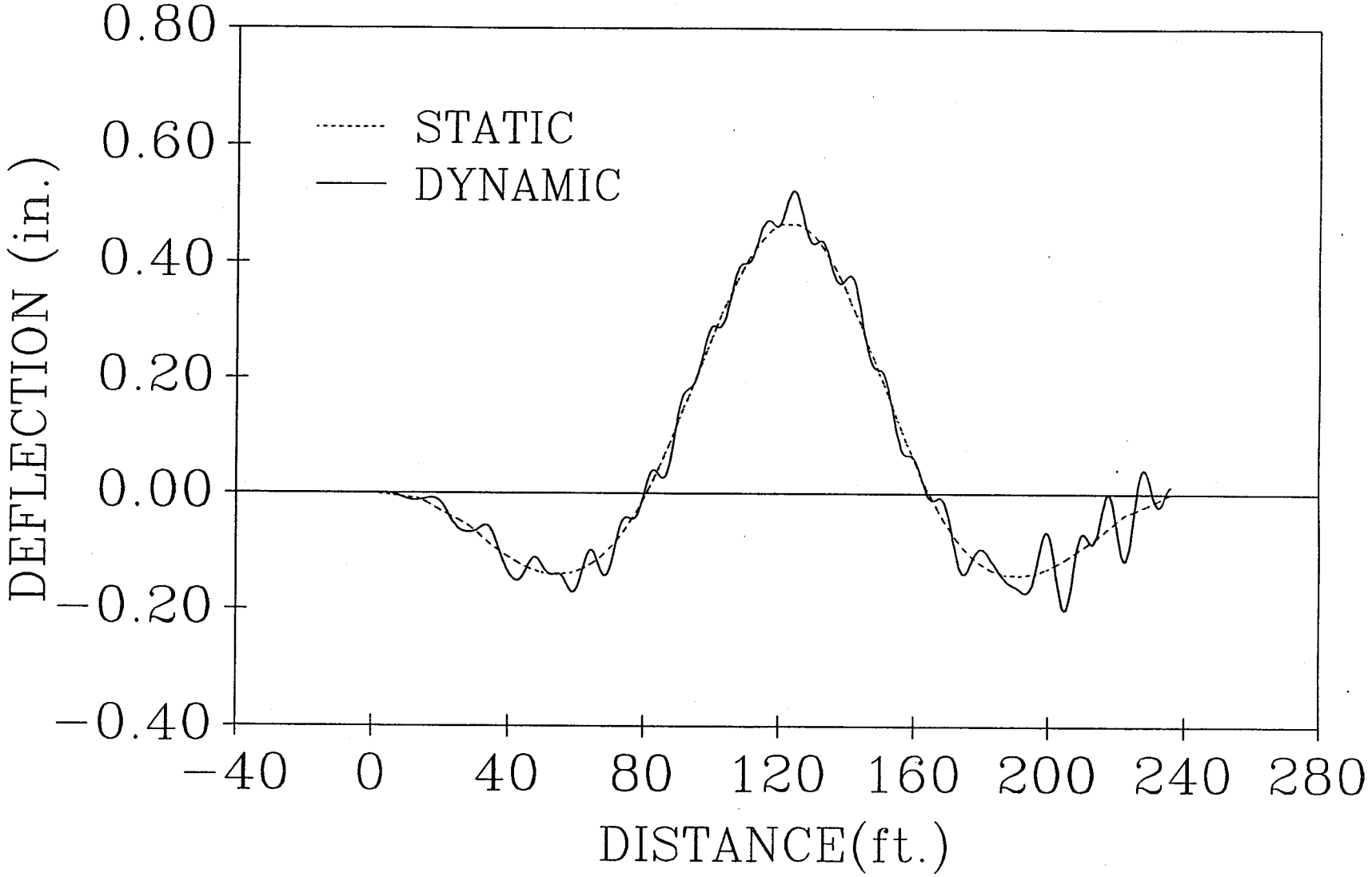

Fig. 3-30. Histories of Deflection at Section 3 of Girder 2

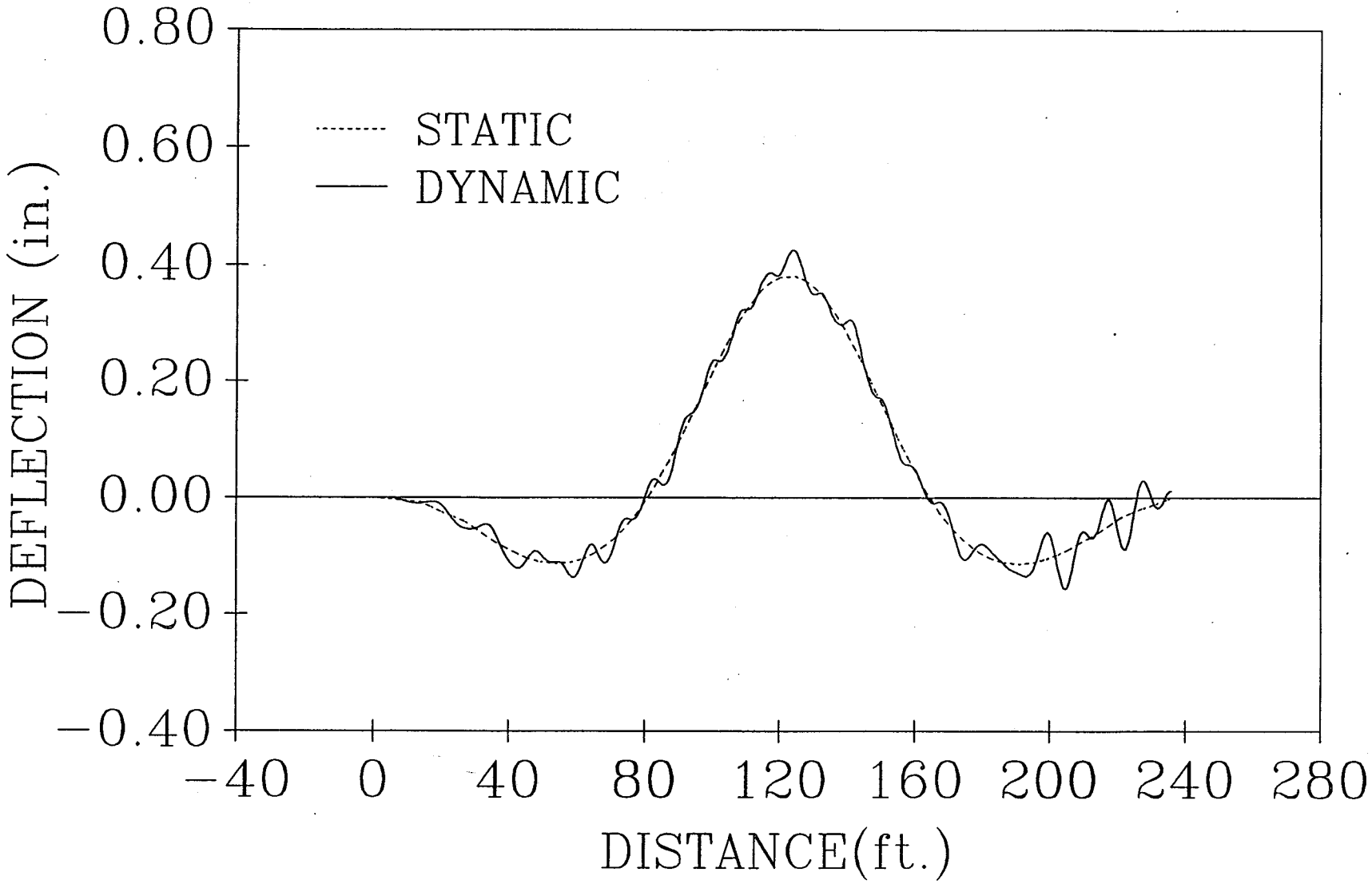

Fig. 3-31. Histories of Deflection at Section 3 of Girder 3

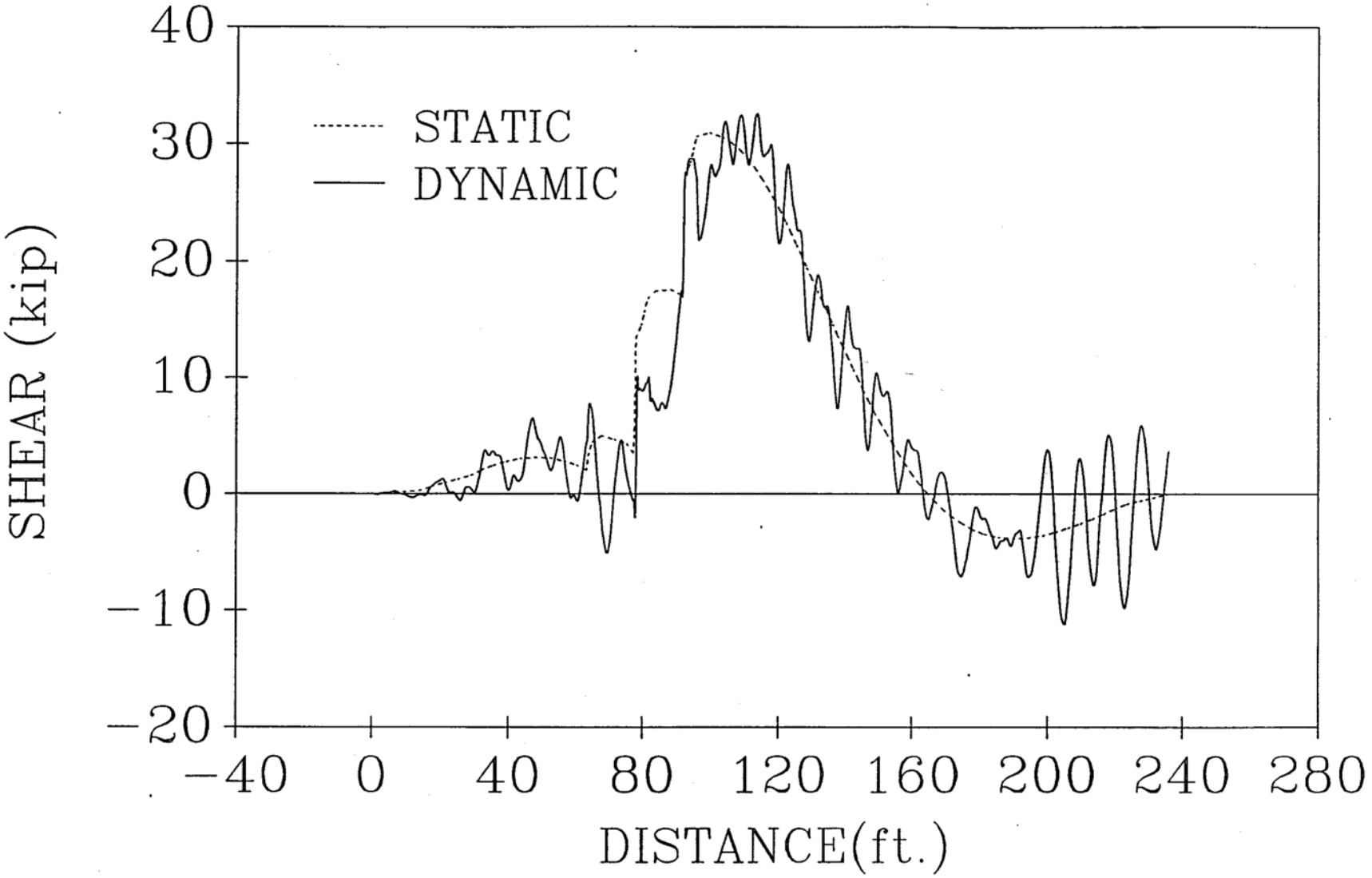

Fig. 3-32. Histories of Shear at Section 2 of Girder 1

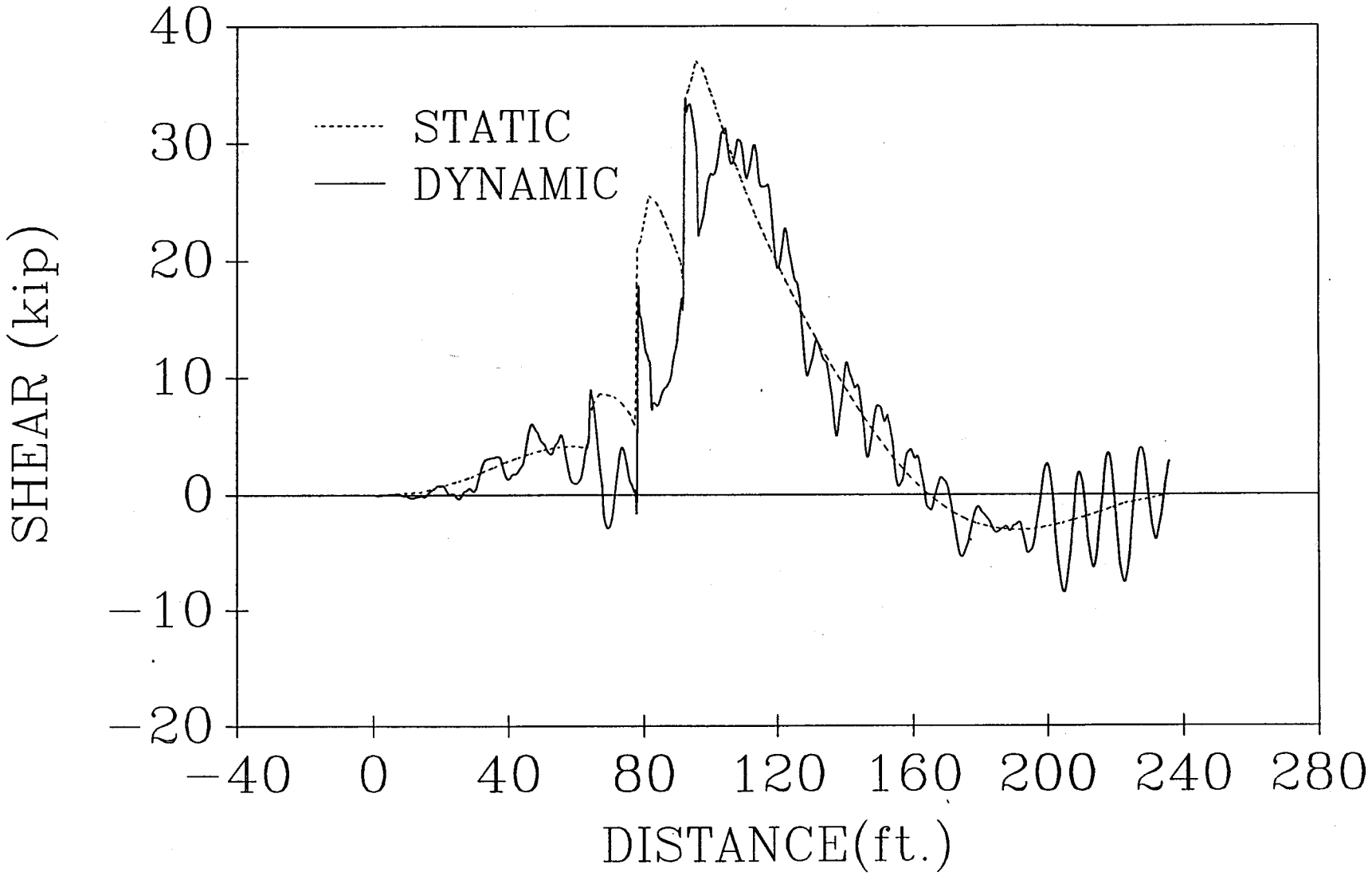

Fig. 3-33. Histories of Shear at Section 2 of Girder 2

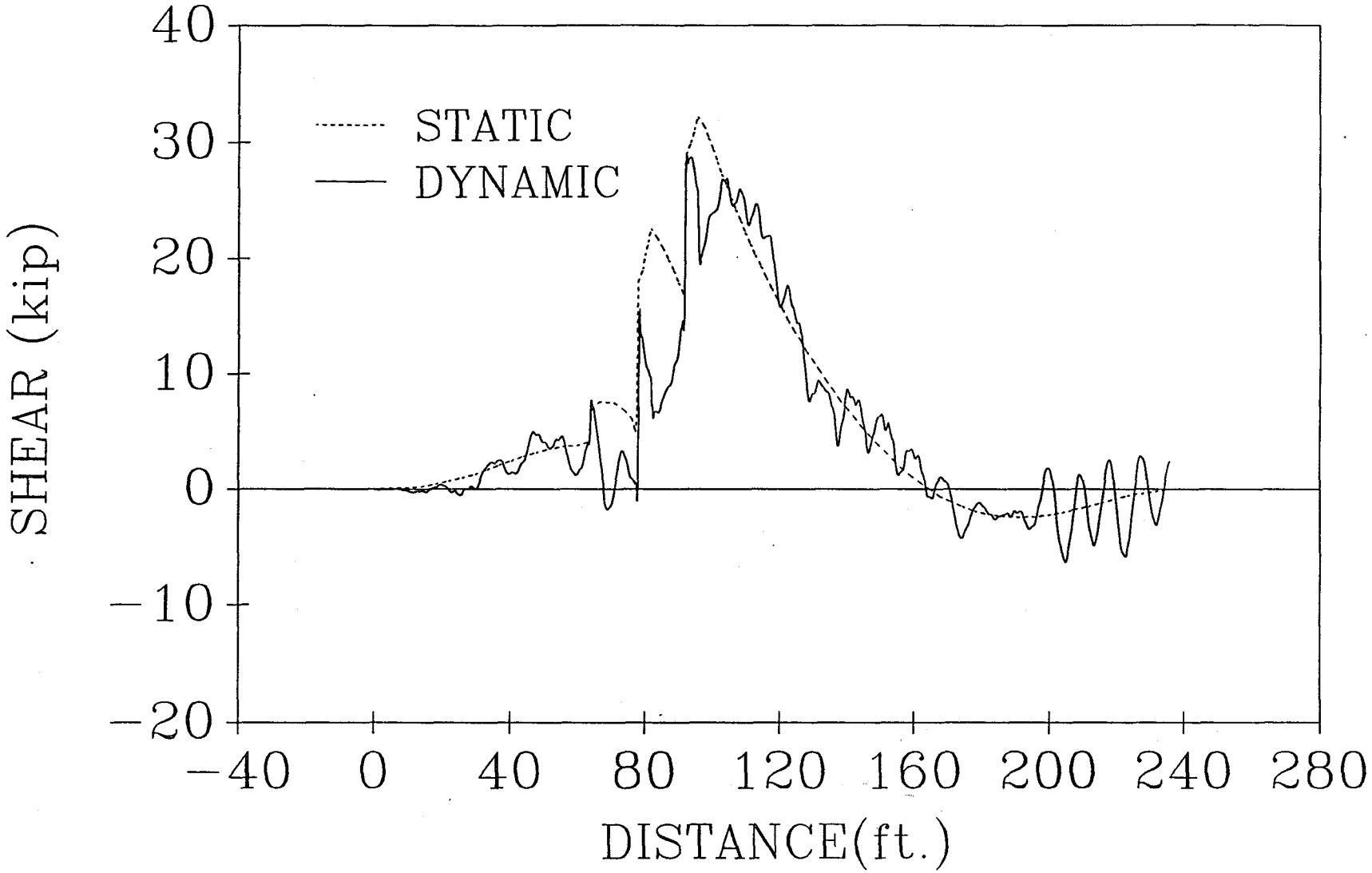

Fig. 3-34. Histories of Shear at Section 2 of Girder 3

bending moment at Section 1 as well as Modes 5, 6 and the influence line of bending moment at Section 2, individually, are very much similar to one another. Therefore, it can be expected that the dynamic response of Sections 3, 1, and 2 is caused mostly by Modes 1, 2, Modes 3, 4 and Modes 5, 6, respectively. Also, from Figs. 3-17 to 3-34, the impact factors of bending moment at Section 2 (over interior supports) are larger than those at Sections 1 and 3 because of the effect of higher modes.

From Fig. 3-17 to 3-34, it can also be observed that all time histories for Girders 1 to 3 at the same section are in similar shape and that the dynamic increments in the center girder are much smaller than those in the exterior girder. This is because the frequencies of bending and torsion (Modes 1 and 2) are quite close.

3.6.3. Parametric Study Effect

of Transverse Stiffness

In an attempt to better understand the influence of transverse stiffness on the dynamic behavior of continuous multigirder bridges, we chose three types of transverse stiffnesses, which are: (1) the original stiffness R (see Table 3-1), (2) 5R, and (3) the stiffness of deck (without transverse beam), for the later analysis.

The maximum static wheel-load distribution and dynamic impact factors of Girders 1 to 3 at different cross-sections, with various transverse stiffness, are listed in Table 3-4. The maximum factors were obtained by changing the position of two-truck loading in transverse 102

Table 3-4. Influence of Transverse Stiffness

Section			1			2			3		
Girder			1	2	3	1	2	3	1	2	3
Static	Distribution Factor	5R	1.177	1.043	0.860	1.239	1.030	0.835	1.165	1.050	0.876
		R	1.138	1.063	0.921	1.178	1.058	0.925	1.139	1.066	0.919
		Deck	1.043	1.117	1.066	1.049	1.136	1.105	1.068	1.102	1.031
Dynamic	Distribution Factor	5R	1.381	1.096	0.874	1.630	1.358	1.081	1.330	1.129	0.926
		R	1.258	1.101	0.910	1.602	1.358	1.105	1.298	1.135	0.954
		Deck	1.157	1.178	1.109	1.436	1.385	1.303	1.214	1.147	1.069
	Impact Factor	5R	11.63	5.16	1.60	31.59	31.49	29.27	14.12	7.51	5.78
		R	10.48	3.52	-1.04	36.26	28.45	19.21	13.81	6.52	3.98
		Deck	11.00	5.43	3.98	36.79	21.98	18.00	13.78	4.06	3.56

direction (refer to Fig. 3-16). It was found that Loading No.4 shown in Fig. 3-16 induces the maximum wheel-load distribution factors of both Girders 1 and 2, while Loading No.3 induces that of center girder. The results presented in Table 3-4 were calculated by considering good road roughness and vehicle speed of 55 MPH for spans of 64 ft.-80 ft.-64 ft.

It can be seen from Table 3-4 that: (1) With the decrease of transverse stiffness, the wheel-load distribution factors of Girder 2 increase and its impact factors at most sections decrease greatly. (2) The impact factors of exterior girder at most sections vary slightly with the increase of transverse stiffness. This is because two predominant effects, the increase of static wheel-load distribution factor and torsion, which contribute to the response of exterior girder are offsetted by each other. (3) With the decrease of transverse stiffness, the static and dynamic wheel-load distribution factors of exterior girder decrease and those of interior girders increase. However, the variation of the factors at most sections is not significant. Therefore, very large transverse stiffness in this kind of steel multigirder bridges seems to be unnecessary.

Effect of Road Surface Roughness and Vehicle Speed

Figs. 3-35 to 3-43 give the variations of impact factors of exterior girders of three bridges with various vehicle speeds for different road surface roughness. It can be observed from these two figures that: (1) Under the condition of very good road surface, the variation of impact factors at all sections vary slightly with vehicle speed and are generally less than 14 % for the bridge with span of 72 ft.-90 ft.-72 ft., 30 % for the bridge with span of 56 ft.-70 ft.-56 ft., and 26 % for the bridge with span of 40-50-40 ft. (2) With the increase of road

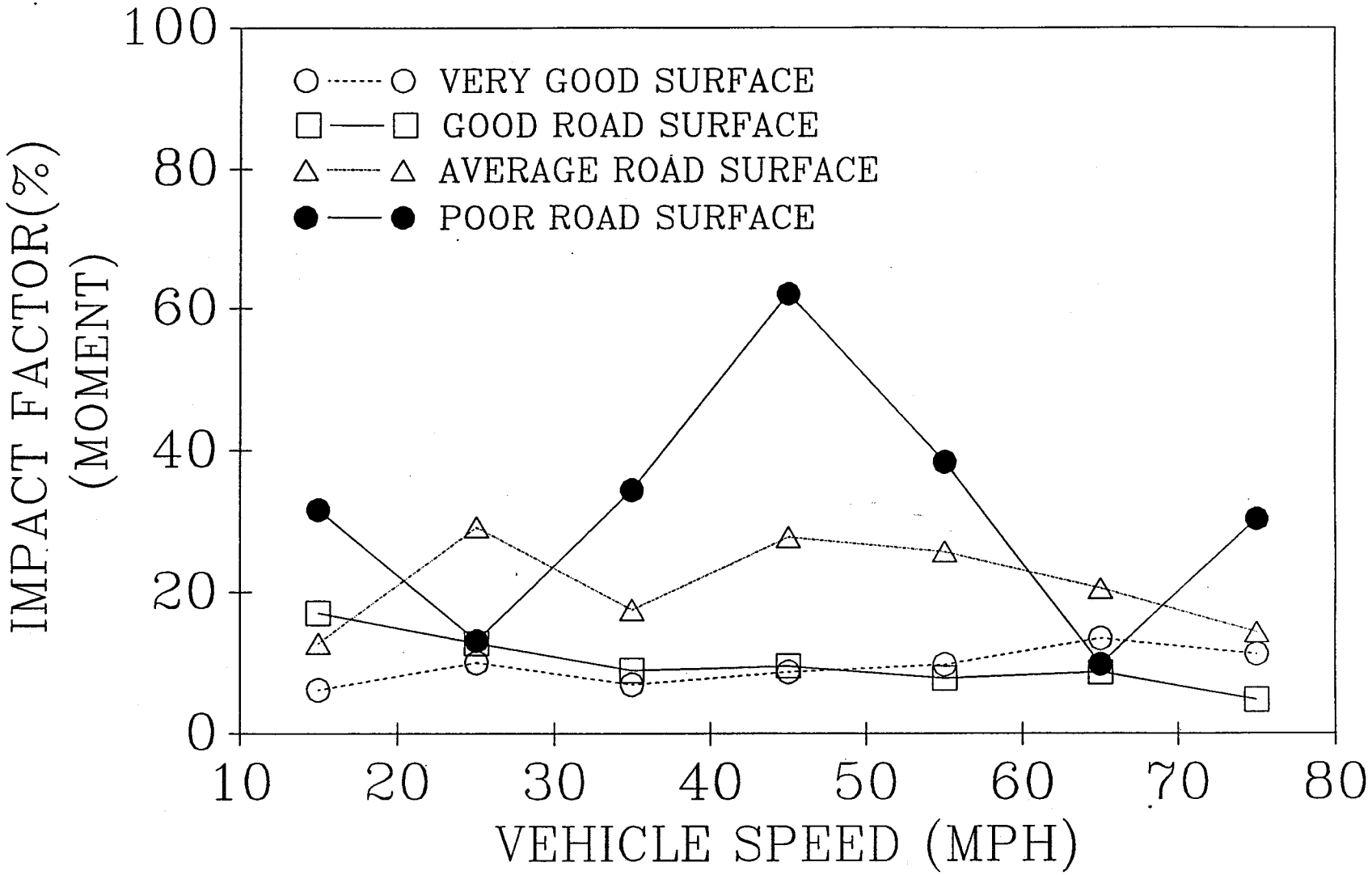

Fig. 3-35. Variation of Impact Factors with Vehicle Speeds at Section 1 of Girder 1 for Bridge of 72-90-72 ft.

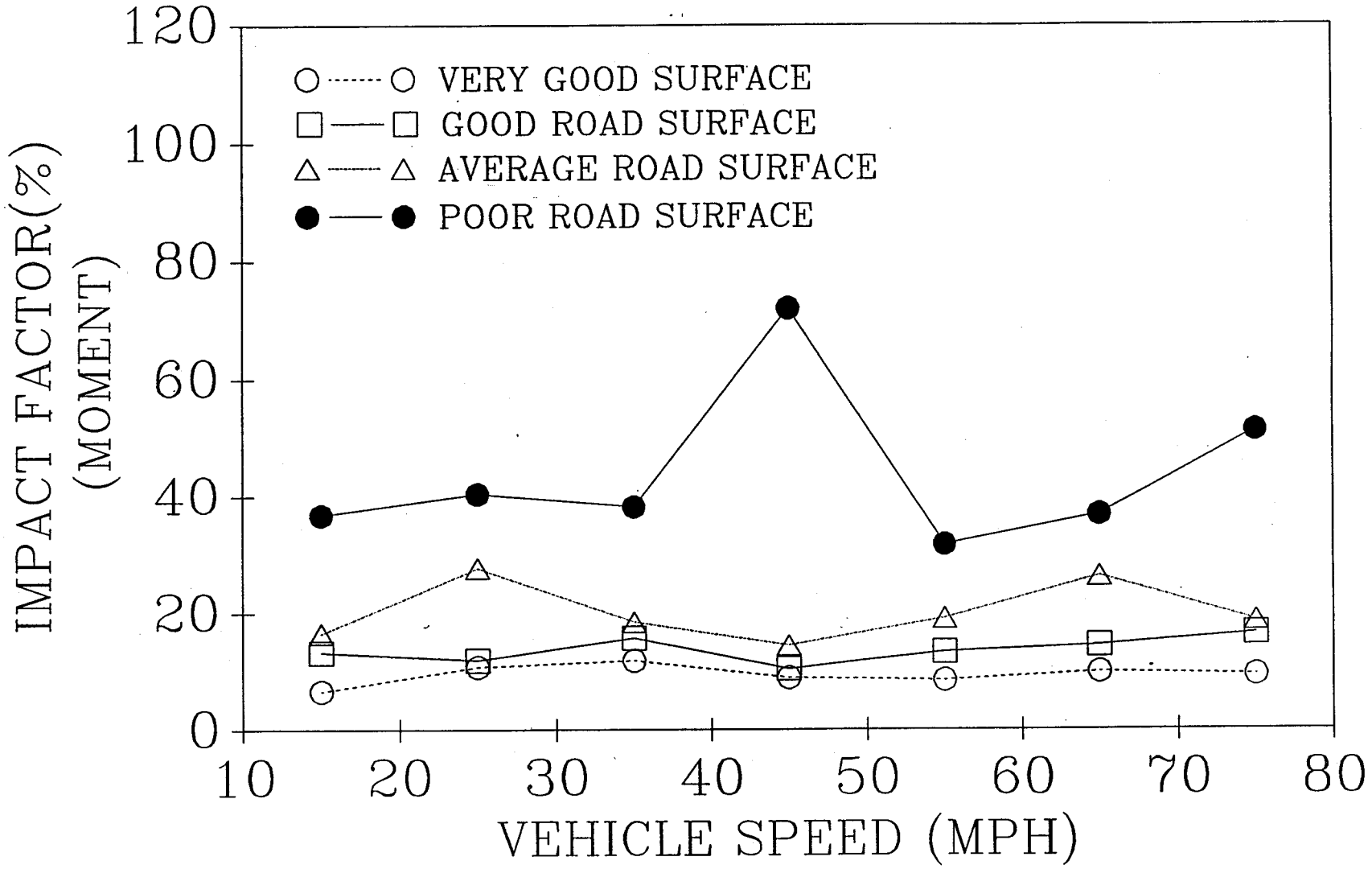

Fig. 3-36. Variation of Impact Factors with Vehicle Speeds at Section 2 of Girder 1 for Bridge of 72-90-72 ft.

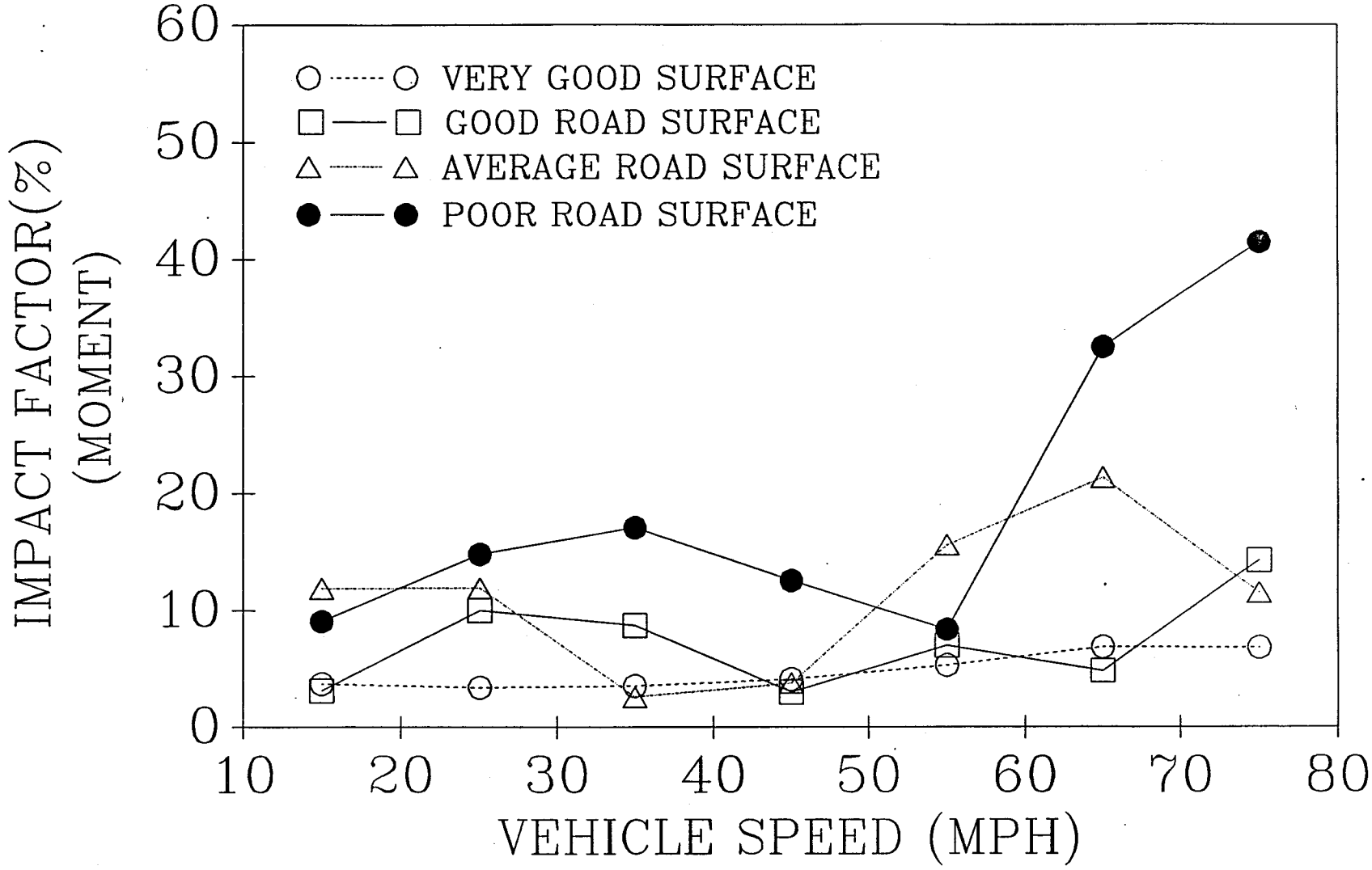

Fig. 3-37. Variation of Impact Factors with Vehicle Speeds at Section 3 of Girder 1 for Bridge of 72-90-72 ft.

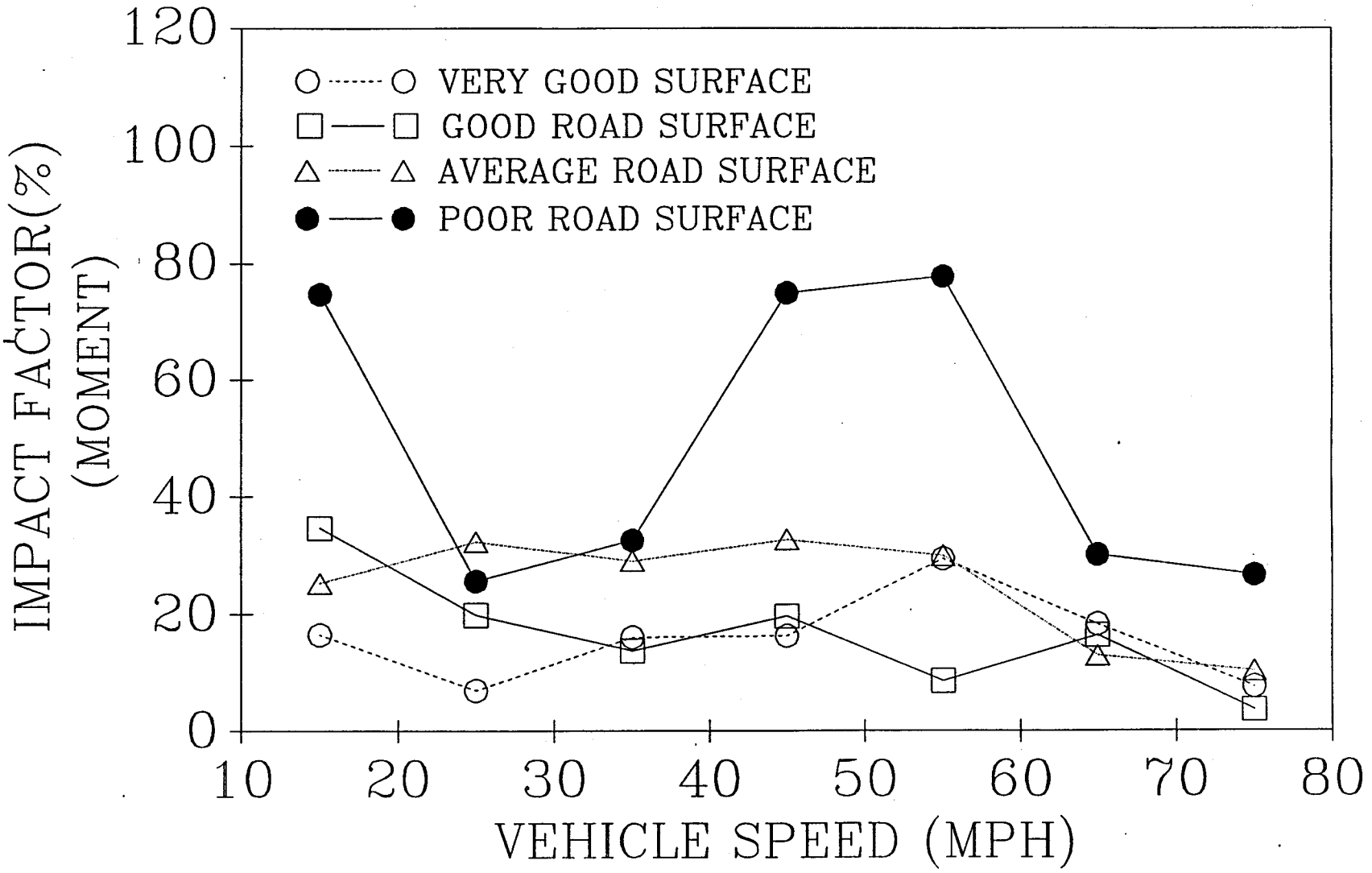

Fig. 3-38. Variation of Impact Factors with Vehicle Speeds at Section 1 of Girder 1 for Bridge of 56-70-56 ft.

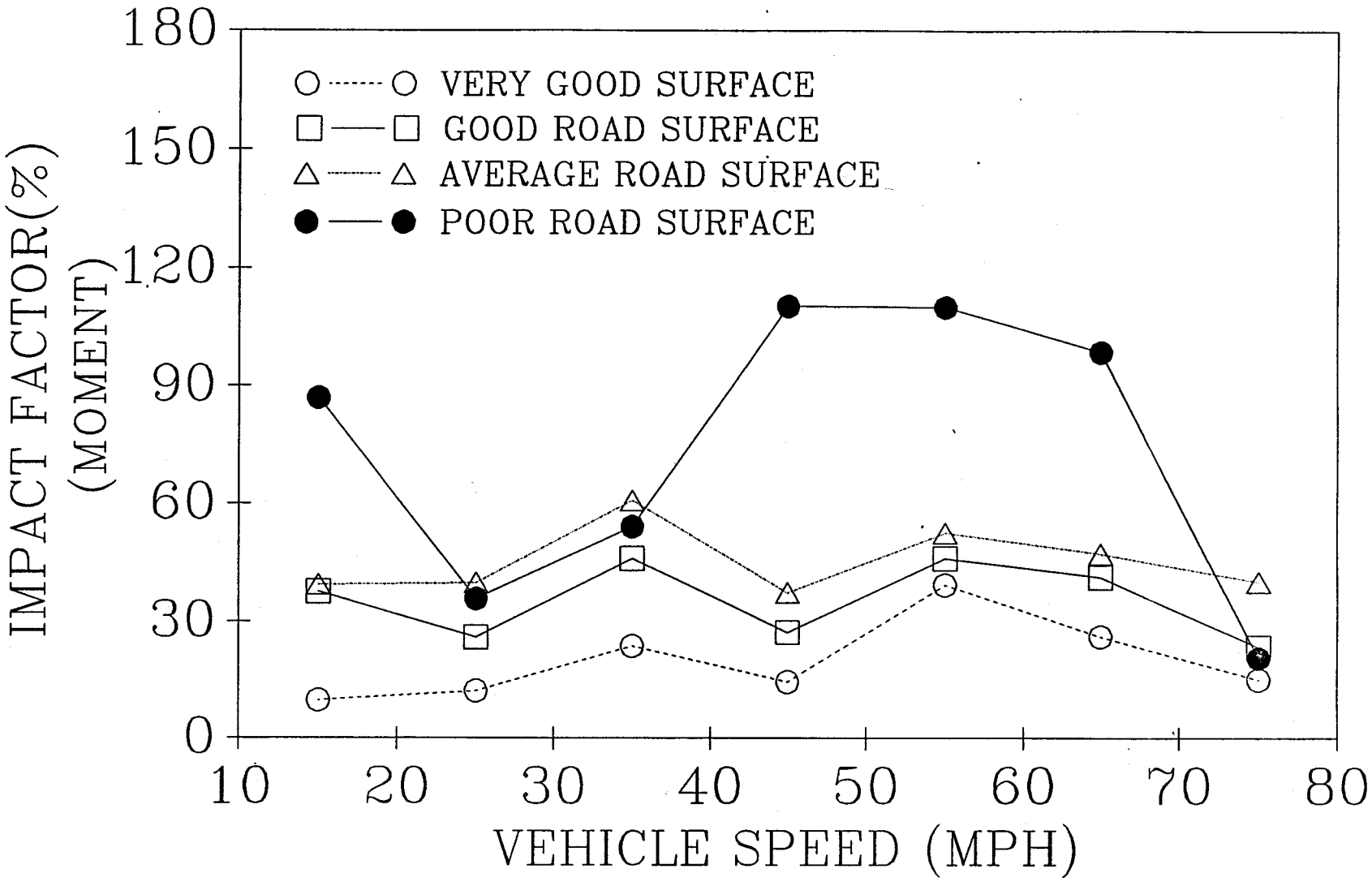

Fig. 3-39. Variation of Impact Factors with Vehicle Speeds at Section 2 of Girder 1 for Bridge of 56-70-56 ft.

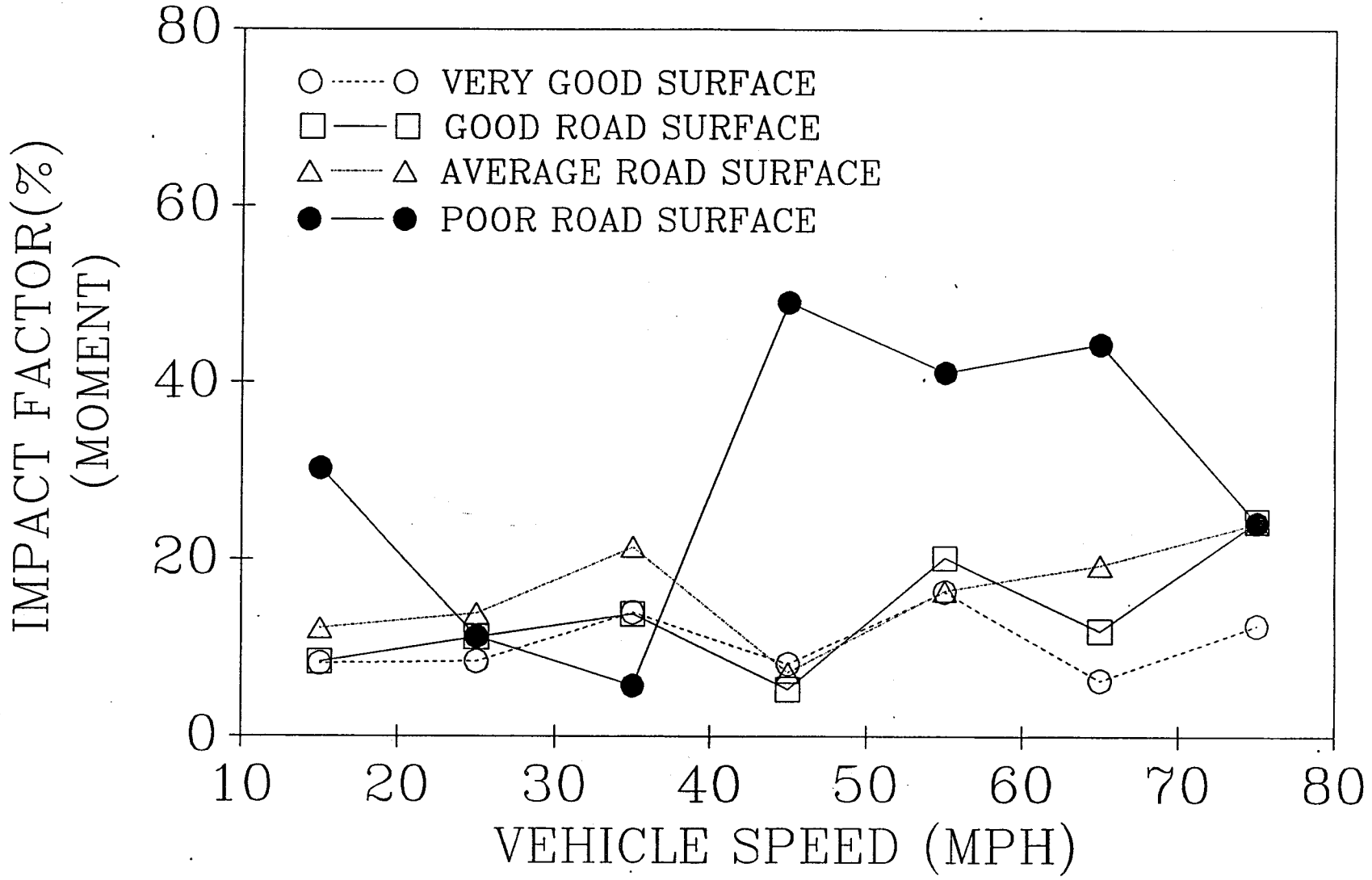

Fig. 3-40. Variation of Impact Factors with Vehicle Speeds at Section 3 of Girder 1 for Bridge of 56-70-56 ft.

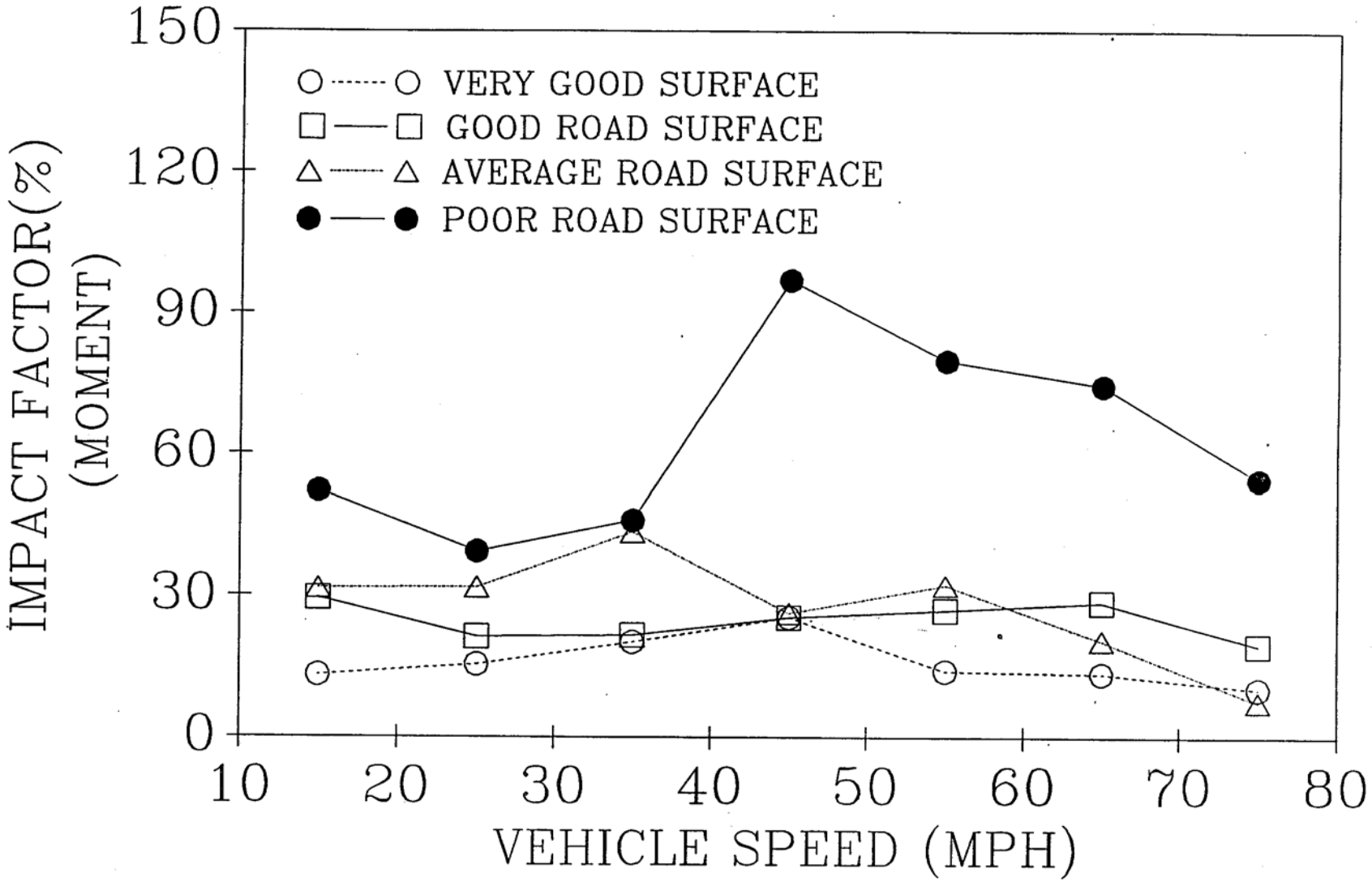

Fig. 3-41. Variation of Impact Factors with Vehicle Speeds at Section 1 of Girder 1 for Bridge of 40-50-40 ft.

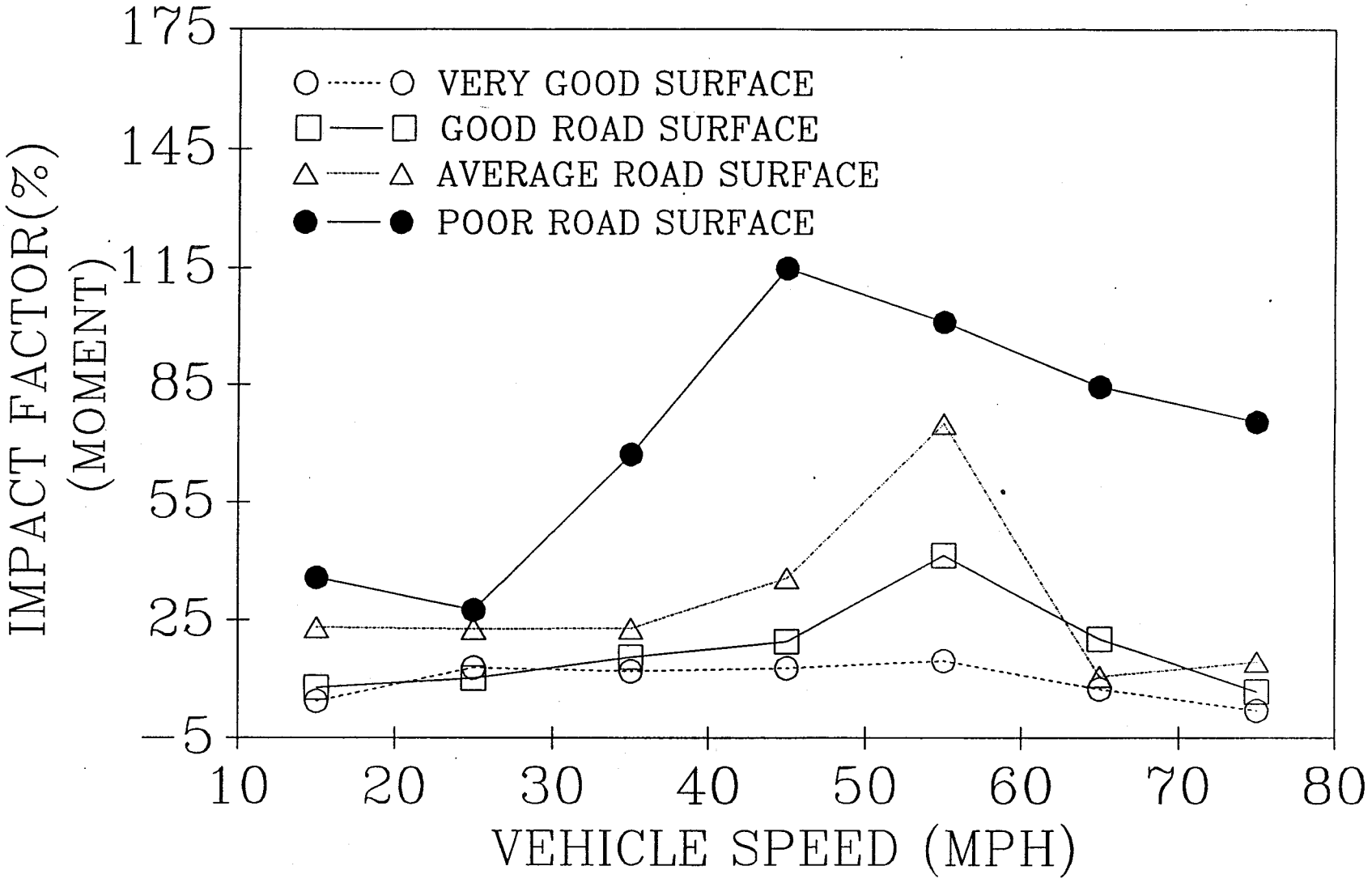

Fig. 3-42. Variation of Impact Factors with Vehicle Speeds at Section 2 of Girder 1 for Bridge of 40-50-40 ft.

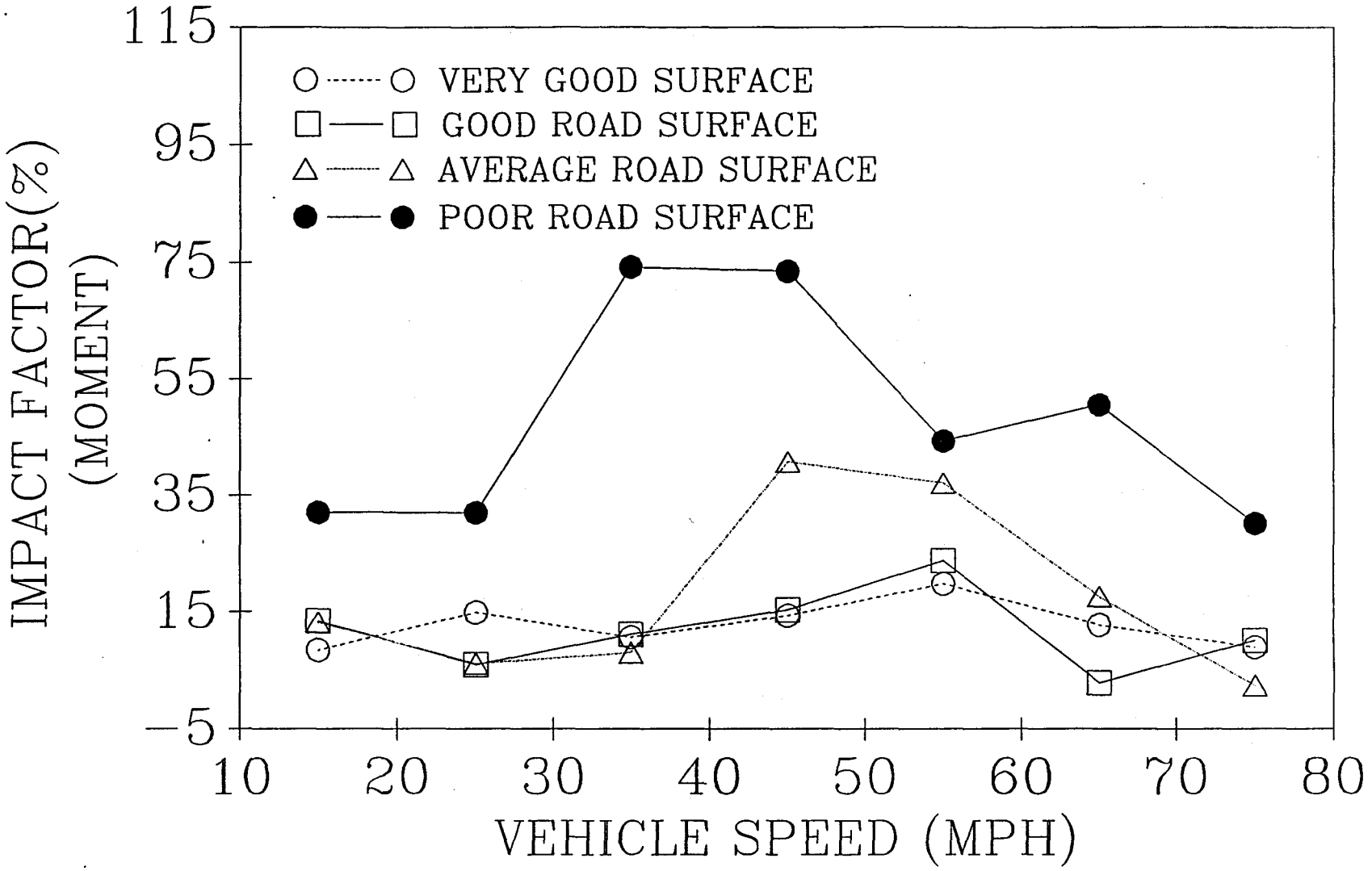

Fig. 3-43. Variation of Impact Factors with Vehicle Speeds at Section 3 of Girder 1 for Bridge of 40-50-40 ft.

the sections over interior supports. (3) With the variation of vehicle speeds, the impact factors at each section appear one or more peak values. The speed corresponding to the peak value of impact factor generally varies with different road roughness, span lengths, and sections. If the frequencies of both vehicle and bridge, which were excited by vehicle moving on rough road surface, are quite close or multiple values with each other, the response of the bridge will reach its peak value. In other words, the appearance of the peak value mainly results from the resonance between bridge and vehicle.

Effect of Span Length

Many investigations have indicated that the span length is one of the major variables affecting the vibration of the bridge. The AASHTO specifications give the impact equation which is the function of the span length that is the length of span under consideration for a positive moment and the average of two adjacent spans for a negative moment. .

In order to know the influence of the span length on the vibration of continuous multigirder bridges, the maximum impact factors of bending moment of six bridges in Girders 1 to 3 at Sections 1 to 5 for different road surface roughnesses were evaluated and given in Tables 3-5 to 3-7. The maximum moment impact factors were computed according to the variation of vehicle speeds from 15 MPH (24.135 km/hr) to 75 MPH (120.675 km/hr) and the variation of transverse position of two-truck loading illustrated in Fig. 3-16. As Sections 1 and 5 as well as Sections 2 and 4 are symmetrical sections about the center section of the bridge, respectively, only the larger impact factors of the symmetrical sections were given in Tables 3-5 to 3-7.

Table 3-5. Maximum Impact Factors of Bending Moments of Bridges.
(Very Good Road Surface Roughness)

Section	Girder	Span Length (ft)					
		80-100-80	72-90-72	64-80-64	56-70-56	48-60-48	40-50-40
No. 1 and No. 5	1	12.46	13.44	16.40	29.33	27.13	25.41
	2	6.37	7.16	8.67	19.25	18.42	14.45
	3	3.04	4.61	5.61	15.34	15.76	11.50
No. 2 and No. 4	1	14.34	14.86	26.61	38.23	32.93	27.34
	2	14.00	11.73	24.24	31.89	25.42	16.25
	3	15.66	11.40	24.11	28.34	19.72	14.19
No. 3	1	7.54	6.88	12.23	16.31	19.19	19.72
	2	3.92	2.67	6.15	9.59	13.09	7.81
	3	3.08	1.27	1.48	8.09	13.23	4.12

Table 3-6. Maximum Impact Factors of Bending Moments of Bridges.
(Good Road Surface Roughness)

Section	Girder	Span Length (ft)					
		80-100-80	72-90-72	64-80-64	56-70-56	48-60-48	40-50-40
No. 1 and No. 5	1	16.44	17.36	24.23	34.64	30.08	31.35
	2	9.40	9.39	19.74	22.52	20.77	22.24
	3	6.58	4.53	18.95	17.51	17.00	19.83
No. 2 and No. 4	1	19.70	18.03	36.29	46.03	40.83	41.54
	2	20.14	16.62	28.90	37.30	33.44	22.47
	3	19.93	17.03	22.17	32.20	27.80	15.25
No. 3	1	14.55	14.28	21.56	24.32	20.38	23.73
	2	10.54	10.01	15.12	18.82	14.80	8.66
	3	9.32	8.99	14.07	18.07	12.22	1.94

Table 3-7. Maximum Impact Factors of Bending Moments of Bridges.
(Average Road Surface Roughness)

Section	Girder	Span Length (ft)					
		80-100-80	72-90-72	64-80-64	56-70-56	48-60-48	40-50-40
No. 1 and No. 5	1	22.34	29.22	36.04	33.12	42.61	47.93
	2	15.74	21.17	25.47	24.33	28.79	27.22
	3	10.46	16.46	17.02	20.04	21.21	24.39
No. 2 and No. 4	1	29.75	29.95	40.62	58.15	69.91	75.09
	2	34.61	25.34	37.72	52.67	56.14	41.54
	3	36.24	25.30	38.28	48.91	52.07	31.59
No. 3	1	18.63	21.35	15.26	23.06	29.83	40.67
	2	9.14	14.85	10.21	16.62	21.32	21.89
	3	7.92	14.60	9.32	14.53	17.80	20.65

It can be seen from Tables 3-5 to 3-7 that: (1) With very good and good surface roughness, the impact factors of most girders of the bridge with span length of 56 ft.-70 ft.-56 ft. at Sections 1, 2, 4 and 5 are larger than those of the other bridges, while the impact factors at Section 3 (middle span) increase with decreasing overall span length. (2) With average road surface roughness, the impact factors of exterior girders at all sections increase with shortening overall span. The phenomenon is due to that the rougher road surface excited the higher modes which affects the response of exterior girders. (3) The impact factors of exterior girders are much larger than those of interior girders and the smallest values of impact factors occurs in center girders at most sections.

In order to explain the effect of span length of continuous girder bridges more clearly, Figs. 3-44 to 3-46 give the curves of impact factors of exterior girder at Section 1 to 3 versus the span length which is defined according to the AASHTO specifications mentioned above. Figs. 3-44 to 3-46 also give the curves of impact factor evaluated based on the AASHTO impact equation for bridges which is presented as

$$I = \frac{50}{L+125} \quad (3\text{-}18)$$

in which L is span length defined above in ft.

From Figs. 3-44 to 3-46, we can observe that: (1) Two groups of the relational curves between impact factors and span lengths shown in Figs. 3-44 and 3-45 are comparatively consistent, especially for very good and good road surfaces. Oppositely, the relations presented

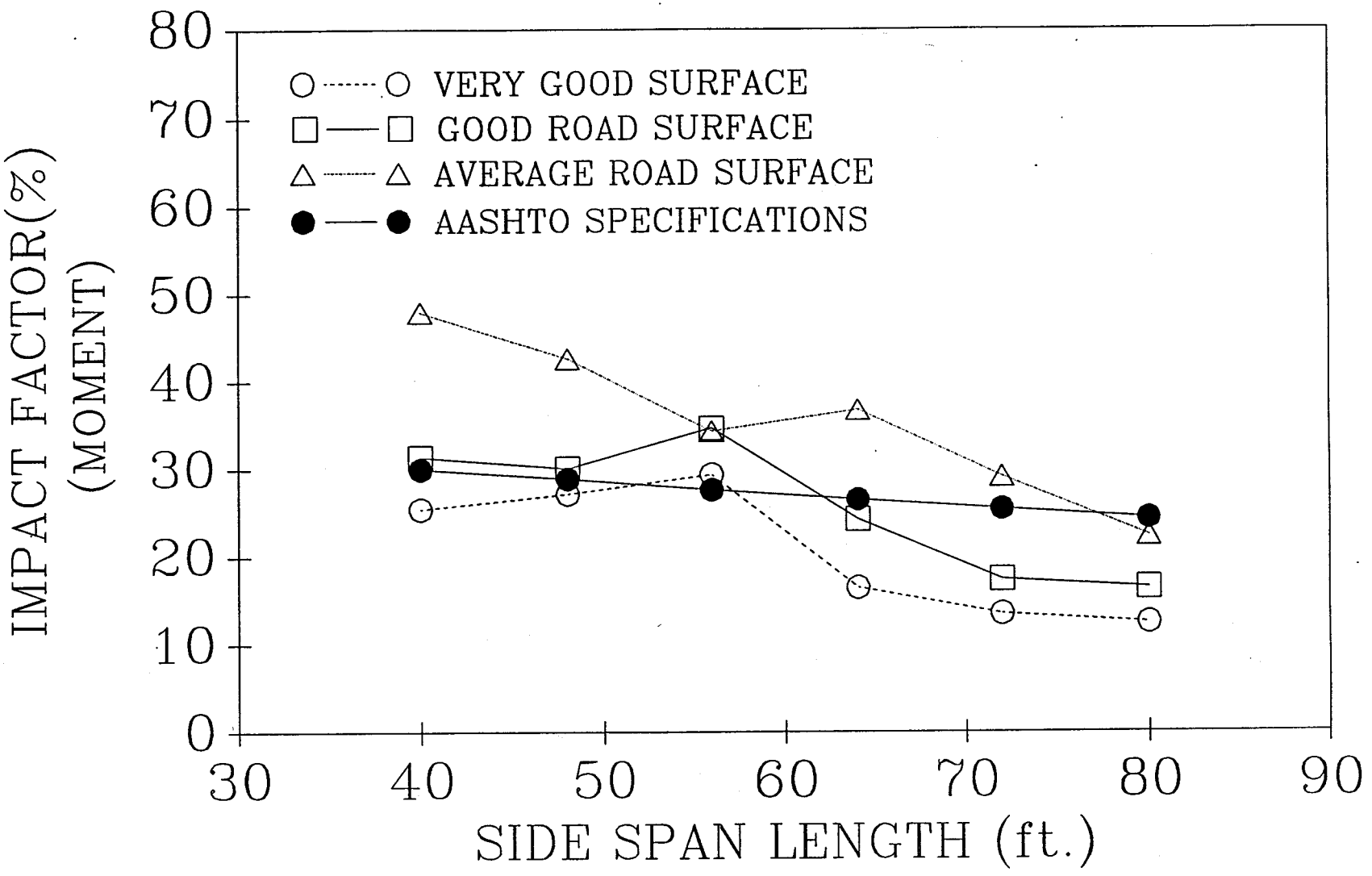

Fig. 3-44. Variation of Impact Factors with Span Lengths at Section 1 of Girder 1

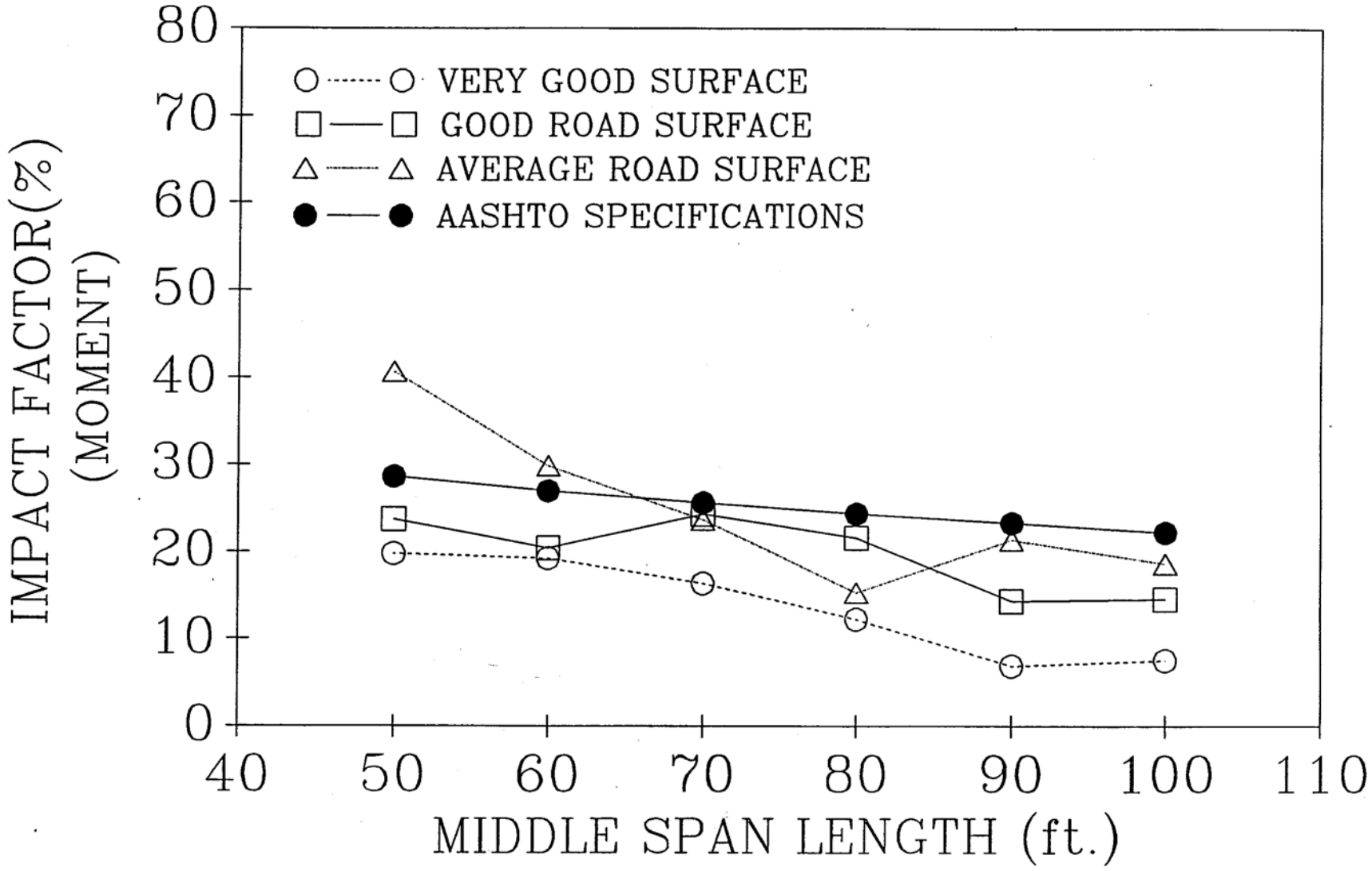

Fig. 3-45. Variation of Impact Factors with Span Lengths at Section 3 of Girder 1

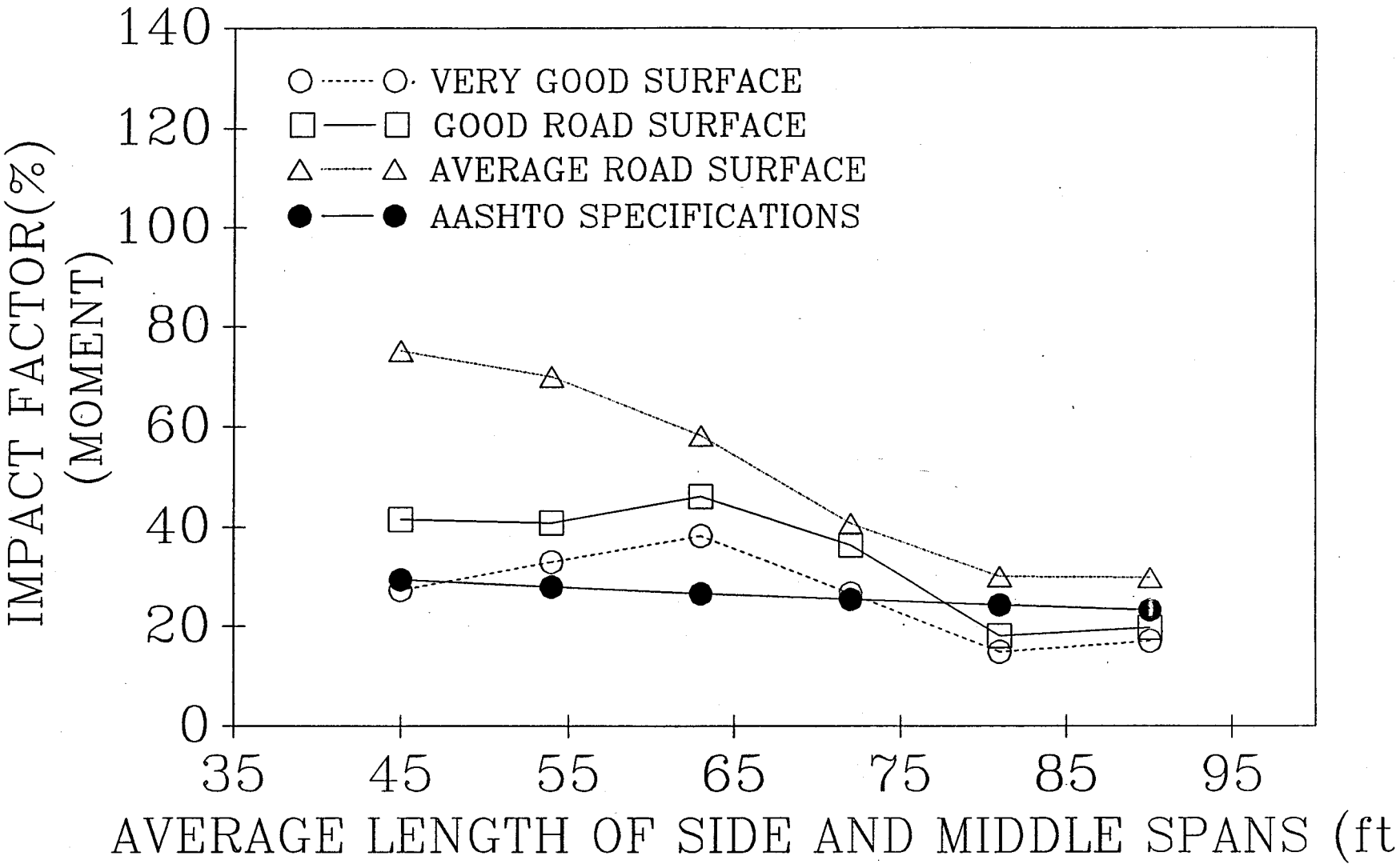

Fig. 3-46. Variation of Impact Factors with Span Lengths at Section 2 of Girder 1

in Fig. 3-46 are quite different from Fig. 3-44 and Fig. 3-45. This situation can be explained from mode shapes as follows (Figs. 3-5 to 3-14): As mentioned before, the first and second modes dominate the response of middle span, while the impact of the side span is principally affected by the third and fourth modes. Based on this, the vibration of both side and middle spans is similar to that of a simple beam. Consequently, the relations illustrated in Fig. 3-44 and Fig. 3-45 for side and, middle spans, respectively, will not be much different. On the other hand, the major effect on the response of the sections over interior supports is due to the fifth and sixth modes which are quite different from those of simple beam, while somewhat like those of fixed beam. As would be expected, the curves shown in Fig. 3-46 will not be consistent with those given in Figs. 3-44 and 3-45. Therefore, it may be more appropriate to use Eq. 3-18 to calculate the impact factor of negative moment over interior support with the distance 1_0 (refer to Fig. 3-10) between two inflexion points in mode 5 or 6, approximately the sum of 0.3 side span and 0.25 middle span length, instead of the average of side and middle spans. However, a more feasible method for predicting the impact factors of continuous girder bridges is yet to be developed. (2) Because of the effect of higher modes, the impact factors at Sections 2 and 4 for all six bridges are much larger than those of the other sections, especially for rougher road surface.

It can also be observed from Figs. 3-44 to 3-46 and Tables 3-5 to 3-7 that: (1) Most impact factors of bending moment of exterior girders at Section 1 with very good and good roads, at Section 3 with very good, good, and average roads as well as at Section 2 with very good roads are lower than the values specified by AASHTO specifications. However, the impact factors over interior supports for bridges with span of 56-70-56 ft. and 48-60-48 ft. exceed the

values evaluated by AASHTO impact factor equation. (2)Under the condition of very good and good roads, most impact factors of interior girders are lower than the values calculated by AASHTO impact equation. (3) Very high impact factors will be found in poor road surface.

It should be noted that the maximum impact factors presented in Tables 3-5 to 3-7 are based on one truck in the longitudinal direction of the bridges. It may be expected that lower impact factors will occur for more heavier design loading.

Effect of Spacing of Girders

The spacing of girders is an important parameter which affects the static wheel-load distribution. In order to understand the influence on dynamic response of the continuous multigirder steel bridges, the spacing of 6.5 ft. (1.9812 m) shown in Fig. 3-3 was changed to 8 ft.(2.4384 m). The maximum static wheel-load distribution and impact factors of bending moment for the bridge with span of 64 ft.-80 ft.-64 ft. were given in Table 3-8. The results listed in Table 3-8 were obtained based on good road surface through changing vehicle speeds and transverse positions of two-truck loading, as described above. It can be observed from Table 3-8 that: (1) With the increase of spacing of girders, the static wheel-load distribution factors of each girder increase, while the impact factors of interior girders decrease. (2) Due to the increase of the spacing, the effect of torsion on exterior girder increases. In consequence, the impact factors at Sections 1 and 3 increase slightly even though their static wheel-load distribution factors increase. However, the variation of most impact factors with the spacing of girders is insignificant.

Section		1			2			3		
Girder		1	2	3	1	2	3	1	2	3
Static Distribution Factor	A`	1.138	1.063	0.921	1.178	1.058	0.925	1.139	1.066	0.919
	B"	1.305	1.199	1.015	1.344	1.187	1.040	1.316	1.200	0.998
Maximum Impact Factor of Moment	A'	17.54	9.01	7.72	36.29	28.90	22.17	21.16	15.12	14.07
	B"	21.37	5.26	2.90	35.14	22.81	17.26	23.58	12.52	11.47

Note: 'A ------ Spacing of 6'-6"
"B ------ Spacing of 8'-0"

Effect of Damping Ratio

In order to know the influence of damping ratio, Table 3-9 presents the impact factors of Girder 1 of the bridge with span length of 64 ft.-80 ft.-64 ft. These data were obtained based on the conditions of good road surface, Loading No. 4 (see Fig. 3-16) and vehicle speed of 55 MPH (88.5 km/hr). From Table 3-9, it can be seen that the influence of damping ratio on the impact factors of each section is different. The impact of Section 3 was affected slightly by increasing damping ratios from 0 % to 3 %. While the impact of Section 2 decreases distinctly with increasing damping ratio. This can be explained by the fact that the fundamental natural mode is the principal contributor to the response at Section 3 and higher modes are the dominant effect of the response at Section 2.

Table 3-9. Effect of Damping Ratio.

Section	Damping Ratio (Impact Factors %)			
	No Damping	1 % for the First and Second Modes	2 % for the First and Second Modes	3 % for the First and Second Modes
1	11.19	10.50	10.14	9.96
2	40.98	36.29	32.94	29.89
3	14.48	14.10	13.89	13.42

CHAPTER IV

DYNANIIC BEHAVIOR OF SLANT-LEGGED RIGID FRAME HIGHWAY BRIDGES

4.1. Introduction

The slant-legged rigid frame bridge is one of the widely used types of highway bridges in the world. Engineers treat the entire super- and substructures as one unit by constructing a continuous steel rigid frame with supporting legs as shown in Fig. 4-1. This type of construction eliminates the need for concrete piers and positions the supports away from the lower roadway, thus giving a safer structure. Generally, this type of bridge can reduce the depth of main girder and save the material in the super structure. Consequently, the ratio of live load to dead load will be comparatively large. Moreover, at present, most of slant-legged rigid frame bridges are short or medium span bridges. Therefore, the investigation of the responses of slant-legged rigid frame bridges due to moving vehicles is very important and practically significant. Unfortunately, little dynamic behavior of slant-legged rigid frame bridges has been reported yet. Most previous research work on dynamic response of bridges due to moving vehicles was concentrated on the beam/girder bridges [2, 9, 12, 14, 26, 27, 29, 31] and some other bridges [10, 16, 30]. In the design of slant-legged rigid frame bridges, engineers use AASHTO impact formula (Eq. 3-18). However, this is still lack of reliable scientific base.

Herein the objective of this study is to investigate the response characteristics of a slant-

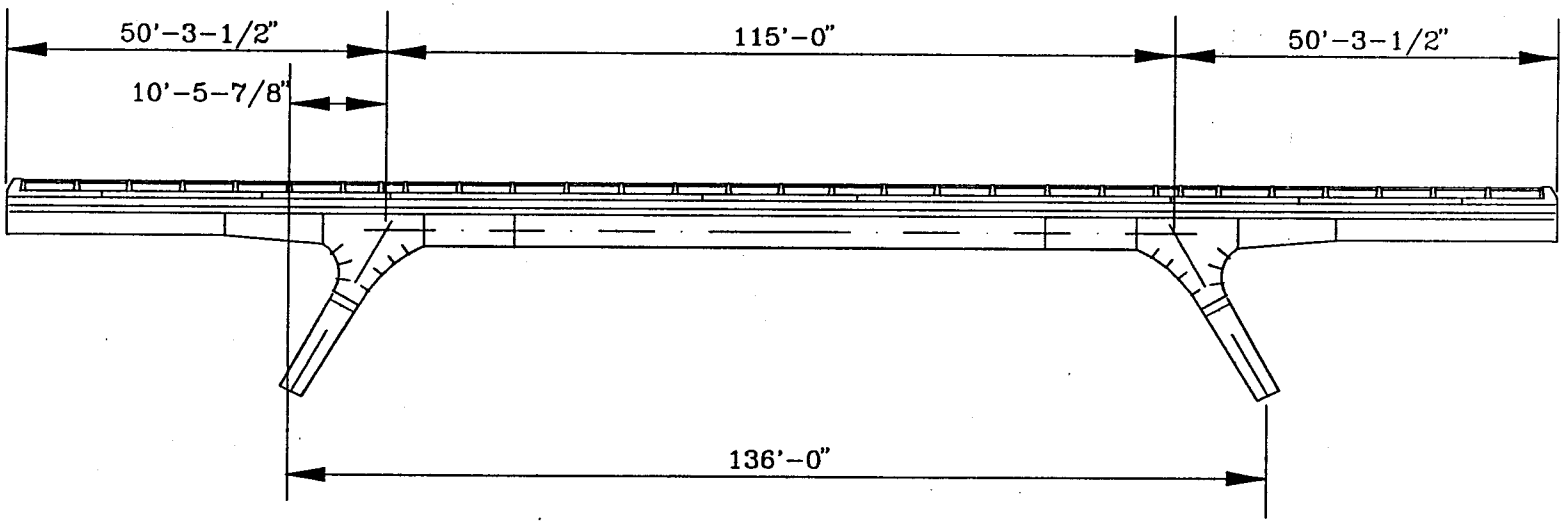

Fig. 4-1. Elevation of Bridge

legged rigid frame bridge for one or two vehicles (side by side) passing over the bridge and to analyze the impact due to the vehicles moving over different classes of road surface roughnesses with various speeds. In this study, the bridge was idealized as a space bar system. The traveling vehicle was treated as a nonlinear space system. Investigation shows that the variation of impact of bending moment along with the longitudinal direction of the bridge is very sharp. The impact behaviors of deflection, moment, and axial force at some design control sections are quite different.

A description of the bridge model is given first. Then, the free vibration characteristics of the slant-legged rigid frame bridge is discussed. Finally, the impact behavior of the bridge is studied. In the later investigation, the vehicle model, road surface roughness, and the numerical method are the same as those described in Chapter III.

4.2. Bridge Model

Figs. 4-1 and 4-2 illustrate the analytical bridge which is chosen from Kinnier and Barton (1975). The bridge is 214.5 ft. (65.38 m) long and consists of five three-span welded rigid frames. The two interior supports are inclined I-shaped columns framed integrally with the welded haunched girders and supported on concrete footing with anchor bolts attached to the web in such a manner as to allow free rotation. The ends of the bridge are simply supported on shelf abutments with allowance for longitudinal movements. The bridge was designed for a HS20-44 live load in accordance with AASHTO specifications (1965). The bridge has a roadway width of 39.33 ft. (11.99 m) and 8 in. (20.32 cm) thick concrete slab which was

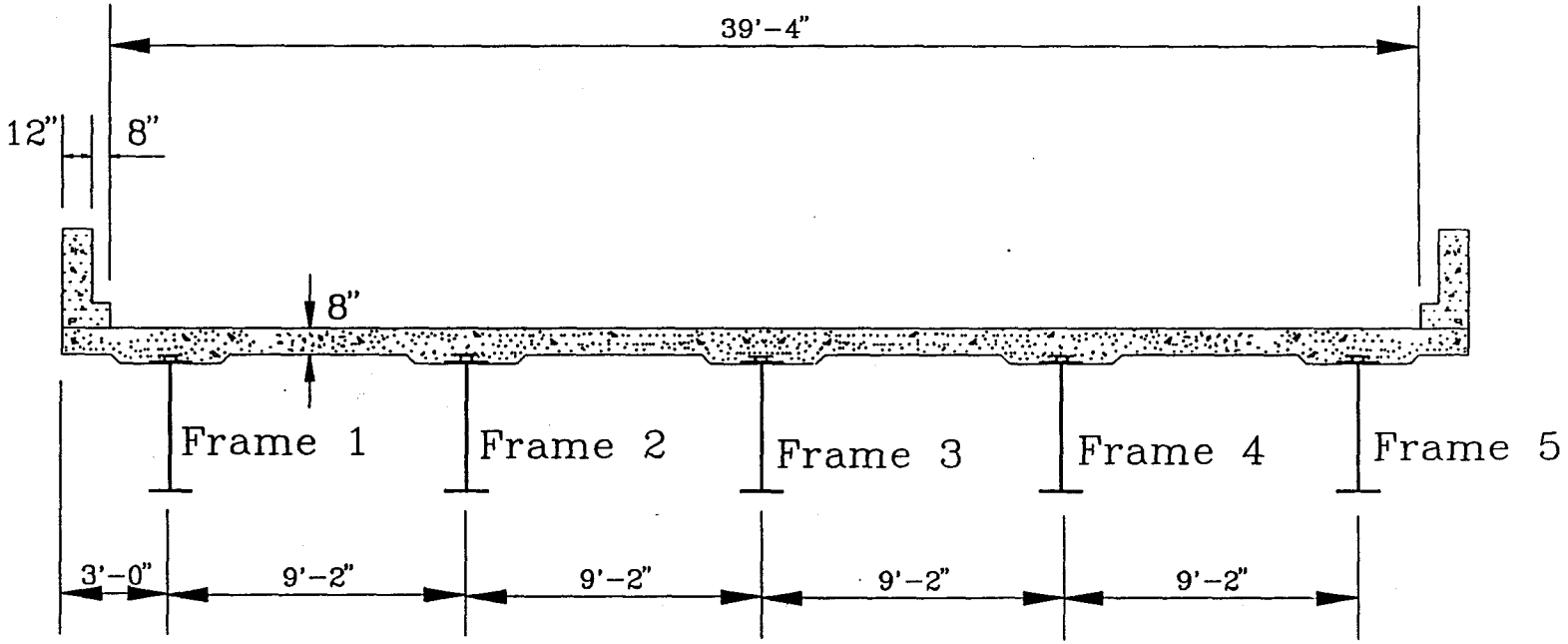

Fig. 4-2. Cross-section of Bridge

connected by shear studs with steel girders.

Based on AASHTO specifications, for composite beams, the concrete deck on the top flange of the girder is counted for the moment of inertia of each cross section. The main data obtained primarily from Kinnier and Barton [15] are listed in Table 4-1. In Table 4-1, the number of segments corresponds to the numbering in Fig. 4-3 and I_z, I_y = the moment of inertia about the z-axis and y-axis, respectively. The coordinate system used herein is a right-handed one (Fig. 4-4). The x-axis is supposed to pass through the centroids of member sections. For elements of frames, including main girders and legs, the y-axis is parallel to the transverse direction of the bridge. For elements of diaphragms and concrete deck, the y-axis is parallel to the longitudinal direction of the bridge.

The bridge is modeled as a space bar system (Fig. 4-5). The dynamic response of the bridge is analyzed by finite element method. Bridge structure is discretized into space beam elements, including girder elements, diaphragms, and concrete deck. The stiffness of girder element includes the composite action of concrete deck. The transverse stiffness of the concrete deck is considered in diaphragm elements and concrete deck elements.

Fig.4-4 shows the orientation of a three dimensional beam element with six degrees of freedom at each end. The node parameters of element are

$$\{\delta\}^e = \begin{Bmatrix} \delta_i \\ \delta_j \end{Bmatrix} \qquad (4-1)$$

Table 4-1. Main Data of the Bridge.

Name	Beam						Leg		Diaphragm
Segment	1	2	3	4	5	6	7	8	9
Area (in^2) $x10^2$	1.023	1.053	1.223	1.541	1.541	1.541	0.525	0.425	0.543
I_y (in^4) $x10^4$	1.835	2.957	18.352	9.360	6.782	6.467	6.065	1.017	6.447
I_z (in^4) $x10^4$	2.716	2.720	2.770	2.840	2.840	2.838	0.260	0.260	8.089
J_d (in^4) $x10^4$	1.641	1.645	1.652	1.720	1.720	1.740	0.150	0.110	0.325
Mass per unit (kip/in)	0.1030		0.1184			0.1178	0.0149	0.0121	0.0042

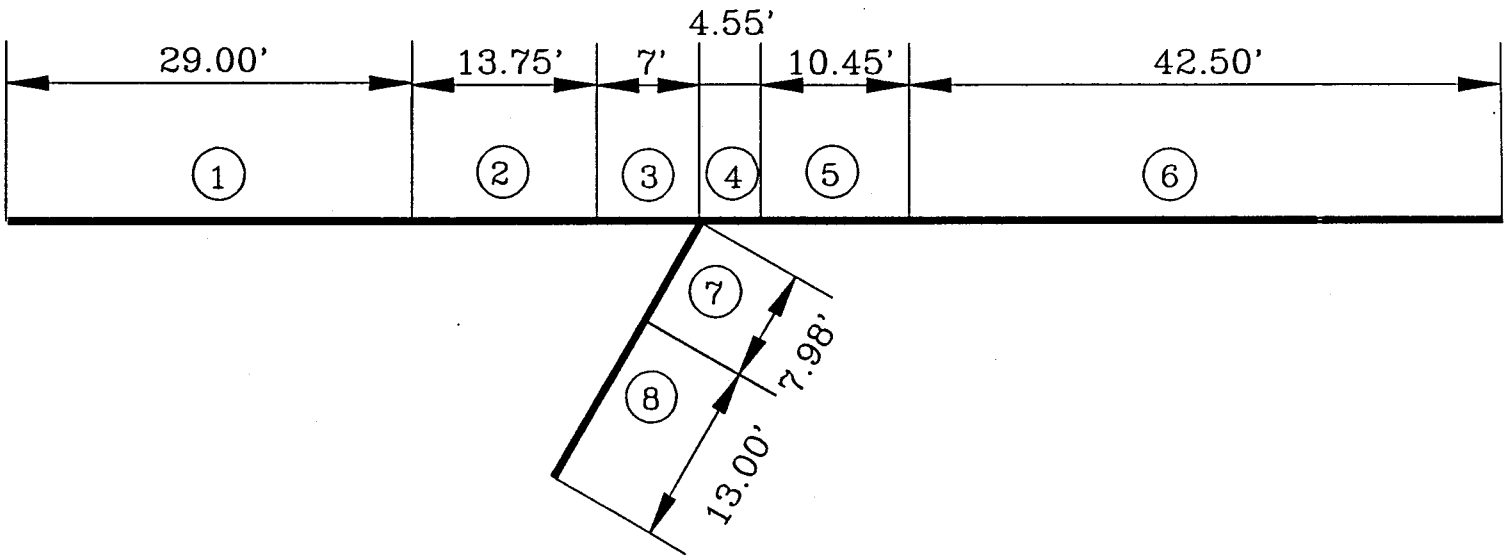

Fig. 4-3. Numbering of Segments

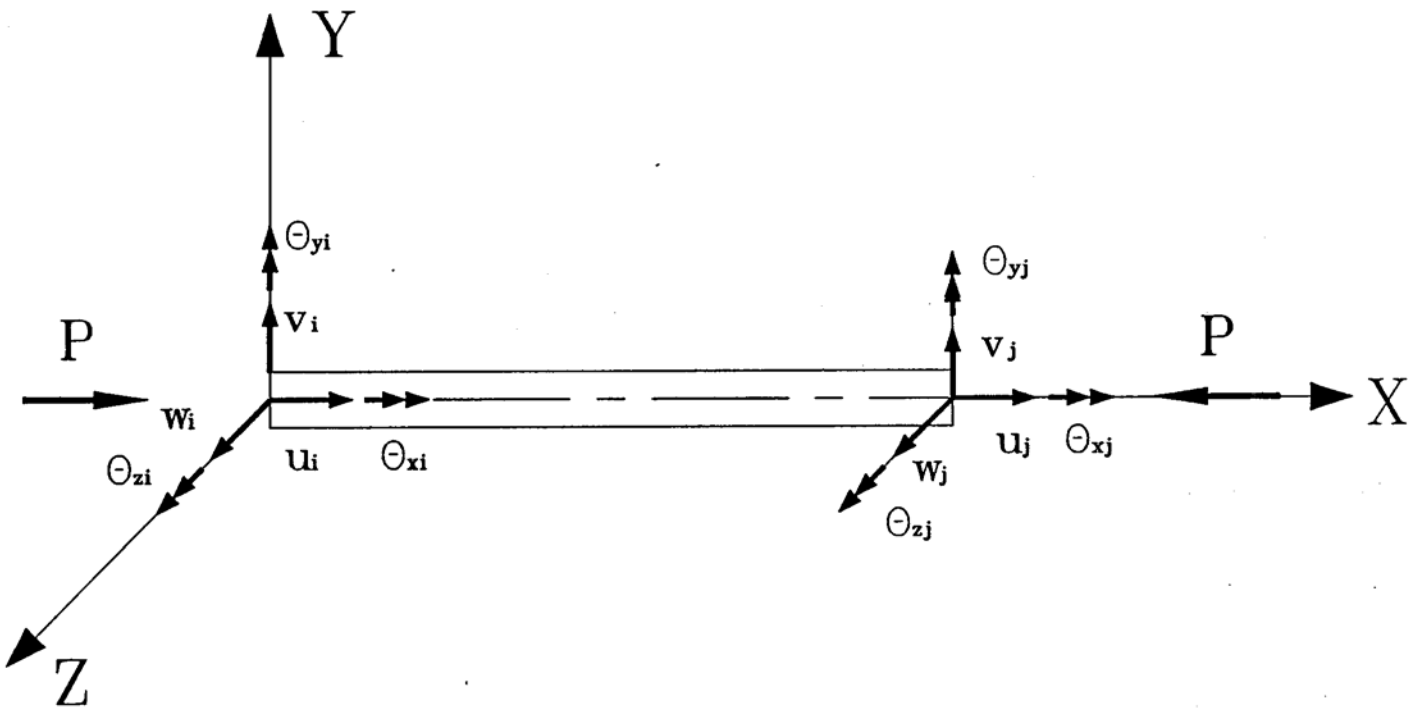

Fig. 4-4. Space Beam Element.

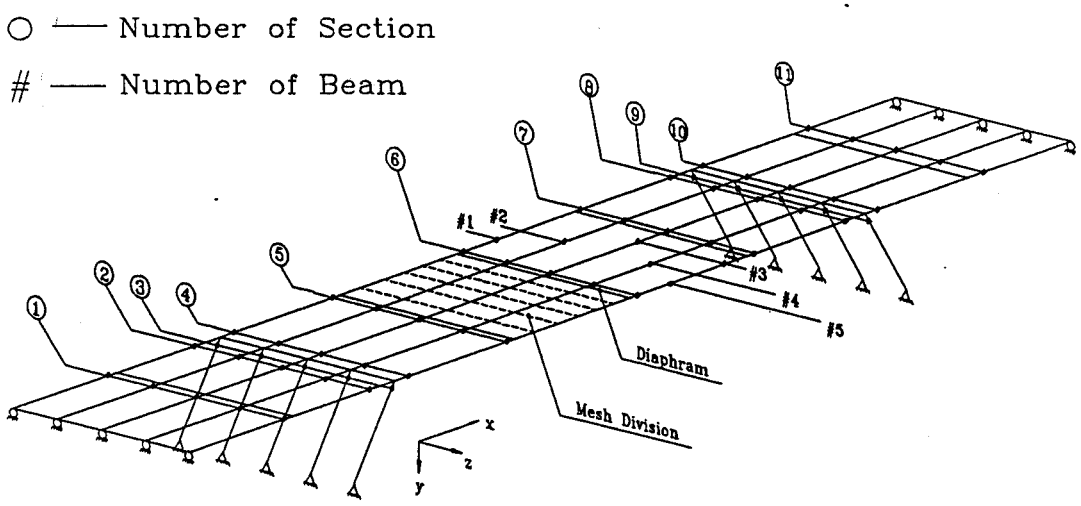
○ —— Number of Section
—— Number of Beam
①
②
③
④
⑤
⑥
⑦
⑧
⑨
⑩
⑪
#1
#2
#3
#4
#5
Diaphram
Mesh Division
x
z
y

in which $\{\delta_i\} = [u_i\ v_i\ w_i\ \theta_{xi}\ \theta_{yi}\ \theta_{zi}]^T$;

$\{\delta_j\} = [u_j\ v_j\ w_j\ \theta_{xj}\ \theta_{yj}\ \theta_{zj}]^T$;

u, v, w = transverse displacements in x, y and z directions, respectively; and

$\theta_x\ \theta_y\ \theta_z$ = rotational displacements in x, y, z directions, individually.

The element stiffness matrix of a prismatic beam (see Fig.4-4) can be written in the form

$$[k] = [k]_l + [k]_g \qquad (4\text{-}2)$$

in which the standard linear stiffness matrix $[k]_l$ is

$$[k]_l = \begin{bmatrix} k_{l11} & Sym. \\ k_{l21} & k_{l22} \end{bmatrix} \qquad (4\text{-}3)$$

$$[k_{l11}] = \frac{E}{l}\begin{bmatrix} A & & & & & \\ 0 & 12I_z/l^2 & & Sym. & & \\ 0 & 0 & 12I_y/l^2 & & & \\ 0 & 0 & 0 & GJ_d/E & & \\ 0 & 0 & -6I_y/l & 0 & 4I_y & \\ 0 & 6I_z/l & 0 & 0 & 0 & 4I_z \end{bmatrix} \qquad (4\text{-}4)$$

$$[k_{l21}] = \frac{E}{l}\begin{bmatrix} -A & 0 & 0 & 0 & 0 & 0 \\ 0 & -12I_z/l^2 & 0 & 0 & 0 & -6I_y \\ 0 & 0 & -12I_y/l^2 & 0 & 6I_y & 0 \\ 0 & 0 & 0 & -GJ_d/E & 0 & 0 \\ 0 & 0 & -6I_y & 0 & 2I_y & 0 \\ 0 & 6I_z & 0 & 0 & 0 & 2I_z \end{bmatrix} \qquad (4\text{-}5)$$

$$[k_{l22}] = \frac{E}{l}\begin{bmatrix} A & & & & & \\ 0 & 12I_z/l^2 & & Sym. & & \\ 0 & 0 & 12I_y/l^2 & & & \\ 0 & 0 & 0 & GJ_d/E & & \\ 0 & 0 & 6I_y/l & 0 & 4I_y & \\ 0 & 6I_z/l & 0 & 0 & 0 & 4I_z \end{bmatrix} \qquad (4\text{-}6)$$

A = area; I_z, I_y = moment of inertia about z-axis and y-axis respectively; J_d = torsion moment of inertia; and l = length of element; and the geometric stiffness matrix $[k]_g$ is

$$[k]_g = \begin{bmatrix} k_{g11} & Sym. \\ k_{g21} & k_{g22} \end{bmatrix} \qquad (4\text{-}7)$$

$$[k_{g11}] = \frac{P}{30l}\begin{bmatrix} 0 & & & & & \\ 0 & 36 & & Sym. & & \\ 0 & 0 & 36 & & & \\ 0 & 0 & 0 & \dfrac{30(I_y+I_z)}{A} & & \\ 0 & 0 & -3l & 0 & 4l^2 & \\ 0 & 3l & 0 & 0 & 0 & 4l^2 \end{bmatrix} \qquad (4\text{-}8)$$

$$[k_{g21}] = -\frac{P}{30l}\begin{bmatrix} 0 & 0 & 0 & 0 & 0 & 0 \\ 0 & -36 & 0 & 0 & 0 & -3l \\ 0 & 0 & -36 & 0 & 3l & 0 \\ 0 & 0 & 0 & \frac{-30(I_y+I_z)}{A} & 0 & 0 \\ 0 & 0 & -3l & 0 & -l^2 & 0 \\ 0 & 3l & 0 & 0 & 0 & -l^2 \end{bmatrix} \qquad (4\text{-}9)$$

$$[k_{g22}] = -\frac{P}{30l}\begin{bmatrix} 0 & & & & & \\ 0 & 36 & & \textit{Sym.} & & \\ 0 & 0 & 36 & & & \\ 0 & 0 & 0 & \frac{30(I_y+I_z)}{A} & & \\ 0 & 0 & 3l & 0 & 4l^2 & \\ 0 & 3l & 0 & 0 & 0 & 4l^2 \end{bmatrix} \qquad (4\text{-}10)$$

The matrix [k], represents the effect of axial force on the bending stiffness of the element. The mechanical behavior of the slant±legged rigid frame bridge is similar to that of the arch bridge. Under dead load, large axial force will be induced in legs and central segments of girders. The axial force will affect the response of a slant-legged rigid frame bridge. The influence of axial force mainly depends on the span length of the bridge. Generally, the longer the span length is , the larger the effect will be. For longer span bridges, the axial force caused by vehicle loads is much smaller. than that induced by dead load. Therefore, hereafter, only the axial forces produced by dead load are considered and treated as a constant in evaluating the 138

dynamic response of the bridge due to moving vehicles.

Element consistent mass matrix was used in the study and can be found in the reference [32].

The equations of motion of the bridge are shown in Chapter III (Eq. 3-2).

4.3. Free Vibration Characteristics

In this study, each of the longitudinal girders was divided into 52 elements and each of the legs was discretized into 5 elements. The eigenvalue problem was solved based on the hypothesis that the bridge is subjected to initial axial forces caused by dead load without initial deformation. The first ten computed three-dimensional mode shapes are shown in Figs. 4-6 to 4-15. As mentioned before, the slant-legged rigid frame bridge possesses the mechanical behavior of arch bridge. Therefore, the first mode shape is antisymmetric mode. The second and fourth modes are vertical bending, lateral bending, and torsional vibration modes. The third and fifth modes are symmetric vertical bending modes. From Figs. 4-6 to 4-15, we can also observe that the bridge has the characteristics of a continuous beam supported by two intermediate elastic supports.

4.4. Dynamic Response

4.4.1. Assumptions

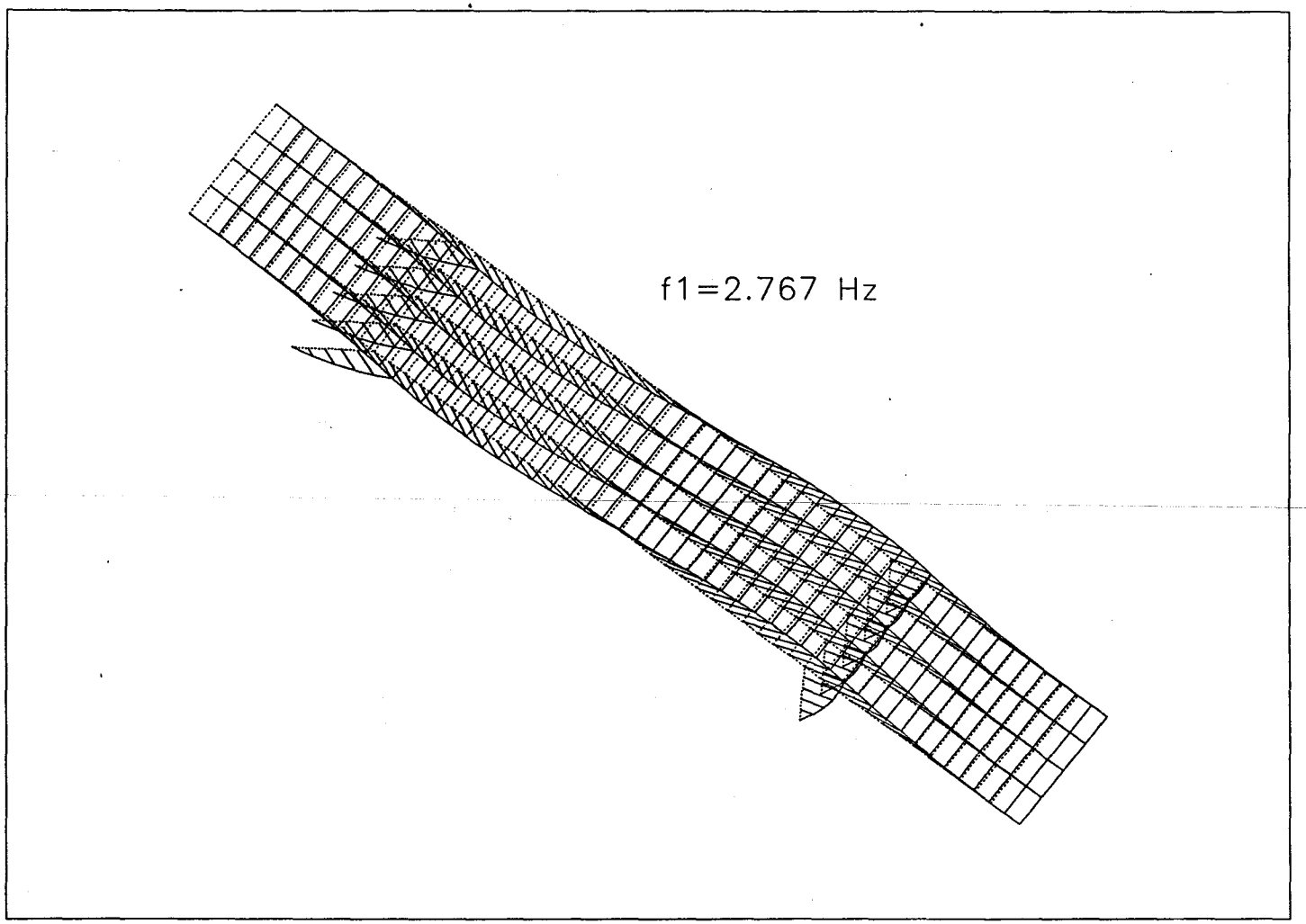

Fig. 4-6. The First Vibration Mode.

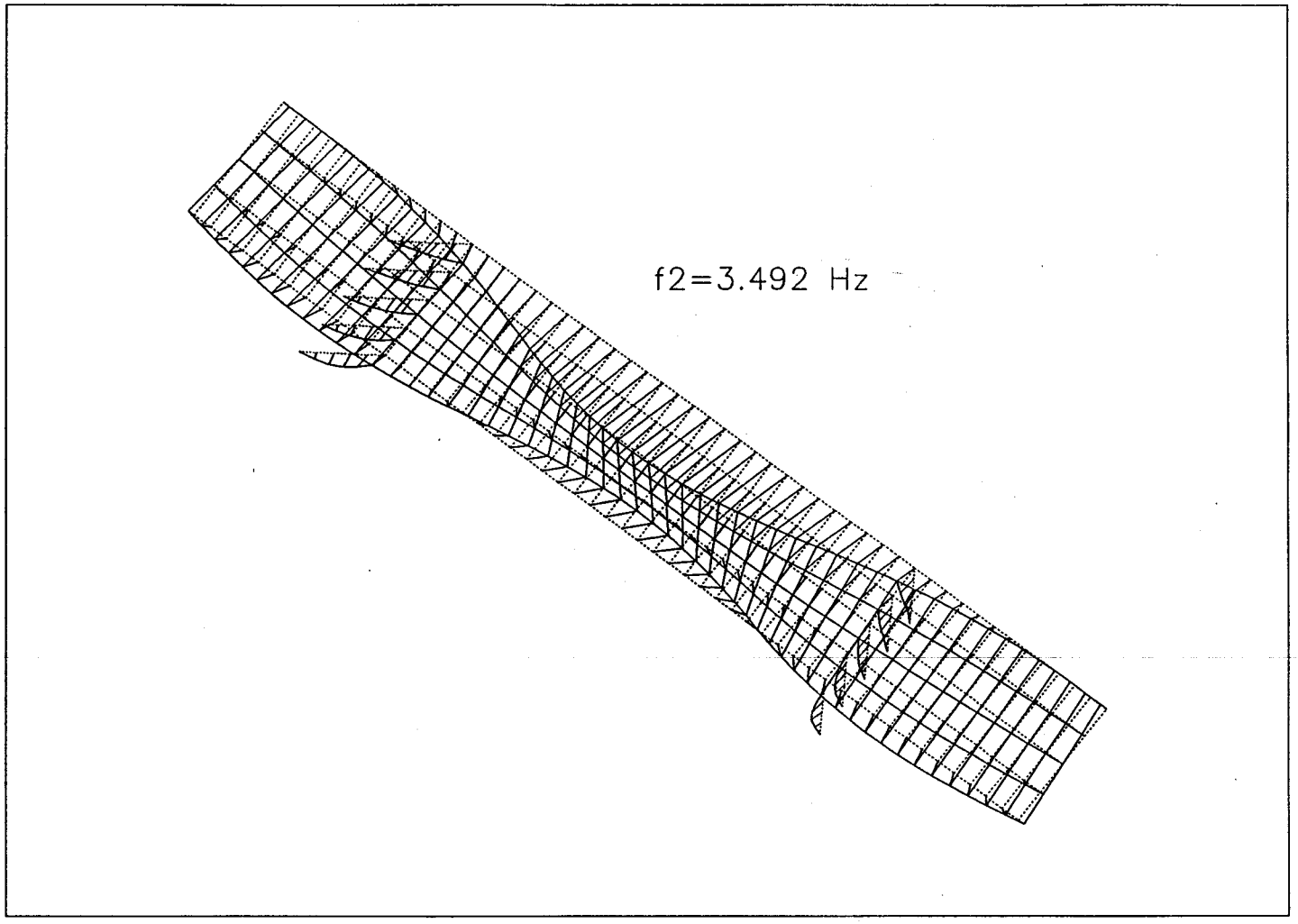

Fig. 4-7. The Second Vibration Mode.

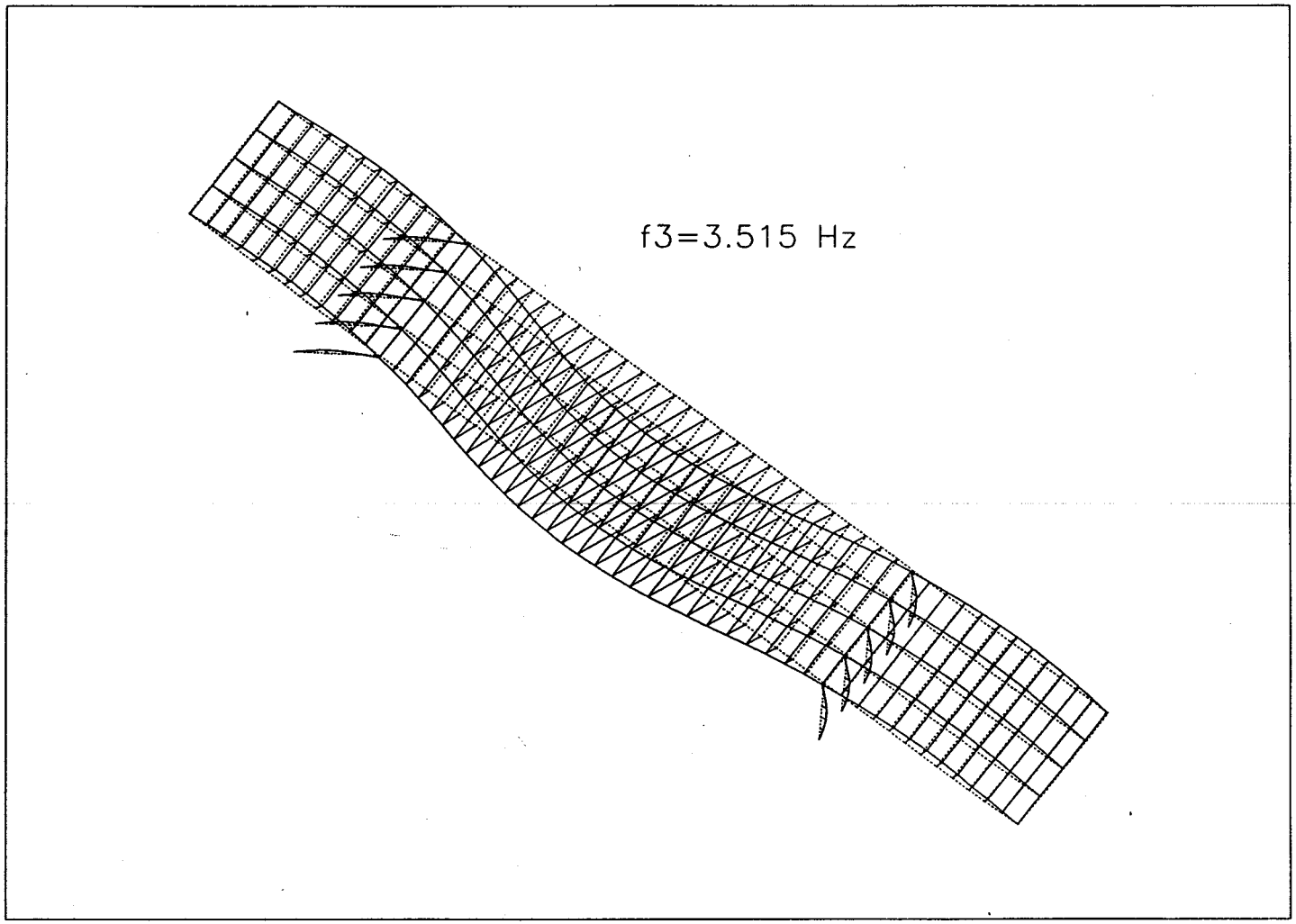

Fig. 4-8. The Third Vibration Mode.

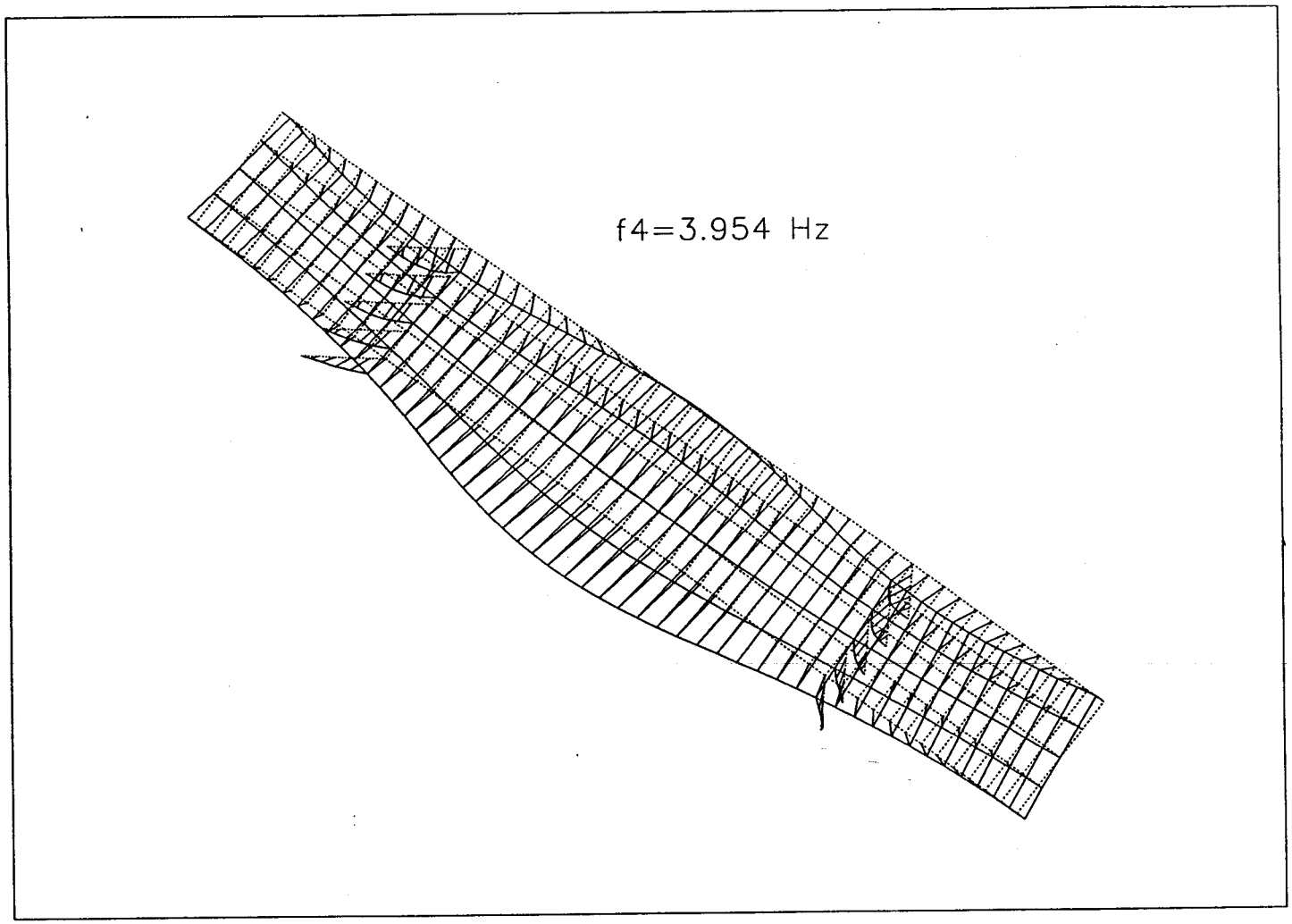

Fig. 4-9. The Fourth Vibration Mode.

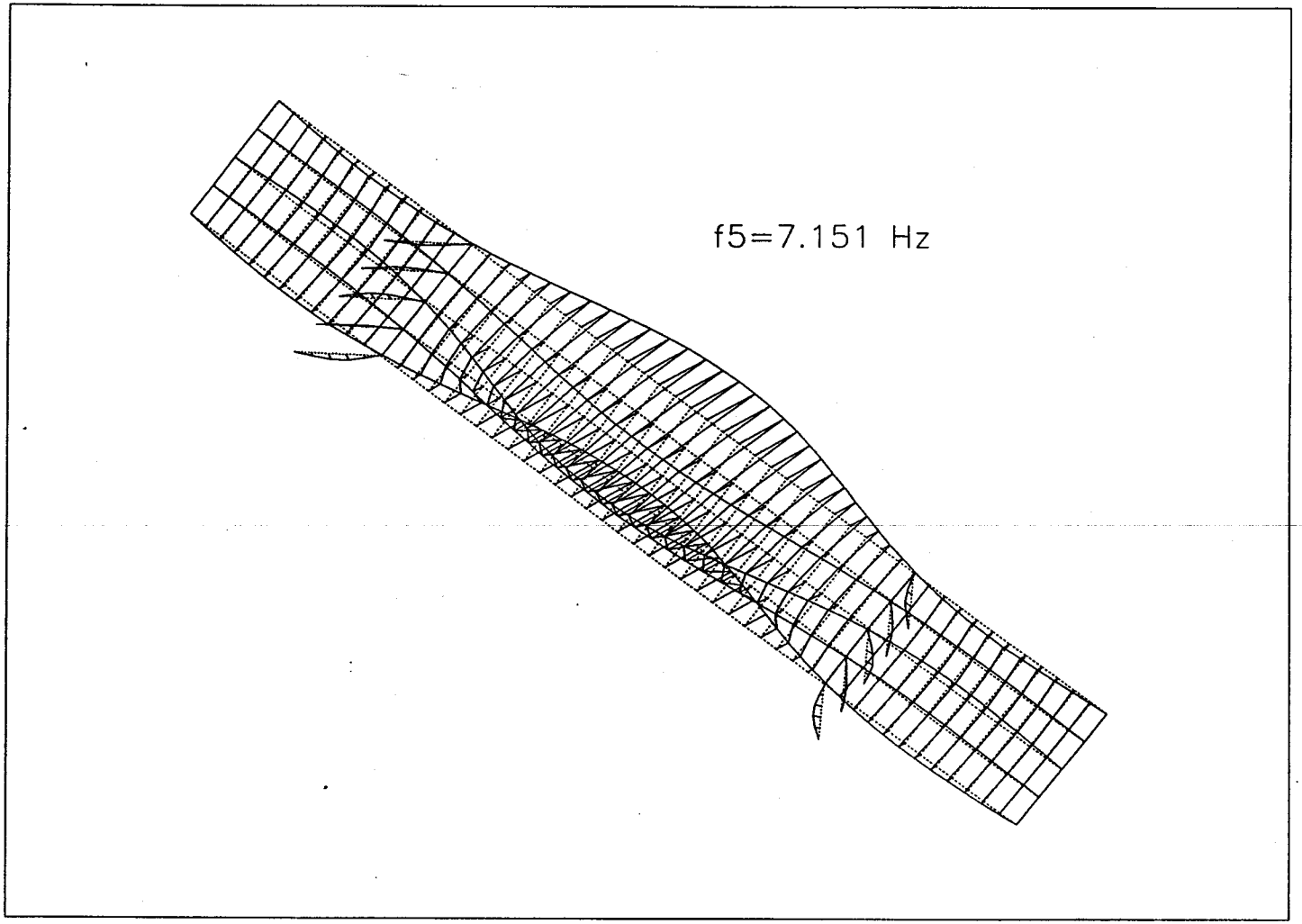

Fig. 4-10. The Fifth Vibration Mode.

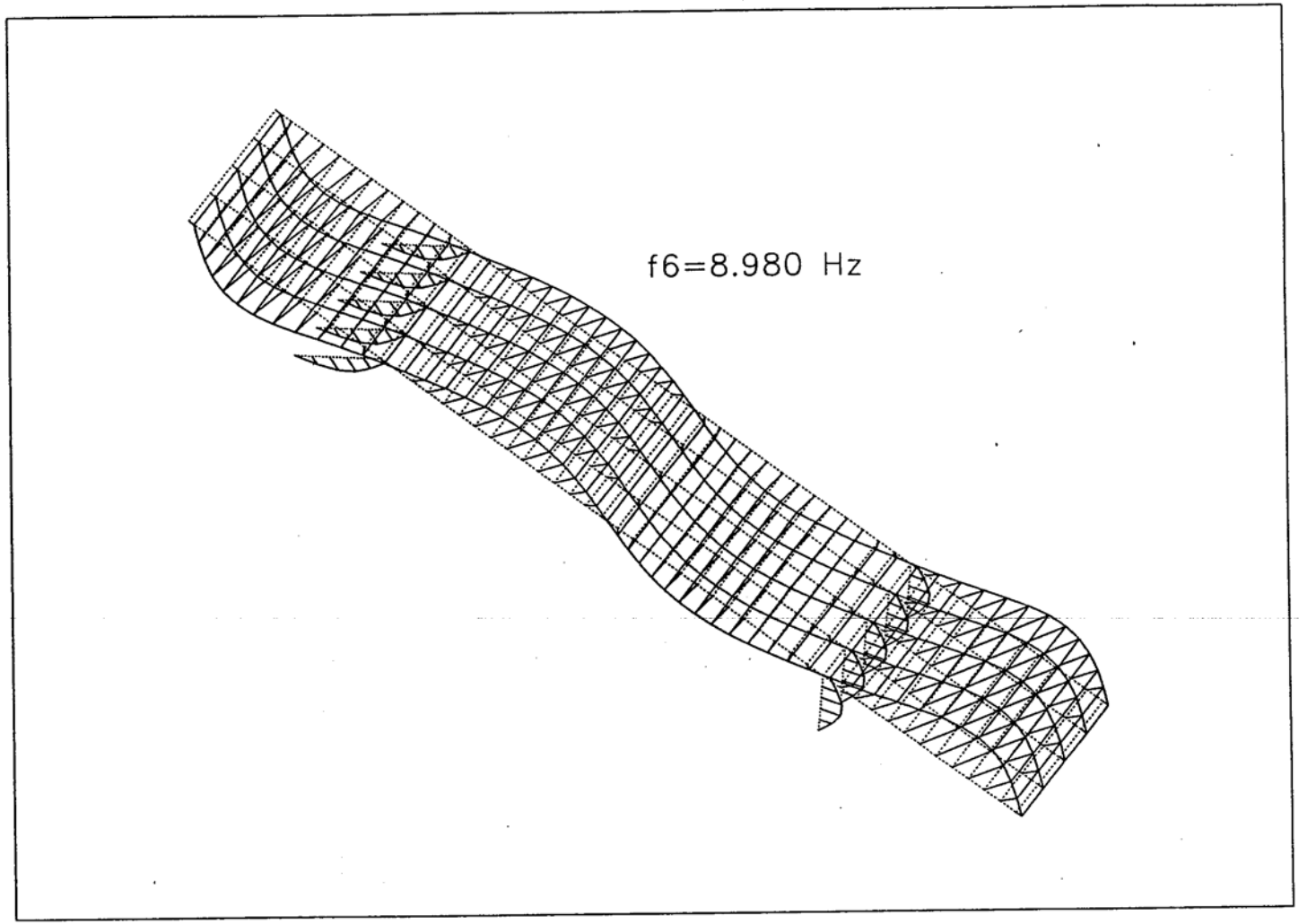

Fig. 4-11. The Sixth Vibration Mode.

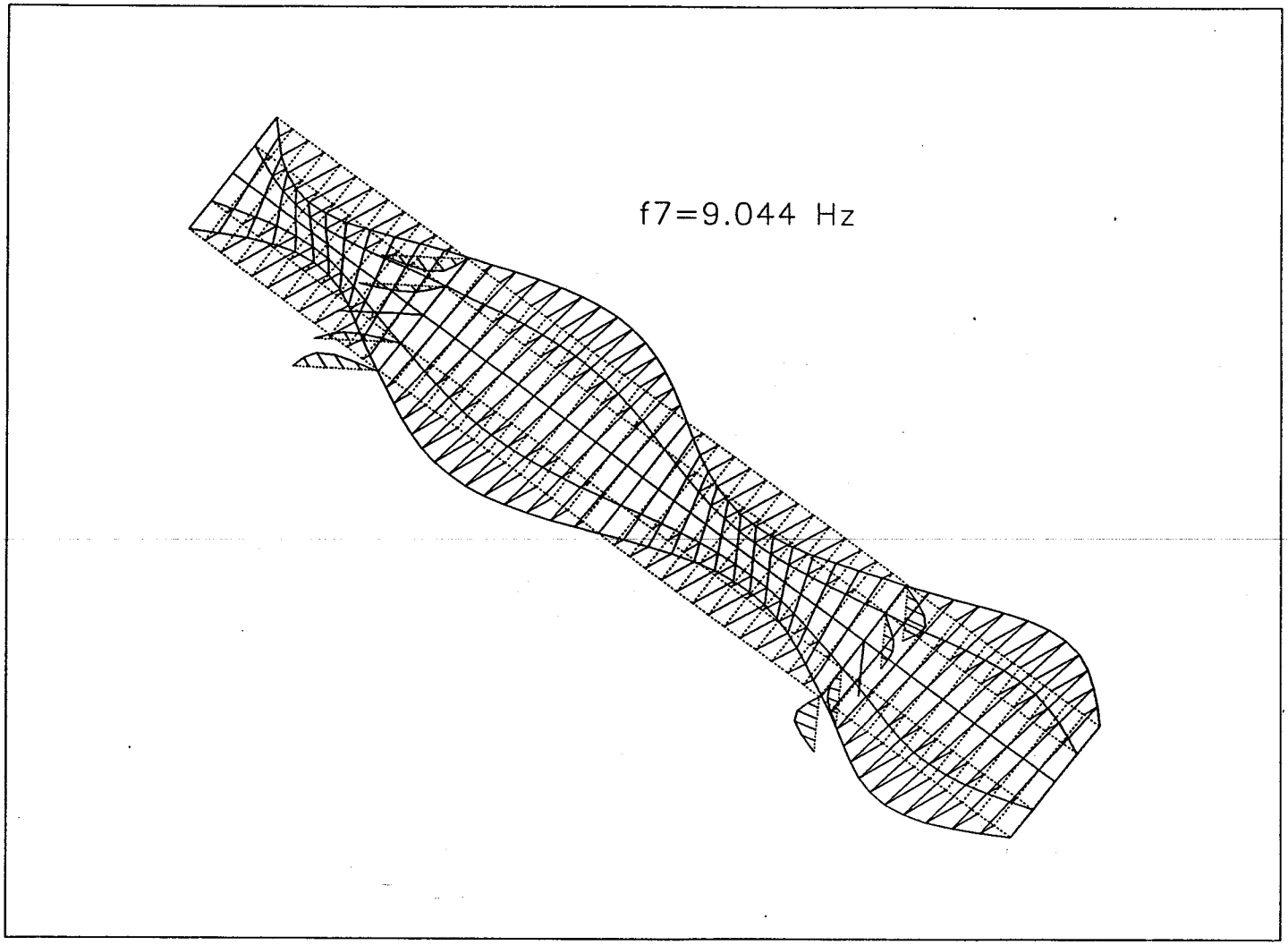

Fig. 4-12. The Seventh Vibration Mode.

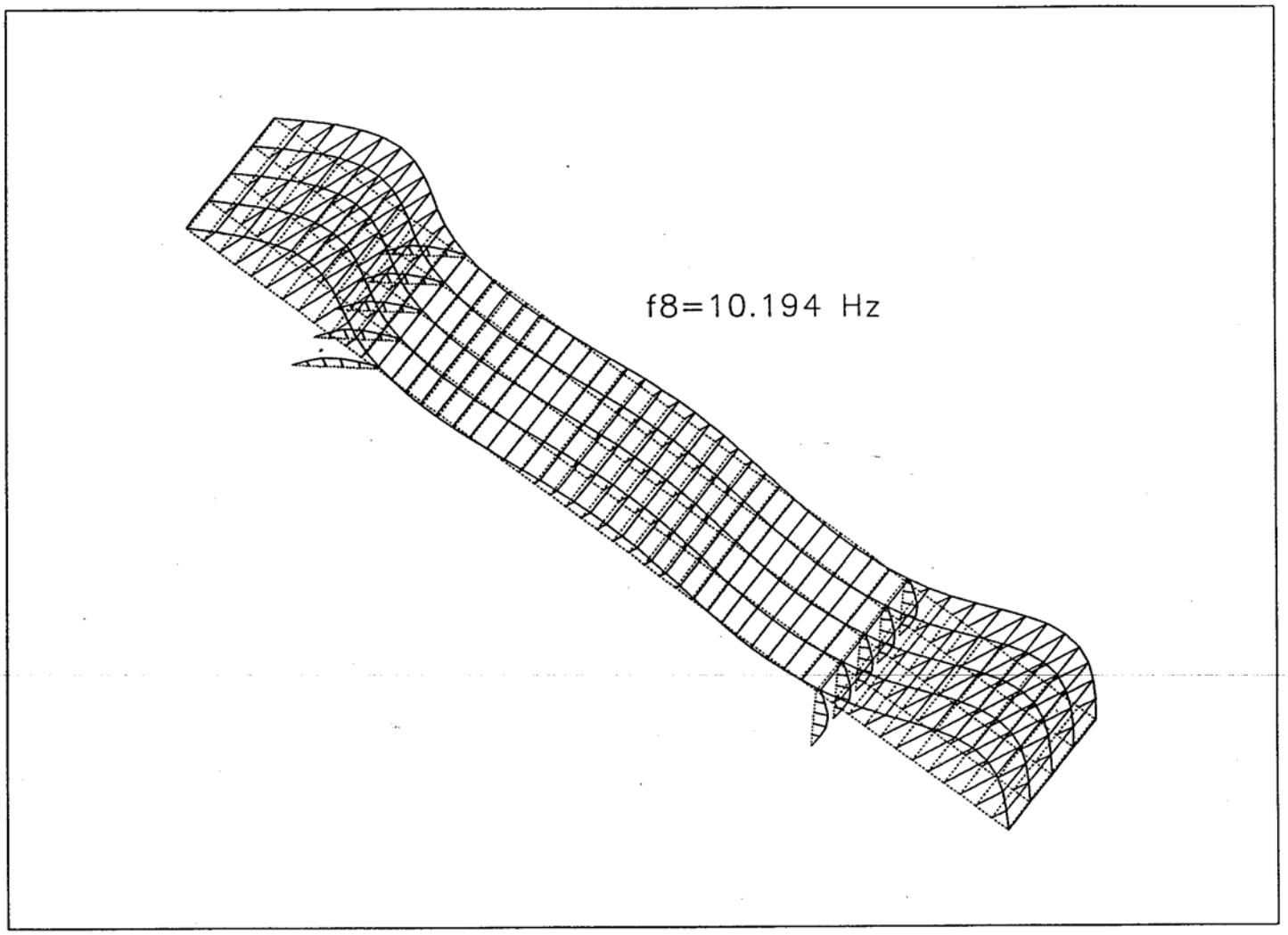

Fig. 4-13. The Eighth Vibration Mode.

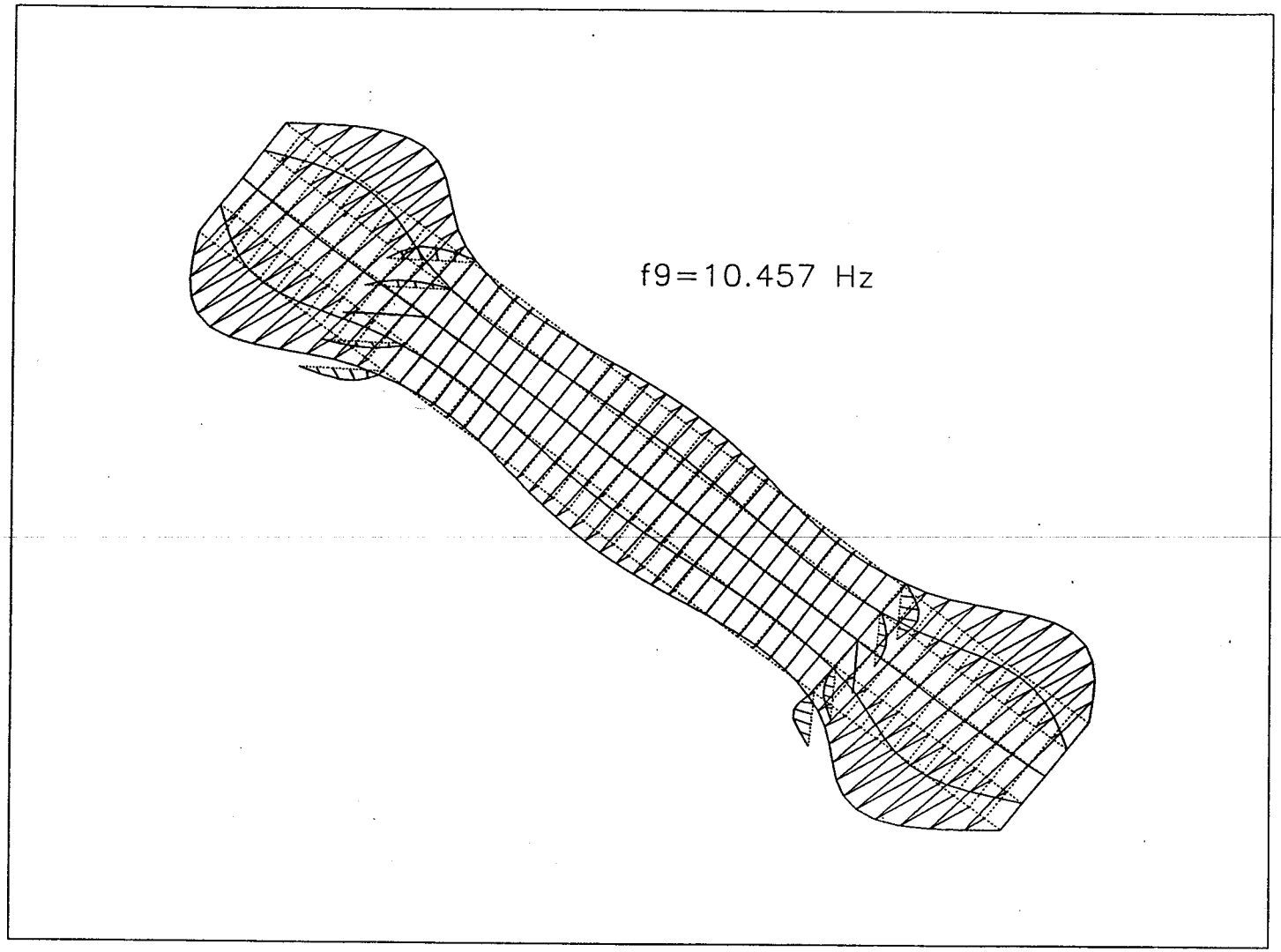

Fig. 4-14. The Ninth Vibration Mode.

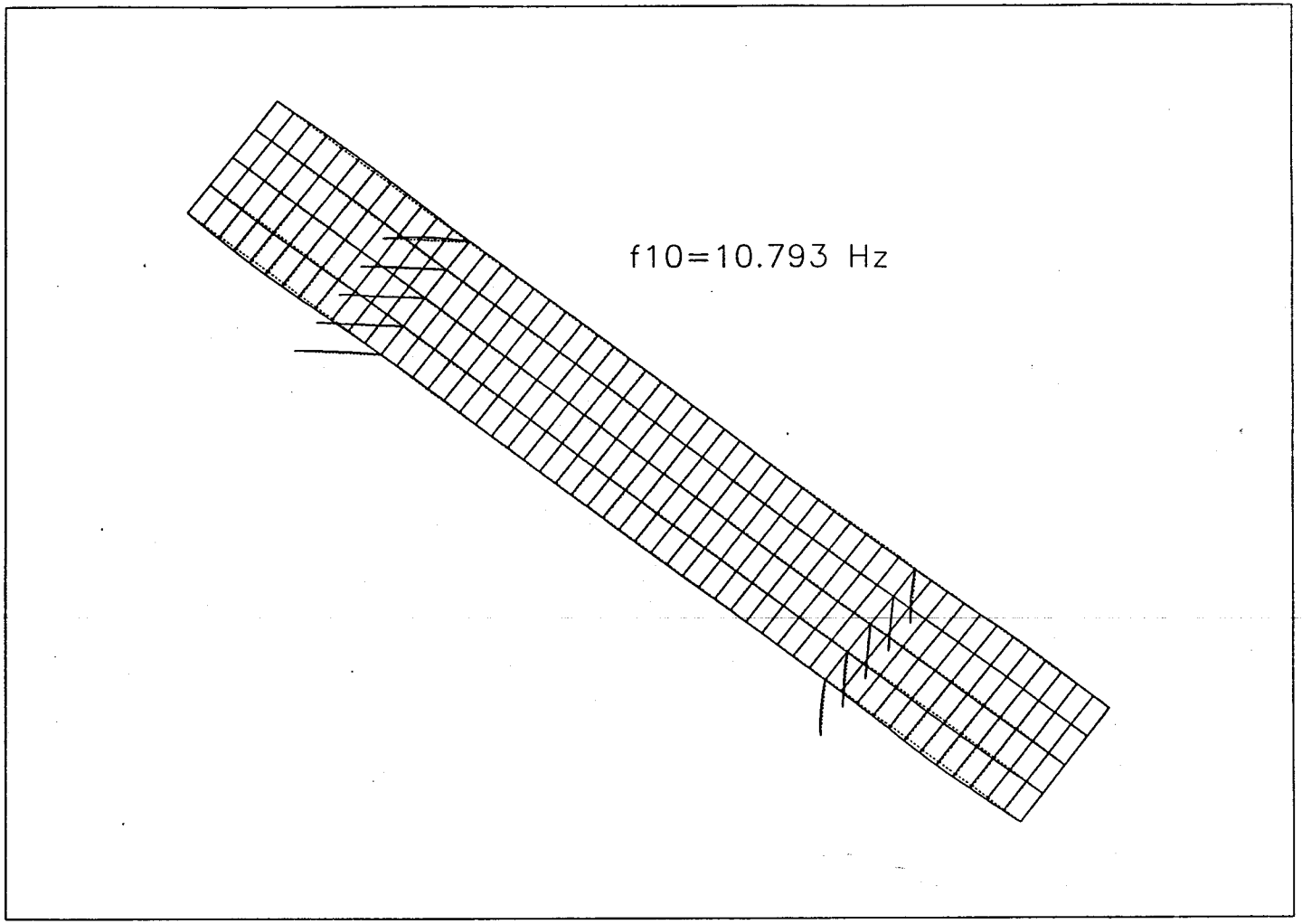

Fig. 4-15. The Tenth Vibration Mode.

The following assumptions have been made in the latter analysis:

1. The bridge has damping characteristics that can be modeled as viscous. One percent of critical damping is adopted for the first and second modes according to Ruhl [20] and Wang and Huang [30]. The mode damping coefficients were determined by using an approach described by Clough and Penzien [3].

2. In order to obtain the initial displacements and velocities of vehicle DOF'S when the vehicle entered the bridge, the vehicle was started the motion at a distance of 140 ft (42.67 m, i.e., a five-car length) away from the left end of the bridge and continued moving until the entire vehicle cleared the right end of the bridge.

3. The same class of road surface was assumed for both the approach roadways and bridge decks. All trucks have same left and right road surface roughnesses.

4.4.2. Convergence

The number of modes used is a very important factor for the accuracy of the dynamic responses which are calculated by mode superposition method. Table 4-2 gives the convergence of response of exterior rigid frame, for several typical sections, with variation of number of modes. Section 1 is located 20.73 ft. (6.32 m) away from left end support. Sections 2 to 4 are located near the haunch. Sections 5 and 6 are the fourth point and mid-span of the central span, respectively. Sections 7 to 11 are symmetrical to Sections 5 to 1. The results were obtained according to vehicle speed of 55 MPH (88.5 krrl/hr), good road surface, and symmetric loading of two trucks (see Fig. 4-16, Loading No: '1). It can be seen from Table 4-2 that the i

Table 4-2. Convergence of Response with Variation of Number of Modes.

Number of modes used	Section 1	Section 2	Section 3		Section 4		Section 6		
	M^{*}(kip-ft) $x10^{2}$	M^{*}(kip-ft) $x10^{2}$	M^{*}(kip-ft) $x10^{3}$	N^{**} (kip)	M^{*}(kip-ft) $x10^{2}$	N^{**} (kip)	M^{*}(kip-ft) $x10^{3}$	N^{**} (kip)	D^{***} (in)
3	-0.643	-1.158	-3.700	-31.3	-4.267	-27.6	3.425	-27.4	0.316
5	-0.765	-1.567	-4.300	-43.4	-5.267	-32.6	4.175	-28.3	0.410
10	1.442	-2.175	-3.767	-45.4	-5.333	-33.5	4.225	-29.6	0.412
15	1.450	-2.183	-3.783	-45.5	-5.342	-33.5	4.233	-29.6	0.414
20	1.475	-2.225	-3.775	-45.7	-5.367	-33.6	4.242	-29.8	0.414
25	2.375	-4.208	-3.492	-55.9	-5.442	-33.2	4.217	-29.4	0.410
30	2.392	-4.225	-3.492	-55.9	-5.442	-33.2	4.233	-29.5	0.411
35	2.383	-4.212	-3.487	-56.0	-5.442	-33.1	4.233	-29.3	0.411

Note:

* -- Moment,
** -- Axial force,
*** -- Deflection.

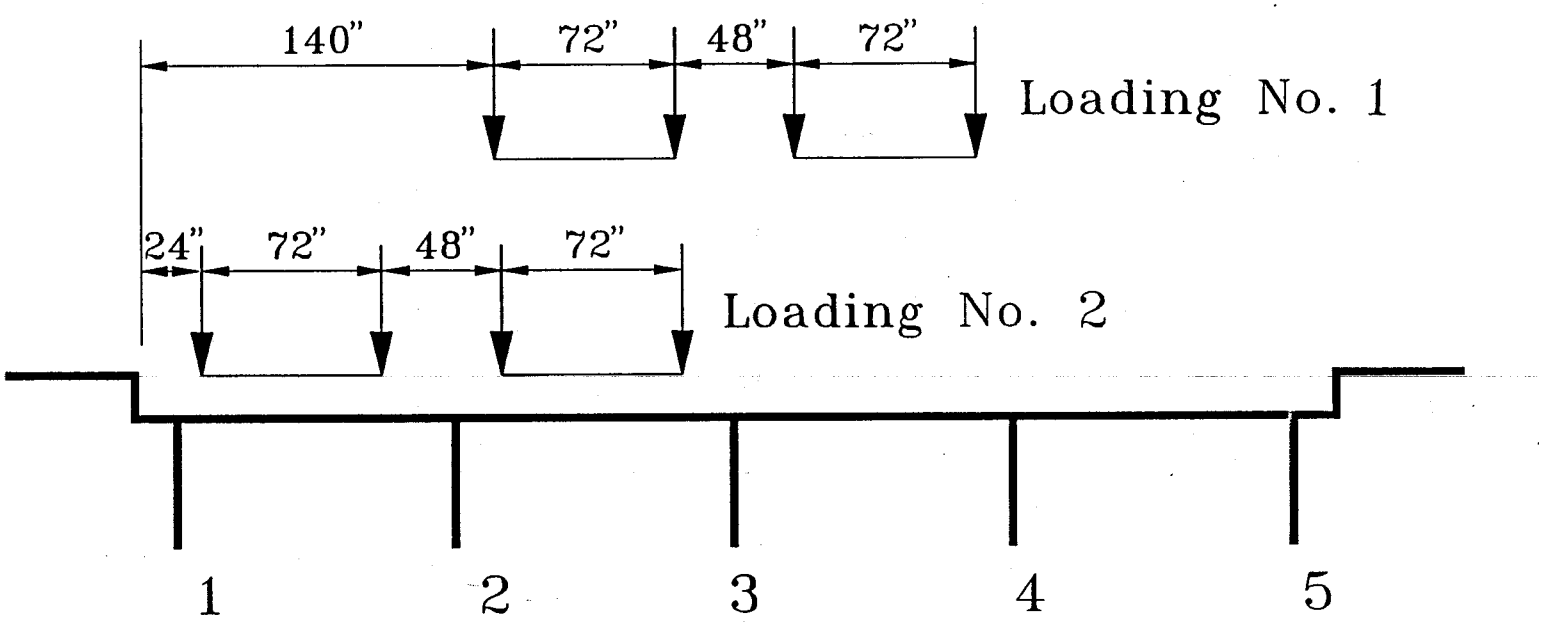

Fig.4-16 Two-truck Loading

convergence of the responses varies with different sections. The response of middle span converges much faster than that of side span. Generally, the response of middle span can reach satisfying results with ten modes. For side span, at least 25 modes should be used in order to obtain reasonable dynamic response. It is obvious that the needed number of modes depends on different sections, structures, and mechanical modes used. For the planar bar system mode, less number of vibration modes will be needed to gain the required accuracy (30]. In the latter investigation, thirty modes will be used.

4.4.3. Representative Histories

Twenty eight time history curves for the bridge are shown in Figs. 4-17 to 4-44. The curves in Figs. 4-17 to 4-35 are for the moment. The history curve of deflection at Section 6 is demonstrated in Figs. 4-36 to 4-38. Figs. 4-39 to 4-44 present the histories of axial force at Sections 4 and 6. The abscissas in Figs. -17 **to 4-44 are the distance measured from the left end of the bridge to the front axle of the vehicle. The results illustrated in those figures were obtained in accordance with good road roughness, symmetric loading of two trucks and vehicle speed of 45 MPH (72.4 km/hr). The solid lines represent the dynamic response, while static response is indicated by dotted lines that can be considered as static influence lines if we treat the truck loading as a unit. Concerning the curves given in Figs. 4-17 to 4-44, the following phenomena can be drawn: The major attribution to the dynamic response of middle span arises from the participation of the first four natural modes. The higher modes greatly affect the dynamic response of side span. The dynamic responses for moment and deflection at Section 6 (mid-span) are quite different. The maximum dynamic deflection is 15% larger than the maximum static deflection. The maximum dynamic moment is 10.3% smaller than the**

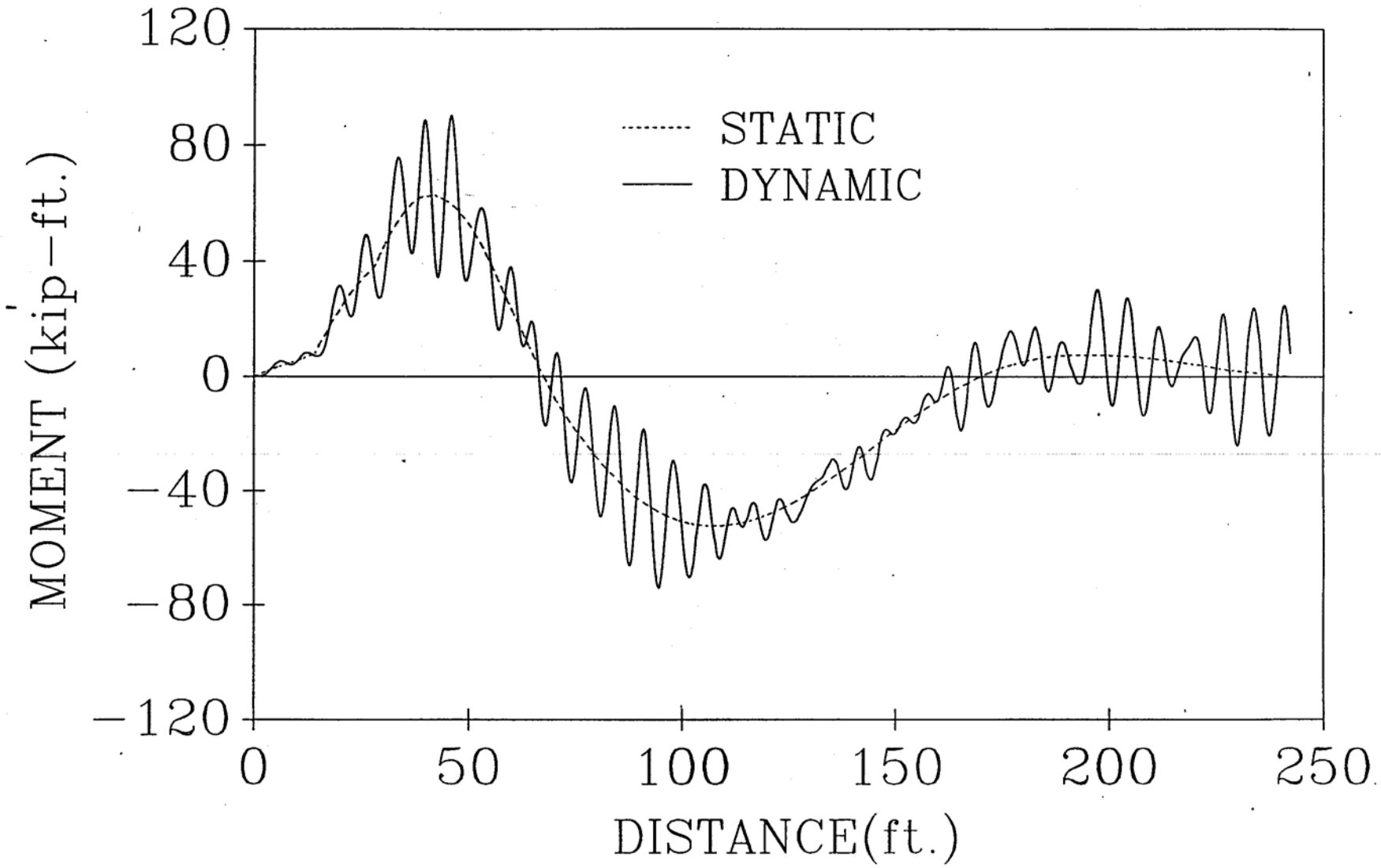

Fig. 4-17 Histories of Moment at Section 1 of Frame 1.

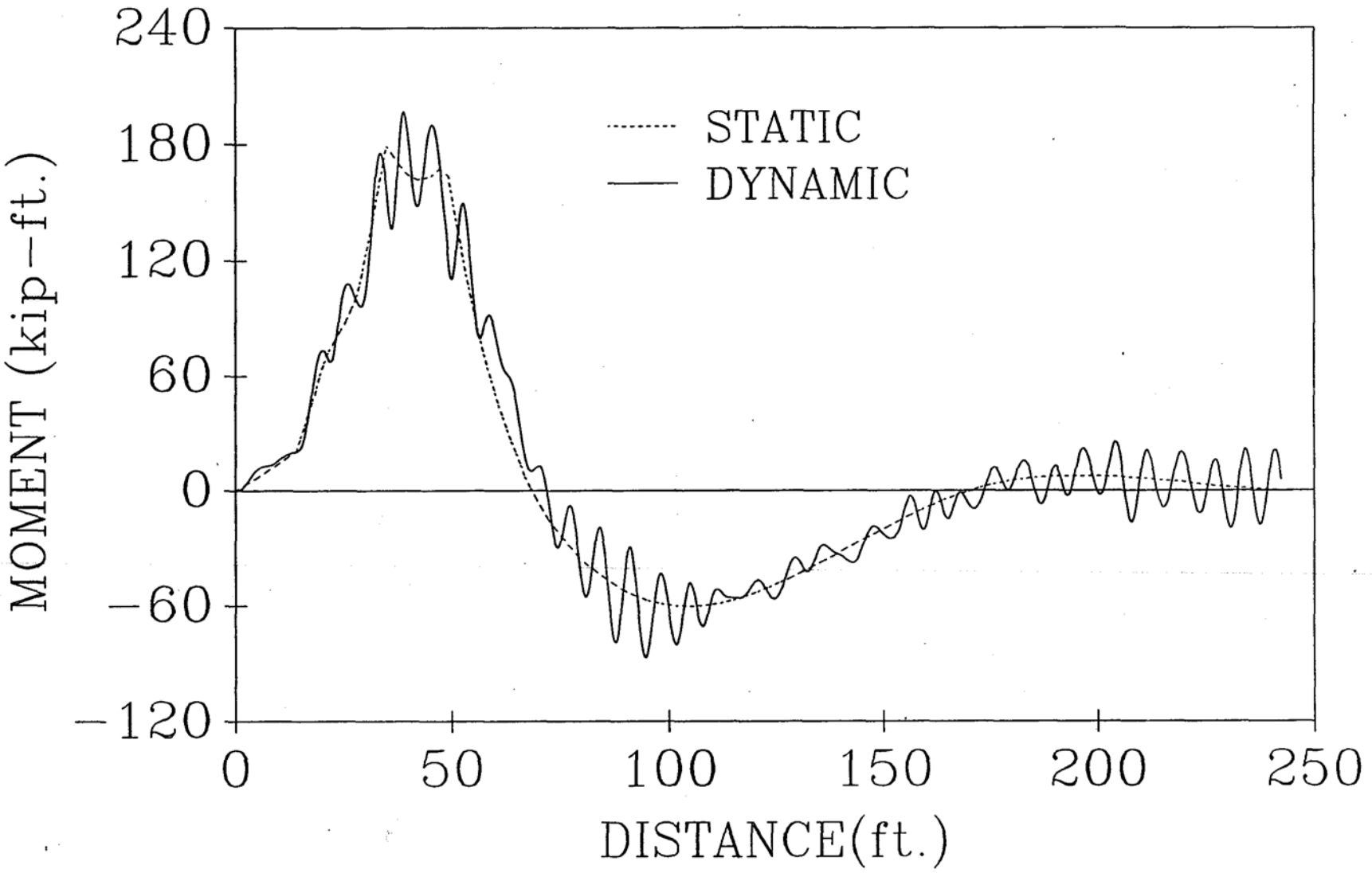

Fig. 4-18 Histories of Moment at Section 1 of Frame 2.

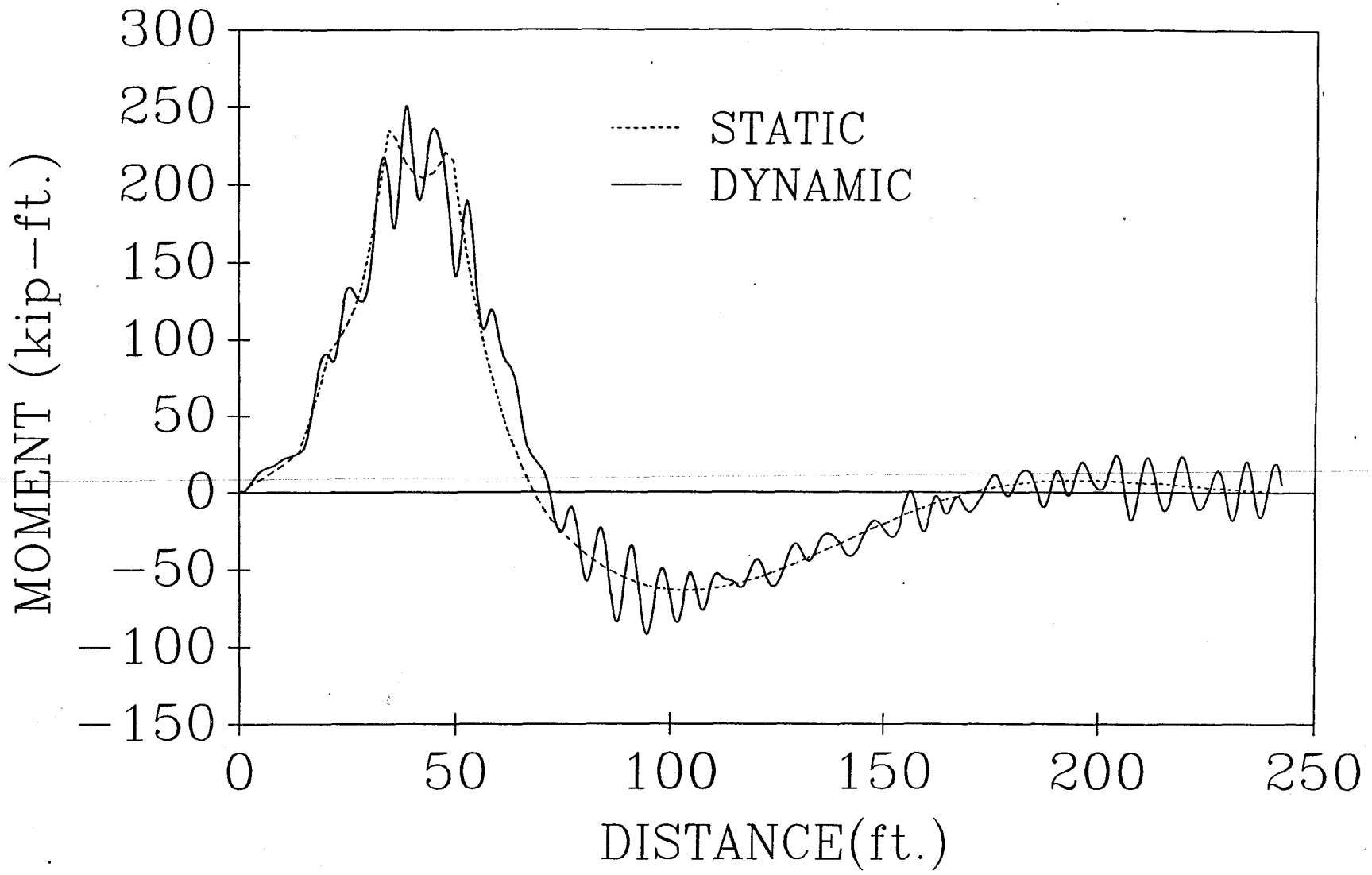

Fig. 4-19 Histories of Moment at Section 1 of Frame 3.

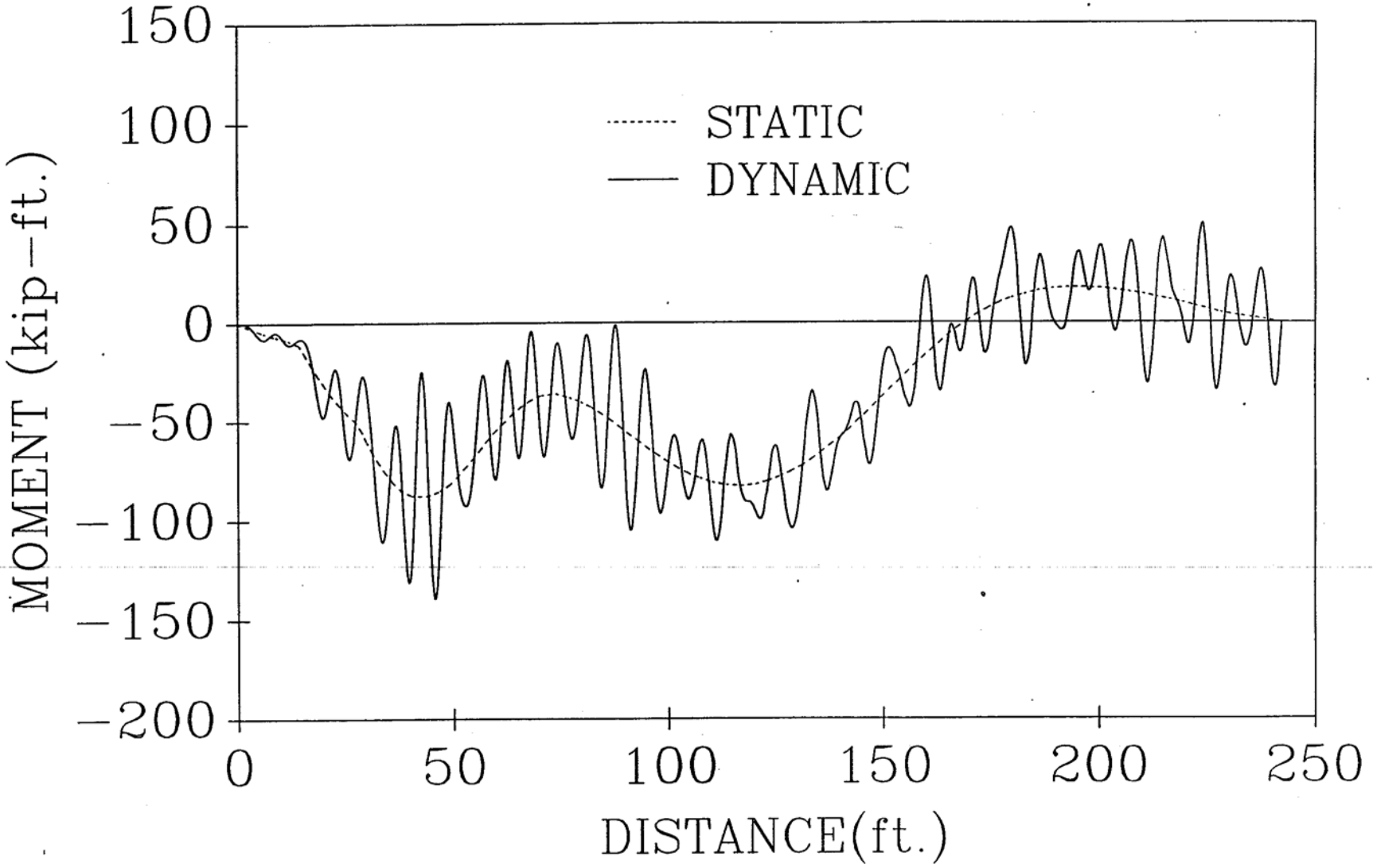

Fig. 4-20 Histories of Moment at Section 2 of Frame 1.

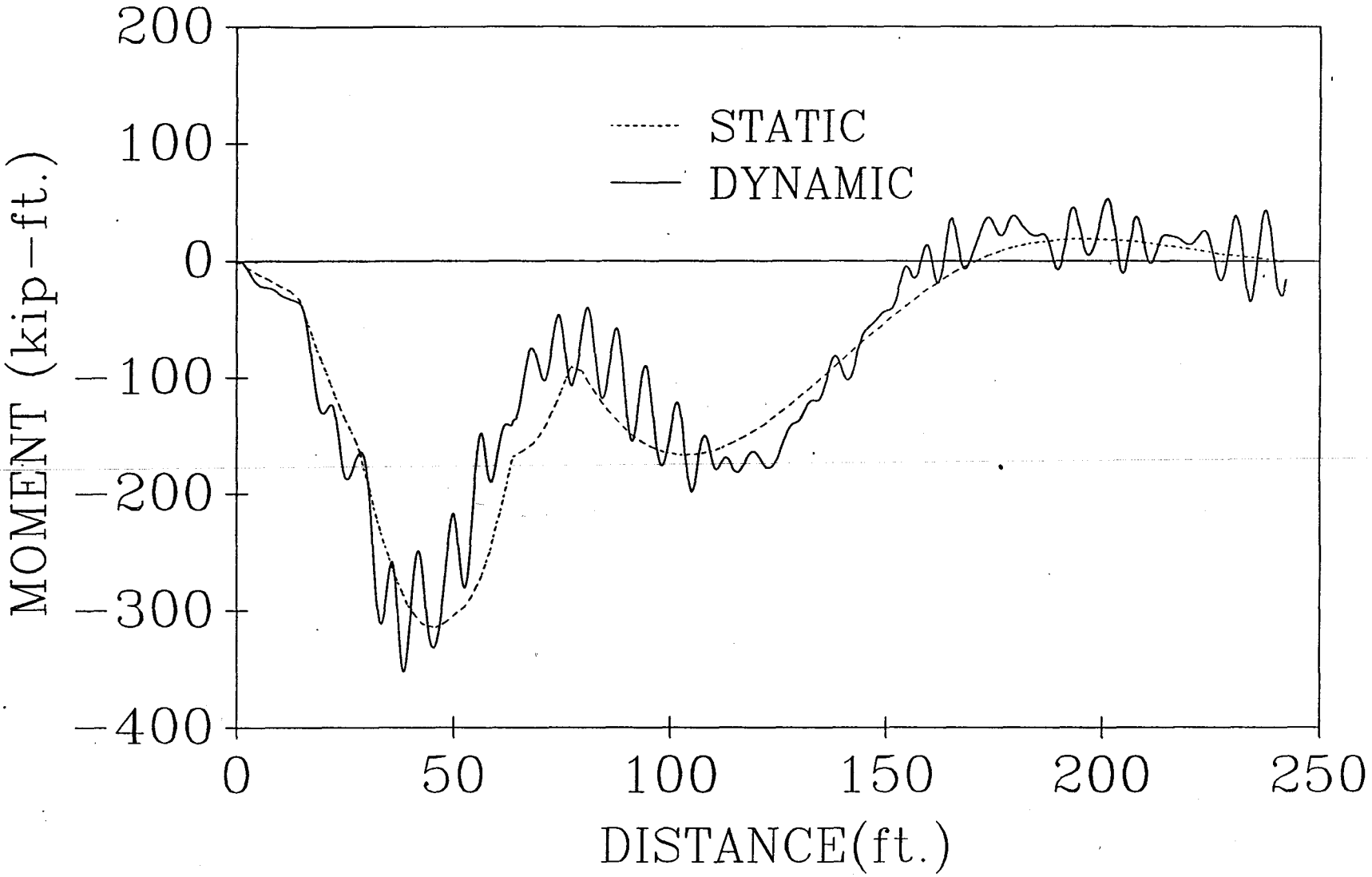

Fig. 4-21 Histories of Moment at Section 2 of Frame 2.

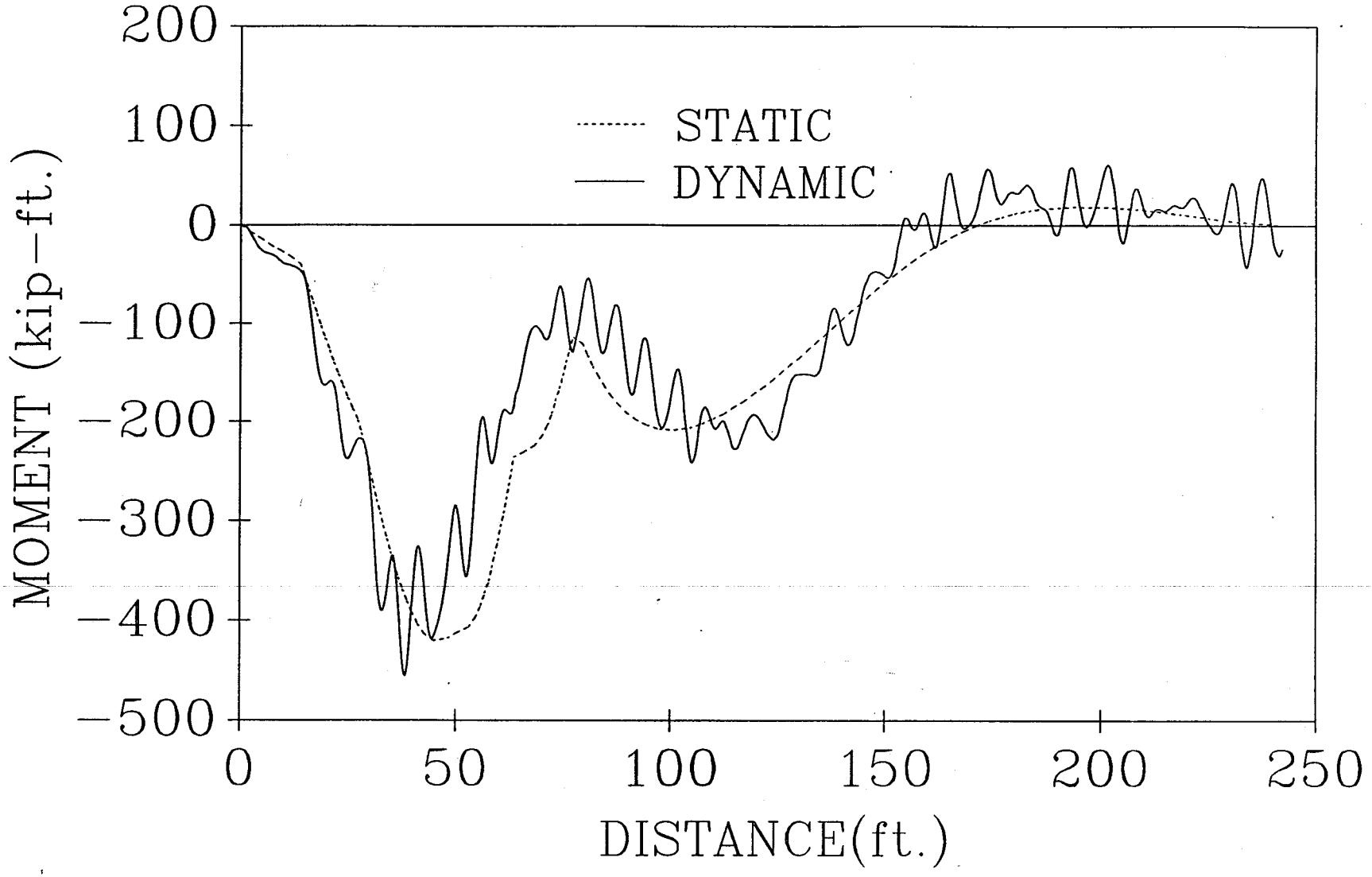

Fig. 4-22 Histories of Moment at Section 2 of Frame 3.

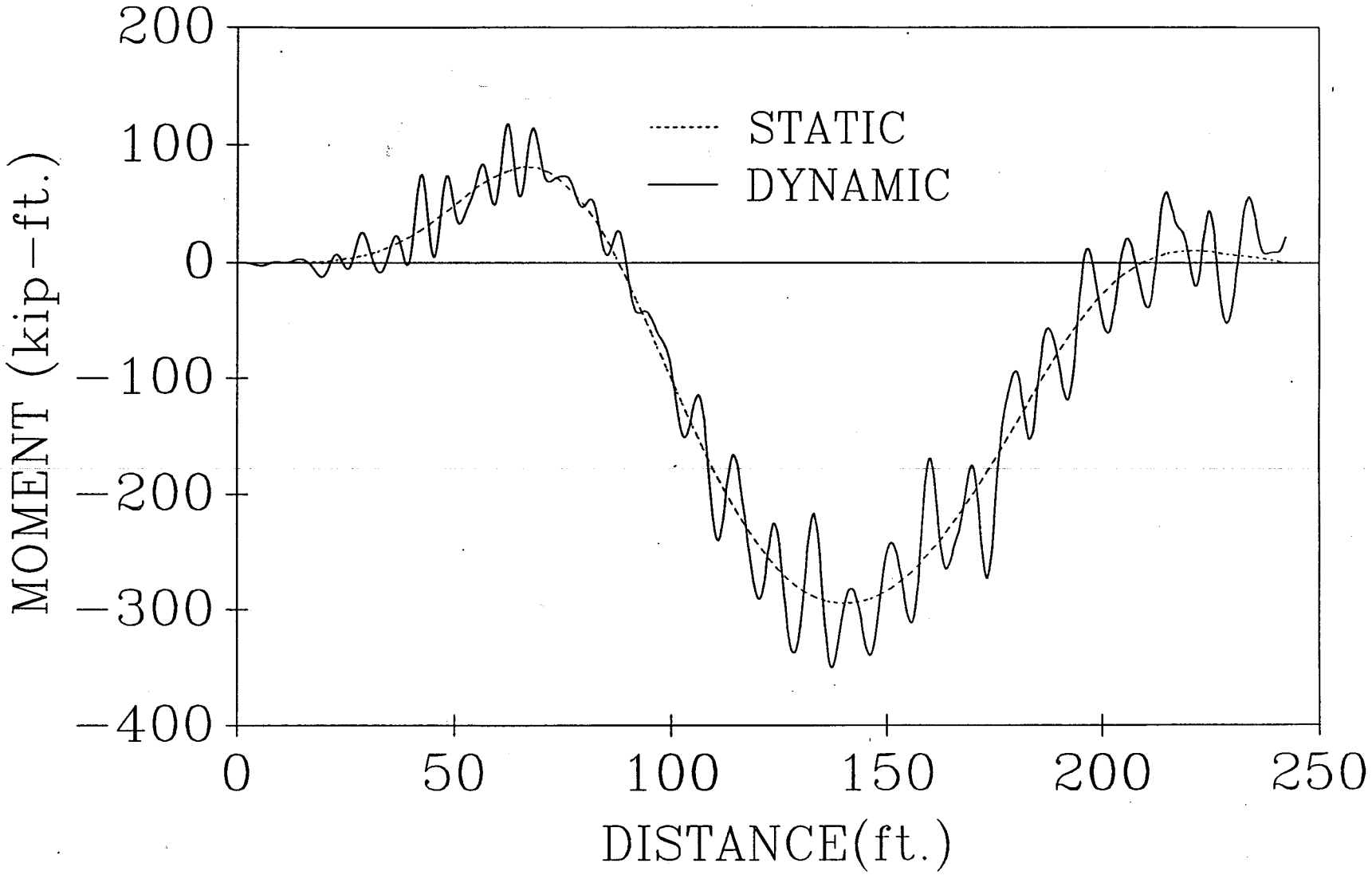

Fig. 4-23 Histories of Moment at Section 3 of Frame 1.

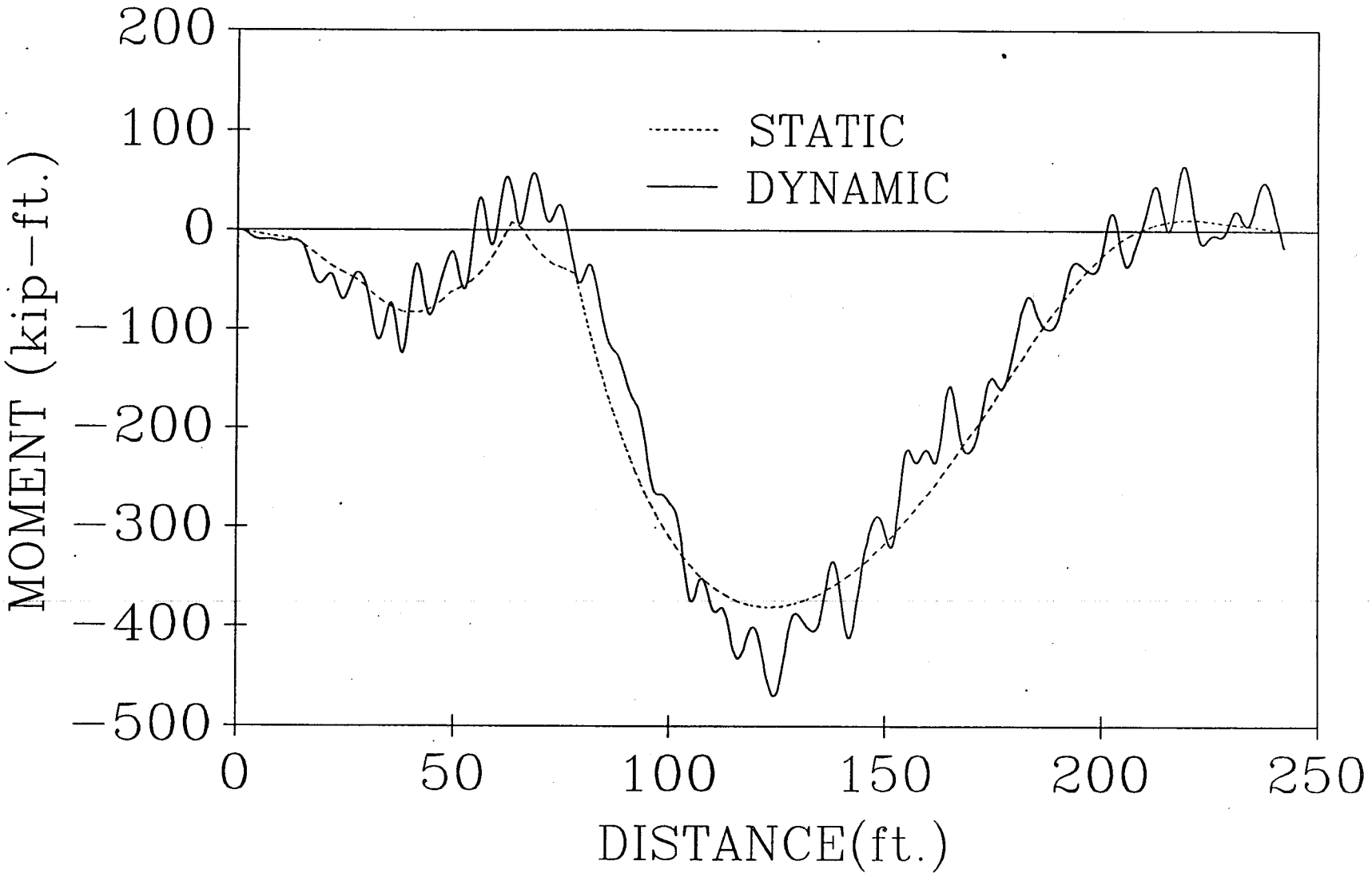

Fig. 4-24 Histories of Moment at Section 3 of Frame 2.

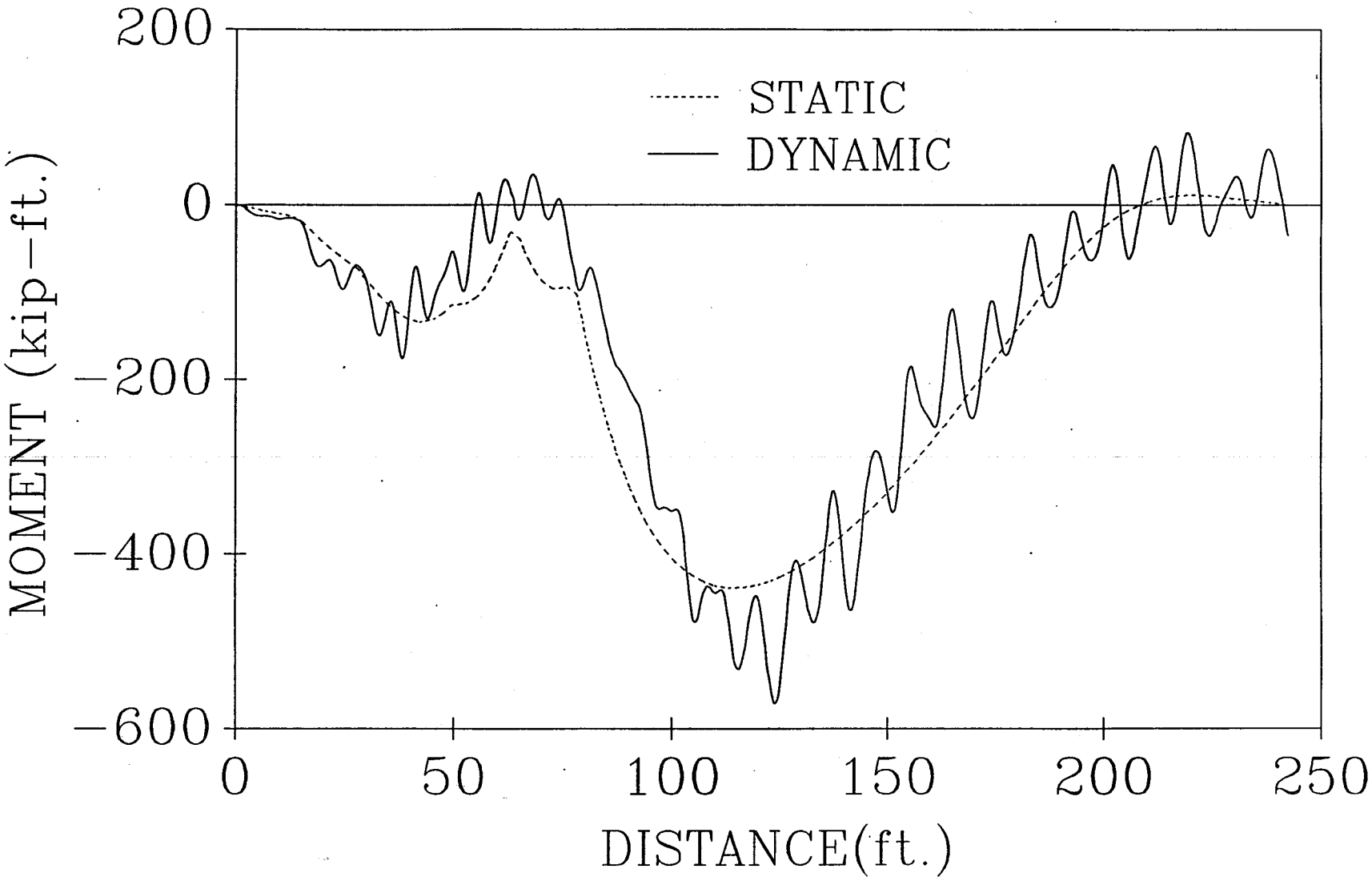

Fig. 4-25 Histories of Moment at Section 3 of Frame 3.

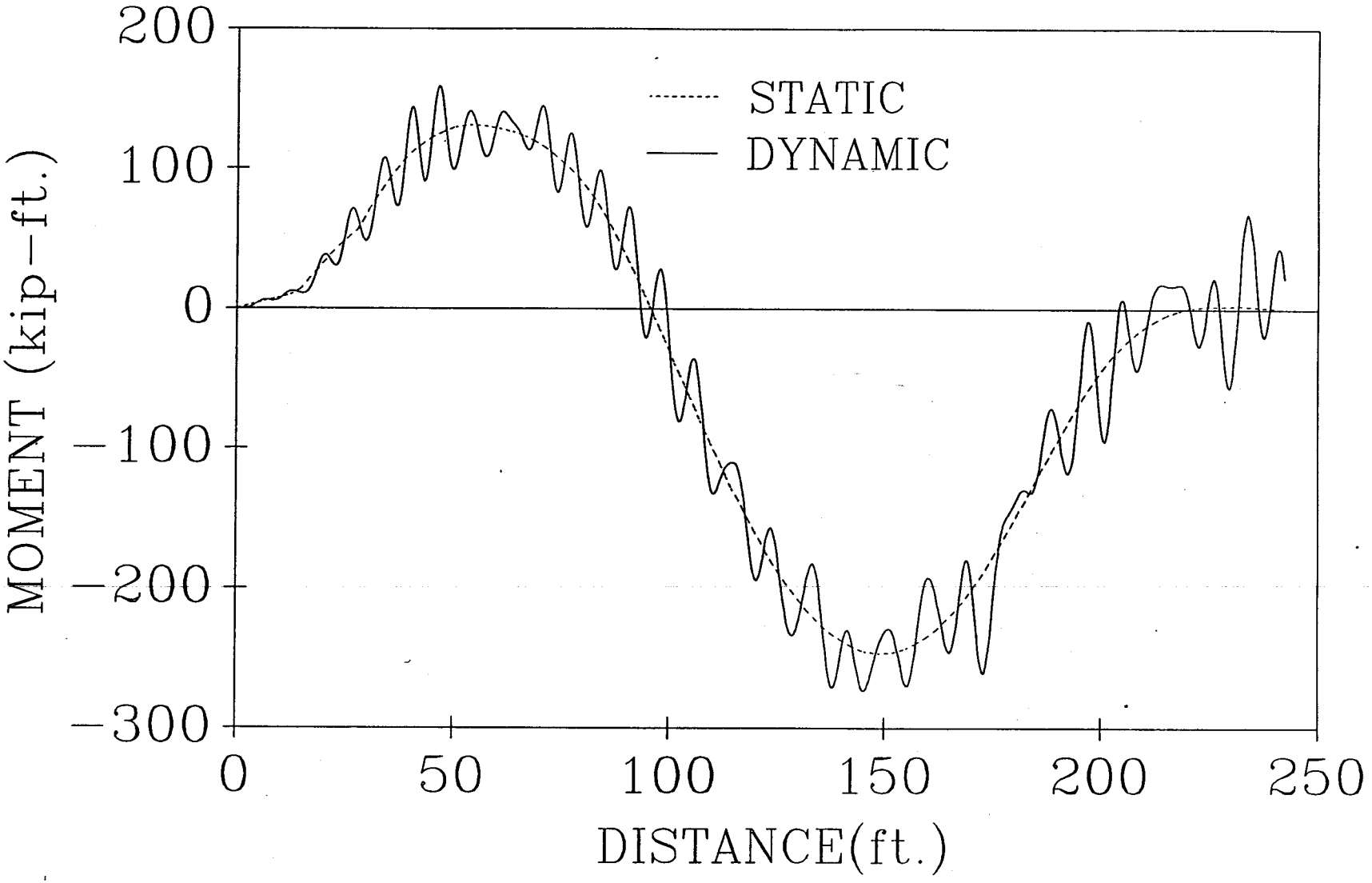

Fig. 4-26 Histories of Moment at Section 4 of Frame 1.

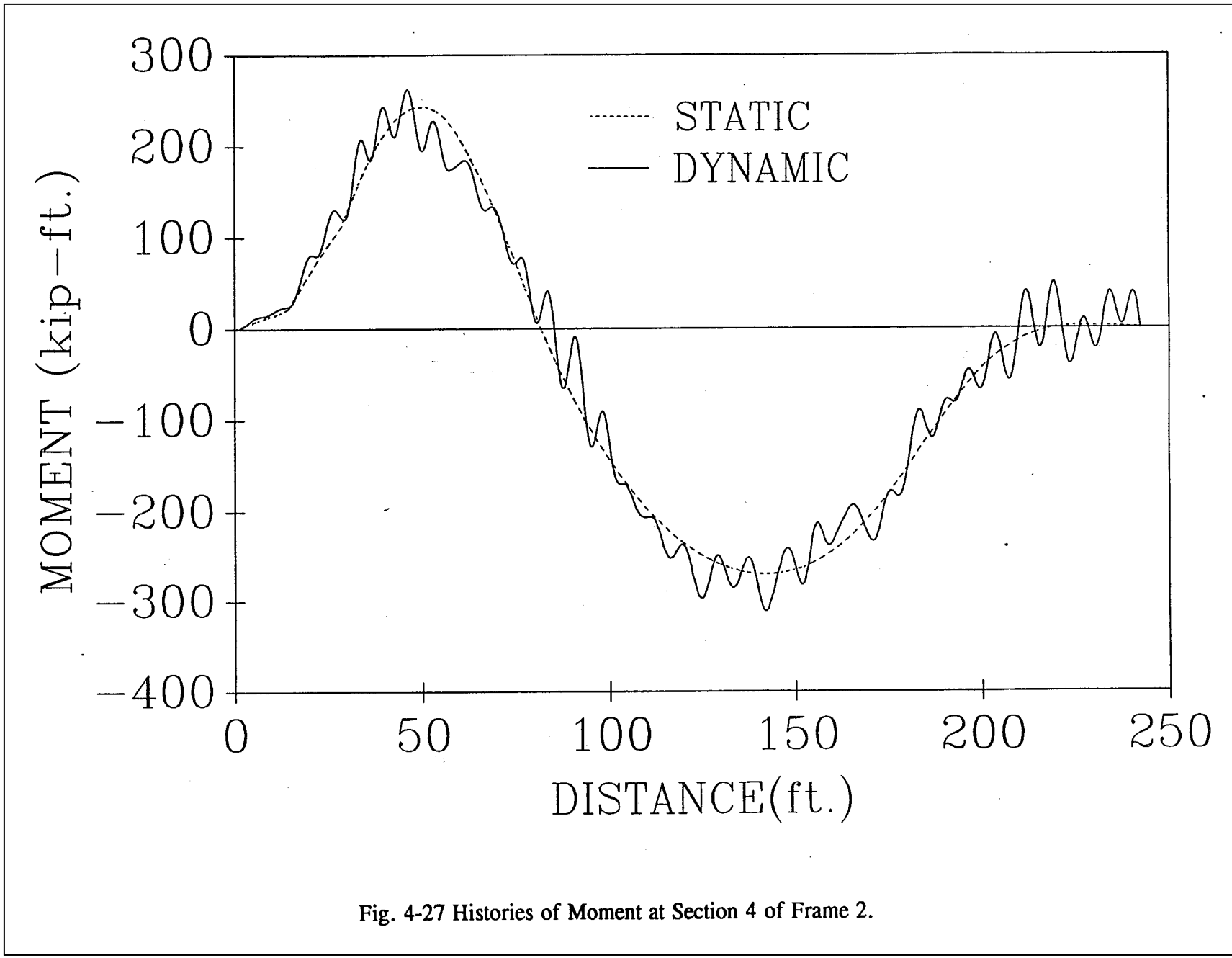

Fig. 4-27 Histories of Moment at Section 4 of Frame 2.

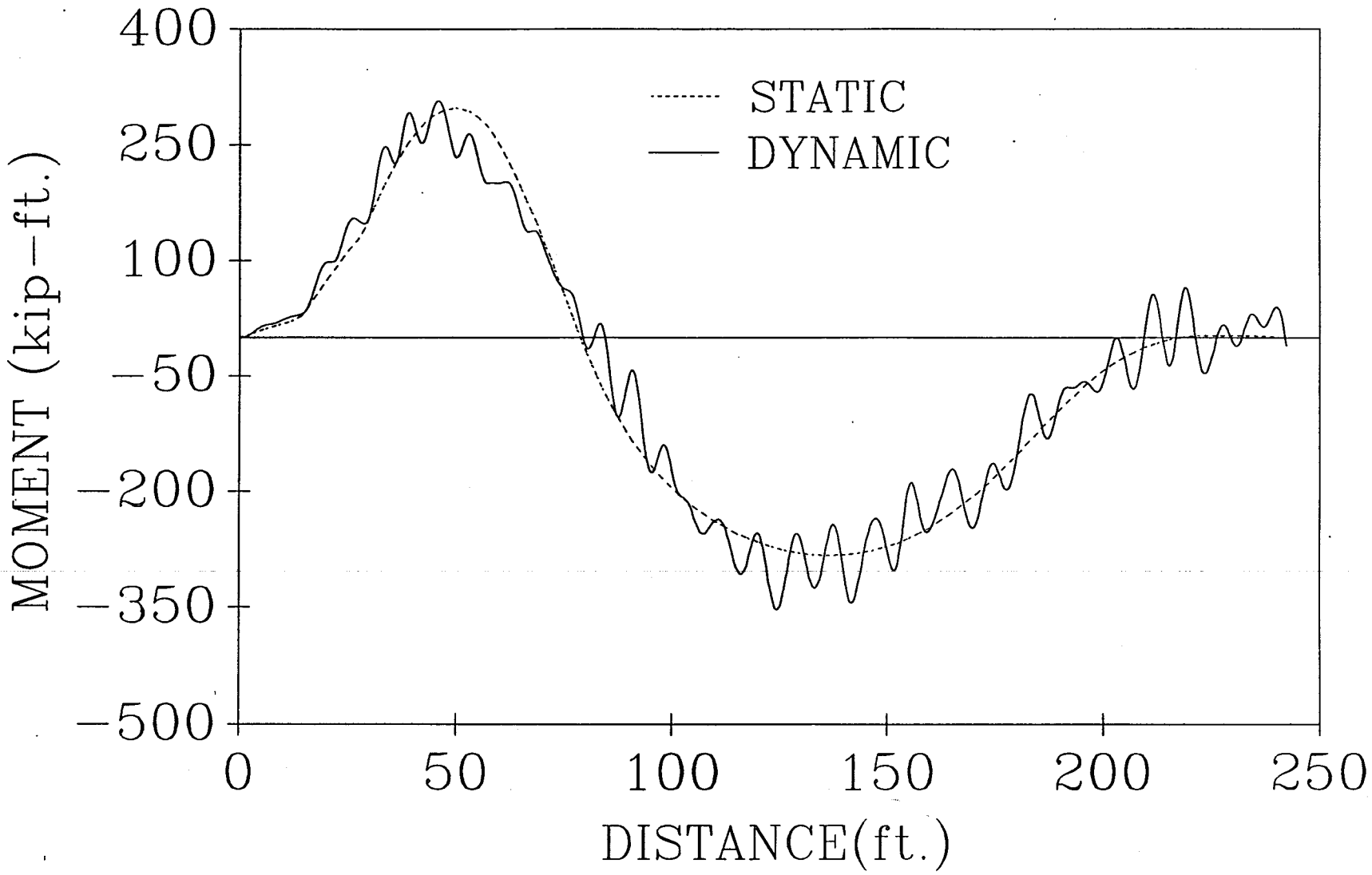

Fig. 4-28 Histories of Moment at Section 4 of Frame 3.

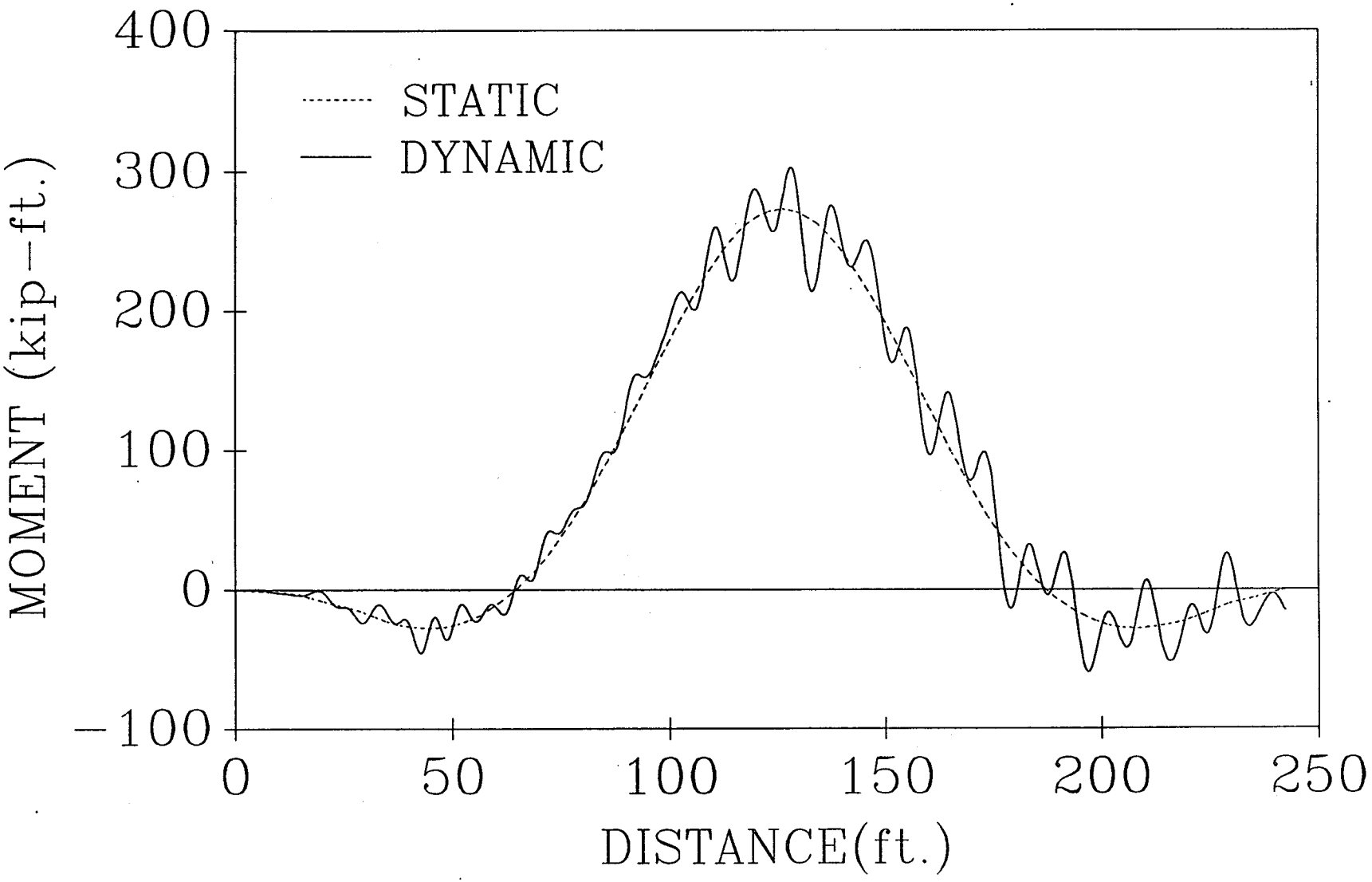

Fig. 4-29 Histories of Moment at Section 6 of Frame 1.

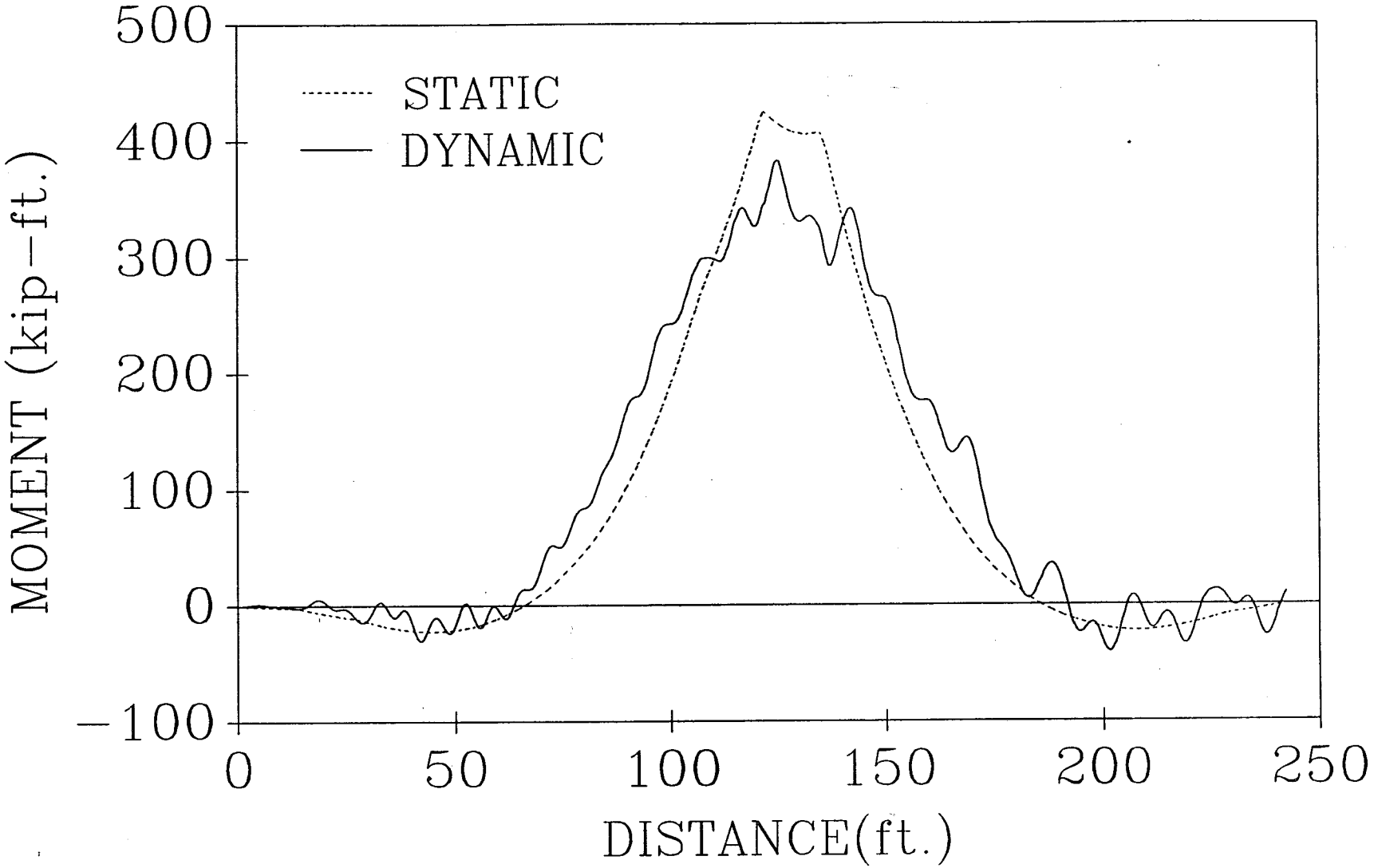

Fig. 4-30 Histories of Moment at Section 6 of Frame 2.

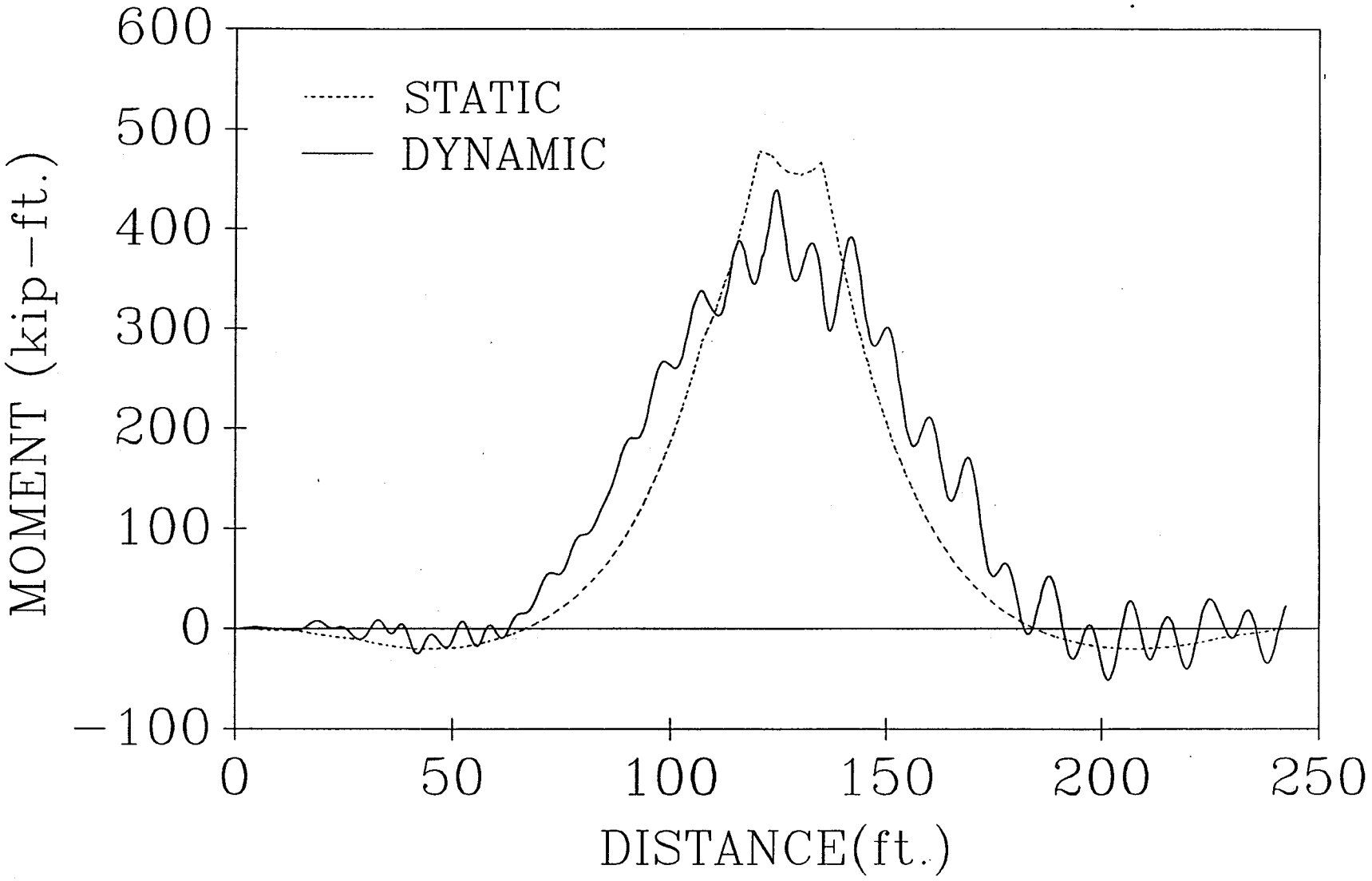

Fig. 4-31 Histories of Moment at Section 6 of Frame 3.

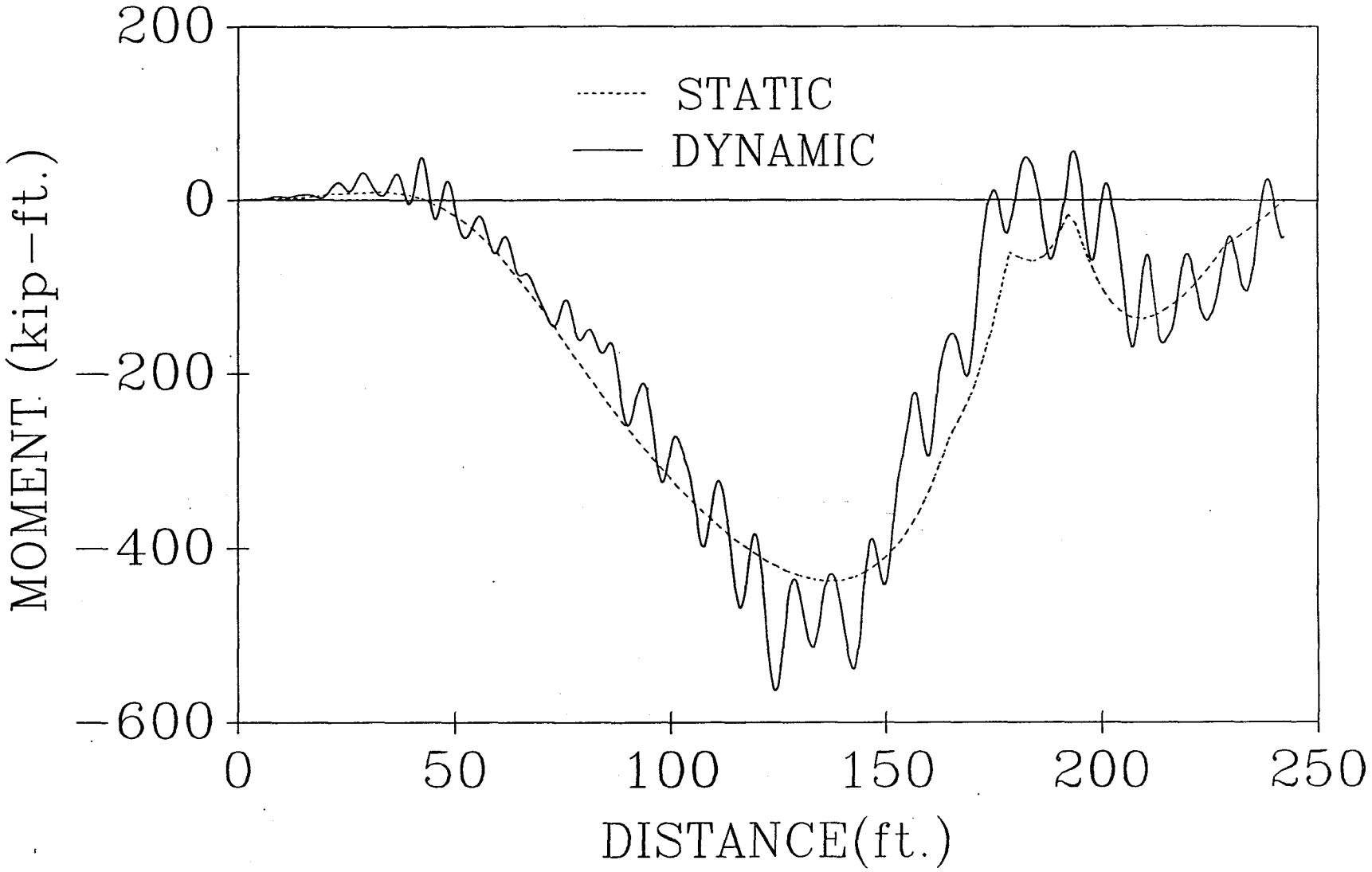

Fig. 4-32 Histories of Moment at Section 8 of Frame 3.

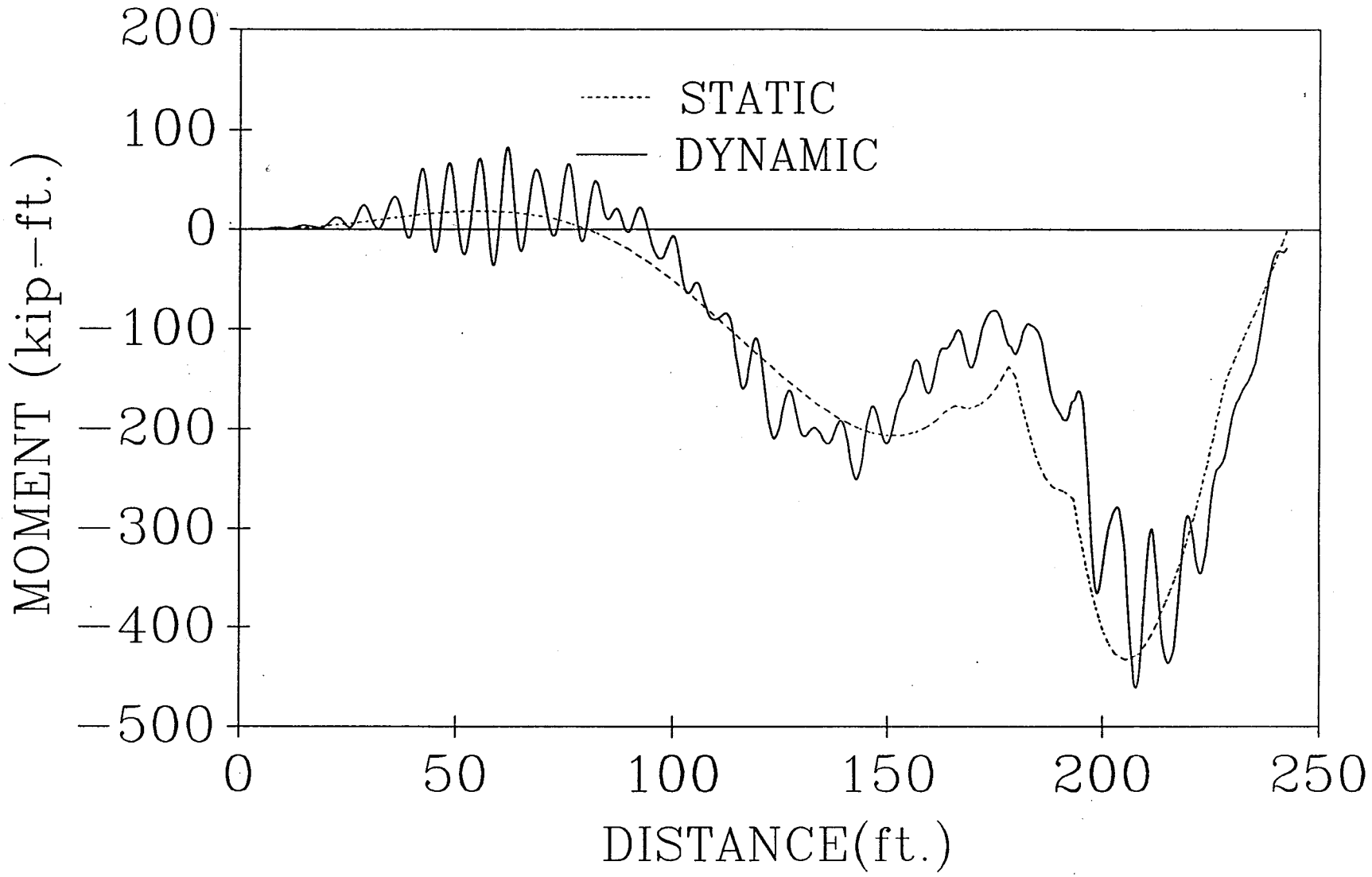

Fig. 4-33 Histories of Moment at Section 9 of Frame 3.

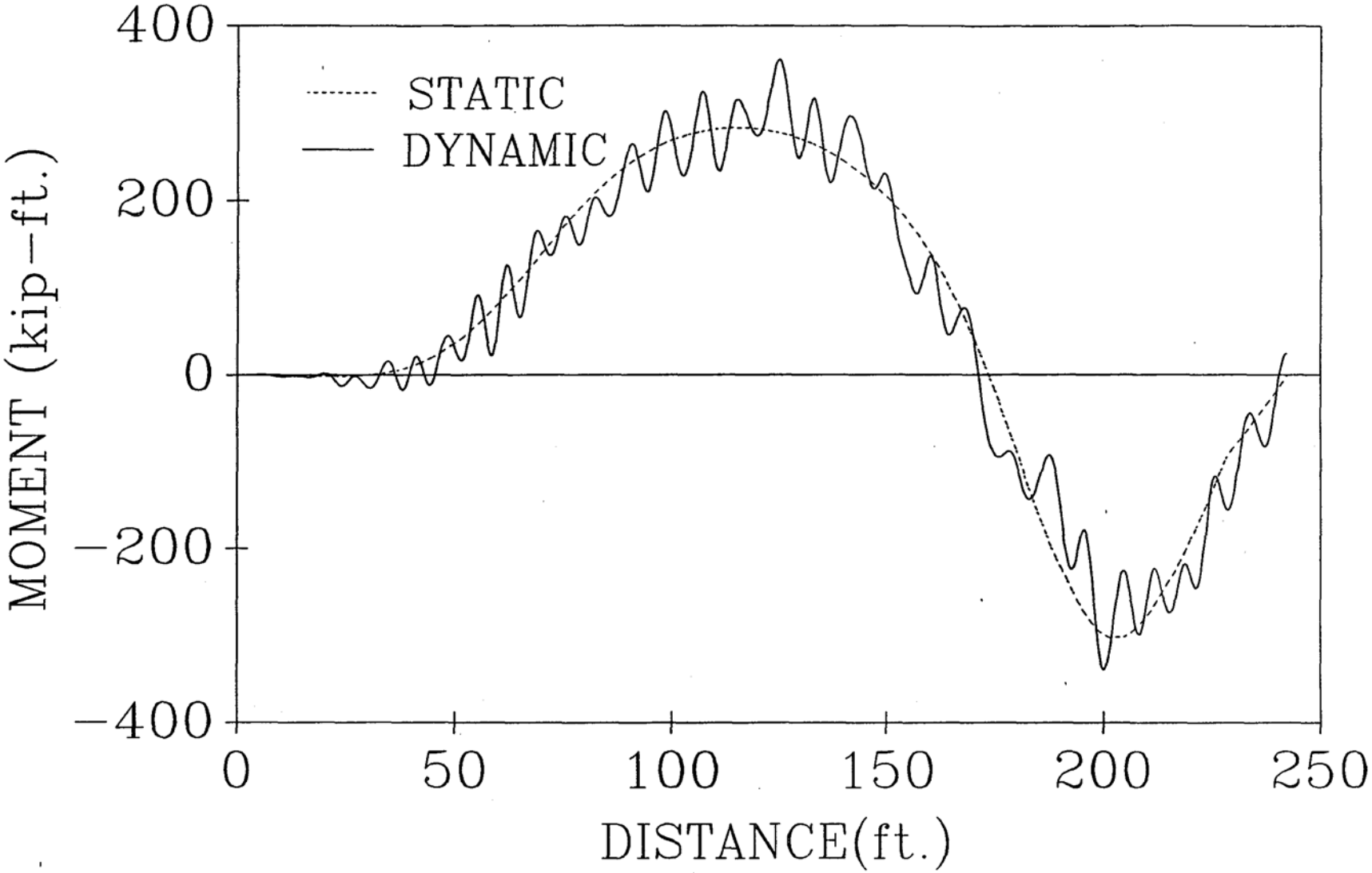

Fig. 4-34 Histories of Moment at Section 10 of Frame 3.

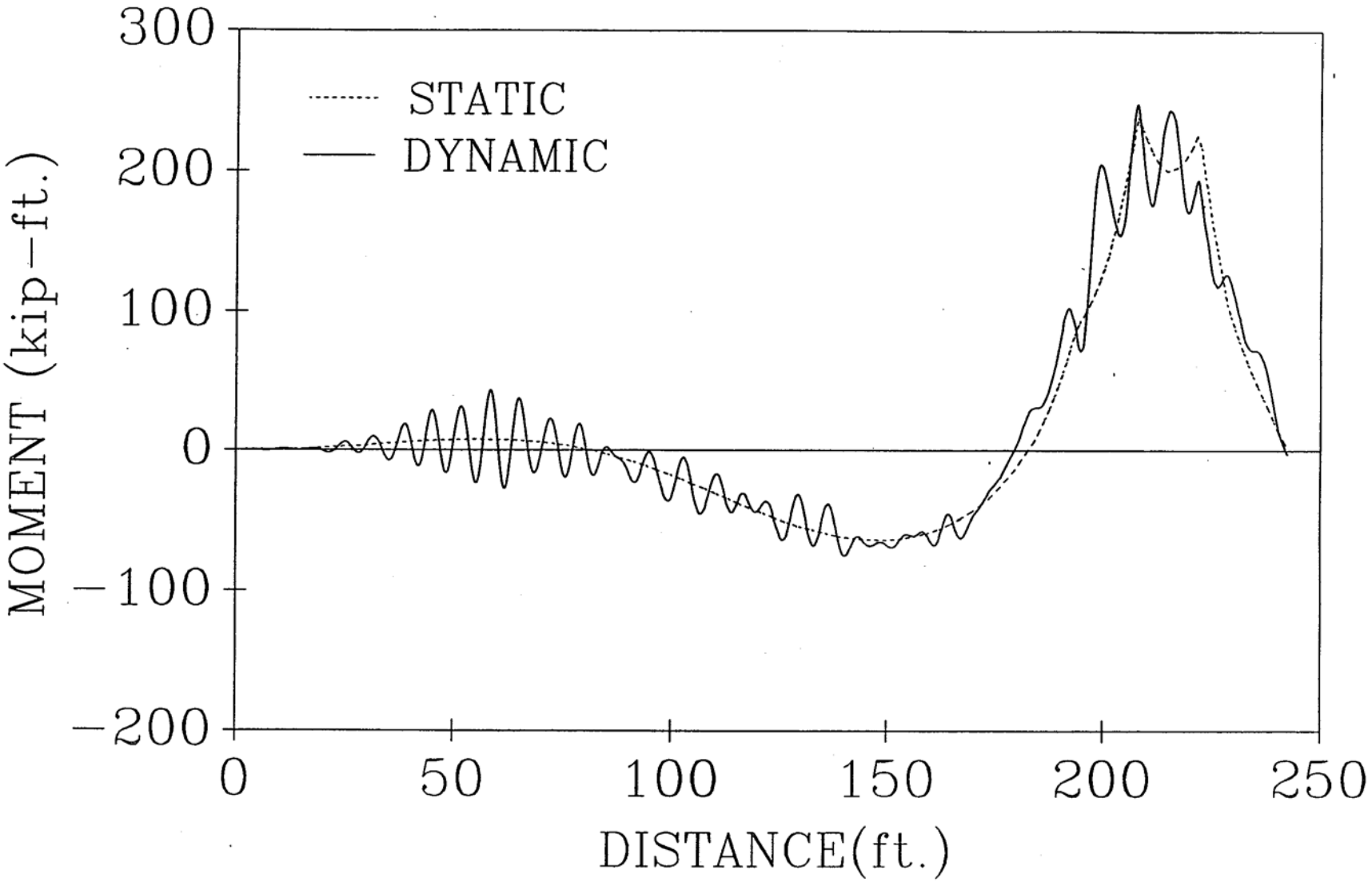

Fig. 4-35 Histories of Moment at Section 11 of Frame 3.

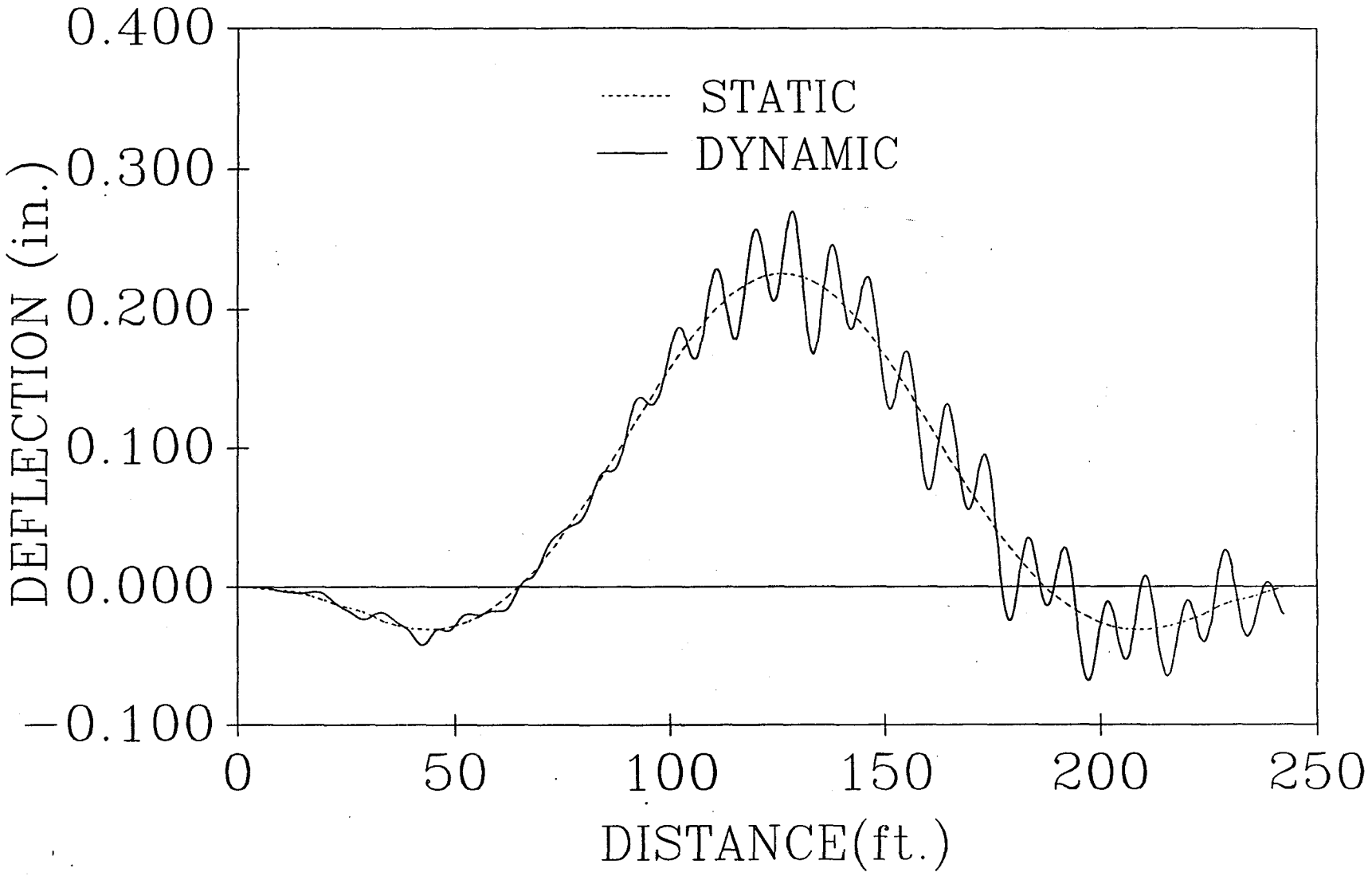

Fig. 4-36 Histories of Deflection at Section 6 of Frame 1.

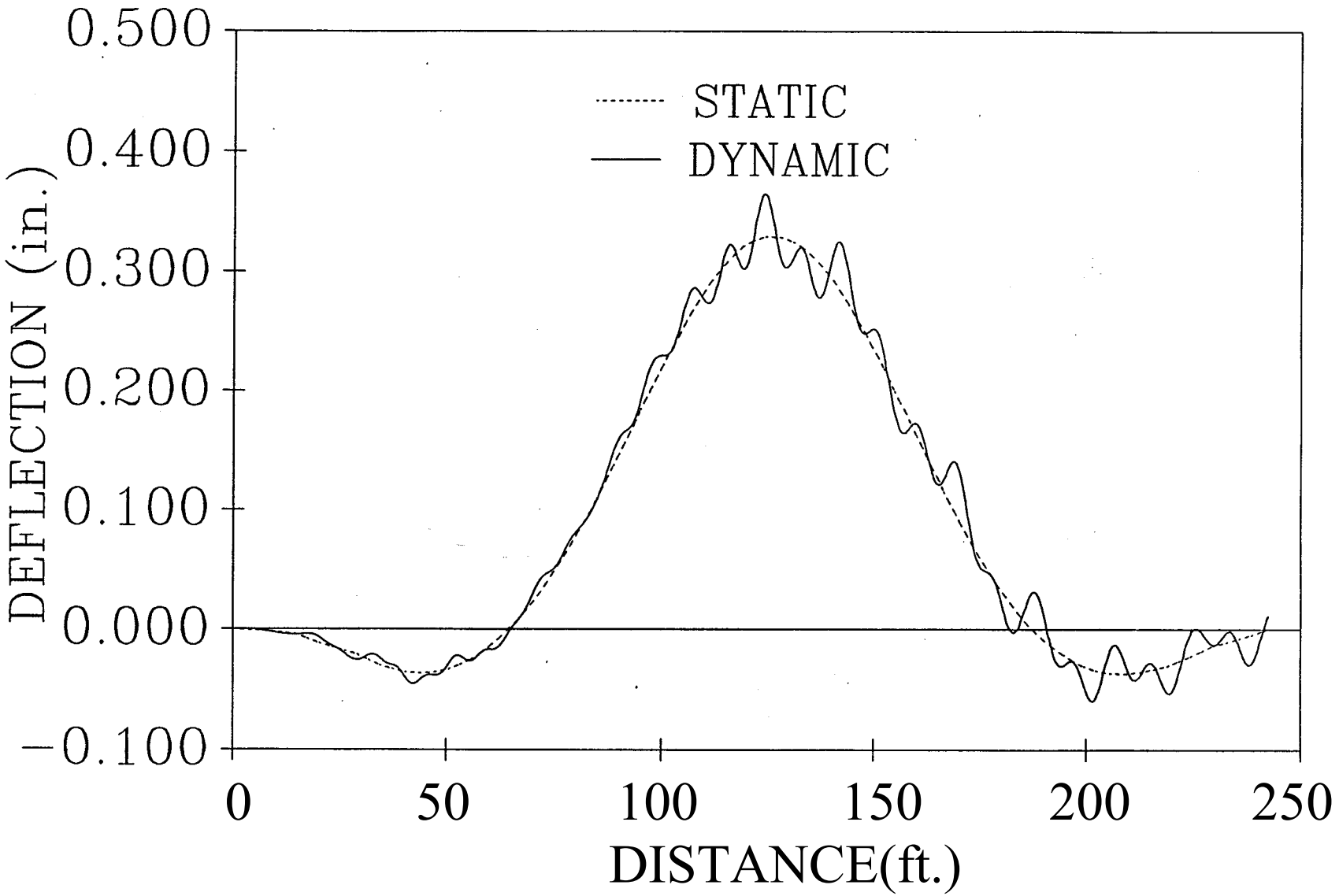

Fig. 4-37 Histories of Deflection at Section 6 of Frame 192.

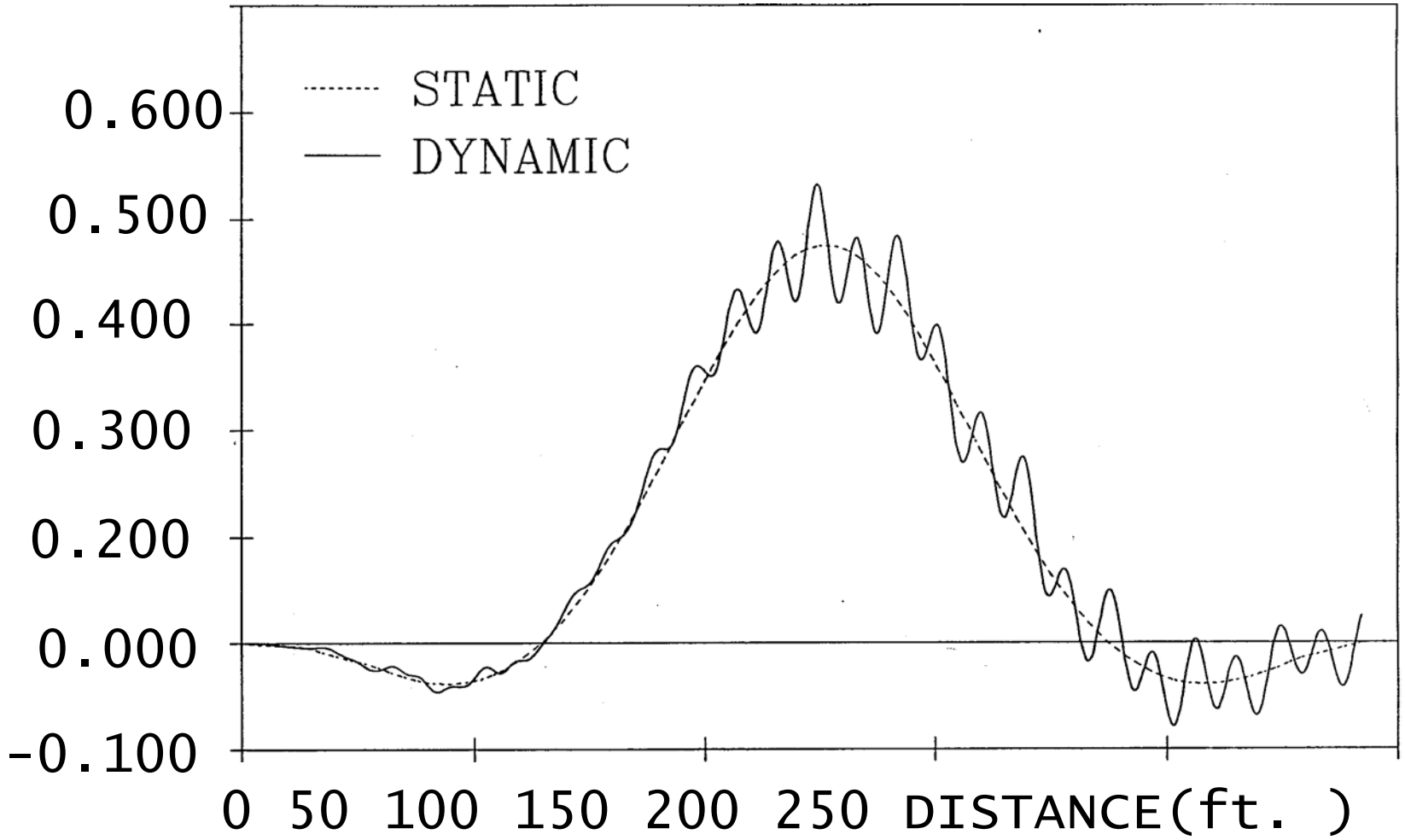

Fig. 4-38 Histories of Deflection at Section 6 of Frame 193.

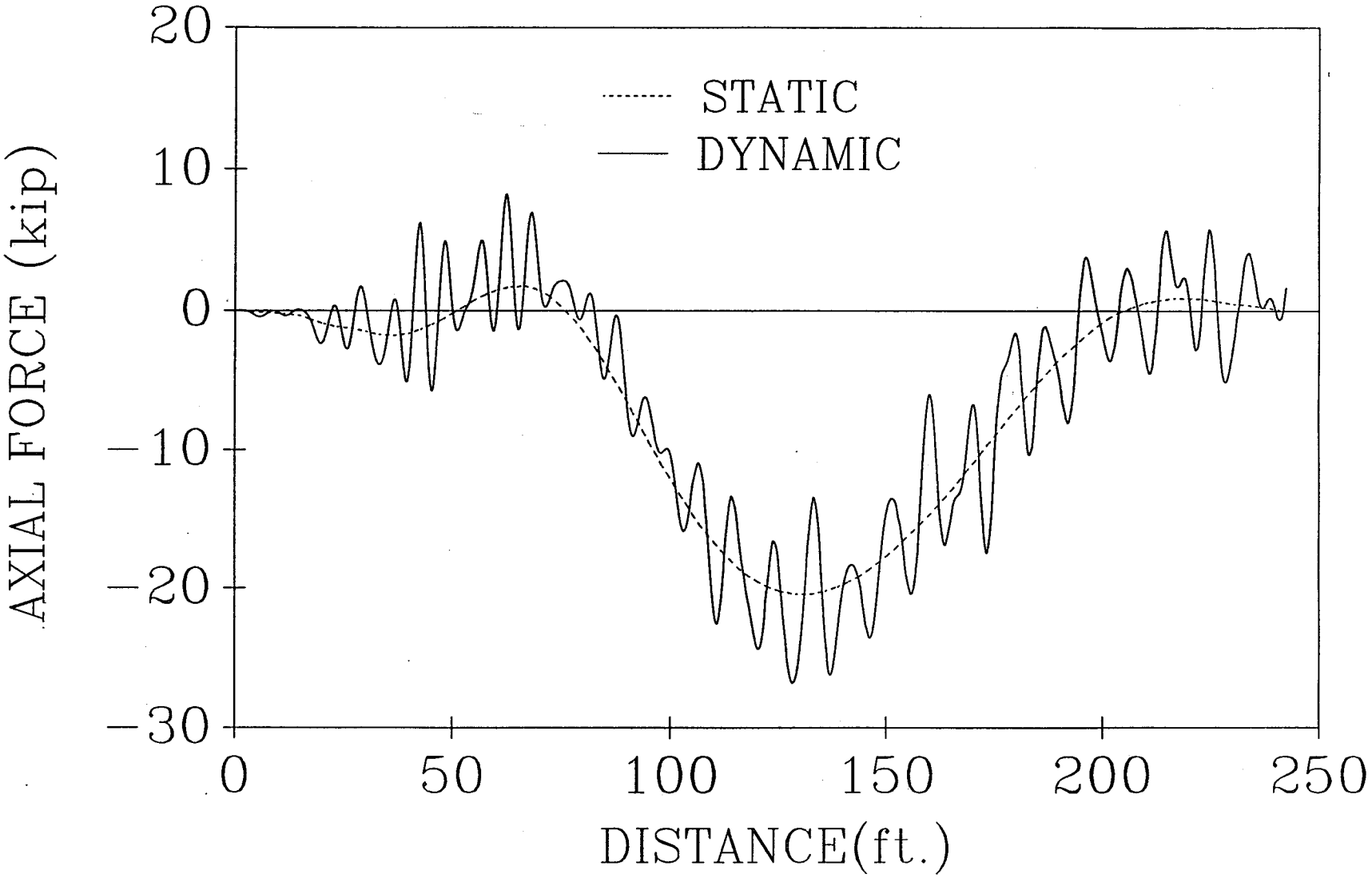

Fig. 4-39 Histories of Axial Force at Section 4 of Frame 1.

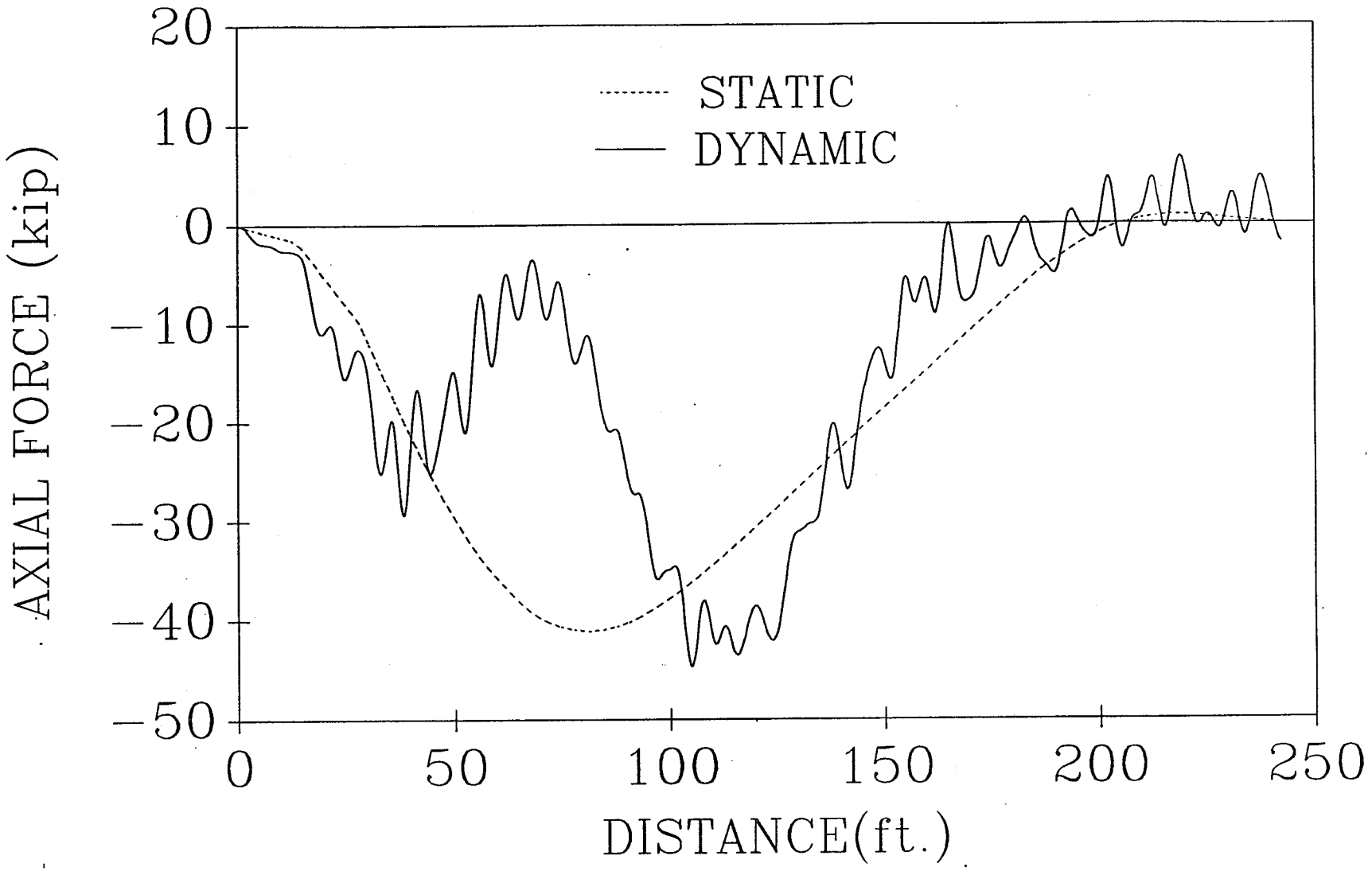

Fig. 4-40 Histories of Axial Force at Section 4 of Frame 2.

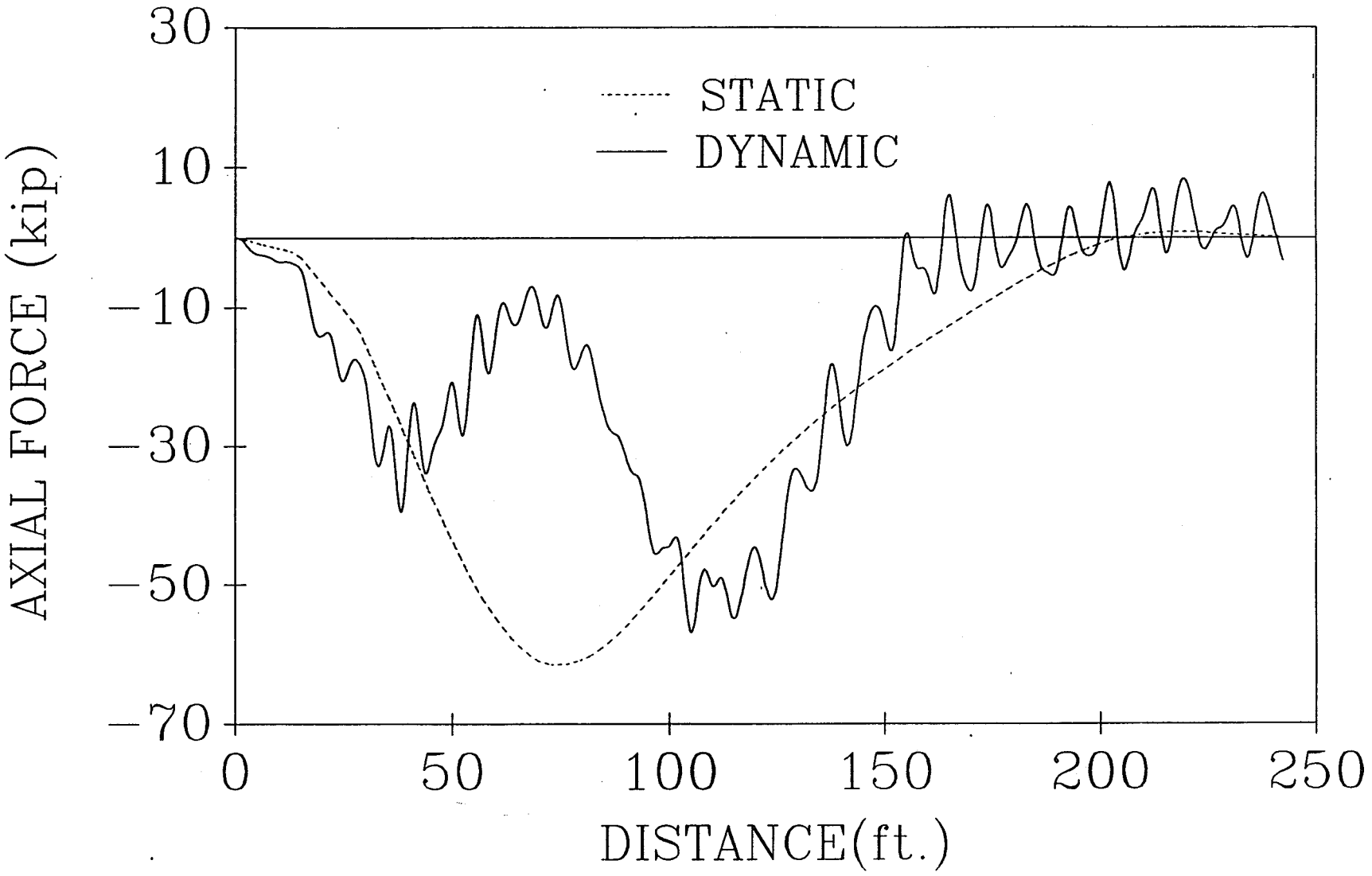

Fig. 4-41 Histories of Axial Force at Section 4 of Frame 3.

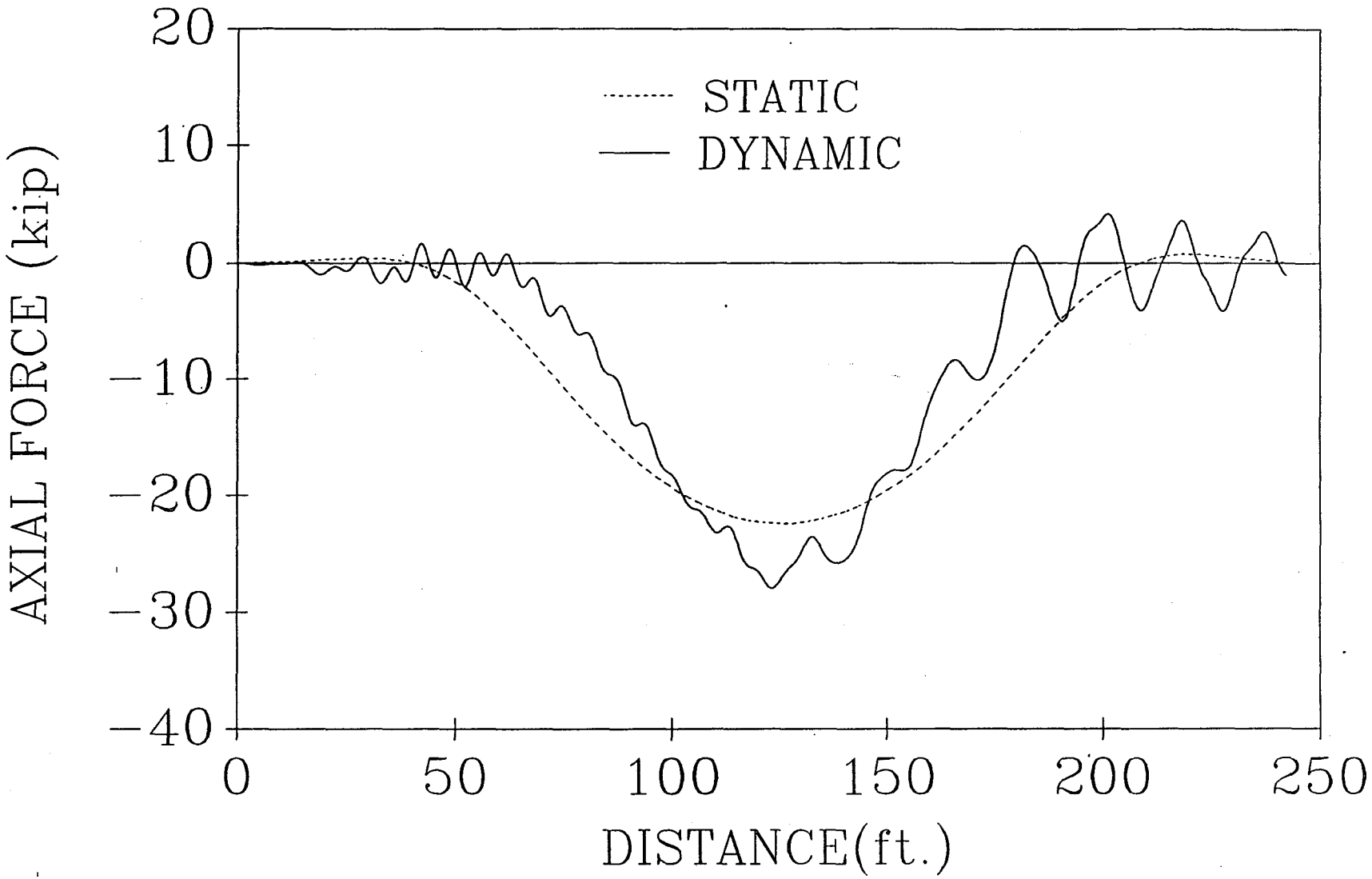

Fig. 4-42 Histories of Axial Force at Section 6 of Frame 1.

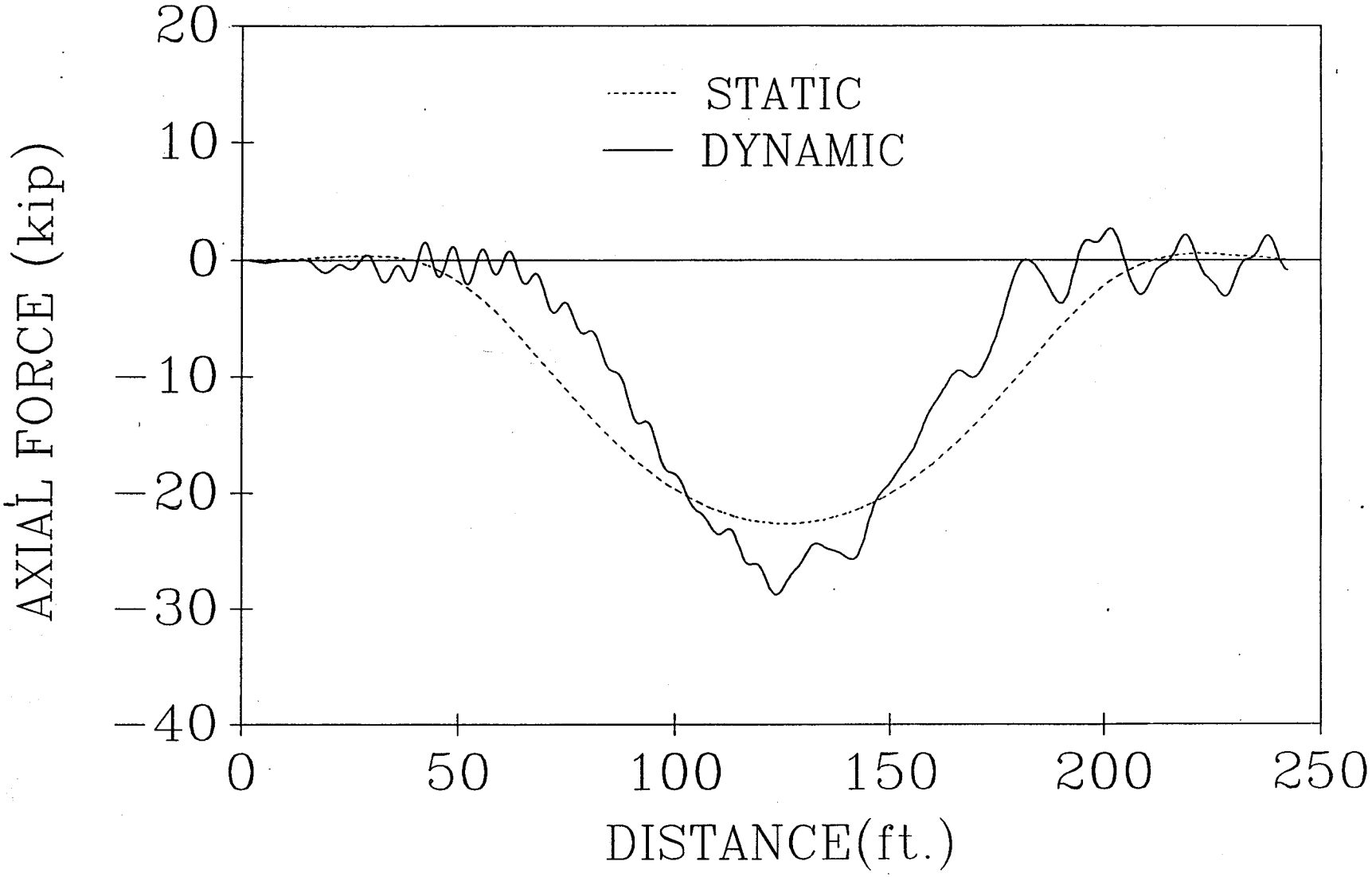

Fig. 4-43 Histories of Axial Force at Section 6 of Frame 2.

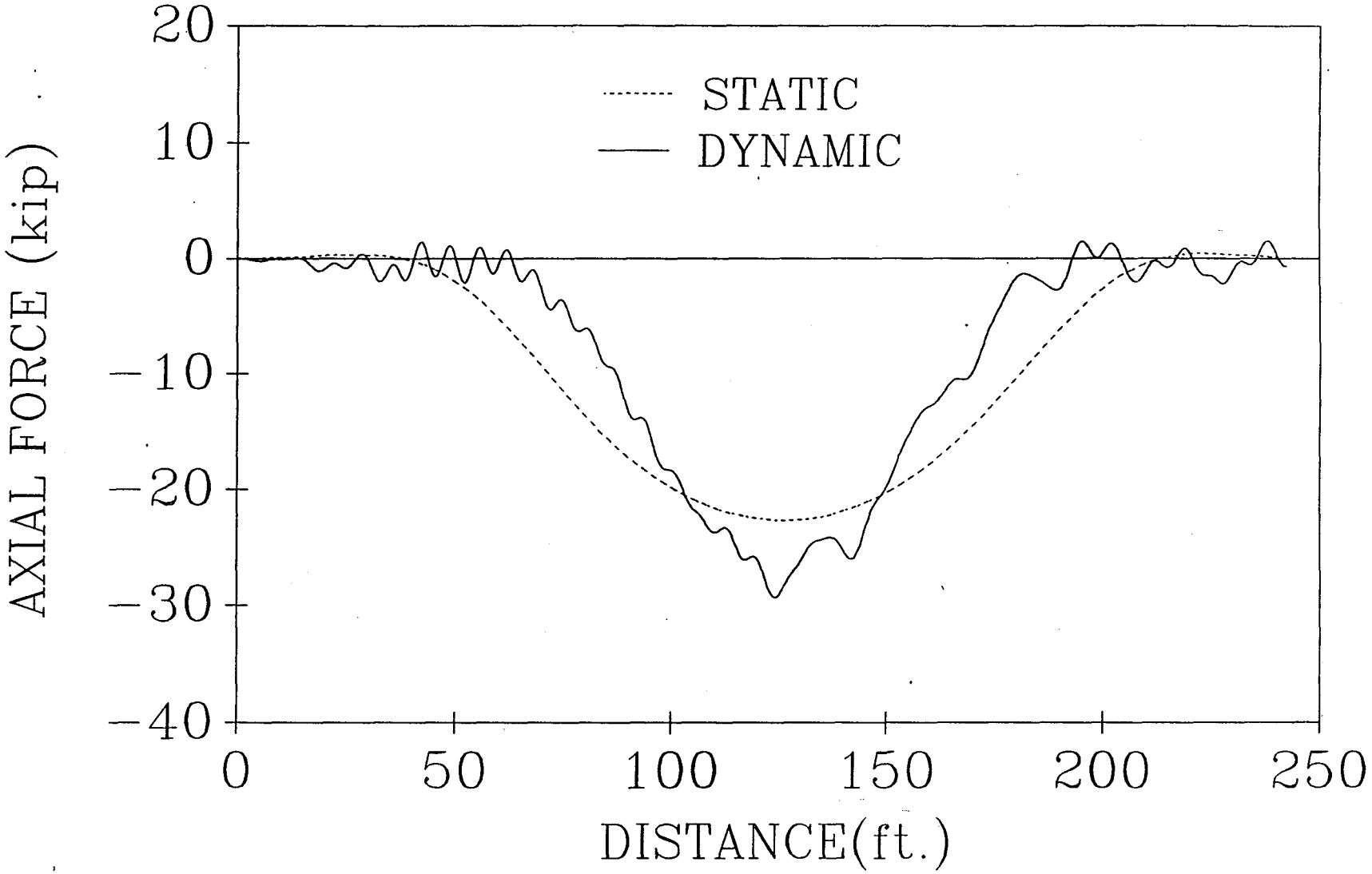

Fig. 4-44 Histories of Axial Force at Section 6 of Frame 3.

corresponding static moment. These differences are due to the fact that the shape of the static influence lines are different in the two cases. The variation of the influence line for moment along the span length is much sharper than that for deflection. Consequently, the length, under which static responses are comparatively larger, for moment is much shorter than that for deflection. The static influence lines of axial forces at Sections 4 and 6 are similar. Their dynamic axial forces will mainly be affected by symmetric modes. It can be expected that the dynamic axial forces at those sections will not have much difference.

4.4.4. Effect of Loading Position

In order to know the effect of lateral loading position on the dynamic response of the slant-legged rigid frame bridge, the transverse wheel-load distribution factors and impact factors of each frame for symmetric and asymmetric one truck loading cases (see Fig. 4-45) were evaluated and given in Table 4-3. The wheel-load distribution factors acquired for the study is defined the same as in Chapter III (Eq. 3-16). The impact factor is defined the same as in Chapter III (Eq. 3-17).

The results illustrated in Table 4-3 were determined on the basis of 55 mph (88.5 km/hr) vehicle speed and good road surface. From Table 4-3, we can observe that: (1) For most section, the loading position affects the impact of each frame greatly. With symmetric loading, the larger the static wheel-load distribution factor is, the smaller the impact factor will be. Under asymmetric loading, most impact factors of exterior frame are larger than those of Frame 2. This is due to the influence of torsion. (2). The influence of loading position on the impact of axial force of girders is comparatively small.

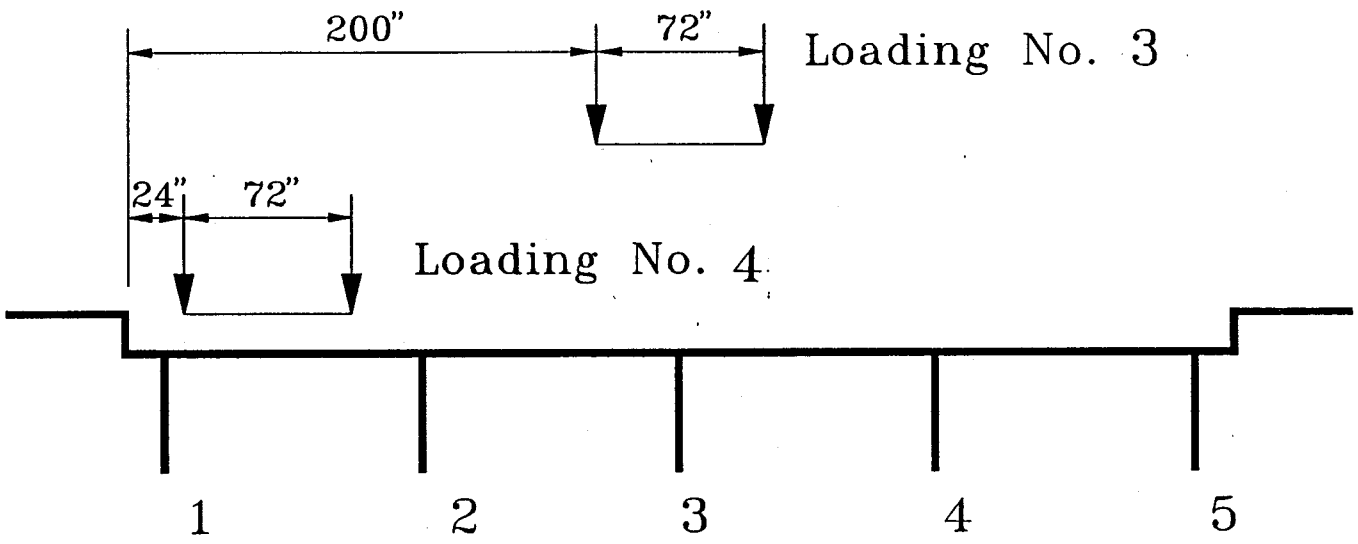

Fig. 4-45 One-truck Loading.

Table 4-3. Effect of Loading Position (Single Car).

Section	Beam	Symmetric Loading				Asymmetric Loading			
		Static Distribution		Impact Factor		Static Distribution		Impact Factor	
		M	N	M	N	M	N	M	N
1	1	-0.197	N/A	68.62	N/A	1.166	N/A	13.09	N/A
	2	0.664	N/A	20.60	N/A	0.707	N/A	11.06	N/A
	3	1.067	N/A	4.81	N/A	0.263	N/A	31.60	N/A
3	1	0.360	0.203	33.14	43.09	0.982	1.162	22.56	13.50
	2	0.399	0.402	19.97	20.23	0.646	0.653	24.92	11.92
	3	0.482	0.791	7.41	-22.78	0.415	0.266	22.91	39.68
6	1	0.267	0.397	20.51	31.56	1.048	1.005	-10.03	29.70
	2	0.465	0.401	-11.37	31.94	0.666	0.701	-6.39	28.99
	3	0.537	0.404	-14.42	32.21	0.339	0.397	0.560	30.34

Note: M and N as Table 2.

4.4.5. Effect of Vehicle Speed and Road Surface Roughness

Figs. 4-46 to 4-49 gives the variation of impact factors of exterior frame with vehicle speed and road surface roughness for asymmetric loading of two trucks. This figure presents some information about the effect of vehicle speed and road profile. With variation of vehicle speed, one or more peak values of impact appear. The speeds at which the peak value of impact occurs change with different sections and different types of internal forces. The primary reason for that is the different sections and types of internal forces have different shapes of static influence lines and their dynamic responses will be dominated by different vibration modes. However, under the situation of very good and good road surface, the impact factors of each section are slightly affected by the variation of vehicle speeds. With increasing the road surface roughness, the impact factors of each section increase tremendously.

4.4.6. Effect of Static Axial Force

The effect of axial force caused by dead load was demonstrated in Table 4-4. The results shown in the table were calculated under the conditions of 55 MPH (88.5 km/hr) vehicle speed and good surface roughness. From Table 4-4, the following conclusion can be drawn. The present of axial force induced by dead load will increase the dynamic moment and deflection at Sections 3 and 6. But the increase is limited for the slant-legged rigid frame bridges with short to medium span length.

4.4.7. Effect of Damping Ratio

Table 4-5 gives the variation of impact factors of exterior frame with the damping ratios changing from 0 to 3 % . The results shown in Table 4-5 were computed according to good road

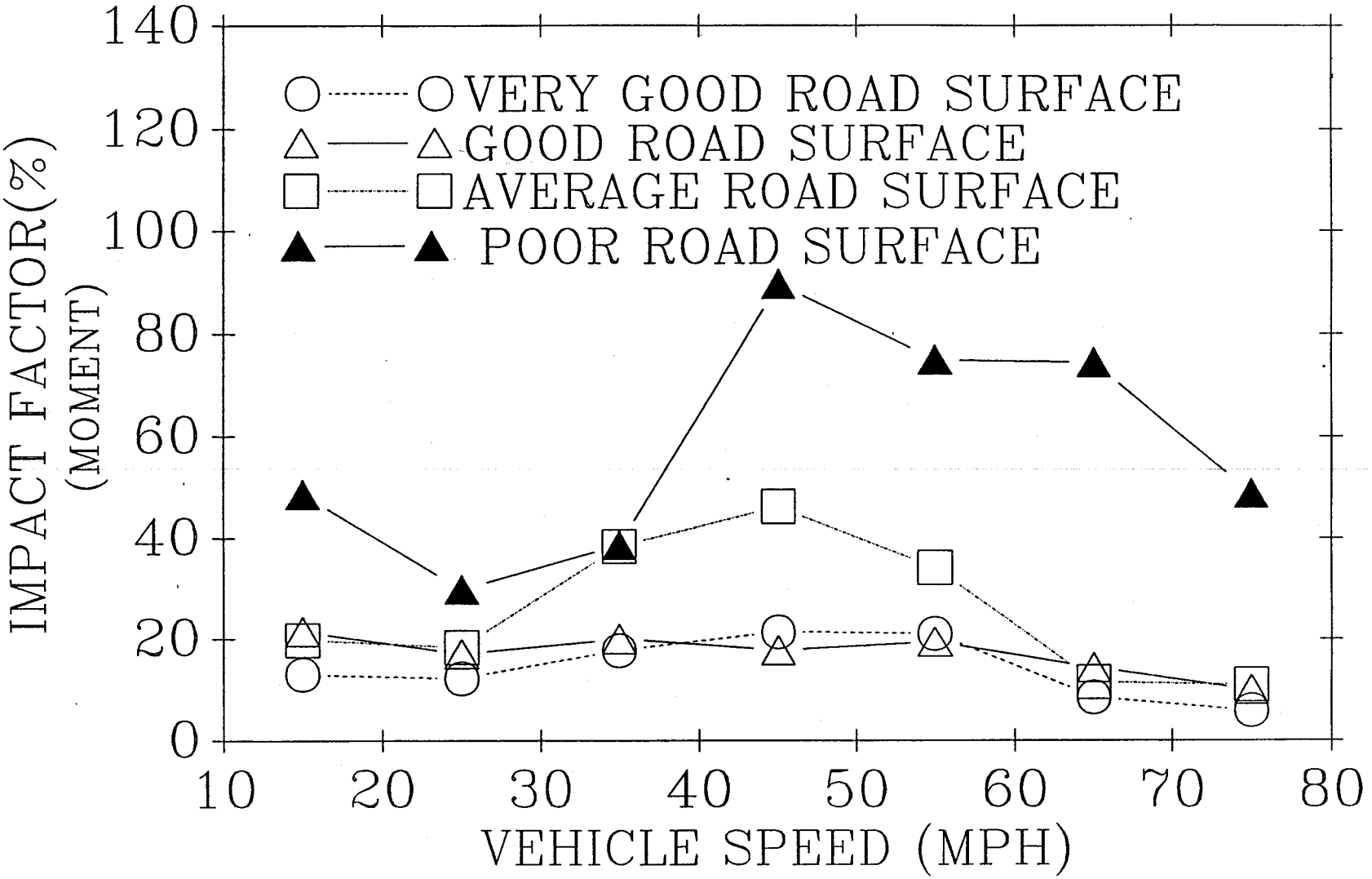

Fig. 4-46 Variation of Impact Factors with Vehicle Speeds at Section 1 of Frame 1.

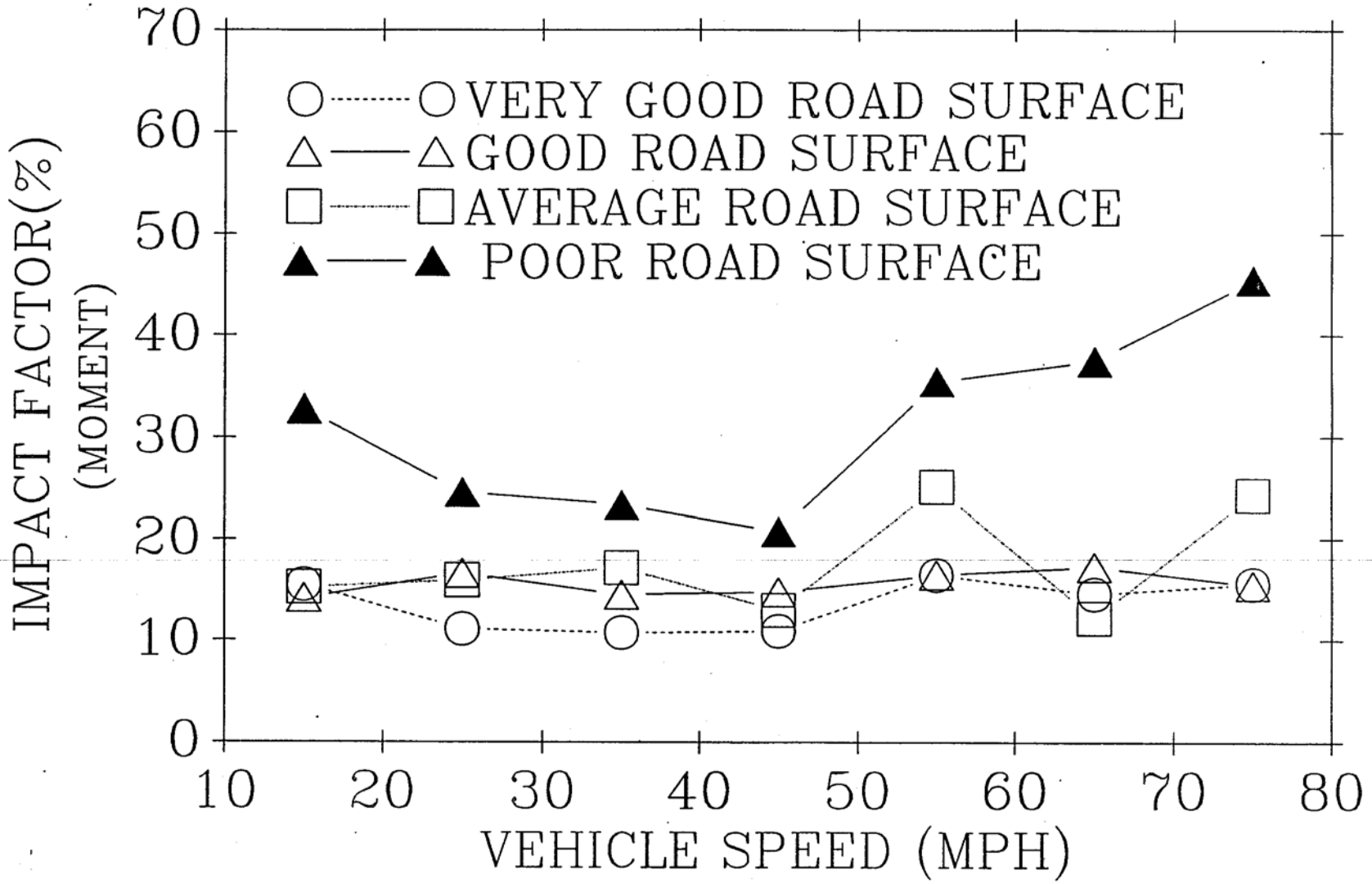

Fig. 4-47 Variation of Impact Factors with Vehicle Speeds at Section 4 of Frame 1.

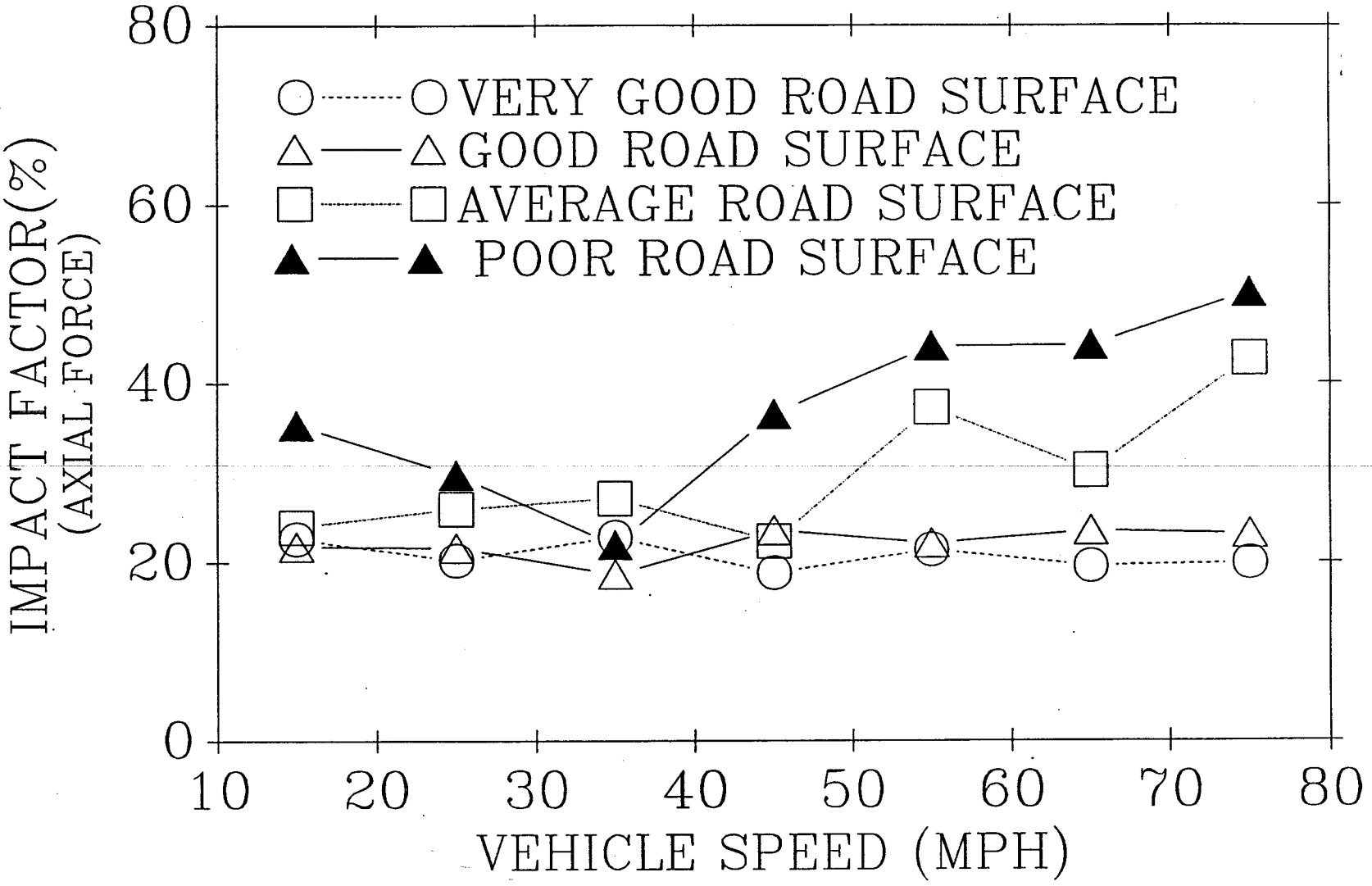

Fig. 4-48 Variation of Impact Factors with Vehicle Speeds at Section 3 of Frame 1.

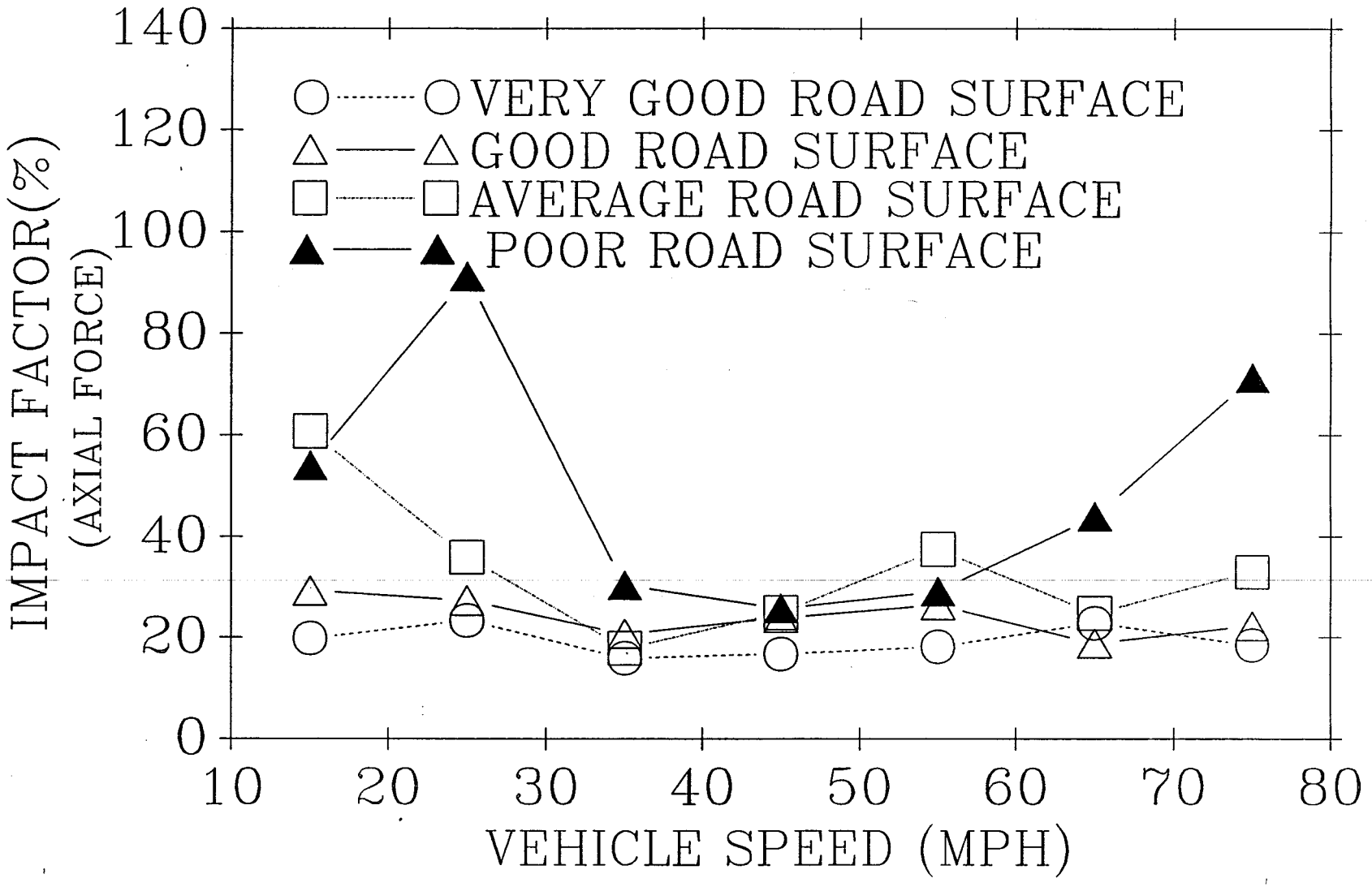

Fig. 4-49 Variation of Impact Factors with Vehicle Speeds at Section 5 of Frame 1.

Table 4-4. Influence of Static Axial Force.

Section	2	3		4		6		
Internal force	M(kip-in) $x10^3$	M(kip-in) $x10^3$	N (kip)	M(kip-in) $x10^3$	N (kip)	M(kip-in) $x10^3$	N (kip)	D (in)
With axial force	-5.06	-4.20	-56.0	-6.52	-33.2	5.09	-29.4	0.412
No axial force	-5.05	-4.15	-56.0	-6.52	-33.2	5.05	-29.4	0.409

Note: M, N, and D as Table 2.

Table 4-5. The Influence of Damping Ratio.

Section	Response	Damping Ratio			
		No Damping	1% for First and Second Modes	2% for First and Second Modes	3% for First and Second Modes
1	M	21.23	19.47	17.83	15.98
2	M	23.19	21.17	19.40	17.34
3	M	26.21	23.08	19.59	16.85
4	M	21.93	16.46	14.91	14.00
	N	34.62	25.75	23.24	21.32
6	M	-5.59	-6.38	-6.67	-6.88
	N	29.38	26.42	24.48	23.63

Note: M and N as Table 2.

surface and _55 MPH (88.5 km/hr) vehicle sped. From Table 4-5, it can be seen that the dynamic response decreases with increasing damping ratios. However, the influence of damping ratio on the impact of bending moment at mid-span and axial force at Section 3 is comparatively smaller, while that of the others are relatively larger.

4.4.8. Maximum Impact Factors

According to the foregoing analysis, the impact is greatly affected by lateral load position, vehicle speed, and different sections. Therefore, it has more practical significance to obtain the maximum impact factors at several control sections.

Table 4-6 gives the maximum impact factors of some typical sections. Only the larger responses of the symmetric sections were listed in the table. The maximum responses were obtained through changing vehicle speeds from', 15 MPH (24.14 km/hr) to 75 MPH (120.68 km/hr) and the transverse loading positions of vehicles, which were found that the Loading No.2 (see Fig. 4-16) will induce the maximum static response of Frames 1 and 2 as well as Loading No. 1 (see Fig. 4-16) will produce that of center frame. From Table 4-6, the following results can be obtained. The maximum impact factors f interior frame, for bending moment of side span and middle span as well as for axial force of slant legs, are much less than those of exterior frames; while the maximum impact factors of each frame for axial force of middle span and moment of slant legs are comparatively uniform. It is worth noting .that: the dynamic characteristics of moment for side span and middle span appear to be similar to those of axial force for slant legs; the dynamic behavior of ax~al force for middle span is similar to those of bending moment for slant legs. It can also be found from Table 4-6 that the maximum impact

Table 4-6. Maximum Impact Factors.

Section	Beam	Road Surface Roughness						AASHTO Specifications
		very Good		good		Average		
		M	N	M	N	M	N	
1 and 11	1	21.42	N/A	35.90	N/A	46.19	N/A	28.52
	2	4.38	N/A	20.58	N/A	24.13	N/A	
	3	12.27	N/A	24.09	N/A	29.96	N/A	
2 and 10	1	22.45	N/A	24.30	N/A	47.12	N/A	24.08
	2	3.68	N/A	9.4	N/A	21.95	N/A	
	3	13.63	N/A	18.13	N/A	32.92	N/A	
3 and 9	1	24.20	24.52	31.17	25.52	34.14	42.70	
	2	25.46	0.15	32.17	-0.21	40.14	10.33	
	3	18.07	-11.61	37.38	-4.56	40.71	-3.10	
4 and 8	1	16.44	23.06	19.32	29.91	29.46	46.26	
	2	18.68	24.55	19.86	28.97	28.26	40.98	
	3	22.40	29.86	30.05	33.06	34.12	42.54	
5 and 7	1	6.42	24.54	15.79	30.06	23.34	57.20	20.83
	2	-5.53	22.79	1.48	28.22	19.48	47.51	
	3	-9.45	26.98	-5.25	31.12	4.94	42.78	
6	1	-7.26	23.34	-5.18	29.21	-1.10	60.72	
	2	-13.34	22.42	-11.15	27.35	-1.25	49.37	
	3	-16.72	24.84	-10.30	29.91	-10.07	37.86	

factors for axial force and moment are quite different, especially at Sections 3, 5 and 6. The impact of axial force at Sections 5 and 6 is extremely larger than that of moment at the same sections. On the contrary, the impact of momen[1] at Section 3 is greatly larger than that of axial force. In this situation, giving the same impact 'actor to different kinds of internal forces seems to be unreasonable.

.I_I

Table 4-6 also gives the impact factors calculated by Eq. (3-18). From the table, it can be seen that, provided with very good road surface, the maximum impact factors obtained by the present theory at most sections are less or close to the values determined by Eq. (3-18). It should be mentioned that the impact factors for Moment at Sections 5 and 6 are distinctly smaller than the value evaluated by Eq. (3-18), while the impact factors of axial force are a little larger than the value. On the whole, based on AASHtO specifications, the design for sections 5 and 6 may seem to conservative if bridges have very' good surface roughness. With increasing road surface roughness, the maximum impact factors", can reach high values.

CHAPTER V

CONCLUSIONS AND RECOMMENDATIONS

In this study, according to the Type 3, Type 3S2, and Type 3-3 truck rating vehicles specified in the AASHTO Guide Specifications for Strength Evaluation of Existing Steel and Concrete Bridges [8], three nonlinear vehicle modes with nine, sixteen, and eighteen degrees of freedom are developed.

Then, six continuous multigirder bridges with different span lengths are designed based on the Standard Plans to Highway Bridge Superstructures of U. S. Bureau of Public Roads. The continuous multigirder bridges are modeled as grillage bea nm systems. The effects of transverse stiffness, road surface roughness, vehicle speed, span length, spacing of girders and damping ratio are analyzed.

' Finally, the slant-legged rigid frame bridge is modeled as a space bar system. The effect of axial force, caused by dead load, on the dynamic response of the bridge is considered. The free and force vibration characteristics, including parametric study, are studied.

Maximum dynamic responses of continuous bridges I and slant-legged rigid frame bridges are determined for two trucks (side by side) through changing their transverse positions with different speeds and road surface roughness. The conclusions of the research for continuous beam bridges are summarized as follows:

1. Impact factors of each girder of continuous multigirder bridges are closely related to its wheel-load distribution factors. The larger the load carried by a girder, the smaller the impact factors will be.

2. Impact factors of exterior girder are affected by both vertical (z-direction) and torsional accelerations of the bridges. Generally, the static and dynamic wheel-load distributions of girders are different and the impact factors of exterior girders of the steel girder bridges are greatly larger than those of interior girders. For this reason, it is not suitable to assign same value of impact factor to all girders in the steel I, bridge design practice.

3. Because of the influence of higher natural frequencies, the impact factors of sections over interior supports are larger than the other sections and the impact of side span is generally larger than the impact of middle span.

4. Under the conditions of very good road surface roughness, the impact factors of most sections of exterior girders of six continuous bridges are less than 30 %. The impact factors of most sections of interior girders are less than 25 %. However, the impact factors increase tremendously with increasing road surface roughness and very high impact will occur for poor road surface roughness.

5. Most impact factors of the six bridges at Section 3 (middle span) with average or better road surface, at Section 1 or 5 (side span) with good or better road surface and at Sections over interior supports with very good road surface are less than those calculated by AASHTO

impact equation. Nevertheless, the impact factors over interior supports for bridges with spans of 56-70-56 ft. and 48-60-48 ft. may exceed the value evaluated according to AASHTO impact factor equation. It seems more suitable to take the sum o~ 0.3 side span length and 0.25 middle span length, instead of the average of side and middle sp~ lengths, as L defined in AASHTO impact formula. Nevertheless, more reasonable impact formula needs to be developed.

6. With the increase of transverse stiffness, the static and dynamic wheel-load distribution factors of exterior girders increase and those of interior girders decrease. However, this variation of the factors at most sections is insignificant. Based on this situation, too large transverse stiffness in this kind of steel multigirder bridges seems to be unnecessary.

7. With changing the spacing of girders from 6.5 ft. to 8 ft., the static wheel-load factors of each girder increase and the impact factors decrease, except that at Sections 1 and 3 of exterior girder. Basically, the variation of maximum impact factors with the spacing of girders is not significant.

8. The existence of damping decreases the response of the bridges, but the influence of damping ratio on the impact of each component is different. The response of sections over interior supports was affected significantly by damping ratio, while the influence of damping ratio on Section 3 (middle span) is comparatively small.

The conclusions of the investigation for the slant-legged rigid frame bridge are:

1. The existence of the static axial force increases the dynamic response of mid span and legs, but the increase is small for the bridges with short to middle span lengths.

2. The number of vibration modes used in the proposed numerical procedure is very important. It depends on different sections and (,different types of responses. Generally, thirty modes are quite enough for all responses of slat-legged rigid frame bridges.

3. Lateral loading position greatly influences the impact of bending moment of girders and the impact of axial force of legs.. Generally, the larger the wheel-load distribution factor is, the smaller the impact will be. The dynamic behavior of this bridge is similar to that of beam/girder bridges [12, 31]. The effect of lateral loading position on the impact of axial force of each girder is comparatively smaller.

4. With changing vehicle speed from 15 MPH (24.14 km/hr) to 75 MPH (120.68 km/hr), impact factors of each section will appear one or more peak values. However, on the basis of very good or good road surface roughness, the variation of impact factors with vehicle speeds is relatively small. With increasing road roughness, the impact of the bridge increases significantly.

5. Increasing damping ratio will decrease', the dynamic response. Nevertheless, the effect of damping ratio varies with different sections and different types of internal forces. The impact of bending moment at mid-span is slightly affected by changing damping ratios from 0 % to 3 and the effect of damping ratio on the others ar6 comparatively larger.

6.The maximum impact factors of the slant-legged', rigid frame bridge vary with different frames, sections, and different types of responses. Owing to the effect of torsion, the maximum impact factors of exterior frame for moment of side span and middle span as well as for axial force of slant legs are greatly larger than that of interior frames. The maximum impact factors of each frame for axial force of middle span and for moment of slant legs do not have much difference.

7. The maximum impact factors of moment and axial force at most sections are quite different. For middle span, the maximum impact factors, of axial force are significantly larger than those of bending moment. Oppositely, for legs, the maximum impact factors of axial force are greatly smaller than those of moment. Under this situation, it seems to be unreasonable to give same impact value to different types of responses in the bridge design practice. Moreover, the impact factors of deflection at Section 6 are distinctly, larger than those of moment. It is not suitable to take the impact factor of deflection as that of',internal forces.

8. Provided with very good road surface, the maximum impact factors at most sections are less than or close to the values determined by AASHTO specifications. Although, the maximum impact factors of axial force at Sections 5 to 7 are a little larger than the value specified by AASHTO, those of moment are greatly smaller than the value. On the whole, the design for Sections 5 to 7 may seem conservative. However, with increasing road surface roughness, the maximum impact factors will distinctively exceed the impact values specified by AASHTO.

The study in this phase is devoted to the impact analysis of straight girder/beam bridge; In Phase III, the dynamic investigation of curved bridges will be carried out.

APPENDIX

EQUATIONS OF MOTION OF VEHICLE MODELS

A.1 Type 3 with 9-DOF's Vehicle Model

I. Degrees of Freedom and Masses of Each Rigid Body:

1. y_{t1}, m_{t1}: Truck vertical displacement and mass
2. ϕ_{t1}, I_{xt1}: Truck roll displacement and mass moment of inertia
3. θ_{t1}, I_{zt1}: Truck pitch displacement and mass moment of inertia
4. y_{a1}, m_{a1}: The first axle vertical displacement and mass
5. ϕ_{a1}, I_{xa1}: The first axle roll displacement and mass moment of inertia
6. y_{a2}, m_{a2}: The second axle vertical displacement and mass
7. ϕ_{a2}, I_{xa2}: The second axle roll displacement and mass moment of inertia
8. y_{a3}, m_{a3}: The third axle vertical displacement and mass
9. ϕ_{a3}, I_{xa3}: The third axle roll displacement and mass moment of inertia

II. Relative Displacement at Spring Locations:

1. Suspension Springs:

$$U_{sy1} = (y_{t1} - y_{a1}) + (s_1/2)(\phi_{t1} - \phi_{a1}) + l_3\theta_{t1}$$

$$U_{sy2} = (y_{t1} - y_{a1}) - (s_1/2)(\phi_{t1} - \phi_{a1}) + l_3\theta_{t1}$$

$$U_{sy3} = (y_{t1} - y_{a2}) + (s_2/2)(\phi_{t1} - \phi_{a2}) - l_4\theta_{t1}$$

$$U_{sy4} = (y_{t1} - y_{a2}) - (s_2/2)(\phi_{t1} - \phi_{a2}) - l_4\theta_{t1}$$

$$U_{sy5} = (y_{t1} - y_{a3}) + (s_3/2)(\phi_{t1} - \phi_{a3}) - (l_2+l_4)\theta_{t1}$$

$$U_{sy6} = (y_{t1} - y_{a3}) - (s_3/2)(\phi_{t1} - \phi_{a3}) - (l_2+l_4)\theta_{t1}$$

2. Tire Springs:

$$U_{ty1} = y_{a1} + (d_1/2)\phi_{a1} - (-u_{SR1})$$

$$U_{ty2} = y_{a1} - (d_1/2)\phi_{a1} - (-u_{SR2})$$

$$U_{ty3} = y_{a2} + (d_2/2)\phi_{a2} - (-u_{SR3})$$

$$U_{ty4} = y_{a2} - (d_2/2)\phi_{a2} - (-u_{SR4})$$

$$U_{ty5} = y_{a3} + (d_3/2)\phi_{a3} - (-u_{SR5})$$

$$U_{ty6} = y_{a3} - (d_3/2)\phi_{a3} - (-u_{SR6})$$

in which: u_{SRi} = road surface roughness under the ith wheel (positive upwards), i = 1 to 6.

III. Equations of Motion:

1. Vertical Displacement of the Truck, y_{t1}:

$$m_{t1}\ddot{y}_{t1} + (F_{sy1} + F_{sy2} + F_{sy3} + F_{sy4} + F_{sy5} + F_{sy6}) + (F_{dsy1} + F_{dsy2} + F_{dsy3} + F_{dsy4} + F_{dsy5} + F_{dsy6}) = m_{t1}g$$

2. Roll Displacement of the Truck, ϕ_{t1}:

$$I_{xt1}\ddot{\phi}_{t1} + (s_1/2)(F_{sy1} - F_{sy2}) + (s_2/2)(F_{sy3} - F_{sy4}) + (s_3/2)(F_{sy5} - F_{sy6}) + (s_1/2)(F_{dsy1} - F_{dsy2}) + (s_2/2)(F_{dsy3} - F_{dsy4}) + (s_3/2)(F_{dsy5} - F_{dsy6}) = 0$$

3. Pitch Displacement of the Truck, θ_{t1}:

$$I_{zt1}\ddot{\theta}_{t1} + l_3(F_{sy1} + F_{sy2}) - l_4(F_{sy3} + F_{sy4}) - (l_2 + l_4)(F_{sy5} + F_{sy6}) + l_3(F_{dsy1} + F_{dsy2}) - l_4(F_{dsy3} + F_{dsy4}) - (l_2 + l_4)(F_{dsy5} + F_{dsy6}) = 0$$

4. Vertical Displacement of the First Axle, y_{a1}:

$$m_{a1}\ddot{y}_{a1} - (F_{sy1} + F_{sy2}) + (F_{ty1} + F_{ty2}) - (F_{dsy1} + F_{dsy2}) + (F_{dty1} + F_{dty2}) = m_{a1}g$$

5. Roll Displacement of the First Axle, ϕ_{a1}:

$$I_{xa1}\ddot{\phi}_{a1} - (s_1/2)(F_{sy1} - F_{sy2}) + (d_1/2)(F_{ty1} - F_{ty2}) - (s_1/2)(F_{dsy1} - F_{dsy2}) + (d_1/2)(F_{dty1} - F_{dty2}) = 0$$

6. Vertical Displacement of the Second Axle, y_{a2}:

$$m_{a2}\ddot{y}_{a2} - (F_{sy3} + F_{sy4}) + (F_{ty3} + F_{ty4}) - (F_{dsy3} + F_{dsy4}) + (F_{dty3} + F_{dty4}) = m_{a2}g$$

7. Roll Displacement of the Second Axle, ϕ_{a2}:

$$I_{xa2}\ddot{\phi}_{a2} - (s_2/2)(F_{sy3} - F_{sy4}) + (d_2/2)(F_{ty3} - F_{ty4}) - (s_2/2)(F_{dsy3} - F_{dsy4}) + (d_2/2)(F_{dty3} - F_{dty4}) = 0$$

8. Vertical Displacement of the Third Axle, y_{a2}:

$$m_{a3}\ddot{y}_{a3} - (F_{sy5} + F_{sy6}) + (F_{ty5} + F_{ty6}) - (F_{dsy5} + F_{dsy6}) + (F_{dty5} + F_{dty6}) = m_{a3}g$$

9. Roll Displacement of the Third Axle, ϕ_{a2}:

$$I_{xa3}\ddot{\phi}_{a3} - (s_3/2)(F_{sy5} - F_{sy6}) + (d_3/2)(F_{ty5} - F_{ty6}) - (s_3/2)(F_{dsy5} - F_{dsy6}) + (d_3/2)(F_{dty5} - F_{dty6}) = 0$$

in which: $F_{syi} = K_{syi}U_{syi} + F_{yi}$, $F_{dsyi} = D_{syi}\dot{U}_{syi}$,

$F_{tyi} = K_{tyi}U_{tyi}$, $F_{dtyi} = D_{tyi}\dot{U}_{tyi}$, i = 1 to 6, and

F_{yi} = the friction force at the ith suspension.

A.2 Type 3S2 (FDOT Truck) with 16-DOF's Vehicle Model

I. Degrees of Freedom and Masses of Each Rigid Body:

1. y_{t1}, m_{t1}: Tractor vertical displacement and mass

2. ϕ_{t1}, I_{xt1}: Tractor roll displacement and mass moment of inertia

3. θ_{t1}, I_{zt1}: Tractor pitch displacement and mass moment of inertia

4. y_{t2}, m_{t2}: Trailer vertical displacement and mass

5. ϕ_{t2}, I_{xt2}: Trailer roll displacement and mass moment of inertia

6. θ_{t2}, I_{zt2}: Trailer pitch displacement and mass moment of inertia

7. y_{a1}, m_{a1}: Steer axle vertical displacement and mass

8. ϕ_{a1}, I_{xa1}: Steer axle roll displacement and mass moment of inertia

9. y_{a2}, m_{a2}: Vertical displacement and mass of forward axle of tractor tandem

10. ϕ_{a2}, I_{xa2}: Roll displacement and mass moment of inertia of forward axle of tractor tandem

11. y_{a3}, m_{a3}: Vertical displacement and mass of aft axle of tractor tandem

12. ϕ_{a3}, I_{xa3}: Roll displacement and mass moment of inertia of aft axle of tractor tandem

13. y_{a4}, m_{a4}: Vertical displacement and mass of forward axle of trailer tandem

14. ϕ_{a4}, I_{xa4}: Roll displacement and mass moment of inertia of forward axle of trailer tandem

15. y_{a5}, m_{a5}: Vertical displacement and mass of aft axle of trailer tandem

16. ϕ_{a5}, I_{xa5}: Roll displacement and mass moment of inertia of aft axle of trailer tandem

II. Relative Displacement at Spring Locations:

1. Suspension Springs:

$$U_{sy1} = (y_{t1} - y_{a1}) + (s_1/2)(\phi_{t1} - \phi_{a1}) + l_5\theta_{t1}$$

$$U_{sy2} = (y_{t1} - y_{a1}) - (s_1/2)(\phi_{t1} - \phi_{a1}) + l_5\theta_{t1}$$

$$U_{sy3} = (y_{t1} - y_{a2}) + (s_2/2)(\phi_{t1} - \phi_{a2}) - l_6\theta_{t1}$$

$$U_{sy4} = (y_{t1} - y_{a2}) - (s_2/2)(\phi_{t1} - \phi_{a2}) - l_6\theta_{t1}$$

$$U_{sy5} = (y_{t1} - y_{a3}) + (s_3/2)(\phi_{t1} - \phi_{a3}) - (l_2+l_6)\theta_{t1}$$

$$U_{sy6} = (y_{t1} - y_{a3}) - (s_3/2)(\phi_{t1} - \phi_{a3}) - (l_2+l_6)\theta_{t1}$$

$$U_{sy7} = (y_{t2} - y_{a4}) + (s_4/2)(\phi_{t2} - \phi_{a4}) - l_9\theta_{t2}$$

$$U_{sy8} = (y_{t2} - y_{a4}) - (s_4/2)(\phi_{t2} - \phi_{a4}) - l_9\theta_{t2}$$

$$U_{sy9} = (y_{t2} - y_{a5}) + (s_5/2)(\phi_{t2} - \phi_{a5}) - (l_4+l_9)\theta_{t2}$$

$$U_{sy10} = (y_{t2} - y_{a5}) - (s_5/2)(\phi_{t2} - \phi_{a5}) - (l_4+l_9)\theta_{t2}$$

2. Tire Springs:

$$U_{ty1} = y_{a1} + (d_1/2)\phi_{a1} - (-u_{SR1})$$

$$U_{ty2} = y_{a1} - (d_1/2)\phi_{a1} - (-u_{SR2})$$

$$U_{ty3} = y_{a2} + (d_2/2)\phi_{a2} - (-u_{SR3})$$

$$U_{ty4} = y_{a2} - (d_2/2)\phi_{a2} - (-u_{SR4})$$

$$U_{ty5} = y_{a3} + (d_3/2)\phi_{a3} - (-u_{SR5})$$

$$U_{ty6} = y_{a3} - (d_3/2)\phi_{a3} - (-u_{SR6})$$

$$U_{ty7} = y_{a4} + (d_4/2)\phi_{a4} - (-u_{SR7})$$

$$U_{ty8} = y_{a4} - (d_4/2)\phi_{a4} - (-u_{SR8})$$

$$U_{ty9} = y_{a5} + (d_5/2)\phi_{a5} - (-u_{SR9})$$

$$U_{ty10} = y_{a5} - (d_5/2)\phi_{a5} - (-u_{SR10})$$

in which: u_{SRi} = road surface roughness under the ith wheel (positive upwards), i = 1 to 10.

III. Equations of Motion:

1. Vertical Displacement of the Tractor, y_{t1}:

$$m_{t1}\ddot{y}_{t1} + (F_{sy1} + F_{sy2} + F_{sy3} + F_{sy4} + F_{sy5} + F_{sy6}) - (l_9/l_8)(F_{sy7} + F_{sy8}) - (1/l_8)(l_4 + l_9)(F_{sy9} + F_{sy10}) + (F_{dsy1} + F_{dsy2} + F_{dsy3} + F_{dsy4} + F_{dsy5} + F_{dsy6}) - (l_9/l_8)(F_{dsy7} + F_{dsy8}) - (1/l_8)(l_4 + l_9)(F_{dsy9} + F_{dsy10}) = m_{t1}g$$

2. Roll Displacement of the Tractor, ϕ_{t1}:

$$I_{xt1}\ddot{\phi}_{t1} + (s_1/2)(F_{sy1} - F_{sy2}) + (s_2/2)(F_{sy3} - F_{sy4}) + (s_3/2)(F_{sy5} - F_{sy6}) + (s_1/2)(F_{dsy1} - F_{dsy2}) + (s_2/2)(F_{dsy3} - F_{dsy4}) + (s_3/2)(F_{dsy5} - F_{dsy6}) = 0$$

3. Pitch Displacement of the Tractor, θ_{t1}:

$$I_{zt1}\ddot{\theta}_{t1} + l_5(F_{sy1} + F_{sy2}) - l_6(F_{sy3} + F_{sy4}) - (l_2 + l_6)(F_{sy5} + F_{sy6}) + l_7(l_9/l_8)(F_{sy7} + F_{sy8}) + (l_7/l_8)(l_4 + l_9)(F_{sy9} + F_{sy10}) + l_5(F_{dsy1} + F_{dsy2}) - l_6(F_{dsy3} + F_{dsy4}) - (l_2 + l_6)(F_{dsy5} + F_{dsy6}) + l_7(l_9/l_8)(F_{dsy7} + F_{dsy8}) + (l_7/l_8)(l_4 + l_9)(F_{dsy9} + F_{dsy10}) = 0$$

4. Vertical Displacement of the Trailer, y_{t2}:

$$m_{t2}\ddot{y}_{t2} - (l_5/l_7)(F_{sy1} + F_{sy2}) + (l_6/l_7)(F_{sy3} + F_{sy4}) + (1/l_7)(l_2 + l_6)(F_{sy5} + F_{sy6}) + (F_{sy7} + F_{sy8} + F_{sy9} + F_{sy10}) - (l_5/l_7)(F_{dsy1} + F_{dsy2}) + (l_6/l_7)(F_{dsy3} + F_{dsy4}) + (1/l_7)(l_2 + l_6)(F_{dsy5} + F_{dsy6}) + (F_{dsy7} + F_{dsy8} + F_{dsy9} + F_{dsy10}) = m_{t2}g$$

5. Roll Displacement of the Trailer, ϕ_{t2}:

$$I_{xt2}\ddot{\phi}_{t2} + (s_4/2)(F_{sy7} - F_{sy8}) + (s_5/2)(F_{sy9} - F_{sy10}) + (s_4/2)(F_{dsy7} - F_{dsy8}) + (s_5/2)(F_{dsy9} - F_{dsy10}) = 0$$

6. Pitch Displacement of the Trailer, θ_{t2}:

$$I_{zt2}\ddot{\theta}_{t2} - l_8(l_5/l_7)(F_{sy1} + F_{sy2}) + l_8(l_6/l_7)(F_{sy3} + F_{sy4}) + (l_8/l_7)(l_2 + l_6)(F_{sy5} + F_{sy6}) - l_9(F_{sy7} + F_{sy8}) - (l_4 + l_9)(F_{sy9} + F_{sy10}) - l_8(l_5/l_7)(F_{dsy1} + F_{dsy2}) + l_8(l_6/l_7)(F_{dsy3} + F_{dsy4}) + (l_8/l_7)(l_2 + l_6)(F_{dsy5} + F_{dsy6}) - l_9(F_{dsy7} + F_{dsy8}) - (l_4 + l_9)(F_{dsy9} + F_{dsy10}) = 0$$

7. Vertical Displacement of the Steer Axle, y_{a1}:

$$m_{a1}\ddot{y}_{a1} - (F_{sy1} + F_{sy2}) + (F_{ty1} + F_{ty2}) - (F_{dsy1} + F_{dsy2}) + (F_{dty1} + F_{dty2}) = m_{a1}g$$

8. Roll Displacement of the Steer Axle, ϕ_{a1}:

$$I_{xa1}\ddot{\phi}_{a1} - (s_1/2)(F_{sy1} - F_{sy2}) + (d_1/2)(F_{ty1} - F_{ty2}) - (s_1/2)(F_{dsy1} - F_{dsy2}) + (d_1/2)(F_{dty1} - F_{dty2}) = 0$$

9. Vertical Displacement of the Forward Axle of the Tractor Tandem, y_{a2}:

$$m_{a2}\ddot{y}_{a2} - (F_{sy3} + F_{sy4}) + (F_{ty3} + F_{ty4}) - (F_{dsy3} + F_{dsy4}) + (F_{dty3} + F_{dty4}) = m_{a2}g$$

10. Roll Displacement of the Forward Axle of the Tractor Tandem, ϕ_{a2}:

$$I_{xa2}\ddot{\phi}_{a2} - (s_2/2)(F_{sy3} - F_{sy4}) + (d_2/2)(F_{ty3} - F_{ty4}) - (s_2/2)(F_{dsy3} - F_{dsy4}) + (d_2/2)(F_{dty3} - F_{dty4}) = 0$$

11. Vertical Displacement of the Aft Axle of the Tractor Tandem, y_{a3}:

$$m_{a3}\ddot{y}_{a3} - (F_{sy5} + F_{sy6}) + (F_{ty5} + F_{ty6}) - (F_{dsy5} + F_{dsy6}) + (F_{dty5} + F_{dty6}) = m_{a3}g$$

12. Roll Displacement of the Aft Axle of the Tractor Tandem, ϕ_{a3}:

$$I_{xa3}\ddot{\phi}_{a3} - (s_3/2)(F_{sy5} - F_{sy6}) + (d_3/2)(F_{ty5} - F_{ty6}) - (s_3/2)(F_{dsy5} - F_{dsy6}) + (d_3/2)(F_{dty5} - F_{dty6}) = 0$$

13. Vertical Displacement of the Forward Axle of the Trailer Tandem, y_{a4}:

$$m_{a4}\ddot{y}_{a4} - (F_{sy7} + F_{sy8}) + (F_{ty7} + F_{ty8}) - (F_{dsy7} + F_{dsy8}) + (F_{dty7} + F_{dty8}) = m_{a4}g$$

14. Roll Displacement of the Forward Axle of the Trailer Tandem, ϕ_{a4}:

$$I_{xa4}\ddot{\phi}_{a4} - (s_4/2)(F_{sy7} - F_{sy8}) + (d_4/2)(F_{ty7} - F_{ty8}) - (s_4/2)(F_{dsy7} - F_{dsy8}) + (d_4/2)(F_{dty7} - F_{dty8}) = 0$$

15. Vertical Displacement of the Aft Axle of the Trailer Tandem, y_{a5}:

$$m_{a5}\ddot{y}_{a5} - (F_{sy9} + F_{sy10}) + (F_{ty9} + F_{ty10}) - (F_{dsy9} + F_{dsy10}) + (F_{dty9} + F_{dty10}) = m_{a5}g$$

16. Roll Displacement of the Aft Axle of the Trailer Tandem, ϕ_{a5}:

$$I_{xa5}\ddot{\phi}_{a5} - (s_5/2)(F_{sy9} - F_{sy10}) + (d_5/2)(F_{ty9} - F_{ty10}) - (s_5/2)(F_{dsy9} - F_{dsy10}) + (d_5/2)(F_{dty9} - F_{dty10}) = 0$$

in which: $F_{syi} = K_{syi}U_{syi} + F_{yi}$, $F_{dsyi} = D_{syi}\dot{U}_{syi}$,

$F_{tyi} = K_{tyi}U_{tyi}$, $F_{dtyi} = D_{tyi}\dot{U}_{tyi}$, i = 1 to 10, and

LIST OF FIGURES

II. Relative Displacement at Spring Locations:

1. Suspension Springs:

$$U_{sy1} = (y_{t1} - y_{a1}) + (s_1/2)(\phi_{t1} - \phi_{a1}) + l_6\theta_{t1}$$

$$U_{sy2} = (y_{t1} - y_{a1}) - (s_1/2)(\phi_{t1} - \phi_{a1}) + l_6\theta_{t1}$$

$$U_{sy3} = (y_{t1} - y_{a2}) + (s_2/2)(\phi_{t1} - \phi_{a2}) - l_7\theta_{t1}$$

$$U_{sy4} = (y_{t1} - y_{a2}) - (s_2/2)(\phi_{t1} - \phi_{a2}) - l_7\theta_{t1}$$

$$U_{sy5} = (y_{t1} - y_{a3}) + (s_3/2)(\phi_{t1} - \phi_{a3}) - (l_2+l_7)\theta_{t1}$$

$$U_{sy6} = (y_{t1} - y_{a3}) - (s_3/2)(\phi_{t1} - \phi_{a3}) - (l_2+l_7)\theta_{t1}$$

$$U_{sy7} = (y_{t2} - y_{a4}) + (s_4/2)(\phi_{t2} - \phi_{a4}) + l_8\theta_{t2}$$

$$U_{sy8} = (y_{t2} - y_{a4}) - (s_4/2)(\phi_{t2} - \phi_{a4}) + l_8\theta_{t2}$$

$$U_{sy9} = (y_{t2} - y_{a5}) + (s_5/2)(\phi_{t2} - \phi_{a5}) - l_{11}\theta_{t2}$$

$$U_{sy10} = (y_{t2} - y_{a5}) - (s_5/2)(\phi_{t2} - \phi_{a5}) - l_{11}\theta_{t2}$$

$$U_{sy11} = (y_{t2} - y_{a6}) + (s_6/2)(\phi_{t2} - \phi_{a6}) - (l_5+l_{11})\theta_{t2}$$

$$U_{sy12} = (y_{t2} - y_{a6}) - (s_6/2)(\phi_{t2} - \phi_{a6}) - (l_5+l_{11})\theta_{t2}$$

2. Tire Springs:

$$U_{ty1} = y_{a1} + (d_1/2)\phi_{a1} - (-u_{SR1})$$

$$U_{ty2} = y_{a1} - (d_1/2)\phi_{a1} - (-u_{SR2})$$

$$U_{ty3} = y_{a2} + (d_2/2)\phi_{a2} - (-u_{SR3})$$

$$U_{ty4} = y_{a2} - (d_2/2)\phi_{a2} - (-u_{SR4})$$

$$U_{ty5} = y_{a3} + (d_3/2)\phi_{a3} - (-u_{SR5})$$

$$U_{ty6} = y_{a3} - (d_3/2)\phi_{a3} - (-u_{SR6})$$

$$U_{ty7} = y_{a4} + (d_4/2)\phi_{a4} - (-u_{SR7})$$

$$U_{ty8} = y_{a4} - (d_4/2)\phi_{a4} - (-u_{SR8})$$

$$U_{ty9} = y_{a5} + (d_5/2)\phi_{a5} - (-u_{SR9})$$

$$U_{ty10} = y_{a5} - (d_5/2)\phi_{a5} - (-u_{SR10})$$

$$U_{ty11} = y_{a6} + (d_6/2)\phi_{a6} - (-u_{SR11})$$

$$U_{ty12} = y_{a6} - (d_6/2)\phi_{a6} - (-u_{SR12})$$

in which: u_{SRi} = road surface roughness under the ith wheel (positive upwards), i = 1 to 12.

III. Equations of Motion:

1. Vertical Displacement of the Tractor, y_{t1}:

$$m_{t1}\ddot{y}_{t1} + (F_{sy1} + F_{sy2} + F_{sy3} + F_{sy4} + F_{sy5} + F_{sy6}) + (l_8/l_{10})(F_{sy7} + F_{sy8}) - (l_{11}/l_{10})(F_{sy9} + F_{sy10}) - (1/l_{10})(l_5 + l_{11})(F_{sy11} + F_{sy12}) + (F_{dsy1} + F_{dsy2} + F_{dsy3} + F_{dsy4} + F_{dsy5} + F_{dsy6}) + (l_8/l_{10})(F_{dsy7} + F_{dsy8}) - (l_{11}/l_{10})(F_{dsy9} + F_{dsy10}) - (1/l_{10})(l_5 + l_{11})(F_{dsy11} + F_{dsy12}) = m_{t1}g$$

2. Roll Displacement of the Tractor, ϕ_{t1}:

$$I_{xt1}\ddot{\phi}_{t1} + (s_1/2)(F_{sy1} - F_{sy2}) + (s_2/2)(F_{sy3} - F_{sy4}) + (s_3/2)(F_{sy5} - F_{sy6}) + (s_1/2)(F_{dsy1} - F_{dsy2}) + (s_2/2)(F_{dsy3} - F_{dsy4}) + (s_3/2)(F_{dsy5} - F_{dsy6}) = 0$$

3. Pitch Displacement of the Tractor, θ_{t1}:

$$I_{zt1}\ddot{\theta}_{t1} + l_6(F_{sy1} + F_{sy2}) - l_7(F_{sy3} + F_{sy4}) - (l_2 + l_7)(F_{sy5} + F_{sy6}) - l_9(l_8/l_{10})(F_{sy7} + F_{sy8}) + l_9(l_{11}/l_{10})(F_{sy9} + F_{sy10}) + (l_9/l_{10})(l_5 + l_{11})(F_{sy11} + F_{sy12}) + l_6(F_{dsy1} + F_{dsy2}) - l_7(F_{dsy3} + F_{dsy4}) - (l_2 + l_7)(F_{dsy5} + F_{dsy6}) - l_9(l_8/l_{10})(F_{dsy7} + F_{dsy8}) + l_9(l_{11}/l_{10})(F_{dsy9} + F_{dsy10}) + (l_9/l_{10})(l_5 + l_{11})(F_{dsy11} + F_{dsy12}) = 0$$

4. Vertical Displacement of the Trailer, y_{t2}:

$$m_{t2}\ddot{y}_{t2} - (l_6/l_9)(F_{sy1} + F_{sy2}) + (l_7/l_9)(F_{sy3} + F_{sy4}) + (1/l_9)(l_2 + l_7)(F_{sy5} + F_{sy6}) + (F_{sy7} + F_{sy8} + F_{sy9} + F_{sy10} + F_{sy11} + F_{sy12}) - (l_6/l_9)(F_{dsy1} + F_{dsy2}) + (l_7/l_9)(F_{dsy3} + F_{dsy4})$$

$$+ (1/l_9)(l_2 + l_7)(F_{dsy5} + F_{dsy6}) + (F_{dsy7} + F_{dsy8} + F_{dsy9} + F_{dsy10} + F_{dsy11} + F_{dsy12})$$

$$= m_{t2}g$$

5. Roll Displacement of the Trailer, ϕ_{t2}:

$$I_{xt2}\ddot{\phi}_{t2} + (s_4/2)(F_{sy7} - F_{sy8}) + (s_5/2)(F_{sy9} - F_{sy10}) + (s_6/2)(F_{sy11} - F_{sy12}) + (s_4/2)(F_{dsy7} - F_{dsy8}) + (s_5/2)(F_{dsy9} - F_{dsy10}) + (s_6/2)(F_{dsy11} - F_{dsy12}) = 0$$

6. Pitch Displacement of the Trailer, θ_{t2}:

$$I_{zt2}\ddot{\theta}_{t2} - l_{10}(l_6/l_9)(F_{sy1} + F_{sy2}) + l_{10}(l_7/l_9)(F_{sy3} + F_{sy4}) + (l_{10}/l_9)(l_2 + l_7)(F_{sy5} + F_{sy6}) + l_8(F_{sy7} + F_{sy8}) - l_{11}(F_{sy9} + F_{sy10}) - (l_5 + l_{11})(F_{sy11} + F_{sy12}) - l_{10}(l_6/l_9)(F_{dsy1} + F_{dsy2}) + l_{10}(l_7/l_9)(F_{dsy3} + F_{dsy4}) + (l_{10}/l_9)(l_2 + l_7)(F_{dsy5} + F_{dsy6}) + l_8(F_{dsy7} + F_{dsy8}) - l_{11}(F_{dsy9} + F_{dsy10}) - (l_5 + l_{11})(F_{dsy11} + F_{dsy12}) = 0$$

7. Vertical Displacement of the Steer Axle, y_{a1}:

$$m_{a1}\ddot{y}_{a1} - (F_{sy1} + F_{sy2}) + (F_{ty1} + F_{ty2}) - (F_{dsy1} + F_{dsy2}) + (F_{dty1} + F_{dty2}) = m_{a1}g$$

8. Roll Displacement of the Steer Axle, ϕ_{a1}:

$$I_{xa1}\ddot{\phi}_{a1} - (s_1/2)(F_{sy1} - F_{sy2}) + (d_1/2)(F_{ty1} - F_{ty2}) - (s_1/2)(F_{dsy1} - F_{dsy2}) + (d_1/2)(F_{dty1} - F_{dty2}) = 0$$

9. Vertical Displacement of the Forward Axle of the Tractor Tandem, y_{a2}:

$$m_{a2}\ddot{y}_{a2} - (F_{sy3} + F_{sy4}) + (F_{ty3} + F_{ty4}) - (F_{dsy3} + F_{dsy4}) + (F_{dty3} + F_{dty4}) = m_{a2}g$$

10. Roll Displacement of the Forward Axle of the Tractor Tandem, ϕ_{a2}:

$$I_{xa2}\ddot{\phi}_{a2} - (s_2/2)(F_{sy3} - F_{sy4}) + (d_2/2)(F_{ty3} - F_{ty4}) - (s_2/2)(F_{dsy3} - F_{dsy4}) + (d_2/2)(F_{dty3} - F_{dty4}) = 0$$

11. Vertical Displacement of the Aft Axle of the Tractor Tandem, y_{a3}:

$$m_{a3}\ddot{y}_{a3} - (F_{sy5} + F_{sy6}) + (F_{ty5} + F_{ty6}) - (F_{dsy5} + F_{dsy6}) + (F_{dty5} + F_{dty6}) = m_{a3}g$$

12. Roll Displacement of the Aft Axle of the Tractor Tandem, ϕ_{a3}:

$$I_{xa3}\ddot{\phi}_{a3} - (s_3/2)(F_{sy5} - F_{sy6}) + (d_3/2)(F_{ty5} - F_{ty6}) - (s_3/2)(F_{dsy5} - F_{dsy6}) + (d_3/2)(F_{dty5} - F_{dty6}) = 0$$

13. Vertical Displacement of the Fourth Axle, y_{a4}:

$$m_{a1}\ddot{y}_{a4} - (F_{sy7} + F_{sy8}) + (F_{ty7} + F_{ty8}) - (F_{dsy7} + F_{dsy8}) + (F_{dty7} + F_{dty8}) = m_{a4}g$$

14. Roll Displacement of the Fourth Axle, ϕ_{a4}:

$$I_{xa1}\ddot{\phi}_{a4} - (s_4/2)(F_{sy7} - F_{sy8}) + (d_4/2)(F_{ty7} - F_{ty8}) - (s_4/2)(F_{dsy7} - F_{dsy8}) + (d_4/2)(F_{dty7} - F_{dty8}) = 0$$

15. Vertical Displacement of the Forward Axle of the Trailer Tandem, y_{a5}:

$$m_{a5}\ddot{y}_{a5} - (F_{sy9} + F_{sy10}) + (F_{ty9} + F_{ty10}) - (F_{dsy9} + F_{dsy10}) + (F_{dty9} + F_{dty10}) = m_{a5}g$$

16. Roll Displacement of the Forward Axle of the Trailer Tandem, ϕ_{a5}:

$$I_{xa5}\ddot{\phi}_{a5} - (s_5/2)(F_{sy9} - F_{sy10}) + (d_5/2)(F_{ty9} - F_{ty10}) - (s_5/2)(F_{dsy9} - F_{dsy10}) + (d_5/2)(F_{dty9} - F_{dty10}) = 0$$

17. Vertical Displacement of the Aft Axle of the Trailer Tandem, y_{a6}:

$$m_{a6}\ddot{y}_{a6} - (F_{sy11} + F_{sy12}) + (F_{ty11} + F_{ty12}) - (F_{dsy11} + F_{dsy12}) + (F_{dty11} + F_{dty12}) = m_{a6}g$$

18. Roll Displacement of the Aft Axle of the Trailer Tandem, ϕ_{a6}:

$$I_{xa6}\ddot{\phi}_{a6} - (s_6/2)(F_{sy11} - F_{sy12}) + (d_6/2)(F_{ty11} - F_{ty12}) - (s_6/2)(F_{dsy11} - F_{dsy12}) + (d_6/2)(F_{dty11} - F_{dty12}) = 0$$

in which: $F_{syi} = K_{syi}U_{syi} + F_{yi}$, $F_{dsyi} = D_{syi}\dot{U}_{syi}$,

$F_{tyi} = K_{tyi}U_{tyi}$, $F_{dtyi} = D_{tyi}\dot{U}_{tyi}$, i = 1 to 12, and

F_{yi} = the friction force at the ith suspension.

REFERENCES

1. Chen, W. L., and Koetje, E. L. (1956). "Model Investigation of the Vibration of Continuous Three-span Steel Bridges." M. S. Thesis, M. I. T.

2. Chu, K. H., Garg, V. K., and Wang, T. L. (1986). "Impact in Railway Prestressed Concrete Bridges." Journal of Structural Engineering, ASCE, Vol. 112, No. 5, 1036-1051.

3. Clough, R. W. and Penzien, J. (1975). Dynamics of Structures, McGraw-Hill Book Co., New York, N.Y.

4. Dodds, C. J. and Robson, J. D. (1973). "The Description of Road Surface Roughness." Journal of Sound and Vibration, Vol. 31, No. 2, 175-183.

5. Eberhardt, A. C. (1972). "A Finite Element Approach to the Dynamic Analysis of Continuous Highway Bridges." Ph.D., Dissertation, University of Illinois, Urbana, IL.

6. Edgarton, R. C., and Bcecroft, C. W. (1958) "Dynamic Stresses in Continuous Plate Girder Bridges." ASCE Transactions, Vol. 123, 266-292.

7. Fenves, S. J., Veletsos, A. S. and Siess, C. P. (1962). Dynamic Studies of Bridges on the AASHO Test Road, Final Report to AASHO Road Test Highway Research Board, National Academy of Sciences-National Research Council, Report No. 71, Washington, D.C.

8. "Guide Specifications for Strength Evaluation of Existing Steel and Concrete Bridges." (1989), American Association of State Highway and Transportation Officials, Washington, D. C.

9. Gupta, R. K. (1980). "Dynamic Loading of Highway Bridges." Journal of the Eng. Mechanics Division. ASCE, Vol. 106, No. EM2, 377-394.

10. Hayashikawa, T. and Watanahe, N. (1981). "Dynamic Behavior of Continuous Beams with Moving Loads." Journal of the Eng. Mechanics Division, ASCE, Vol. 106, No. EM1, 229 -246.

11. Hayes, J. M., and Sbarounis, J. A. (1956). "Vibration Study of Three-span Continuous I-beam Bridge." Highway Research Board, Bulletin 124, 47-78.

12. Huang, D. Z., Wang, T. L. and Shahawy, M. (1992), "Impact Analysis of Continuous Multigirder Bridges Due to Moving Vehicles," Journal of Structural Engineering, ASCE, Vol. 118, No. 12.

13. Huang, T. (1960). "Dynamic Response of Three-Span Continuous Highway Bridges." Ph.D.

Dissertation, University of Illinois, Urbana, IL.

14. Hwang, E. S. and Nowak, A. S. (1991). "Simulation of Dynamic Load for Bridges." Journal of Structural Engineering, ASCE, Vol. 117, No. 5, 1413-1434.

15. Kinnier, H. L. and Barton,F. W.(1975),"A Study of a Rigid Frame Highway Bridge in Virginia, Virginia Highway and Transportation Research Council, Department of Highway, Charlottesville, Virginia, VHTRC 75-R47.

16. Klöppl, K. and Lie, K. H./Li, G. H. (1942), "Lotrechte Schwingungen von Hangeruchen", Ingenicur-Archiv, Vol. 13, 211-266.

17. Li, G. H. (1983), Theory of Bridges and Structures (in Chinese), Publishing House of Shanghai Science and Technology, Shanghai, China .

18. Louw, J. M. (1958). "Dynamic Response of Continuous Span Highway Bridges to Moving Vehicle Loads." Ph.D. Dissertation, M. I. T.

19. Nieto Ramirez, J. A. (1964). "Response of Three-span Continuous Highway Bridges to Moving Vehicles." Civil Engineer Studies, SRS, No. 276, University of Illinois, Urbana.

20. Ruhl, J. (1974). Stress Histories for Highway Bridges Subjected to Traffic Loading." Ph.D. Dissertation, University of Illinois, Urbana-Champaign.

21. Shi, D., Shi Z. Y. and Huang, D. Z. (1989). Application of Computers in Bridge Engineering, Tongji University Publishing House, China. (in Chinese).

22. "Standard Plans for Highway Bridge Superstructures." (1957, 1968), U.S. Department of Commerce, Bureau of Public Road.

23. "Standard Specifications for Highway Bridges." (1989). 14th Ed., American Association of State Highway and Transportation Officials, Washington, D.C.

24. Trakool, A. (1974). "Highway Bridge Vibration Studies." Ph.D. Dissertation, Purdue University.

25. Vandegrift, L. E. (1944). "Vibration Studies of Continuous Span Bridges." Bulletin 119, Engineering Experiment Station, Ohio State University.

26. Veletsos, A. S. and Huang, T. (1970). "Analysis of Dynamic Response of Highway Bridges." Journal of the Eng. Mechanics Division, ASCE, Vol. 90, No. EM5, 1648-1659.

27. Wang, T. L. (1990). "Ramp/Bridge Interface in Railway Prestressed Concrete Bridges." Journal of the Structural Engineering, ASCE, Vol. 116, No. 6, 1648-1659.

28. Wang, T. L., Garg, V. K., and Chu, K. H. (1991). "Railway Bridge/Vehicle Interaction

Studies with a New Vehicle Model." Journal of Structural Engineering, ASCE, Vol. 117, No. 7, 2099-2116.

29. Wang, T. L. and Huang, D. Z. (1992). "Computer Modeling Analysis in Bridge Evaluation." Interim Research Report, Florida Department of Transportation, Report No. FL/DOT/RML/054-3392, Tallahassee, FL.

30. Wang, T. L. and Huang, D. Z. (1992). "Cable-stayed Bridge Vibration due to Road Surface Roughness." Journal of Structural Engineering, ASCE, Vol. 118, No. 5, 1354-1374.

31. Wang, T. L., Huang, D. Z. and Shahawy, M. (1992), "Dynamic Response of Multigirder Bridges", Journal of Structural Engineering, ASCE, Vol. 118, No. 8.

32. Weaver, W. and Johnston P. R. (1987) "Structural Dynamics by Finite Elements", PRENTICE-HALL, INC. Englewood Cliffs, New Jersey.